The Sol-Gel Chemistry

and

Electrochemistry

of Niobium (V).

a thesis presented by

GEORGE ROBERT LEE

to the

UNIVERSITY OF ST. ANDREWS

in application for

THE DEGREE OF DOCTOR OF PHILOSOPHY

St. Andrews May 1992

DECLARATION

I, George Robert Lee, hereby certify that this thesis has been composed by myself, that it is a record of my own work, and that it has not been accepted in partial or complete fulfillment of any other degree or professional qualification.

Signed . Date 20/5/92

I was admitted to the Faculty of Science of the University of St. Andrews under Ordinance General No. 12 on 1 October 1989
and as a candidate for the degree of Ph.D. on 1 October 1989

Signed Date 20/5/92

I hereby certify that the candidate has fulfilled the conditions of the Resolution and Regulations appropriate to the degree of Ph.D.

Signature of supervisor

Date 20/5/92

Copyright

To

Jenn

"...Nature cannot be fooled."

Richard Feynman

ACKNOWLEDGEMENTS

I would like to express my sincere thanks to Dr. Joe Crayston for his untiring encouragement, guidance and enthusiasm during the course of my postgraduate studies.

Thanks also go to:-

Dr. John Walton for his help and advice with the ESR studies.

Dr. Frank Riddell and Dr. San Arumagum for their help with the ^{93}Nb NMR studies.

Dr. Trevor Dines, University of Dundee, for the Raman Spectroscopy and Dr Steve Jones, British Gas, for the CO_2 absorbance pore size data.

The technical staff at St. Andrews; in particular, Jim Bews (computing), Colin Smith (glass blower), Melanja Smith (NMR), Silvia Smith (microanalysis) and Colin Miller (gcms).

The occupants of Lab 248, past and present, for their good humour and for occasionally leaving me some of my clean dry glassware to work with!

I am indebted to BP Reseach (Sunbury) for a Research Studentship.

List of Abbreviations

AN	acetonitrile
BiSCCO	bismuth strontium calcium copper oxide
BN	phenyl acetonitrile
CV	cyclic voltammetry
DMF	dimethylformamide
DMSO	dimethyl sulfoxide
EDAX	energy dispersive analysis by X-rays
ESR	electron spin resonance
FWHM	full width at half maxima
GITT	galvanostatic intermittent titration technique
Glymo	3-(glycidoxypropyl)trimethoxysilane
ITO	indium tin oxide
NMR	nuclear magnetic resonance spectroscopy
PMN	lead magnesium niobate
PZT	lead zirconium titanate
SEM	scanning electron microscopy
SGP	sol-gel processing
TBA	tetra butyl ammonium ion
TBAOMe	tetra butyl ammonium methoxide
TBAHFP	tetra butyl ammonium hexafluorophosphate
TBADHP	tetra butyl ammonium dihydrogenphosphate
TPM	triphenyl methanol
YBCO	yttrium barium copper oxide
9F	9-fluorenemethanol

ABSTRACT

^{93}Nb NMR has been used to investigate and characterise the precursor species present in alcohol solutions of niobium (V) chloride. It reveals the presence of all possible substitution products $NbCl_{5-x}(OR)_x$, and that the solution composition is both temperature and concentration dependent. Investigations of the sol-gel processing properties of these solutions reveals that the gelation rates of these solutions is dependent not only on the concentration of niobium but also the pKa of the parent alcohol and the ratio of chloride ions to niobium atoms.

Sol-gel processing of niobium chloroethoxide solutions, via spin coating, can be used to form thick (5 μm) and thin (0.1 μm) films of hydrated Nb_2O_5. The thick films have limited durability and crack upon drying, however application of a second coating containing a mixed NbO/silicone solution produces a more durable Nb_2O_5/silicone composite film. Chronoamperometry and chronabsorptiometric measurements upon the three types of film reveal that the thick films have H^+ diffusion coefficients of the order of 10^{-8} cm^2s^{-1} comparable to previously reported sputtered Nb_2O_5 films, whereas the thin films have H^+ diffusion coefficients of the order of 10^{-13} cm^2s^{-1}, due to their dense, non-microporous, glass-like structure.

The electrochemistry and electrodeposition properties of a number of niobium (V) compounds have been investigated, using cyclic voltammetry and constant potential electrolysis. Although it proved possible to electrodeposit films of niobium oxide, the production of gas (O_2 or H_2) at the very large negative potentials required limit the practical applications of these systems.

CONTENTS

Chapter Three: Gelation Studies of Niobium Chloroalkoxides

Chapter Four: Techniques for Film Formation of Nb_2O_5

Chapter Five: Electrochromic Properties of Nb_2O_5 Films

Chapter Seven: Electrochemical Deposition of Niobium Oxide

Chapter Eight: Novel Chemistry of Nb(V) Compounds

Chapter Nine: Experimental

Chapter 1

Introduction

1.1 Advanced Ceramic Materials

Ceramic objects have been with us for tens of thousands of years and can probably lay claim to be the first fruits of high temperature chemistry practised by man. For centuries their use was limited to clay based items such as cooking containers and tiling. However, in the past few decades a new group of ceramics have appeared – the "advanced" ceramic materials, and have found uses in many technologically important areas.

These advanced ceramics have many favourable properties when compared to metals, and so have many potential applications. Thus, silicon nitride (Si_3N_4) with its higher melting point and greater strength than nickel superalloys seems an ideal choice for the replacement of the nickel superalloys used in gas turbines and reciprocating engines. The greater operating temperatures afforded by the use of Si_3N_4 would lead to greater efficiencies.

Novel glass ceramics have found many applications, such as the Li_2O-Al_2O_3-SiO_2 system which is used in heat exchangers and cooking utensils, or the MgO-Al_2O_3-SiO_2 system used in missile radar domes.[1] Likewise, aluminium titanate is used to make port liners in car engines as it has a low thermal conductivity (2 W m^{-1} K^{-1}) which reduces heat flow to the cylinder block and thus the amount of cooling required.[1]

Ceramic coatings have also found many uses, often as optical coatings (eg. TiO_2-SiO_2 which is used for graded refractive index systems) or for their thermal, wear or corrosion resistance properties. Thus an RB211 gas turbine engine coated with a 50 μm thick ZrO_2 film enjoys an increased lifetime over uncoated versions, due to a reduction in turbine substrate temperature of up to 50K.[2]

Electronic ceramics comprise one of the largest and most mature areas of the advanced ceramic materials, dating from the 1940's when Al_2O_3 was used in spark plugs because of its insulating properties. Almost all electronic ceramics are dielectric materials. This means that they are able to store electrostatic charge. The dielectric constant (a measure of the materials ability to store charge) can vary with temperature, crystal structure, structural defects and the

frequency of an applied ac field. The commonest use of dielectric materials is in the production of capacitors, where the dielectric material increases the charge storage capacity of a capacitor by neutralising some of the free charges which would otherwise contribute to the potential difference opposing the battery voltage. Thus, more charge can flow into the capacitor, which then has an increased storage capacity given by $\varepsilon_r C_o$ where C_o is the original capacity in air and ε_r is known as the dielectric constant or relative permittivity of the material (see Fig. 1.1).[2]

Fig. 1.1

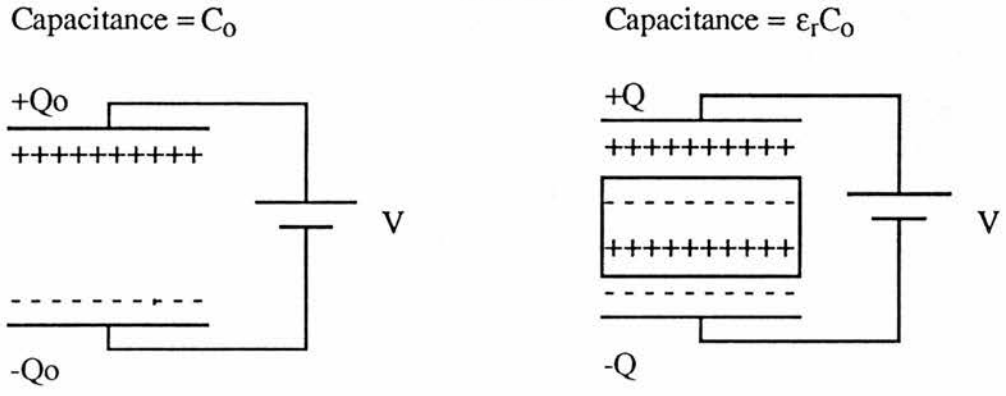

In normal dielectric materials the permittivity decreases with decreasing temperature. The majority of capacitors produced are based on $BaTiO_3$ as it has a very high dielectric constant. Dielectric ceramics can have useful other properties, some of which are outlined below.

1.1.1 Piezoelectric Materials

Piezoelectric materials are compounds which produce electricity when subjected to pressure. Charges appear on a piezoelectric crystal surface when it is stressed, because the stress separates the centre of gravity of the positive charge from the centre of gravity of the negative charge, producing a dipole moment.[2] Thus the effect can only be observed in crystals not having a centre of symmetry, because applying uniform stress to centro-symmetric crystals does not separate the centre of gravity of the charges. When an electric field is applied to a piezoelectric crystal it will strain mechanically. Piezoelectric materials have many uses, ranging from mechanical sensors, such as stereo record-player needles, through acoustic transducers

used to change the electrical signal back into sound in a pair of headphones, to quartz electronic oscillators used in quartz watches.

1.1.2 Pyroelectric and Ferroelectric Materials

Ferroelectric and pyroelectric crystals have an electric dipole moment even in the absence of an external electric field. This arises because the centre of positive charge in the crystal does not coincide with the centre of negative charge, producing permanent electrostatic charge on the crystal surfaces. This spontaneous polarization is strongly dependent upon temperature because the atomic dipole moments vary as the crystal expands or contracts. Normally the surface charge on a crystal with a permanent electric dipole is not observed since atmospheric ions neutralise the charge. However heating the crystal will tend to desorb the neutralising ions (charging the surface) and change the polarisation; this effect is known as the pyroelectric effect. A ferroelectric crystal is defined as possessing two (or more) orientation states of polarization, and can be switched from one to the other.by application of an electric field. Most pyroelectrics are also ferroelectrics.[2] The Curie temperature (T_c) of a ferroelectric material is defined as the temperature at which, when cooled, a crystal will undergo phase transition to a ferroelectric phase. Thus, below T_c spontaneous polarization develops, whereas above T_c the crystal phase is too symmetrical to exhibit spontaneous polarization. This means that, unlike normal dielectric materials, in ferroelectric materials the dielectric constant increases with decreasing temperature, going through a sharp maximum at T_c and thereafter falling.

Ferroelectrics have many applications. They are used in miniature capacitors because they have large dielectric constants. The ability to switch between two polarization states is used in non-volatile memories (for instance in pocket calculators/computers). The polarization of the crystal by application of an electric field is also used in optics as the oscillating dipoles can broadcast electromagnetic radiation (electro-optics) and modulate and deflect laser beams. Because the induced polarization (and hence optical modification) is a nonlinear function of the applied field the effect is termed "non-linear optics". The temperature dependence of spontaneous polarization exhibited by both ferroelectrics and pyroelectrics is used to create thermal and infrared detectors.[2]

Many other examples of electronic ceramics exist, including the recently discovered high temperature superconductors such as yttrium barium cuprate ($YBa_2Cu_3O_{7-d}$ ($0<d<1$)).[1] However these many forms of advanced ceramics all have a common requirement. That is a need for a high degree of control in chemical purity and ceramic formation in order to achieve optimum performance.

In the past this was achieved by sintering powders of the required ceramic (obtained by grinding bulk materials) to form films and layers in a device. Whilst allowing a fair degree of control in the ceramic formation, the powders were easily contaminated with impurities during grinding and the whole process was very energy inefficient, requiring high temperatures to form defectless films. Nowadays low temperature methods have been developed, using such methods as sputtering (ion beam and laser ablation) and chemical vapour deposition. Unfortunately, these methods are expensive and not very efficient since there is a high degree of waste. However one technique that has been developed, that is both a low temperature process and reasonably inexpensive, is sol-gel processing of ceramics.

1.2 Sol-Gel Processing of Ceramics

Traditional ceramics have been made by mixing fine grained solid powders (>50 μm particle size) of oxides such as SiO_2, Al_2O_3, Fe_2O_3 in a water based slurry or clay and then subjecting them to temperatures between 1000°C-1500°C in order for them to react. The problems associated with this method are well known:- (i) high temperatures are required to sinter large particles in order to facilitate diffusion across the large distances between the particles; (ii) large particles lead to defects and voids which can have a deleterious effect on the electrical and optical properties of the ceramic or lead to cracks in engineering ceramics; (iii) the successful mixing of the components to achieve the correct atomic scale stoichiometry and chemical homogeneity depends on the particle size; (iv) high temperatures may destroy metastable phases, cause volatilization of some component oxides or loss of O_2 from the surface. Whilst the level of component mixing acheived with large particles (>50μm) is adequate for rough-grained "low-tech." ceramics, it is difficult to produce advanced, high technology ceramics, glasses and composites from these particle sizes. Thus, much research

has centred on chemical solutions to these problems – by chemically creating ultra-fine, chemically homogeneous powders, films and monolithic glasses the need for high sinter temperatures and problems with atomic-scale homogeneity are circumvented.

Around the turn of the century attention focused on colloidal sols, ie. submicroscopically homogeneous suspensions of solid particles in a liquid which can be manipulated to form a gel (the sol-gel process). Whilst chemists such as Lord Raleigh[3] worked on precipitation phenomena of these sols, and H.B. Weiser and W.O. Milligan[4] worked on oxide sols and gels, there was little work done on actually applying these chemical studies to the production and use of ceramics.

The first time that colloid science was applied to the production of ceramics came prior to World War II. Ewell and Insley [5] coprecipitated gels of SiO_2 and Al_2O_3, and Iler pioneered the chemical synthesis of micas and clays by the sol-gel route,[6] leading to the commercial development of colloidal silica powders. However, it was not until after the war that sol-gel processing (SGP) blossomed. The sol-gel process thus developed has two basic approaches:

a) dispersion of the colloidal particles (often oxide) in a liquid to form a sol which, upon manipulation eg pH or concentration, then undergoes gelation;

b) preparation of an organometallic precursor in solution (often an alkoxide) which upon the addition of water undergoes gelation.

The gelation products thus produced can take many different physical forms depending on the gelation and drying technique. Thus thin films, fibres, spheres, grains, powders and amorphous gels are all common products. The advantages of the sol-gel process over the old "grind and fire" method are apparent. It allows for the rational manipulation of inorganic species at the molecular level (thereby achieving chemical mixing and homogeneity on a 0.5nm scale rather than 50μm scale) and the controlled growth of particle size from nm dimensions upwards. Furthermore the components can be made extremely pure and lower firing temperatures are required because of the smaller particle size and greater homogeneity. Finally, the shaping and forming of the ceramic via the sol-gel route is often easier than with the old conventional method and almost all ceramic materials are accessible, as shown in Fig. 1.2:

Fig. 1.2

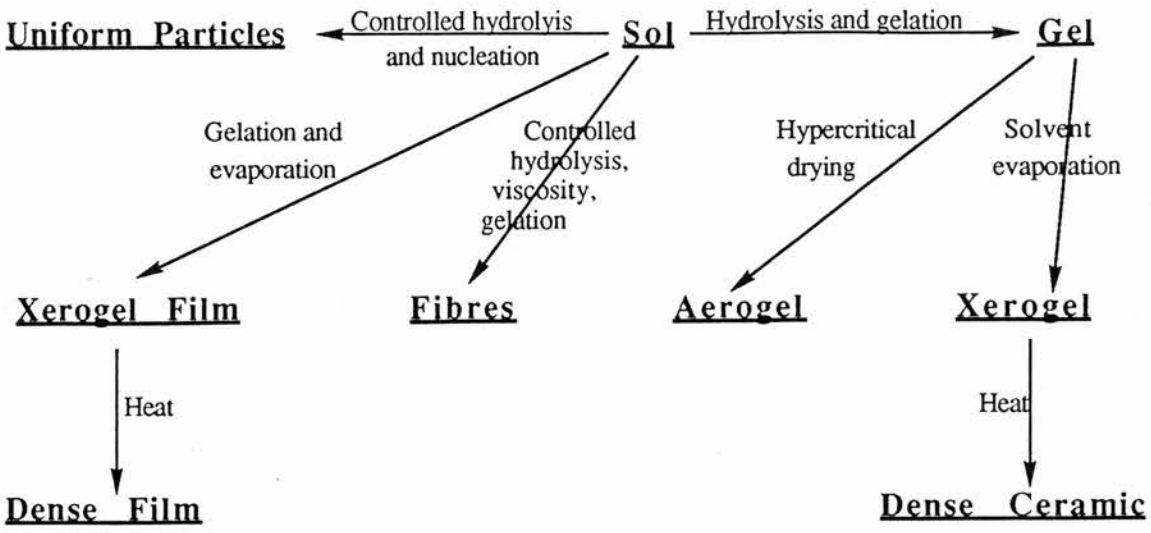

The postwar development of SGP was rapid and occurred simultaneously on a number of fronts. The nuclear industry was a big sponsor of the sol-gel process – it required the production of mixed $(Th,U)O_2$ fuel pellets without the production of radioactive dust particles. To this end, Dean et al [7,8] developed the following technique: superheated steam (748K) was used to strip HNO_3 from hydrated thorium nitrate, the residue formed being redissolved in dilute HNO_3 or uranyl nitrate solution to form a ThO_2 sol. This sol could be tray dried at 363K to give cracked gel fragments, which when compacted and calcined at 1423K in air and then 4% H_2/Ar (to reduce UO_3 to UO_2) gave a homogeneous solid with 98% theoretical density. These solids were achieved at significantly lower temperatures than required by conventional fabrication techniques, where 2000K was often used to achieve densification.

Internal gelation of the sol, to form spheres, was pioneered in the Netherlands in the 60's by Hermans[9] and developed by the UKAEA and AGIP Nucleare Sp. A. Milan in the 70's.[10] The technique developed entails feeding solutions of plutonium and uranyl nitrates (containing an organic gelling aid and modifying agent for stabilization) through a vibrating orifice which forms droplets. These fall into aqueous ammonia where they form mixed hydroxide gel spheres. The spheres are dried and then debonded in CO_2 to remove organics and sintered to dense solids at 1723K in 5% H_2/Ar. This process has been successfully developed to produce highly uniform spheres with two diameters of 80 and 800 μm, which are

then loaded into fast reactor pins by vibrocompaction – again without the production of radioactive dusts.

At the same time Roy and coworkers[11-14] were using the sol-gel route to synthesize a large number of novel multicomponent ceramic oxides, eg. Al, Si, Ti, Zr etc. from organometallic precursors rather than metal mineral salt precursors. Thus tetraethyl orthosilicate (TEOS), aluminium isopropoxide and tetrabutyl titanate were hydrolysed in alcohol solutions to create, upon drying, amorphous ceramic powders which were then sintered to form glassy melts of the following multi component systems; (MgO-Al_2O_3-SiO_2),[15] (TiO_2-SiO_2), (BaO-TiO_2-SiO_2) and (BaO-CaO-TiO_2-SiO_2).[16] Like the thorium systems described above, the powders obtained from this sol-gel process when sintered formed ultrahomogeneous glasses at temperatures hundreds of degrees below the normal melting range.[17]

Much attention has been paid to the production of monodispersed submicron powders, in order to obtain denser packing and lower sintering temperatures than can be achieved with non spherical grains and powders. The principles that determine the formation of monodispersed particles were detailed back in the 40's by La Mer et al [18,19] on sulphur sols. The sulphur particle growth occurred in acidified sodium thiosulphate or ethanolic sulphur solutions diluted in water. They found that the molecular sulphur concentration in H_2O could be increased past the saturation concentration to a super-saturation concentration. Homogeneous self-nucleation then occurred, followed by particle growth due to diffusion of molecular sulphur to the nuclei, until the molecular sulphur concentration equalled the saturation concentration and growth stopped. By using low concentrations (10^{-2} mol dm^{-3} or less), only a single burst of nucleation occurs, in a short time interval, and uniform growth follows because diffusion of the molecular sulphur to the nuclei does not cause a large enough increase in the local molecular sulphur concentration around the nuclei to cause further bursts of nucleation.

Stober et al [20] extended these qualitative findings to show that, when using ammonia as a catalyst for the hydrolysis of TEOS, the morphology and the size of the powders formed could be controlled by a number of factors, including the type and concentration of catalyst used for gelation, type of alkoxide used and reactant temperature and thus developed the

so-called "Stober spherical silica powder". The qualitative approach to homogeneous nucleation has been applied to many sol-gel processes, for example: hydrothermal processing of solutions, vapour-phase reactions and the controlled hydrolysis of alkoxides.

Since then the work of the nuclear industry, Roy and Iler has been built upon, and there is now a plethora not only of colloidal powders but films, glasses, fibres etc that can be made from the sol-gel route using such techniques as spray drying, spin coating and hypercritical drying. Many different types of ceramics are now available, such as oxides, carbonates, hydroxides and sulfides of Al, Si, Ti, Zr, Fe, Co, V, Nb, Ce, Cr, Y, Sr, U and the range is still growing.

The sol-gel processing of transition metal oxides was extensively reviewed by Livage et al [21] in 1988, and since then the field, especially the use of transition metal alkoxides, has flourished. Without doubt, the two biggest areas of research in the sol-gel processing of transition metal alkoxides have been in the formation of high temperature superconductors (such as yttrium barium cuprate) and ferroelectric materials such as the titanates, though numerous other systems have been examined. The sol-gel route is attractive both in achieving atomic scale mixing of the components and as a method for thin film growth.

1.2.1 High Temperature Superconductors

Sol gel processing of $YBa_2Cu_3O_{7-x}$ (YBCO) and bismuth - strontium - calcium - copper - oxygen (BiSCCO) superconductors, through the variation of the process parameters, offers a high degree of microstucture control, homogeneity and lower sinter temperatures. In the formation of YBCO films, soluble copper (II) methoxyethoxide ($Cu(MoE)_2$)[22-24] is now the preferred precursor due to the insoluble oligomeric nature of many other copper(II) alkoxides. Alkoxides used for yttrium and barium vary from ethoxide [25,26] and ethylene glycoxide[26] to methoxyethoxide[22,27,28] whilst highly polar solvents such as methoxy ethanol, methyl ethyl ketone[22,24,28] or amines[25,26] are used in order to promote the solubility and complexation of the metal alkoxides in solution.[24]

Epitaxial thin films of YBCO can be grown on such substrates as $SrTiO_3$,[29] ZrO_2,[30] and sapphire.[22] For these films the water to metal alkoxide ratio affects the transition

temperature (the temperature at which zero resistance is observed,T_c(zero) = 78-83K) and sharpness of the paramagnetic to diamagnetic transition.[27] Addition of organic additives such as pyridine, lutidine and toluene 2,4 disulfonic acid to the precursor solutions affects the ability of the sols to cover the various substrates, such as $SrTiO_3$, ZrO_2, sapphire, SiO_2 and Si.[22,28]

Sintering rates and temperatures of the films are important; for example, the copper concentration on the surface layer increases upon elevation of the heat treatment temperature due to Y and Ba diffusing into the bulk phase.[31] The 123 superconducting phase undergoes initial crystal growth at <700°C and forms single phase 123 YBCO at 850°C.[23,30] At >900°C the films react with the substrate, decomposing to give the 211 YBCO phase (ie Y:Ba:Cu is 2:1:1) and CuO.[30]

Pellets of 123 and 124 phase YBCO have been prepared by the production of powders from citrate and oxalate precursors.[32-34] The procedure is highly reproducible, and permits easy fabrication of highly pure and homogeneous superconductors by eliminating the need for such steps as centrifugation, filtration, and pH control.[33] Powders with particle sizes of lower than 3μm lead to pure phase superconducting powders (>99.5% purity) after firing in flowing O_2 at 900°C (for the citrate precursors) and 950°C (for the oxalate precursors).[32,33] The 123 phase pellets formed after annealing in flowing O_2, at 750 and 800°C exhibited zero resistance at 70K and 80K respectively.[34] The 124 phase pellets formed after annealing at 780°C and 1 atmosphere of O_2 followed by furnace cooling to room temperature or quenching in liquid N_2 (124 phase), exhibited a T_c(onset) of 80-83K and a T_c(zero) of 76-69K.[34] Finally, fibres of 123 phase have been prepared from a single heterometal alkoxide precursor using ethyl acetoacetate and ethylenediamine. After firing at 950°C for 10 hours in O_2, the T_c(onset) of these fibres was 94K.[35]

Films of sol gel processed Bi-Sr-Ca-Cu-O have also been prepared. Excess Ca and Cu and firing at 850°C for 48hrs at a 30° /min heating and cooling rate, are used to counter losses due to volatility and are effective in processing films with a T_c(onset) of 125K and a T_c(zero) of 115K.[36] Likewise, pellets of sol gel processed, lead-doped Bi-Sr-Ca-Cu-O have been characterized.[37] Prepared via an oxalate precursor, in ethylene glycol, the pellets gave a T_c(onset) of 140K and a T_c(zero) of 104K. Analysis by FTIR and XRD suggests that lead

doping (Ca_2PbO_4) catalyses the formation of Ca_2CuO_3 at 650°C. This phase acts as a flux to fuse $Bi_2Sr_2CaCu_2O_{8+x}$, CuO and excess Ca_2CuO_3 to give the high-T_c 2223 phase, $Bi_2Sr_2Ca_2Cu_3O_{10+x}$ at 840K. Finally, $Tl_2CaBa_2Cu_2O_{8+x}$ superconducting powders with transition temperatures of between 100 and 110K have been developed using Ba, Ca, Tl, methoxyethoxides and copper ethoxide in a mixed 2-methoxyethanol/methyl ethylketone/toluene solvent system.[38]

1.2.2 Ferroelectric materials

Titanates

The potential market for thin films of ferroelectric materials for non-volatile semiconductor memories is calculated to be $1 billion within the next three years.[39] Non-volatile memories have the advantages of high access speed, high density, radiation-hardness and low operating voltage. The titanates form a very large percentage of the currently available ferroelectric materials. Thus, $BaTiO_3$ is a diclectric and has applications as a capacitor and sensor. Conventional processing of these materials relies on high temperature solid state reactions (1100-1350°C), and tends to produce coarse and inhomogeneous materials. Furthermore, impurities introduced by ball milling greatly lowers the electrical characteristics of these materials. Sol gel processing circumvents many of these problems.

A large number of the useful phases of the barium titanate system have now been obtained by the hydrolysis of metal alkoxide precursors. Unlike the high temperature superconductors, there does not seem to be a solubility problem in using short alkyl chain alcohols as alkoxide precursors. Thus, $Ba(OEt)_2$ and $Ti(OEt)_4$[40-42] are commonly used as well as $Ba(OAc)_2$ and $Ti(O^iPr)_4$.[43,44] Recently, there has been interest in the synthesis of bimetallic barium titanium alkoxides, as precursor materials; compounds such as $Ba_4Ti_{13}(\mu_3\text{-}O)_{12}(\mu_5\text{-}O)_6(\mu_1\text{-}\eta^1\text{-}OCH_2CH_2OCH_3)_{12}[(\mu_1,\mu_3)\text{-}\eta^2\text{-}OCH_2CH_2OCH_3]_{12}$ have been synthesized and characterized as single crystals by x-ray diffraction, and ^{13}C, ^{17}O, and ^1H NMR in the solid and solution states.[45]

$BaTiO_3$ powders with 90% relative density have been obtained from the hydrolysis of barium acetate and titanium (IV) isopropoxide, in the presence of acetic acid, followed by sintering at 1000°C.[46] $BaTiO_3$ powders with a high dielectric constant (4000) at 20°C were obtained upon direct sintering at 1150°C and exhibited a fine grain microstructure.[46] This dielectric constant decreased in samples sintered above 1200°C due to the high grain growth rate at elevated temperatures. $BaTiO_3$ pellets have also been prepared from the calcined $BaTiO_3$ powders.[41] Prehydolysing $Ti(OEt)_4$ and then mixing with $Ba(OMe)_2$ to give Ba/Ti ratios of 2:9 and 1:5 yielded powders of, $BaTi_5O_{11}$ at 700°C from the 1:5 precursor, and $Ba_2Ti_9O_{20}$ at 1200°C from the 2:9 precursor.[42] Crystalline $BaTi_4O_9$ powders have also been formed.[44]

Lead zirconium titanate (PZT) has numerous uses. As a ferroelectric it is used as a non-volatile memory. It is used as an IR detector because it is a pyroelectric and its nonlinear optical properties find many uses, such as in thin film waveguides where laser light is "channeled" or directed and modified.[39] A recent review of this area focuses on the process optimization and characterization of "device-worthy" sol-gel based PZT for ferroelectric memories.[47] High quality films and mouldings of PZT have been prepared from Pb, Zr and Ti alkoxides such as eg $Pb(OBu)_2$, $Ti(OBu)_4$ and $Zr(OBu)_4$.[48,49] To grow PZT films a stabilising agent is usually added to prevent abrupt hydration. When this agent is acetate ($\geq$5 mols acetate/mol Pb salt), $PbZr_{0.0\text{-}1.0}Ti_{0.0\text{-}1.0}O_3$ films have been prepared having a dielectric constant of 150-4000, a dielectric loss factor of 0.001-0.08 and a saturation polarization of 0-80 μCcm^{-2}.[49] PZT crystals (Curie temperature of 340°C) and monodispersed PZT particles have also been prepared by the hydrolysis of a mixed metal alkoxide.[50,51]

Like PZT, lead titanate is a ferroelectric material which, due to its pyroelectric and piezoelectric properties is used as a pyrodetector and acoustic transducer.[39] Films, powders and gels of $PbTiO_3$ have all been prepared by sol-gel routes, usually using lead acetate, $Pb(OOCMe)_2$, and titanium alkoxides such as titanium isopropoxide and titanium methoxyethoxide in methoxyethanol.[52-54] ^1H and ^{13}C NMR have been used to identify the actual precursors present in methoxyethanol solution when titanium isopropoxide and lead acetate are used as the starting alkoxides. These techniques reveal that the precursors present in solution are $Pb(OOCMe)(OC_2H_4OMe).xH_2O$ ($x<0.5$) and $Ti_2(OC_2H_4OMe)_8$ respectively, as

well as a mixed Pb-Ti complex.[52] $PbTiO_3$ powders show an increase in surface area, pore diameter and pore volume with increasing water concentration during the hydrolysis step.[53] Thus, organic decomposition temperatures decreased with increasing water concentration.

Niobates

Whilst sol-gel processing of the niobates is not, presently, as common as that of the titanates, there is reason to expect this route to gain in popularity. Both niobium ethoxide and tantalum ethoxide offer very convenient precursor materials for the sol-gel synthesis of the niobates, and are currently the main ones in use, although their use seems to have been limited to the production of lithium niobate and tantalate.[55-58] Lithium niobate ($LiNbO_3$) is a piezoelectric material, used as a pyrodetector. Lithium tantalate ($LiTaO_3$) is a non-linear optical material used as a waveguide device, optical modulator (converting acoustic frequencies into light intensities) and second harmonic generator (frequency doubling,modifying an input frequency (ω) to give an output frequency of (2ω).[39] $Pb(Mg_{1/3}Nb_{2/3})O_3$ (PMN) is a dielectric material and is used as a capacitor and memory.[39]

$LiNbO_3$ films have been prepared using lithium ethoxide or lithium methoxyethoxide.[55,56] Upon sintering, randomly orientated polycrystalline layers on Si and grain orientated layers on sapphire and Pt substrates may be grown.[55] The morphology of the films formed from a Li and Nb ethoxide solution was dependent on substrate, precursors and grain growth at high annealing temperatures.[56] Prehydrolysis of the lithium and niobium ethoxide solution promoted polycrystalline films, whereas nonhydrolysis produced solid state epitaxial growth of $LiNbO_3$ films.[56] Whilst prehydrolysis of the alkoxides causes greater hydrolysis and condensation (leading to greater loss of organics, less "burn-out") and thus lowered the temperature at which grain growth occurred, the nonhydrolysed precursor on sapphire produced a denser film and unexpectedly large single phase domains.[56]

$LiTaO_3$ powders produced by the sol-gel synthesis of Li and Ta alkoxides enabled the elaboration of ceramics at temperatures below 1150°C.[57] These ceramics showed a higher shrinkage coefficient and lower sintering temperatures than similar ceramics produced by solid state reactions. The thermal dependence of the permittivity and Curie temperature was correlated with the microstructure of the ceramic and the quantity of water used to hydrolyse

the sample.[57] Use of lithium acetate, instead of alkoxide, gave upon hydrolysis gels whose gelation time decreased with the increase in either acid or base concentrations or higher water concentrations.[58] These amorphous gels became crystalline after firing in air at 450°C for 2 hours.

Perovskite phase PMN powders have been prepared at sinter temperatures of ~700°C. The perovskite phase developed at a faster rate in gels prepared with higher water content.[59] Approximately 95% perovskite phase developed after 1 hour at 700°C or 5 minutes at 775°C. Films of PMN were formed on Pt coated Si and the perovskite phase formed by fast firing the films at 800°C. The dielectric constant for these films was 1000-1250 at room temperature [59]

1.2.3 Other Sol-Gel Processed Transition Metal Oxides

Zirconia

Zirconia (ZrO_2) is an important structural and high temperature material, whose fibres are used for thermal insulators, catalyst conductors and reinforcements for metals, plastics and ceramics.[60] It is also a high performance ceramic with possible uses as the solid electrolyte in third generation fuel cells and as a substrate for the oxide superconductors.[60] Simple alkoxides and chloroalkoxides of butanol,[60] propanol,[61-64] and ethanol[65] are the usual precursor compounds for the sol-gel synthesis of zirconia. The hydrolysis and condensation steps occurring have been studied in some detail. Raman spectroscopy shows that hydrolysis occurs immediately water is added.[61] A mechanism for the growth of the gel backbone has been proposed which describes the aggregation of the primary clusters formed in the sol upon addition of water.[61] The gel thus formed is amorphous Zr hydroxoxide. The particle size of ZrO_2 powders produced via hydrolysis of Zr alkoxides increases as the ageing temperature, or the water/ alkoxide ratio or the size of the alkyl groups on the solvent increase.[66] Xerogels are formed when the water/alkoxide ratio is less than 4 and the pH of the hydrolysis water is 2.[66]

Amorphous thin films (<0.1μm) of zirconia can be formed upon sintering dip-coated layers of zirconium alkoxide or chloroalkoxide at ≤450°C.[63,65] Upon sintering at ≥500°C, these films form orientated tetragonal ZrO_2 monocrystals.[65] Fibres of zirconia with diameters of 5-10μm and 3-30μm were drawn from $H_2O_2/HNO_3/Zr(OBu)_4$ and $H_2O/Pr^iOH/Zr(O^iPr)_4$

systems respectively.[60,62] The sintered fibres had fine microstructure and very narrow size distribution. The grain size increased from 0.1μm at ≤1000°C to 1μm at 1500°C.[60]

Mixed metal zirconia fibres and films have also been prepared by the sol-gel method. CaO_2-ZrO_2 and CeO_2-ZrO_2 fibres, sintered at 1000°C, with maximum tensile strengths of 0.8-1.0GPa and 1.0-1.2GPa, respectively, and diameters of 10-15μm, have been prepared from $Zr(O^nPr)_4$, $Ce(NO_3)_3.6H_2O$, $Ca(NO_3)_2.4H_2O$ and $Ca(MeCOO)_2$.[67] Interestingly, the strength of the acetate-derived films decreased at a faster rate, with increasing fibre diameter, than the nitrate-derived fibres. This feature was ascribed to the sudden removal of acetate, at a given and unique temperature, which caused microcracks in the fibres. Addition of small amounts of CuO as a sintering aid greatly improves the mechanical properties of the fibres, with tensile strengths of 1.8-2.0GPa achieved. Y_2O_3-ZrO_2 crystalline films have been obtained upon sintering at >500°C. The crystal phases of ZrO_2 within these films is dependent upon the percentage composition of ZrO_2 and the sintering temperature.[68]

Titania

The photoelectrochemistry of TiO_2 is of great interest as both the rutile and anatase phases can act as catalysts for the photochemical cleavage of water.[69] The anatase phase is a stronger catalyst and greater absorber of O_2 and H_2O than the rutile phase due to its defective crystal structure.[69] As anatase is a thermodynamically metastable phase, single crystals and sintered bodies of anatase cannot be obtained by conventional methods. Sol-gel processing of TiO_2 offers a method of obtaining this metastable phase, due to its lower sinter temperatures.[69]

Films of TiO_2 have been prepared from the hydrolysis of $Ti(O^iPr)_4$,[69,70] and $Ti(OA)_4$,[71] where OA = OEt,OBu^n or poly(n-Bu methacrylate). Below 500°C the films remain amorphous; however, between 500-800°C the anatase phase is formed, and above 800°C the rutile phase forms.[69-71] A maximum photocurrent is observed after the gel is heated at 900°C. The increase in photocurrent with increasing heating is due to an initial increase in the concentration of Ti^{3+} caused by the reduction of Ti^{4+} by undecomposed organic residue. Further heating, however, causes a decrease in the specific surface area and Ti^{3+} concentration due to the reoxidation of Ti^{3+} to Ti^{4+}, resulting in a lower photocurrent.[69] Monodispersed TiO_2 particles can be formed by the hydrolysis of $Ti(OA)_4$ where OA=OEt or O^iPr.[72,73] They

have diameters of ~0.7μm and transform from the amorphous state to anatase at ~400°C and the rutile phase at ~900°C.

A number of mixed metal titania systems have been prepared by the sol-gel process using metal alkoxide precursors, including CeO_2-TiO_2,[74] $LiTi_2(PO_4)_2$,[75] and SiO_2-ZrO_2-TiO_2-Al_2O_3.[76 77]

Vanadates

V_2O_5 gels have been prepared from vanadium oxo-alkoxides[78,79] and alkoxides.[80] The red "jammy" gels derived from hydrolysis of $VO(OAm^t)_3$ with a large excess of water exhibit electronic and ionic behaviour comparable to V_2O_5 prepared using inorganic precursors, whereas stoichiometric hydrolysis of $VO(OPr^n)_3$ gives gels which are orange monoliths and have a highly branched polymeric molecular structure.[78] Amorphous V_2O_5 particles have been prepared, due to inhibited or incomplete hydrolysis of $VO(OBu^n)_3$.[79] If the condensation reactions are inhibited then green precipitates are formed from aggregates of particles with small molecular weights. These have short structural units with terminal hydroxide groups. If the hydrolysis is incomplete, red precipitates are formed with terminal alkoxide groups in their structural units.[79] Coatings of V_2O_5/GeO_2 (70:30) were prepared from $VO(OCHMe_2)_3$ and $Ge(OEt)_4$.[81] The films, dried under vacuum at 500°C, showed apparent reversible transmission hysteresis with temperature, indicating the possibility of their use as erasable optical storage media.[81]

Vanadium dioxide (VO_2) undergoes a reversible, thermally induced semiconductor to metal phase transition at 68°C, and exhibits large changes in its optical, electrical and magnetic properties around this transition. This behaviour has prompted considerable interest in VO_2.[82] Thin films of VO_2 were prepared from $V(O^tBu)_4$ in Pr^iOH. After annealing at 600°C, they underwent a reversible semiconductor to metal phase transition at 72°C, exhibiting resistive and spectral switching comparable with VO_2 films produced by other techniques.[82] If they are doped with hexavalent transition metal oxides, the transition temperature drops.

Tungsten, Molybdenum and Tin Oxides

WO_3 gels have been prepared from $W(OEt)_6$ and $[WOCl_{4-x}(O^iPr)_x]_n$ precursors.[83,84] Hydrolysis gives a tungsten oxide colloid sol, which can be dip coated to give amorphous thin

films. These films have electrochromic properties (see section 1.3). Left at room temperature in humid air they form crystalline $WO_3.H_2O$. Upon sintering at 410°C the amorphous films form crystalline WO_3.[83,84]

$MoOCl_{4-x}(O^nPr)_x$ reportedly hydrolyses to form xerogels of $(MoO_2Cl_2)_2$.[85,86] Sintering of the xerogel at 600°C transformed the oxide into MoO_3 and upon further heating at 900°C produced Mo_8O_{23}. These latter two oxides were characterised by IR spectroscopy.

A couple of studies have been reported on the mechanisms and products of Sn(IV) alkoxide hydrolysis and condensation. $Sn(O^tBu)_4$ was studied in solution as a model system, in order to establish whether it is possible to distinguish between different Sn-alkoxide ligand bonding modes i.e. terminal vs doubly bridging vs triply bridging.[87] The sol-gel condensation of $Sn(OEt)_4$ has also been examined.[88] Under basic conditions it produced spherical 2-3nm size Sn(IV) oxide (cassiterite) particles. Hydrolysis of $ZnSn(OEt)_6$ under identical conditions produced spherical or octahedral crystalline particles of $ZnSn(OH)_6$ depending upon the solvent used.[88] Sintering of $ZnSn(OH)_6$ resulted in the formation of $ZnSnO_3$ at ~676°C. Hydrolysis of $ZnSn(OEt)_6$ at neutral pH resulted in the formation of a high surface area powder ($261 m^2g^{-1}$).

Thus research in the sol-gel processing of advanced ceramics is both extensive and vigourous since it offers a low temperature route to high purity ceramics and has the added advantage of offering a high degree of control and manipulation of the physical forms of the product ceramic.

1.3 Electrochromism

Electrochromism is defined as a persistent but reversible optical change produced electrochemically. That is to say, a material which can be reversibly coloured by the application of an electric field or the passage of current and ions through it, is called an electrochromic material. A major requirement of an electrochromic material is that it exhibits mixed conduction, ie. both electronic and ionic conductivity. Typically a metal redox centre is generated by injecting electrons, and for charge neutrality to be preserved cations must be allowed into the material. Since it is usually the movement of ions which is rate-limiting,

materials with fast ion conduction at room temperature are desired (usually with H^+, Li^+ or Na^+ ions). Often such materials are amorphous and of low density so as to provide an open framework for rapid ionic diffusion. Amorphous materials also have the advantages of flexibility of composition, high concentrations of vacancies for ionic motion and generally are more easily prepared as thin coatings necessary for display devices. A common feature of an electrochromic material is that, unlike liquid crystal displays, once the material is coloured the applied voltage can be switched off and the colour is retained, making the device more energy efficient. Thus, industrial research is intensely active in this area because of the potential applications in energy efficient display devices.

Research in this area came out of work done in the 60's on photochromism, which at the time was hoped to produce a technique for high density information recording.[89] A number of transition metal oxides were examined (WO_3, MoO_3, TiO_2, V_2O_5) but when films of these oxides were irradiated with UV light, the colour change observed was irreversible. However, Deb realised[90,91] that amorphous films of these metal oxides and specifically films of WO_3 could be reversibly coloured and bleached by the application of an electric field across the WO_3 with the injection of H^+ and e^- ions, rather than by UV light. This led to intensive investigation of electrochromic materials, such as WO_3,[92] WO_3/MoO_3,[93,94] Prussian Blue[95] and organic molecules such as alkyl viologens.[96] Although a wide variety of compounds exhibit electrochromism, most work in this area has been directed at metal oxides with much attention given to WO_3.[97,98] The reason that metal oxides and inparticular, WO_3, are so popular is that they satisfy two basic requirements of good electrochromic performance, ie, that they are fast-ion conductors, thus allowing for relatively fast insertion of ionic charge, and that they have highly absorbing colour centres, thus giving a large visible change in colour upon ion insertion.[93]

Tungsten (VI) oxide is known as an ion insertion material,[99] that is to say, amorphous WO_3 is a mixed conductor (electronic and ionic) in which ions can be rapidly and reversibly inserted. A typical electrochromic cell is shown in Fig. 1.3. The WO_3 film (on an electrode surface, commonly indium-doped tin oxide (ITO) glass) is placed in contact with a medium (liquid, gel or solid) which can supply ions (M^+). For ease of transport, small singly charged

Fig. 1.3

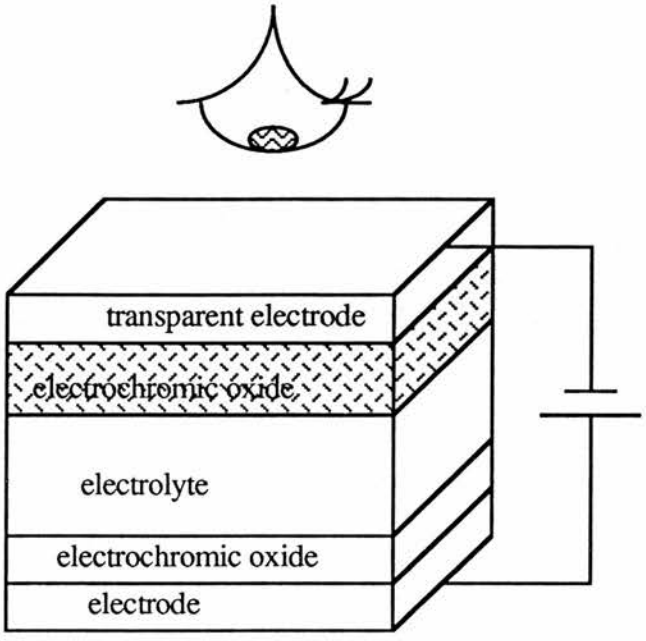

ions such as H^+, Li^+ and Na^+ are commonly used. A cathodic voltage is applied across the WO_3 of sufficient strength to enable two migratory process to occur: (i) electrons are drawn into the WO_3 from the electrode/WO_3 interface, and (ii) M^+ diffuses into the WO_3 from the WO_3/electrolyte interface. This voltage is known as the "colouring voltage". The injection of electrons and ions into the WO_3 forms a "tungsten bronze" of formula M_xWO_3 causing the blue colour seen in the bronze (see eq. 1.1):

$$xM^+ + xe^- + WO_3 \rightleftharpoons M_xWO_3 \qquad (1.1)$$

yellow blue W-bronze

M^+ can be H^+, Li^+, Na^+, and so on.

When an anodic voltage (bleaching voltage) is applied, the reverse reaction occurs with the M^+ ions moving out of the M_xWO_3 and bleaching the WO_3 back to its normal pale yellow colour. A second electrochromic oxide layer is often applied to the counter electrode, so that the redox efficiency of the counter electrode matches that of the working electrode, thus assuring long term stability. In cathodic colouration working electrode cells, an anodically coloured counter electrode film can also be used.

Many different morphologies of WO_3 have been used, from amorphous thermally evaporated to polycrystalline radio-frequency sputtered films in contact with a wide variety of electrolytes. However, the creation of stable practical devices has been hindered by the

problems of film dissolution in the electrolyte. The use of aqueous sulphuric acid solutions as electrolytes causes the slow dissolution of WO_3 into the acid at up to 2.5 nm/day.[91,92,100,101] The use of nonaqueous solvents containing electrolytes such as $LiClO_4$ also causes dissolution of the WO_3 as well as slow response times and irreversible colouring.[92,102-104] Finally the use of gel/solid electrolytes, such as Na-β-alumina gives slow response times.[98,105]

Much research has been devoted to solving these problems and not surprisingly interest has turned to electrochromic metal oxides other than WO_3 which might not dissolve so readily in liquid electrolytes. In 1980, Reichman and Bard reported the electrochromic behaviour of Nb_2O_5 in both aqueous sulphuric acid (1mol dm^{-3}) and acetonitrile/$LiClO_4$ (0.8mol dm^{-3}) solutions.[106] The Nb_2O_5 did not appear to dissolve in either sets of solutions and exhibited a fairly reasonable response time (ie the time required to complete a colouration or bleach cycle) of 1-2 secs. This stability and response time also makes Nb_2O_5 ideal for use as a counter electrode coating. The Nb_2O_5 was prepared by heating a rod of pure niobium in air at 500°C for 10 minutes and then scrapping off patches for electrical contact. Similarly, thin Nb_2O_5 films have been prepared by anodic[107-109] oxidation of the metal, and by oxidation of sputtered NbN_x.[110] Unfortunately, although they can be used in reflectance mode, the metal oxidation routes preclude the use of the electrochromic films in most display devices where the metal oxide is sandwiched between optically transparent electrodes. Finally, it is also possible to sputter Nb_2O_5 thin films.[111] However, we decided that the sol-gel processing of niobium (V) oxide offered a potentially cheap, flexible and effective method for producing such displays and for modification of the films formed by the production of multicomponent mixed metal/silicone composites.

1.4 Sol-gel Processing of Nb_2O_5

Nb_2O_5 has a high melting point (1500°C)[112] and is resistant to all acids and alkalis except HF and molten alkalis.[113] These properties make it an excellent corrosion inhibitor if applied as a film coating to devices, and also enhance its potential use as an electrochromic material in large area displays. Furthermore, it is a good catalyst for selective dehydrogenation of propane (450-620°C),[114] and the ammoxidation of ethane to acetonitrile.[115]

Current methods of producing Nb_2O_5 films are inadequate for the production of either electrochromic display devices or corrosion resistant films. Sol-gel processing of Nb_2O_5 films offers a solution to these problems. It has the advantages of control of porosity and structure, convenience and the ability to coat large objects with adherent films.[116,117] Furthermore, the method has already been successfully employed in the synthesis of V_2O_5, TiO_2[118] and WO_3[119] electrochromic devices.

However, the sol-gel process can only be used to make crack-free films of thickness $\leq$0.5 μm. Typical electrochromic efficiencies are 10 mC cm^{-2} for V_2O_5, corresponding to an optical density of ca 0.5 in a film of thickness 0.5μm.[118] Thus for greater display densities a method for producing thick (5 μm), crack-free electrochromic films with fast response times would also be desirable. This is acheived by the application of a mixed niobium oxide/silicone coating to thick (5 μm) films of Nb_2O_5. The silicone coating dries to give a flexible, microporous solid which "supports" the original Nb_2O_5 film and slows crack propagation.

1.4.1 Niobium chloroalkoxides and Thesis Summary

For the sol-gel synthesis of niobium (V) oxide and niobium (V) oxide composites a number of possible routes present themselves, the two classical ways being the destabilisation of a niobium sol and the hydrolysis of a niobium alkoxide. Alquier et al[120] conducted a study of these routes and drew the following conclusions:

i) Nb_2O_5 aqueous sols could be created by the action of deionised water upon $NbCl_5$ to give a white gel of hydrated niobium oxide. This gel could then be redissolved in acidic water (pH<2) over a period of 24 hours to give the niobium sol. The sol thus obtained was found to be extremely sensitive to electrolytes and pH changes, flocculating immediately, whilst use of temperature to destabilise the sol required long ageing times (48 hours+). The relatively long times required for this synthesis and its lack of reproducibility precluded its use as a route to reproducible niobium (V) oxide gels. Furthermore, although hydrolysing the $NbCl_5$ in hydrogen peroxide gave reproducible sols and gels, the procedure was lengthy.

ii) Niobium alkoxides dissolved in dry alcohol can be hydrolysed to give niobium (V) oxide. Whilst quick and simple, the alkoxides are expensive and thus a cheaper route would be preferred.

iii) Dissolution of niobium (V) chloride in alcohol gives a solution of niobium chloroalkoxides which, upon addition of water, hydrolyse to give niobium (V) oxide. Not only is this method quick, simple and reproducible, but niobium (V) chloride is about 10 times cheaper than niobium (V) ethoxide (the only commercially available niobium alkoxide). These advantages make it a very attractive route for the sol-gel synthesis of Nb_2O_5.

In chapter 2, ^{93}Nb NMR and ^{1}H NMR is described as a means of identifying the substitution products, $(NbCl_{5-x}(OMe)_x)_2$ formed by the stepwise substitution of $NbCl_5$ by MeOH in non-coordinating solvents. These techniques reveal evidence for all of the possible substitution products, $NbCl_{5-x}(OMe)_x$, whilst phase equilibria favours the formation of $(NbCl_4(OMe))_2$ and $(NbCl_2(OMe)_3)_2$ dimer species over $(NbCl_3(OMe)_2)_2$ in mixed MeOH/aromatic solvents. In coordinating solvents such as acetonitrile ^{93}Nb NMR is able to distinguish between the uncoordinated dimeric $(NbCl_{5-x}(OMe)_x)_2$ species and the monomeric adduct species $NbCl_{5-x}(OMe)_x.AN$. Thus ^{93}Nb NMR monitoring of $NbCl_5$ solvolysis in ROH (R=Me, Et, ^{i}Pr) is able to identify the $(NbCl_{5-x}(OR)_x)_2$ species present and reveals that the solution composition is both concentration and temperature dependent. This refutes earlier beliefs that the reaction of $NbCl_5$ with ROH proceeds:

$$NbCl_5 + xROX \longrightarrow NbCl_{5-x}(OR)_x + xHCl \qquad (1.2)$$

where x=2 or 3,[121] or x=3 when an excess of ROH is added.[120,122]

Chapter 3 is concerned with the investigation of the sol-gel processing properties (eg. hydrolysis and gelation rates) of various $(NbCl_{5-x}(OR)_x)_2$ solutions in their parent alcohol. This includes studies of the effects of manipulation (concentration, acid catalysis, alcohol type and $Nb:H_2O$ ratio) upon the hydrolysis and gelation rates of these solutions, as well as detailed analysis of the gelation products which prove hydrated Nb_2O_5 is formed, rather than $NbCl_2(OH)_3$, as proposed by Alquier et al.[120] A discussion of the possible mechanisms of the observed gelation rates is also undertaken.

Chemical additive methods for forming thick uncracked films of Nb_2O_5 are investigated in chapter 4 and include the use of surfactants, drying control chemical additives and "plasticizers". The use of spin coating techniques allows the successful production of thin (<0.1μm) and thick (5μm) films of hydrated Nb_2O_5 via sol-gel processing of $(NbCl_{5-x}(OR)_x)_2$ solutions, whilst the application of a second mixed NbO/silicone coating to the thick Nb_2O_5 films produces more durable thick (5μm) Nb_2O_5/silicone composite films.

In chapter 5, by the use of chronoamperometric, chronoabsorptiometric and a.c. impedance spectroscopy techniques the electrochromic efficiency, kinetics and lifetimes of the films prepared in Chapter 4 are measured, compared and discussed. Although the lifetimes of the thick films are found to be limited, the diffusion coefficients of these films are comparable to those of previously reported sputtered Nb_2O_5 films. However, the thin films are shown to have a dense durable glass structure that inhibits diffusion and acts in a similar manner to conducting polymer films.

Chapter 6 investigates the electrochemistry, studied by cyclic voltammetry, of a number of Nb(V) precursor species (eg $NbCl_5$, $(Nb(OEt)_5)_2$) in organic and aqueous solvents prior to the attempted electrodeposition (in chapter 7) of films of Nb_2O_5, from these solutions, by modified sol-gel techniques.

Chapter 8 covers two sets of novel chemistry of Nb(V) compounds discovered during the course of our research, not covered elsewhere in the thesis. These are the reaction with ferrocene of $CsNbCl_6$ and $NbCl_5$.AN to form Cs_2NbCl_6 and $Cp_2FeNbCl_6$ (Cp_2Fe^+ is the ferricenium ion) respectively and the unexpected hydrolysis of solvent acetonitrile to NH_4Cl in solutions containing $NbCl_5$ and ROH. Samples of $Cp_2FeNbCl_6$ have been investigated by ESR spectroscopy and show the ferricenium spectra at 293K. Multinuclear NMR of the NH_4Cl forming solutions reveals that the hydrolysis route is via a Pinner synthesis mechanism.

Finally, in chapter 9, details of instrumental, preparative and electrochemical methods used in the course of this research are given.

References

1. D. Segal, " Chemical Synthesis of Advanced Ceramic Materials", Cambridge Uni. Press, 1989.
2. (a) G.W. Meetham, *Chem. and Ind.*, 1986, 636.
   (b) J.C. Anderson, K.D. Leaver, R.D. Rawlings, J.M. Alexander,"Materials Science", Chapman and Hall, London, 1990, p518-542.
   (c) R.M. Rose, L. A. Shepard, J. Wulff, "The Structure and Properties of Materials", Vol. 4, Wiley, London, 1967, p251-267.
3. Lord Raleigh, *Philos. Mag.*, 1919, **38**, 738.
4. H.B. Weiser, W.D. Milligan, "Advances in Colloid Science", Ed. E. Kraemar, Interscience, New York, 1942, vol. 1, p227-246.
5. R.S. Ewell, H. Insley, *J. Res. Natl. Bur. Stand.*,1935, **15**, 173.
6. R.K. Iler, " The Colloid Chemistry of Silica and Silicates", Cornell Univ. Press, Ithaca, 1955.
7. O.C. Dean, C.C. Haws, A.T. Kleinstreuber, J.W. Snider, "Proceedings of the Thorium Fuel Cycle Sym.", Gaithersburg, 5-7 Dec. 1962, TID 7650, bk. II, p519-42.
8. D.E. Ferguson, O.C. Dean, D.A. Douglas, "3rd UN Int. Conf. on Peaceful Uses of Atomic Energy.",1964, A/CONF 28/P/237.
9. M.E.A. Hermans, "Sol-gel Processes for Ceramic Nuclear Fuels", IAEA, Vienna, 1968, p 21-32.
10. G. Brambilla, P. Gerontopoulos, *D. Neri, Energia Nucleare*, 1970, **17**, 217.
11. D.M. Roy, R. Roy, *Am. Mineral*, 1954, **39**, 957.
12. R. Roy, *J. Am. Ceram. Soc.*, 1956, **39**, 145.
13. R. Roy, *J. Am. Ceram. Soc.*, 1969, **52**, 344.
14. G.J. McCarthy, R. Roy, J.M. McKay, *J. Am. Ceram. Soc.*, 1971, **54**, 637.
15. D.M. Roy, R. Roy, *Am. Mineral*, 1955, **40**, 147.
16. R.C. DeVries, R. Roy, *J. Am. Ceram. Soc.*, 1955, **38**, 142 and ibid 155.
17. R. Roy, *Science*, 1987, **238**, 1664.
18. E.M. Zaiser, V.K. La Mer, *J. Colloid Sci.*, 1948, **3**, 571.

19. V.K. La Mer, R.H. Dinegar, *J. Am. Chem. Soc.*, 1950, **72**, 4847.

20. W. Stober, A. Fink, E Bohn, *J. Colloid Interface Sci.*, 1968, **26**, 62.

21. J. Livage, M. Henry, C. Sanchez, *Progress in Sol. State Chem.*,1988, **18**, 259.

22. D.S. Kenzer, M.R. Teepe, G.A. Moore, G. Kordas, "Better Ceramics Through Chemistry 4", Materials Research Society, Pittsburgh, 1990, p947-52.

23. G. Kordas, G.A. Moore, J.D. Jorgensen, F. Rotella, R.L Hitterman, K.J. Volin, J. Faber, *J. Mater. Chem.*, 1991, **1**, 175.

24. G. Moore, S. Kramer, G. Kordas, *Mater. Lett.*, 1989, **7**, 415.

25. T. Monde, H. Kozuka, S. Sakka, *Chem. Lett.*, 1988, **2**, 287.

26. M. Saito, Jpn. Kokai Tokkyo Koho JP 01122960 A2 16 May 1989 Heisei, 4 pp.

27. S. Kramer, K. Wu, G. Kordas, *J. Electron. Mater.*, 1988, **17**, 135.

28. G. Kordas, G.A. Moore, M.B. Salamon, J.B. Hayter, *J. Mater. Chem.*, 1991, **1**, 181.

29. S.A. Kramer, G. Kordas, J. McMillan, G.C. Hilton, D.J. Van Harligen, *Appl. Phys. Lett.*, 1988, **53**, 156.

30. Y. Masuda, K. Matubara, T. Tateishi, R. Ogawa, Y. Kawate, *Funtai oyobi Funmatsu Yakin*, 1990, **37**, 772.

31. M. Muroya, Y. Takemoto, T Hatayama, K. Yamamoto, T. Yoshida, E. Tada, "Prog. High Temp. Supercond.", 15 (Int. Symp. New Dev. Appl. Supercond., 1988) 1989, 267-72.

32. R. Sanjines, K.R Thampi, J. Kiwi, *J. Am. Ceram. Soc.*, 1988, **71**, C512.

33. M. Kakihana, L. Boerjesson, S. Eriksson, P. Svedlindh, *J. Appl. Phys.*, 1991, **69**, 867.

34. H. Murakami, S. Yaegashi, J. Nishino, Y. Shiohara, S. Tanaka, *Jpn. J. Appl. Phys.*, Part 1, 1990, **29**, 2715.

35. S. Katayama, M. Sekine, *J. Mater. Res.*, 1991, **6**, 1629.

36. S. Katayama, M. Sekine, *Nippon Seramikkusu Kyokai Gakujutsu Ronbunshi*, 1991, **99**, 345.

37. F.H. Chen, H.S. Koo, T.Y. Tseng, *J. Mater. Sci.*, 1990, **25**, 3338.

38. G. Kordas, M.R. Teepe, *Appl. Phys. Lett.*, 1990, **57**, 1461.

39. L. M. Sheppard, *Ceram. Bull.*, 1992, **17**, 85.

40. Y. Ozaki, Y. Shinohara, Jpn. Kokai Tokkyo Koho JP 62265118 A2 18 Nov 1987 Showa, 3.

41. G. Limmer, H. Buerke, R. Kohl, G. Tomandl, *Sprechsaal*, 1988, **121**, 1099.

42. H.C. Lu, L.E. Burkhart, G.L. Schrader, *J. Am. Ceram. Soc.*, 1991, **74**, 968.

43. A. Ooga, A. Itani, T. Myazaki, Jpn. Kokai Tokkyo Koho JP 01111724 A2 28 Apr 1989 Heisei, 4pp.

44. P.P. Pradeep, S.H. Risbud, "Better Ceramics Through Chemistry 3", Materials Research Society, Pittsburgh, 1988, 275.

45. J.F. Campion, D.A. Payne, H.K. Chae, J.K. Maurin, S.R. Wilson, *Inorg. Chem.*, 1991, **30**, 3244.

46. F. Chaput, J.P. Boillot, *Sci. Ceram.*, 1988, **24**, 133.

47. B.M. Melnick, J.D. Cuchiaro, L.D. McMillan, C.A. Paz de Araujo, J.F. Scott, *Ferroelectrics*, 1990, **112**, 329.

48. T. Sato, K. Ayusawa, T. Arai, Jpn. Kokai Tokkyo Koho JP 02281769 A2 19 Nov 1990 Heisei , 3pp.

49. P. Groves, N.I. Steward, R.R. Landham, S.J. Teat, T.E Warrender, PCT Int Appl. WO 9012755 A1 1 nov 1990, 21p.

50. F. Imoto, S Hashimoto, Y. Ogawa, *Shizuoka Daigaka Kogakubu Kenkyu Hokoko*, 1988, **39**, 9.

51. T. Ogihara, H. Kaneko, N. Mizutani, M. Kato, *J. Mater. Sci. Lett.*, 1988, **7**, 867.

52. S.D. Ramamurthi, D.A. Payne, *J. Am. Ceram. Soc.*, 1990, **73**, 2547.

53. R.W. Schwartz, D.A. Payne, A.J. Holland, "Ceramic Powder Processing Science, Proc. Int. Conf., 2nd", Meeting Date 1988, Eds H. Hausner, G.L. Messing, S. Hirano. Dtsch. Keram. Ges., Cologne, 1989, p165-72.

54. S. Sun, Y. Li, W. Rei, Q. Zhou, X. Wu, L. Zhang, X. Yao, *Ferroelectrics*, 1990, **108**, 9.

55. D.S. Hagberg, D.J. Eichorst, D.A. Payne, *Proc. SPIE-Int Soc. Opt. Eng.* 1990, **1328**, 466.

56. K. Nashimoto, M.J. Cima, W.E. Rhine, *Mater. Res. Soc. Symp. Proc.* 1991, **202**, 439.

57. J.Ravez, N. Puyoo-Castaings, F. Duboudin, *Ferroelectrics*, 1988, **81**, 313.

58. J.H. Jean, *J. Mater. Sci.* 1990, **25**, 859.

59. L.F. Francis, Y.J. Oh, D.A. Payne,*J. Mater. Sci.*, 1990, **25**, 5007.

60. C. Sakurai, T. Fukui, M. Okuyama, *Am. Ceram. Soc. Bull.*, 1991, **70**, 673.

61. A. Ayral, T. Assih, M. Abenoza, J. Phalippou, A. Lecomte, A. Dauger, *J. Mater. Sci.*, 1990, **25**, 1268.

62. G. De, A. Chatterjee, D. Ganguli, *J. Mater. Sci. Lett.*, 1990, **9**, 845.

63. D. Kundu, P.K. Biswas, D. Ganguli, *Thin Solid Films*, 1988, **163**, 273.

64. V.V. Nazarov, N.E. Sizov, S.Y. Dou, Y.G. Frolov, *Zh. Prikl. Khim.*,1991, **64**, 201.

65. L. Yang, J. Cheng, *J. Non-Cryst. Solids*, 1989, **112**, 442.

66. H. Saito, H. Suzuki, H. Hisoa, *Nippon Kagaku Kaishu*, 1988, **9**, 1571.

67. K. Kamiya, K. Takahashi, T. Maeda, H. Nasu, T. Yoko, *J. Eur. Ceram. Soc.* 1991, **7**, 295.

68. Y. Tanaka, N. Iwamoto, N. Umesaki, *Koon Gakkaishi*, 1991, **17**, 146.

69. T. Yoko, A. Yuasa, K. Kamiya, S. Sakka, *J. Electrochem. Soc.*, 1991, **138**, 2279.

70. Y. Tanaka, *Aichi-ken Kogyo Gijutsu Senta Hokoku*, 1989, **25**, 7.

71. K.A. Mauritz, C.K. Jones, "Proc. Water-Borne Higher -Solids Coat. Symp.", 16th, 1989, 212.

72. Y. Azuma, H. Terada, N. Ohshima, *J. Adv. Sci.*, 1990, **2**, 145.

73. Y.P. Ahn, S.H. Choi, *Yoop Hakhoechi*, 1988, **25**, 677.

74. A. Makishima, M. Asami, K. Wada, *J. Non-Cryst. Solids*, 1990, **121**, 310.

75. Z.N.J. Tohge, T. Minami, *Chem. Express*, 1990, **5**, 973.

76. P. Colomban, L. Mazerolles, *J. Mater. Sci.*, 1991, **26**, 3503.

77. C.J.R. Gonzalez Oliver, *Bol. Soc. Esp. Ceram. Vidrio*, 1990, **29**, 145.

78. C. Sanchez, M. Nabavi, F. Taullelle, "Better Ceramics Through Chemistry 3", Materials Research Society, Pittsburgh, 1988, p93-104.

79. S. Hioki, T. Ohishi, K. Takahashi, T. Nakazawa, *Nippon Seramikkusu Kyokai Gakujutsu Ronbunshi*, 1989, **97**, 628.

80. M. Nabavi, C. Sanchez, J. Livage, *Solid State Inorg. Chem.*, 1991, **28**, 1173.

81. L. Hou, S. Sakka, *J. Non-Cryst. Solids*, 1989, **112**, 424.

82. K.R. Speck, H.S.W. Hu, R.A. Murphy, R.S. Potember, "Better Ceramics Through Chemistry 3", Materials Research Society, Pittsburgh, 1988, p667-72.

83. A. Takase, K. Miyakawa, *Jpn. J. Appl. Phys., Part 2*, 1991, **30**, L1508.

84. P. Judeinstein, J. Livage, J. *Mater. Chem.*, 1991, **1**, 621.

85. J. Mendez-Vivar, T. Lopez, A. Campero, C. Sanchez, *Langmuir*, 1991, **7**, 704.

86. J. Mendez-Vivar, *Inorg. Chim. Acta*, 1991, **179**, 77.

87. M.J. Hampden-Smith, T.A. Wark, L.C. Jones, C.J. Brinker, A.L. Rheingold, *Polym. Prep.*, 1991, **32**, 510.

88. E.A. Gulliver, J.W. Garvey, T.A. Wark, M.J. Hampden-Smith, A. Dayte, *J. Am. Ceram. Soc.*, 1991, **74**, 1091.

89. S.K. Deb, L.J. Forrestal, "Photochromism", Ed G.H. Brown, Wiley Interscience, 1971, p 633.

90. S.K. Deb, *Appl. Optics, Suppl.*, 1969, **3**, 192.

91. S.K.Deb, *Philos. Mag.*, 1973, **27**, 801.

92. B. Reichman, A.J. Bard, *J. Electrochem. Soc.*, 1979, **126**, 583.

93. B. W. Faughnan, R.S. Crandall, P.M. Heyman, *RCA Rev.*, 1975, **36**, 177.

94. V. Wittwer, O.F. Schirmer, P. Schlotter, *Solid State Comm.*, 1978, **25**, 977.

95. K. Itaya, I. Uchida, *Acc. Chem. Res.*, 1986, **19**, 162.

96. R.E. Malpas, A.J. Bard, *Analyt. Chem.*, 1980, **52**, 109.

97. G.Beni, "Electrochromism and Electrochromic Displays Seminar", Lectures given at the Seminar, Uni. of Rome Press, Rome, Nov.1982, p1-38.

98. M. Green,."Electrochromism and Electrochromic Displays Seminar", Lectures given at the Seminar, Uni. of Rome Press, Rome, Nov.1982, p39-62.

99. "Fast Ion Transport in Solids", Eds. P. Vashishta,J.N. Mundy, G.K. Shenoy, N. Holland, 1979.

100. H.N. Hersch, W.E. Kramer, J.H. McGee, *Appl. Phys. Lett.*, 1975, **27**, 646.

101. I.F. Chang, B. L. Gilbert, T. I. Sun, *J. Electrochem. Soc.*, 1975, **122**, 955.

102. J.P. Randin, *J. of Electronic Materials*, 1978, **2**, 42.

103. T.B. Reddy, E.A. Battistelii, "95th Conf. on Electronics Materials", Cornell Uni. Press, Ithaca, June 1977, Abs. G-4.

104. T.J. Knowles, H.N. Hersch, W. Kramer,"95th Conf. on Electronics Materials", Cornell Uni. Press, Ithaca, June 1977, Abs. I-3.

105. P. Judeinstein, J. Livage., A. Zarudiansky, R. Rose, *Solid State Ionics*, 1988, **28-30**, 1722.

106. B. Reichman and A.J. Bard, *J. Electrochem. Soc.*, 1980, **127**, 241.

107. S. Rigo, J. Siejka, *Solid State Commun.*, 1974, **15**, 259.

108. C.K. Dyer and J.S.L. Leach, *J. Electrochem. Soc.*, 1978, **125**, 23.

109. R.M. Toresi and F.C. Nant, *Electrochim. Acta*, 1988, **33**, 1015.

110. R. Cabanet, J. Chaussy, J. Mazuer, G. De la Bouglise, J.C. Jubert, G. Barral and C. Montella, *J. Electrochem. Soc.*, 1990, **137**, 1444.

111. N. Machida, M. Tatsumisaga and T. Minami, *J. Electrochem. Soc.*, 1986, **133**, 1963.

112. F. Fairbrother, " The Chemistry of Niobium and Tantalum.", Elesevier, London, 1967, p27.

113. F.A. Cotton, G. Wilkinson, "Advanced Inorganic Chemistry", Wiley Interscience, London, 1988, p781.

114. R.H.H. Smits, K. Seshan, J.R.H. Ross, *J. Chem. Soc., Chem. Comm.*, 1991, 558.

115. R. Catani, G. Centi, *J. Chem. Soc., Chem. Comm.*, 1991, 1081.

116. C.J. Brinker and G. Scherer, "Sol-gel Science", Academic Press, New York, 1989.

117. J. Livage, *Prog. Solid State Chem.*, 1988, **18**, 259.

118. M. Nabari, S. Doeff, C. Sanchez and J. Livage, *Mater. Sci. Eng.*, 1989, **133**, 203.

119. (a) A. Chemseddine, R. Monneau and J. Livage, *Solid State Ionics*, 1983, **5**, 357; (b) C. Sanchez, J. Livage, M. Henry and F. Babonneau, *J. Non-Cryst. Solids*, 1988, **100**, 65: (c) O. Kamaguchi, D. Tonihisa, H. Kawabata and K. Shimizer, *J. Am. Ceram. Soc.*, 1987, **70**, C94; (d) K. Yamanaka, *J. Appl. Phys.*, 1981, **20**, L307.

120. C. Alquier, M.T. Vandenborne and M. Henry, *J. Non-Cryst. Solids,* 1986, **79**, 383.

121. L.G Hubert-Pfalzgraf, M. Postel and J.G. Riess, " Comprehensive Coordination Chemistry" ed. G.Wilkinson, Pergamon, 1987, Vol.3, p 585-698.

122. C.Sanchez, J. Livage, M. Henry and F. Babonneau, *J. Non-Cryst. Solids,* 1988, **100**, 65.

Chapter 2

NMR Studies of Niobium Chloroalkoxides

2.0 Introduction

Sol-gel processing of metal alkoxides offers a convenient route to single-component and mixed metal oxide ceramics from pure starting materials.[1] This route is also extremely useful in casting thin ceramic films.[2] In work aimed at producing sol-gel derived electrochromic thin films[3] of Nb_2O_5 we became interested in the reactions of $NbCl_5$ with alcohols to give chloroalkoxides which are precursors to Nb containing oxides and ceramics in the sol-gel process. A precise knowledge of these precursors is necessary for full elaboration of the sol-gel processing mechanism, in order to permit rational modification of the final ceramic. In a recent review[4] the reaction of $NbCl_5$ with ROH proceeds to give $NbCl_{5-x}(OR)_x$, where x = 2 or 3:

$$NbCl_5 + xROX \longrightarrow NbCl_{5-x}(OR)_x + xHCl \qquad (2.1)$$

However, other workers have claimed that only one species, $NbCl_2(OR)_3$, was present when excess ROH is added to $NbCl_5$.[5-7a]

We felt that a detailed ^{93}Nb NMR investigation of this system would resolve this problem, in a similar manner to the study of $[NbCl_{6-x}Br_x]^-$ species.[8,9] Although ^{93}Nb is quadrupolar ($I = {}^9/_2$, $Q/10^{-28}m^2 = -0.2$)[9] the broadness of the lines is compensated for by a wide Nb(V) chemical shift range (–1500 to +500 p.p.m.) and good sensitivity (^{93}Nb is in 100% abundance). Nevertheless, the lines are too broad for spin-spin coupling to be observed.

Results and Discussion

2.1 Model Systems

2.1.1 Synthesis of $NbCl_{5-x}(OMe)_x$ Species in Aromatic Solvents

In order to determine the identity of all probable species present in the alcohol solutions, controlled equivalents of MeOH were added to a 0.05 mol dm^{-3} suspension of $(NbCl_5)_2$ in

benzene and the solutions sonicated for 15 minutes. The ^{93}Nb spectrum of $(NbCl_5)_2$ in benzene consists of a single peak at ~2.6 p.p.m., slightly broader at (FWHM = "full width at half maximum" = 20Hz) than the $[NbCl_6]^-$ reference peak (FWHM 7Hz) run under the same conditions. On incremental addition of MeOH, much HCl gas and heat is liberated. The solutions change in colour from red through orange to pale yellow, and the ^{93}Nb spectra, for the various Nb:MeOH ratios are shown in Fig. 2.1(a-e). One would expect to see five peaks, one for each of the $NbCl_{5-x}(OMe)_x$ species (x=1,2,3,4,5), yet only four different peaks are observed during the experiment and in each spectrum one peak is dominant. Assignments are given in Table 2.1.

Fig.2.1 (a) shows that upon addition of 1:1 Nb:MeOH, the $NbCl_5$ species is replaced by a single peak at -495ppm, whilst in the ^1H spectra only a single peak at 3.80ppm and no free methanol peak (3.5ppm) is observed, implying that all the MeOH has coordinated with the $NbCl_5$ to form $NbCl_4(OMe)$. The possibility of Nb=O species being formed can be ruled out, since addition of wet benzene to a suspension of $(NbCl_5)_2$ in benzene gave a sharp signal at -535ppm, and -515ppm in toluene, due to the previously observed $NbOCl_3$ [9] and ruling out an oxygen abstraction reaction by the niobium with the methanol to give $NbOCl_3$. On standing small amounts of the $NbCl_4(OMe)$ species precipitated out. The assignment of the ^{93}Nb peak to $NbCl_4(OMe)$ was confirmed by dissolving an authentic sample in deuterated toluene (see experimental). It gave a single ^{93}Nb peak at -495ppm (FWHM 1200Hz).

Schonherr and Kolditz have shown by use of ebullioscopic measurements that, in benzene, $NbCl_4(OMe)$ exists as the dimer, even down to concentrations of 10^{-3} mol dm^{-3}.[7a] It seems highly probable then that in toluene $NbCl_4(OMe)$ would exist as the dimer $(NbCl_4(OMe))_2$ and low temperature ^1H NMR of $NbCl_4(OMe)$ in deuterated toluene confirms this; 2 peaks are seen in a 1:1 ratio (Table 2.2) due to the axial and equatorial methoxy groups of the dimer. However, the absence of bridging methoxy ^1H resonances is surprising since bridging/ terminal exchange should have been frozen out at this low temperature. We can only conclude that the thermodynamically most stable isomers are those with bridging Cl^- ligands. These axial/equatorial methoxy peaks coalesce at about 293K. V.C. Gibson[7b] has recently obtained the crystal structure for $(NbCl_4(OR))_2$ (R is a Me or Et group) and shown that the

Fig. 2.1

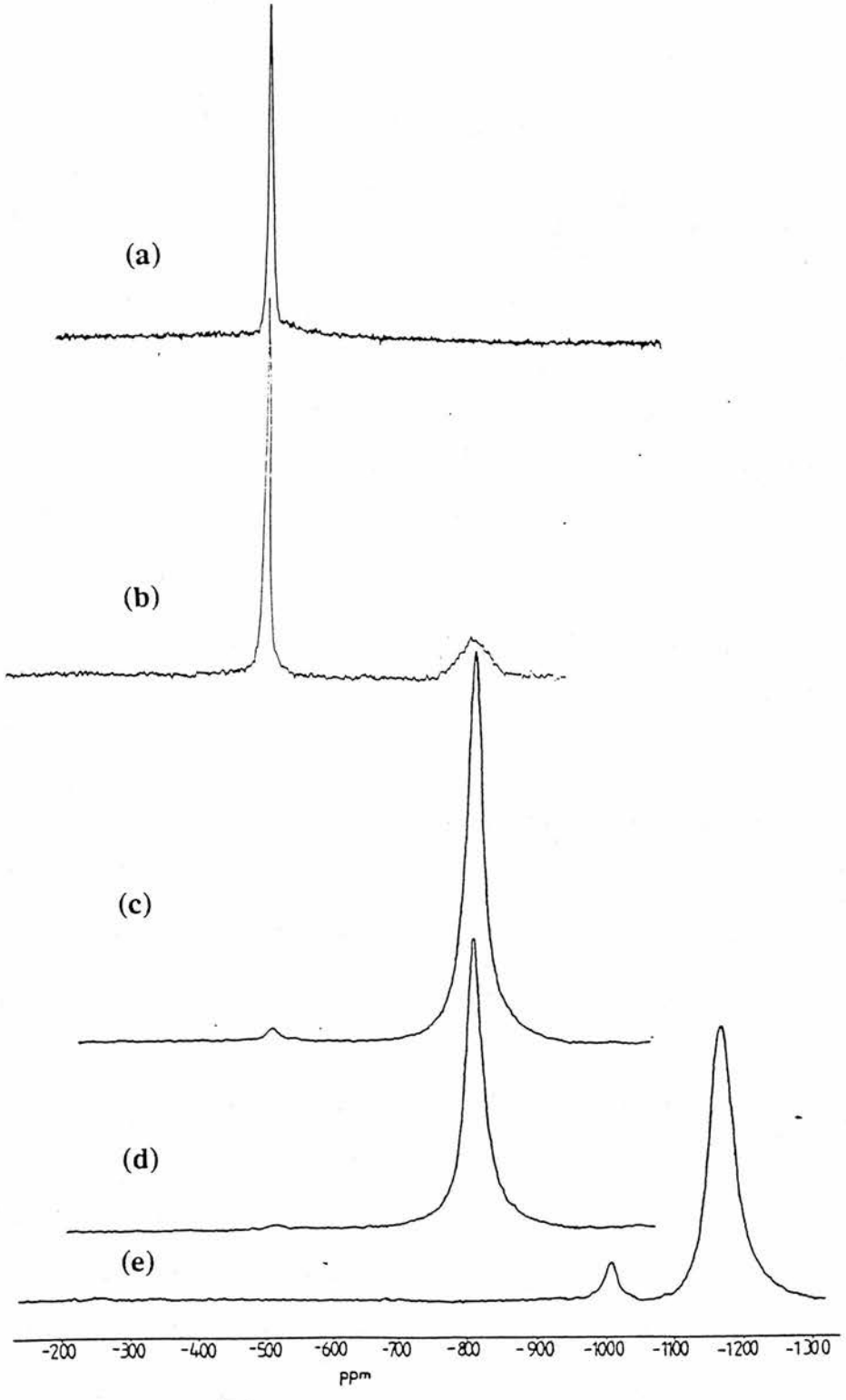

Fig. 2.1. ^{93}Nb NMR spectra (at 293K) of 0.05 mol dm^{-3} $(NbCl_5)_2$ in benzene with the following added molar ratios of MeOH: (a) 1; (b) 2; (c) 3; (d) 5, (e) 5 + NH_3 bubbling to force complete conversion to $Nb(OMe)_5$

Table 2.1

	Assignment of ^{93}Nb NMR Signals (ppm)[a] to $(NbCl_{5-x}(OMe)_x)_2$ Species					
solvent	x=0	x=1	x=2	x=3	x=4	x=5
Benzene	2.6	-497	-650	-810	-1010	-1160
Toluene	2.0	-495		-810	-1005	-1150
Acetonitrile	-0.5/-55	-495/-560		-850		-1160

(a) All signals ± 7ppm

Table 2.2

	^1H NMR Signals Observed For $NbCl_{5-x}(OMe)_x$ Species at Given Temperatures[a] (ppm)					
Deuterated Solvent	Species	200K	220K	233K	255K	310K
Toluene	$(NbCl_4OMe)_2$	3.62 3.12 (1) (1)		3.78 3.15 (1) (1)		3.75 (broad)
Toluene	$NbCl_4OMe.AN$			3.90 2.35 (1) (1)	3.98 2.38 (1) (1)	
Toluene	$(NbCl_2(OMe)_3)_2$					4.10
Toluene	$(Nb(OMe)_5)_2$		4.28 4.24 4.03 (2) (2) (1)		4.26 4.02 (4) (1)	4.25
Acetonitrile	$(Nb(OMe)_5)_2$		4.25 4.15 3.95 (2) (2) (1)			3.95

(a) Figures in parentheses are the relative signal areas.

alkoxide ligand is found only in the terminal positions. Low temperature ^{93}Nb studies on $(NbCl_4(OMe))_2$ in toluene did not reveal two peaks due to the two geometric isomers but gave a single peak that broadened in line width (FWHM) from 1200Hz (-497ppm) at 298K to 25kHz (-516ppm) at 205K. The failure to see the two isomers by ^{93}Nb NMR is not surprising considering the broadness of the peaks and is discussed later.

Schonherr and Kolditz[7a] prepared $NbCl_2(OMe)_3$ by addition of 5 equivalents of MeOH to a suspension of $(NbCl_5)_2$ and observed that the further addition of MeOH did not give $NbCl(OMe)_4$. Fig. 2.1(d) shows that upon reaction of a 5:1 MeOH:Nb mixture in benzene a single peak is observed at -810ppm due to $NbCl_2(OMe)_3$ in the ^{93}Nb spectra. The ^1H spectra of the 5MeOH:Nb in C_6D_6 shows a peak due to free MeOH at 3.5ppm in addition to a second peak at 4.10ppm assigned to $NbCl_2(OMe)_3$ (see Table 2.1). The ratio of the peak areas is 2:3 implying that two molecules of MeOH per Nb have failed to react and that the species $NbCl_2(OMe)_3$ is in fact formed. On standing the $NbCl_2(OMe)_3$ species separated out from the benzene solvent as a dense lower layer. To confirm this assignment, authentic $NbCl_2(OMe)_3$ dissolved in deuterated toluene exhibits a single peak at -810ppm (FWHM 9600Hz) in the ^{93}Nb spectrum, whilst in the ^1H spectrum at low temperatures, a complex pattern is observed. Riess et al[10] observed an identical pattern of peaks, allowing for minor solvent shifts, for the dimer $(NbCl_2(OMe)_3)_2$ in $CDCl_3$. They attributed the peaks to a mixture of isomers and redistribution products. The peaks coalesce near 265K and imply that to some extent the large width of the ^{93}Nb peak (at 293K) is due to the averaging of the isomers by kinetic scrambling of the methoxy groups.

Complete substitution to yield $Nb(OMe)_5$ was enforced by bubbling NH_3 through the solution.[11] In practice if only 5 equivalents of MeOH is added to 1 equivalent of $NbCl_5$, rather than an excess, then the ^{93}Nb spectra displays a small peak at -1010ppm, assigned to the $NbCl(OMe)_4$ species, as well as a major peak at -1160ppm attributable to $Nb(OMe)_5$ (see Fig. 2.1(e)). When an authentic $Nb(OMe)_5$ sample is dissolved in toluene it gives a peak at -1150ppm (FWHM 9600Hz) in the ^{93}Nb spectra and an identical temperature-dependent ^1H spectrum to that observed by other authors[12-15] for the dimer $(Nb(OMe)_5)_2$ (see Table 2.2). At temperatures below 238K, three peaks are seen in the ^1H spectrum, in a 2:2:1 ratio at 4.26,

4.24 and 4.03ppm respectively due to equatorial, axial, and bridging methoxy groups in the dimer. The equatorial and axial peaks coalesce at 238K to give a single peak at 4.26ppm, with a peak area of 4:1 with respect to the bridging peak at 4.02ppm. These two peaks in turn coalesce at 309K to give a single peak at 4.25ppm. These temperatures compare with the two coalescence temperatures found by Riess and Hubert Pfalzgraf[14] of 218K and 278K and Holloway [16] of 228K and ~292K. Holloway further showed that the activation energy for the intramolecular scrambling of the terminal and bridging methoxy groups was about 45 kJ mol^{-1}.

2.1.2 Linewidths of $(NbCl_{5-x}(OMe)_x)_2$ Species

The linewidth at half height ($W_{1/2}$) for mobile molecular fluids containing quadrupolar nuclei ($I>1/2$) is given by:[17]

$$W_{1/2} = (T_q)^{-1} = \frac{3(2I+3)(2\pi e^2qQ)^2(3+a^2)\tau_c}{120I^2(2I-1)h^2} \qquad (2.2)$$

where T_q ($=T_2=T_1$) is the relaxation time, e^2qQ the nuclear quadrupole coupling constant, (eq being the largest component of the electric field gradient at the nucleus with assymmetry parameter, a,) τ_c is an effective correlation time for the molecular tumbling. Therefore, the higher the local electronic symmetry (ie the lower the electric field gradient (efg) with which the nuclear electric quadrupoles couples) the less quadrupole broadening of the peaks occurs. Thus the linewidth can be a useful indicator of the symmetry of the coordination shell of the quadrupolar nuleus.[17] It is interesting to note that as the degree of substitution increases from $(NbCl_5)_2$ to $(NbCl_2(OMe)_3)_2$, the ^{93}Nb peak line widths at half height increase from 20Hz to 9600Hz, yet further substitution does not increase the line width: $(NbCl_2(OMe)_3)_2$ has the same line width as $(Nb(OMe)_5)_2$ This increased line width can be explained by two processes: (a) the fluxionality of the methoxy groups causing a kinetic scrambling of the isomers and hence an averaging of the isomeric peak positions; (b) quadrupolar broadening associated with an increase in the efg due to the lowering of local electronic symmetry about the Nb atoms. This lowering of symmetry has two sources: (i) replacing species X by Y in an octahedral environment dominated by X; (ii) the ability of OMe to bend and take up different conformations with respect to the Nb atom. Thus the increase of line width from $(NbCl_5)_2$ to

$(Nb(OMe)_5)_2$ is to be expected , while the similar line width of $(NbCl_2(OMe)_3)_2$ compared to $(Nb(OMe)_5)_2$ must come about by the fortuitous interaction of these factors. Likewise the increased linewidth of $(NbCl_5)_2$ compared to $[NbCl_6]^-$ reflects the lower pseudo-octahedral symmetry about Nb in the dimer $(NbCl_5)_2$ compared to $[NbCl_6]^-$.

It might also be expected that Nb-Nb coupling should be observed in these dimeric species. However this is not the case, because in $(NbCl_5)_2$ and $(Nb(OMe)_5)_2$ the niobium atoms within each molecule are in identical environments, and in the other $NbCl_{5-x}(OMe)_x$ species the fluxionality of the methoxy groups gives very similar environments for the niobium atoms within a molecule, lowering any potential coupling factor to such a stage that it is swamped by the large line width.

2.1.3 Disproportionation of $(NbCl_3(OMe)_2)_2$

The preceding ^{93}Nb and ^1H NMR data provides good evidence for the assignment of x=1,3,4,5 species (Table 2.1 and 2.2). However, it will be noted that a ^{93}Nb peak due to $(NbCl_3(OMe)_2)_2$ is not observed. When MeOH:Nb=2 (Fig. 2.1(b)), only peaks assigned to $(NbCl_4(OMe))_2$ and $(NbCl_2(OMe)_3)_2$ are observed. Therefore it is proposed that in non-coordinating solvents, such as benzene and toluene, $(NbCl_3(OMe)_2)_2$ rapidly disproportionates to give $(NbCl_4(OMe))_2$ and $(NbCl_2(OMe)_3)_2$.

$$2(NbCl_3(OMe)_2)_2 \rightarrow (NbCl_4(OMe))_2 + (NbCl_2(OMe)_3)_2 \qquad (2.3)$$

The driving forces for this reaction are the lower solubility of $(NbCl_4(OMe))_2$ and the stability of the $(NbCl_2(OMe)_3)_2$. Furthermore, at >2 equivalents MeOH, there is always some unreacted MeOH present, and this separates into a lower MeOH layer largely containing $(NbCl_2(OMe)_3)_2$, in which it is more soluble.

Plotting peak position against degree of substitution gives the graph shown in Fig. 2.2. As can been seen, $(NbCl_3(OMe)_2)_2$ should be expected in the region of -650ppm. It is believed that $(NbCl_3(OMe)_2)_2$ is seen at high concentrations (>0.25 mol dm^{-3}) of $(NbCl_5)_2$ in benzene when 2 equivalents of MeOH are added. As well as the peaks due to $(NbCl_4(OMe))_2$ and $(NbCl_2(OMe)_3)_2$, a small peak (no more than 5% of total peak area) is observed at -650ppm.

Fig. 2.2

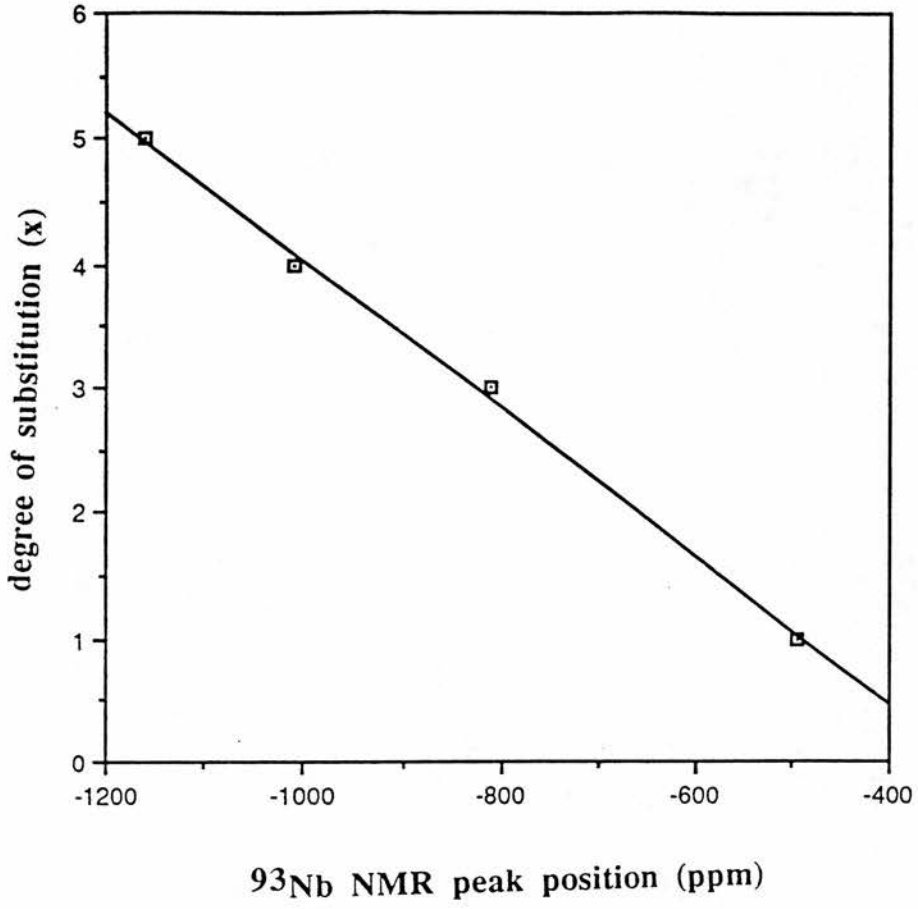

Fig. 2.2. Plot of the degree of substitution (x) vs observed ^{93}Nb NMR peak position (ppm) in the species $NbCl_{5-x}(OMe)_x$, dissolved in aromatic solvent.

2.1.4 Attempted Synthesis of $(NbCl_3(OMe)_2)_2$ from $(NbCl_5)_2$ /$(Nb(OMe)_5)_2$ Mixtures

The ^{93}Nb spectra of redissolved $(NbCl_4(OMe))_2$, $(NbCl_2(OMe)_3)_2$ and $(Nb(OMe)_5)_2$ confirm the assignments given in Table 2.1 of the peaks seen in Fig. 2.1(a-e) but did not answer the question of why $(NbCl_3(OMe)_2)_2$ was not seen. A different approach was tried in an attempt to prepare this species, namely the addition of controlled amounts of $(Nb(OMe)_5)_2$ to the $(NbCl_5)_2$ solution.

A 0.041 mol dm^{-3} solution of $(NbCl_5)_2$ and a 0.050 mol dm^{-3} solution of $(Nb(OMe)_5)_2$ in toluene were mixed together in the following ratios, Cl: OMe, 4:1, 3:2, and 2:3. Gut et al[18] claimed this produced $NbCl_4(OMe)$, $NbCl_3(OMe)_2$, and $NbCl_2(OMe)_3$ respectively. The species in solution appear to undergo instantaneous redistribution on mixing giving the spectra shown in Fig. 2.3(a-c). As would be expected, the 4: 1 Cl:OMe solution (see Fig. 2.3(a)) gives a single peak for $(NbCl_4(OMe))_2$, likewise the 2:3 solution (see Fig. 2.3(c)) gives a single peak for $(NbCl_2(OMe)_3)_2$. However the 3:2 solution (see Fig. 2.3(b)) did not give a single peak at -650ppm but 2 peaks at the positions for $(NbCl_4(OMe))_2$ and $(NbCl_2(OMe)_3)_2$. If it had, as proposed, disproportionated to give these two species then they should occur in equal amounts. Despite the apparent differences in peak height and broadness, integration of the two peaks in Fig. 2.3(b) gives a ratio of 45:55 $(NbCl_4(OMe))_2$: $(NbCl_2(OMe)_3)_2$, implying that $(NbCl_3(OMe)_2)_2$ does indeed disproportionate.

As $(NbCl_3(OMe)_2)_2$ at these concentrations and temperature appears to be unstable, a low temperature study was undertaken. The $(NbCl_5)_2$ solution was frozen in the N.M.R. tube by placing it in liquid N_2 . The $(Nb(OMe)_5)_2$ solution was then poured on top and likewise frozen (Cl:OMe 1:1) . The frozen sample was then placed in the N.M.R. spectrometer and held at 223K. Unfortunately atmospheric moisture froze the tube to the spectrometer, so stationary spectra had to be taken. As the layers thawed, spectra were taken every 100s to try and observe formation of $(NbCl_3(OMe)_2)_2$. Initially at 223K only $(NbCl_5)_2$ was seen, but after 100s some $(NbCl_4(OMe))_2$ appeared. Over the 19 spectra taken the $(NbCl_5)_2$ decreased in size whilst the $(NbCl_4(OMe))_2$ peak increased. At this point the temperature was raised to 253K. In the time it took to raise the temperature some $(NbCl_2(OMe)_3)_2$ had been formed. After a further 29

Fig. 2.3

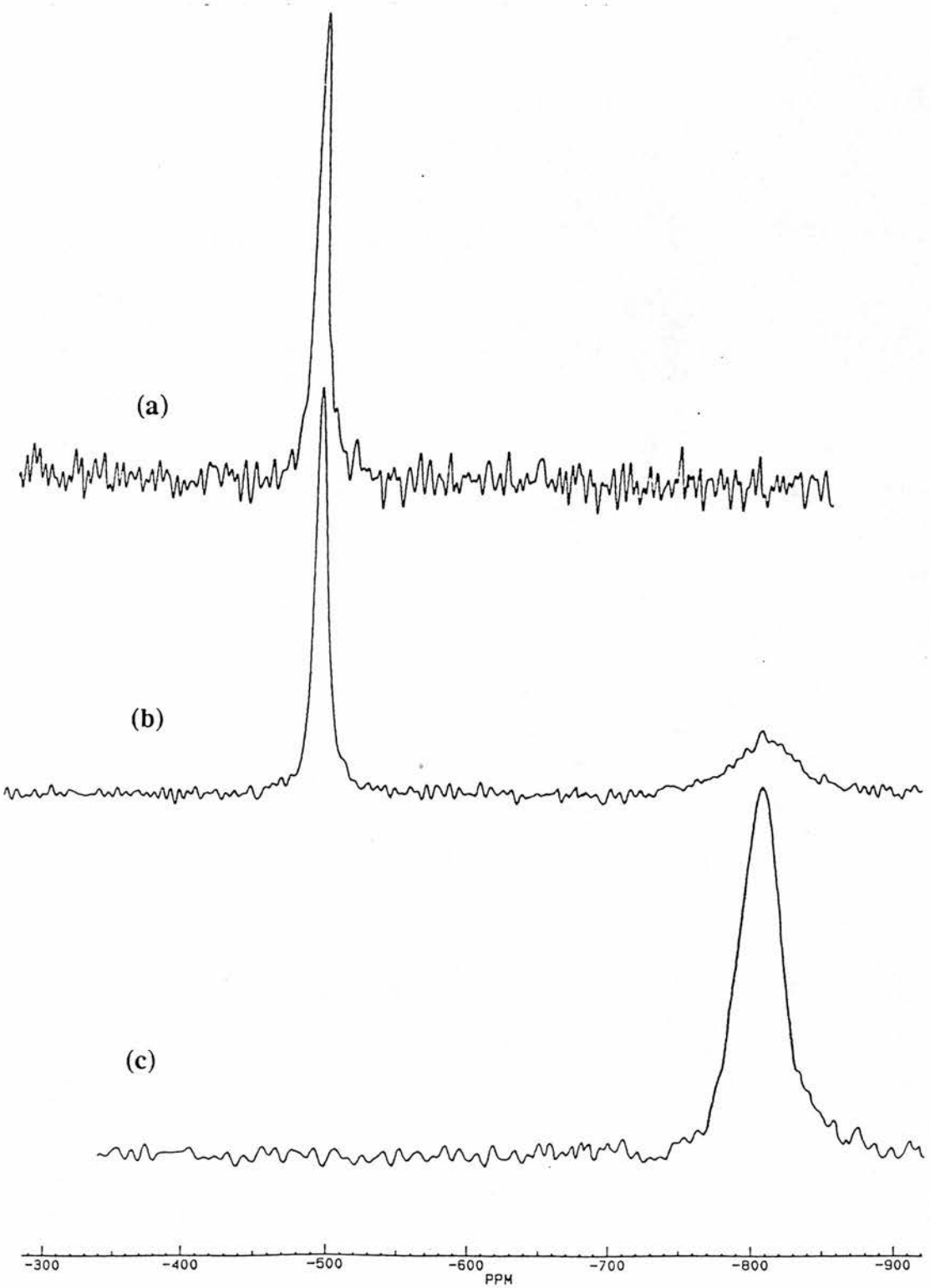

Fig. 2.3. ^{93}Nb NMR spectra of 0.041 mol dm^{-3} $(NbCl_5)_2$ and 0.049 mol dm^{-3} $(Nb(OMe)_5)_2$ in toluene, mixed in the following ratios, Cl:OMe; (a) 4:1,(b) 3:2,(c) 2:3.

spectra had been taken, only peaks due to $(NbCl_4(OMe))_2$ and $(NbCl_2(OMe)_3)_2$ were observed and at no time was a peak at -650ppm seen. On elevating the temperature to 293K the sample could be spun and the two peaks were found to be in the ratio 20:80 $(NbCl_4(OMe))_2$: $(NbCl_2(OMe)_3)_2$. For a 1:1 mixture that had fully disproportionated to these species the ratio should be 25:75. For better resolution of the $(NbCl_3(OMe)_2)_2$ peak, the spectral width was limited to the area in which it might occur and so the $(Nb(OMe)_5)_2$ resonance was not monitored.

2.1.5 The "Half" Species

As the $NbCl_{5-x}(OMe)_x$ series of molecules exist as dimers in non coordinating solvents, it should be possible to create dimers which have an odd number of Cl and methoxy groups. This would give non-equivalent Nb sites within the dimer, each having a different number of Cl and OMe groups attached. eg. $Nb_2Cl_3(OMe)_7$ or $(NbCl_{3/2}(OMe)_{7/2})_2$ – the "Half" species. As the methoxy groups on the $NbCl_{5-x}(OMe)_x$ series of molecules are fluxional it seems likely that in such "half" species the peak positions for the two types of niobium would be averaged to give a single peak. Although no experiments have been conducted to look specifically for these species, evidence for the formation of these species is believed to have been seen.

Immediately after mixing a 0.041 mol dm^{-3} solution of $(NbCl_5)_2$ and a 0.050 mol dm^{-3} solution of $(Nb(OMe)_5)_2$ in toluene (Cl:OMe ratio of 1:4) 5 peaks are observed in the ^{93}Nb spectrum. Three peaks, each ~30% of total peak area, occur at -810ppm, -1005ppm and -1150ppm and are due to $(NbCl_2(OMe)_3)_2$, $(NbCl(OMe)_4)_2$ and $(Nb(OMe)_5)_2$ respectively. The equal intensities imply incomplete redistribution. The other two peaks, each of ~5% total peak area occur at -900ppm and -1080ppm. These match the predicted positions, taken from Fig. 2.2, of $Nb_2Cl_3(OMe)_7$ and $Nb_2Cl(OMe)_9$ respectively Upon sonication for 15 minutes, only one peak is observed, at -1005ppm due to $(NbCl(OMe)_4)_2$.

However although similar experiments have been run at Cl:OMe ratios of 1:1 (ie. possible $Nb_2Cl_5(OMe)_5$ formation) and 3:2 (see earlier), no peaks for $Nb_2Cl_5(OMe)_5$ or

$Nb_2Cl_7(OMe)_3$ have been observed. The reason for this is not clear but it seems likely that they disproportionate to $(NbCl_4(OMe))_2$ and $(NbCl_2(OMe)_3)_2$. Why they should disproportionate is not easy to explain, except that both of these dimer species can be thought of as containing one monomer unit of $NbCl_3(OMe)_2$ which has been shown to disproportionate.

Finally, it has been noticed that upon addition of 1 equivalent of MeOH to a suspension of $NbCl_5$ in benzene/toluene, and the ^{93}Nb spectrum being run immediately a very broad peak (~9.7KHz) at -440ppm is observed that disappears over time or upon sonication to give the expected peak at -495ppm. It may be that this is the species Nb_2Cl_9OMe.

2.1.6 Acetonitrile Adducts $NbCl_{5-x}(OMe)_x.AN$

The ^{93}Nb peak positions of $(NbCl_5)_2$, $(NbCl_4(OMe))_2$, $(NbCl_2(OMe)_3)_2$ and $(Nb(OMe)_5)_2$ when dissolved in acetonitrile (AN) are given in Table 2.1. Kepert and Nyholm[19] have shown that in non-coordinating solvents such as carbon tetrachloride, $NbCl_5$ exists as the dimer $(NbCl_5)_2$ but in acetonitrile it forms the monomer $NbCl_5.AN$, with ^{93}Nb peak position at -55ppm.[9] Upon dissolution of $(NbCl_5)_2$ in acetonitrile at 293K, we observed two peaks in the ^{93}Nb spectrum, at -0.5ppm (FWHM 20Hz) characteristic of the dimer species, and at -55ppm (FWHM 1kHz) characteristic of the monomer adduct $NbCl_5.AN$. The relative intensities of these peaks change over time from 70:30 $(NbCl_5)_2$:$NbCl_5.AN$ within 3 minutes of dissolution of the $(NbCl_5)_2$ in the acetonitrile, to 20:80 after 30 minutes. Gentle heating (318K) gave a single peak at -55ppm indicative of the monomer adduct.

It seems highly probable then that in toluene $NbCl_4(OMe)$ would exist as the dimer but that in acetonitrile it could exist as the monomer $NbCl_4(OMe).AN$ .This is in fact what appears to be observed. In toluene a single peak is observed at -495ppm due to the dimer, whereas in acetonitrile two peaks are observed at -495ppm (FWHM 1kHz) and -560ppm (FWHM 1.5kHz). The latter is shifted upfield from the dimer by the appropriate amount for a monomeric niobium acetonitrile adduct.[9] This acetonitrile adduct is isolated by removal of

excess solvent to give an orange solid whose FTIR spectrum confirmed the presence of bound acetonitrile.[19,20] The orange $NbCl_4(OMe).AN$ was then added to deuterated toluene and two new peaks were seen to arise in the low temperature ^1H spectrum in a 1:1 ratio (Table 2.2) and a new peak was observed at -550ppm in the ^{93}Nb spectrum. The ^1H peaks can be assigned to NbOMe (3.90ppm) and Nb.NCMe (2.35ppm)[21] confirming the presence of $NbCl_4(OMe).AN$.

Riess and Hubert-Pfalzgraf[13,14,22] have shown that $Nb(OMe)_5$ is dimeric in both toluene and acetonitrile. Thus whilst $NbCl_5$ and $NbCl_4(OMe)$ have been shown to exist as separate monomer adducts, it might be predicted that $NbCl_2(OMe)_3$ would exist in a fluxional state between the monomer and dimer. When $(NbCl_2(OMe)_3)_2$ is dissolved in acetonitrile it gives a single peak at -850ppm (FWHM 10.5kHz) in the ^{93}Nb spectra, rather than two peaks for the monomer and dimer. This peak is shifted upfield from the dimeric species in toluene, implying the formation of an acetonitrile adduct species. Removal of the acetonitrile solvent gives a yellow solid whose FTIR not only contains $(NbCl_2(OMe)_3)_2$ but also shows shifted acetonitrile stretches confirming the formation of some monomer adduct $NbCl_2(OMe)_3.AN$. When the sample is redissolved in deuterated toluene it gives rise to a complex pattern of peaks in the low temperature ^1H NMR spectrum. Apart from a peak at 2.35ppm (Nb-NCMe) it has proved impossible to assign the peaks.

Although the preceding experiments had provided information on some of the $NbCl_{5-x}(OMe)_x.AN$ adducts, they did not answer the question of whether the monomer $NbCl_3(OMe)_2.AN$ would disproportionate in the same way as the dimer species. To answer this question a 0.0993 mol dm^{-3} solution of $(NbCl_5)_2$ and a 0.01696 mol dm^{-3} solution of $(Nb(OMe)_5)_2$ in acetonitrile were mixed in the following Cl:OMe ratios:- 4:1, 3:2, 2:3, and sonicated for 5 minutes. The ^{93}Nb spectra of the resulting solutions were run and found to give similar results to the experiments run in toluene (see section 2.1.4). The 4:1 Cl:OMe solution gave two peaks at -495ppm and -560ppm (16% and 84% respectively) due to $(NbCl_4(OMe))_2$ and $NbCl_4OMe.AN$. The 2:3 Cl:OMe solution gave a single peak at -854ppm due to $(NbCl_2(OMe)_3)_2/NbCl_2(OMe)_3.AN$ and the 3:2 Cl:OMe solution gave three peaks at -495ppm,

-560ppm, and -845ppm, with an integrated area of $NbCl_4OMe$: $NbCl_2(OMe)_3$ of 47:53, indicating $NbCl_3(OMe)_2$.AN had disproportionated like its dimer counterpart.

$(Nb(OMe)_5)_2$ in acetonitrile gives a ^{93}Nb peak at -1160ppm and the classic low temperature ^1H spectrum of the dimeric species, identical to that found in toluene but solvent-shifted (see Table 2.2). A small peak at -1185ppm is also observed, along with 9 corresponding peaks and a free methanol peak in the ^1H low temperature spectra . It is believed that this is due to an oligomer of $Nb(OMe)_5$ rather than a hydrolysis product, as addition of 1 equivalent of water does not cause this peak to grow, but rather creates a new peak at -1260ppm in the ^{93}Nb spectra. Further evidence for this belief is that upon mixing $NbCl_5$ and $Nb(OMe)_5$ solutions in acetonitrile in 4:1, 3:2, 2:3, ratios, no hydrolysis products (eg. $NbOCl_3$) are observed. $NbOCl_3$ should be observed if the peak at -1185ppm is due to a hydrolysis product. The peak at -1260ppm is thought to be due to a partial hydrolysis species of the type, $Nb_8O_{10}(OR)_{20}$, prepared by Bradley.[23]

2.1.7 $[NbCl_{6-x}(OMe)_x]^-$ Species

Initially it was hoped to generate these anionic monomer species by the mixing, in solution, of $CsNbCl_6$ and NaOMe in the required ratios. However, no common solvent was found for both NaOMe and $CsNbCl_6$.

To obtain a soluble methoxide salt, tetrabutyl ammonium methoxide (TBAOMe) was prepared. TBAOMe and $CsNbCl_6$ in acetonitrile (0.04 mol dm^{-3}) were mixed in various ratios to generate the $[NbCl_{6-x}(OMe)_x]^-$ series. However, it proved impossible to totally dry the TBAOMe and so apart from a peak at -425ppm, the only species observed was that of $NbCl_4OH/NbOCl_3$ at -495ppm.

Finally, a 0.1 mol dm^{-3} solution of $CsNbCl_6$ in acetonitrile was prepared and to this solution 1 to 5 equivalents of MeOH were added. These solutions gave a set of results similar to those observed with $(NbCl_5)_2$ in benzene/MeOH, except that the initial substitution of the $[NbCl_6]^-$ ion by the nucleophile, MeOH, proved harder than for $(NbCl_5)_2$. Thus, when 1

equivalent of MeOH was added, two peaks were observed at 0ppm and -425ppm (FWHM 4.6kHz). As more MeOH was added, the peak at 0ppm due to $[NbCl_6]^-$ decreased in size and a third peak appeared at -745ppm (FWHM 9kHz). By 5 equivalents of MeOH, only the peak at -745ppm remained. It seems probable that the peak at -425ppm is due to $[NbCl_5(OMe)]^-$, however the peak at -745ppm is less easily assigned and may be due to either $[NbCl_4(OMe)_2]^-$ or $[NbCl_3(OMe)_3]^-$.

2.2 Chemical Shift Dependence

2.2.1 Early Transition Metals

The overall shielding (σ) of a nucleus is defined as;[24]

$$\sigma = \sigma_d + \sigma_p + \sigma_o \qquad (2.4)$$

where σ_d is the diagmagnetic shielding of the atom, σ_p the paramagnetic shielding and σ_o is the shielding contribution of the other atoms. For atoms heavier than Be σ_p dominates (σ_d is approximately constant and small compared to σ_p for each element). Thus chemical shifts (δ) and nuclear magnetic shielding (σ) are defined with opposite sign, so that an increase in δ is given by an increase in the absolute magnitude of σ_p.[17,24]

A simple ligand field formulation for a transition metal nucleus in a d^6 octahedral complex is:[17]

$$-\sigma_p = \frac{\mu_o e^2 (r^{-3})_{nd} \langle 0/L^2/0 \rangle}{4\pi m^2 \Delta E} \qquad (2.5)$$

where μ_o is the permeability of free space, e and m the electronic charge and mass $(r)_{nd}$ the valence d electron radius and ΔE the excitation energy associated with the angular momentum operator L, with the origin at the metal nucleus. ΔE is effectively the ligand field splitting.[17] If ΔE is dominant, then σ_p increases with a decrease in the ligand field splitting parameter (Δ) and follows the spectrochemical series:[17]

$$H,C,N,O,F,S,Cl,Br,I \rightarrow (\text{increasing } \delta, \text{ decreasing } \Delta) \qquad (2.6)$$

This means that the chemical shift of a metal complex increases with a decrease in substituent electronegativity, with an increase in the λ of UV/vis absorption of the molecules and is observed for many early transition metal systems eg. Ti,[25] Co[26] and V.[27] This dependence is known as the "spectrochemical" dependence or "inverse halogen " dependence, the latter because δ increases as Δ decreases. The dependence of chemical shift upon electronegativity is often either a first order effect[28] (metal-ligand interactions dominant) or a second order effect[29] (ligand-ligand interactions important) and is discussed below with reference to the niobium species described in this chapter.

2.2.2 The Linear Dependence of ^{93}Nb Shift With Coordination Composition

Plotting peak position vs degree of substitution for the dimeric species gives a straight line for x=1,2,3,4,5 (see Fig.2.2). This is perplexing as it implies that after a large initial methoxide substitution, further substitution is a linear function. In attempting to provide a theoretical interpretation for the composition dependence of chemical shift of a molecule, there are two approaches;

i) A first order approach, based on a simple summation of substituent electronegativities and governed by the relationship:-

$$\delta calc = n/5(\delta NbCl_5) + (5-n)/5(\delta Nb(OMe)_5) \qquad (2.7)$$

ii) A second order approach, based on the "trans" model of Buslaev.[29] This approach recognizes that the shielding change caused by one substituent is apparent in neighbouring substituents and thus the chemical shift for the central atom is calculated by summing the pairwise interaction parameters for all substituents taken as opposite (trans) pairs. This has successfully been used to rationalize the chemical shift of the $[NbCl_{6-x}Br_x]^-$ series.[29]

Application of the first order approach gives wildly inaccurate predictions for the chemical shifts of the $(NbCl_{5-x}(OMe)_x)_2$ and $NbCl_{5-x}(OMe)_x.AN$ species. For example the following ^{93}Nb shifts are predicted: $(NbCl_4OMe)_2$ = -230ppm; $NbCl_4OMe.An$ = -285ppm; $(NbCl_2(OMe)_3)_2$ = -690ppm. Its main failure is its inability to predict the large shift observed in $(NbCl_4OMe)_2$. Because it fails to do this, all the calculated chemical shifts are inaccurate.

Application of the second order approach is more complex. For the dimeric series, each niobium in the dimer is in an octahedral environment, and so has 3 trans pairwise interactions. There are seven types of additivity parameters:-ηCl-Cl, ηCl-OMe, ηOMe-OMe, ηCl-Cl_{Br}, ηCl-OMe_{Br}, ηCl_{Br}-OMe, ηOMe-OMe_{Br}, and these can be calculated from the observed chemical shifts of the $(NbCl_{5-x}(OMe)_x)_2$ series. An assumption has been made in the predictions of the additivity parameters, that is, that the value for ηCl-Cl is 0ppm – this is not unreasonable as $[NbCl_6]^-$ has a chemical shift of 0ppm. A summary of the calculated shifts for the kinetically scrambled isomers is shown in Table 2.3.

Table 2.3

	ηCl-Cl	ηCl-Cl_{Br}	ηCl-OMe	ηCl_{Br}-OMe	ηCl-OMe_{Br}	ηOMe-OMe	ηOMe-OMe_{Br}	Obs.δ (ppm)	Calc.δ (ppm)
$(NbCl_5)_2$	2	4						2.6	2.6
$(NbCl_4(OMe))_2$	1	3	1	1				-495	-491.1
$(NbCl_3(OMe)_2)_2$	0.6	1.2	1.2	1.6	0.8	0.2	0.4	-650	-649.2
$(NbCl_2(OMe)_3)_2$	0.2	0.4	1.2	0.8	1.6	0.6	1.2	-810	-810
$(NbCl(OMe)_4)_2$			0.75	1	0.75	1.25	2.25	-1010	-1010
$(NbOMe_2)_2$						2	4	-1160	-1160

where ηCl-Cl=0ppm, ηCl-OMe=-482.4ppm, ηOMe-OMe=-350.65ppm, ηCl-Cl_{Br}=0.65ppm, ηCl-OMe_{Br}=78.375ppm, $\eta$$Cl_{Br}$-OMe=-10.65ppm, ηOMe-OMe_{Br}=-114.675ppm.

As can be seen in Table 2.3 the second order approach works. It shows that the trans interactions of non-bridging groups are the dominant additivity parameters in a upfield shift of the chemical shift, and that the Cl-OMe_{Br} interaction is the sole additivity parameter to cause an downfield shift in δ. Thus the large change in shift observed for the $(NbCl_4(OMe))_2$ species can now be explained. It contains no bridging methoxide groups and so has no downfield component in the summation of its pairwise parameters, giving it a very large upfield shift compared to the the other substituted chloroalkoxides.

Use of the "trans" pairwise additivity interaction model to predict the chemical shifts of the $NbCl_{5-x}(OMe)_x$.AN and $[NbCl_{6-x}(OMe)_x]^-$ series fails because of the lack of known chemical shifts for these series. Furthermore, use of the "cis" pairwise additivity interaction model, proposed by Vladimiroff and Malinowski[30] (and successfully used to rationalise the chemical shifts of systems such as boron-11,[30] carbon-13,[31] aluminium-27,[32] and germanium-73.[33]) fails to correctly predict the observed chemical shifts of the $(NbCl_{5-x}(OMe)_x)_2$ series. This is because there are ten "cis" additivity parameters, too many to be calculated using the six observed chemical shifts. Likewise, use of the assumption that the bridging groups can be considered similar to non bridging groups in order to reduce the numbers of "cis" additivity parameters to three gives wildly inaccurate results.

2.3 Alcohol Solutions

2.3.1 Alcohol Solutions of $CsNbCl_6$

The ^{93}Nb spectra obtained upon dissolving $CsNbCl_6$ in MeOH at different concentrations are shown in Table 2.4.

Table 2.4

Conc. (M)[c]	Peak Positions[a,b] Observed (ppm) and FWHM for Solutions of $CsNbCl_6$ in McOII						
1.0	-483 (6)		-853 (47)	-1005 (47)			
0.5	-490 (15)	-810 (35)		-1022 (45)			-1161 (5)
0.1					-1031 (90)	-1110 (10)	

(a). ±7ppm

(b) Figures in parentheses are approximate relative proportions.

(c) M = mol dm^{-3}.

Unlike the model systems so far described, alcohol solutions of $CsNbCl_6$ are not so easily characterized. This is due to the fact that the niobium chloroalkoxide species may be present either as monomers (anions or neutral solvent adducts) or dimers. Thus the assignment of any of the observed peaks to specific species is tenuous. Whilst some of the peaks observed *might possibly* be assigned to dimer species, ie, -485ppm = $(NbCl_4(OMe))_2$ (FWHM 3.6kHz), -810ppm = $(NbCl_2(OMe)_3)_2$ (FWHM 9kHz), -1005/-1022ppm = $(NbCl(OMe)_4)_2$ (FWHM 10kHz), -1161ppm = $(Nb(OMe)_5)_2$, others can not, ie, -853ppm (FWHM 12kHz), -1031ppm (FWHM 8.5kHz), -1110ppm (FWHM 8.5kHz). However, these latter three peaks may be tentatively assigned to $[NbCl_3(OMe)_3]^-$, $[NbCl_2(OMe)_4]^-$ and $[NbCl(OMe)_5]^-$, respectively, although they could just as likely be due to $NbCl_3(OMe)_2.MeOH$, $NbCl_2(OMe)_3.MeOH$ and $NbCl(OMe)_4MeOH$ or an equilibrium between these two types of monomers. For example:

$$[NbCl_3(OMe)_3]^- \underset{-H^+}{\overset{H^+}{\rightleftharpoons}} NbCl_3(OMe)_2.MeOH \qquad (2.8)$$

Table 2.4 also shows that as the concentration of $CsNbCl_6$ increases, the degree of OMe substitution per Nb (V) atom decreases.

2.3.2 $(NbCl_5)_2$ Dissolved in Neat Alcohols

When $(NbCl_5)_2$ is dissolved in MeOH the ^{93}Nb NMR spectrum at 293K consists of a set of lines, the number and intensity of which is heavily dependent on the concentration of $(NbCl_5)_2$ (see Fig. 2.4). The niobium chloroalkoxide species may be present as dimers or monomers (anionic or solvent adduct) – Bradley et al[11] have shown that $Nb(OR)_5$ in ROH exists as a monomer/dimer equilibrium mixture, and that $Nb(OMe)_5$ in MeOH (0.009 to 0.053 mol dm^{-3} of Nb) exists in equilibrium as 40% $(Nb(OMe)_5)_2$ and 60% $Nb(OMe)_5$.MeOH. When the ^{93}Nb spectrum of $Nb(OMe)_5$ is run in MeOH (0.02 mol dm^{-3}) it gives a single broad peak at -1170ppm implying peak averaging between the monomer and dimer species. As the observed peak positions for $(NbCl_5)_2$ in alcohol are very similar to those found for the dimeric species the peaks are now assigned to dimeric species (see Table 2.5), although it seems probable that they are in fact due to peak averaging between the dimeric species and monomer alcohol adduct.

Table 2.5

	Approximate Relative Percentage Proportions of $(NbCl_{5-x}(OMe)_x)_2$ in Various Alcohols and at Different Concentrations of $(NbCl_5)_2$.				
Concentration and Alcohol	x=1	x=2	x=3	x=4	x=5
1.65 mol dm^{-3} MeOH	50		35	15	
0.50 mol dm^{-3} MeOH		5	50	45	
0.25 mol dm^{-3} MeOH			30	60	10
0.05 mol dm^{-3} MeOH			20	45	35
0.50 mol dm^{-3} EtOH	15		85		
0.25 mol dm^{-3} EtOH	5	10	45	25	5
0.05 mol dm^{-3} EtOH			20	70	10
0.50 mol dm^{-3} Pr^iOH	25	45	35		

These lines sharpen on warming to 343K. On cooling back to 293K, the original spectrum is reproduced except for the most concentrated solution (1.65 mol dm^{-3}). The initial

Fig. 2.4

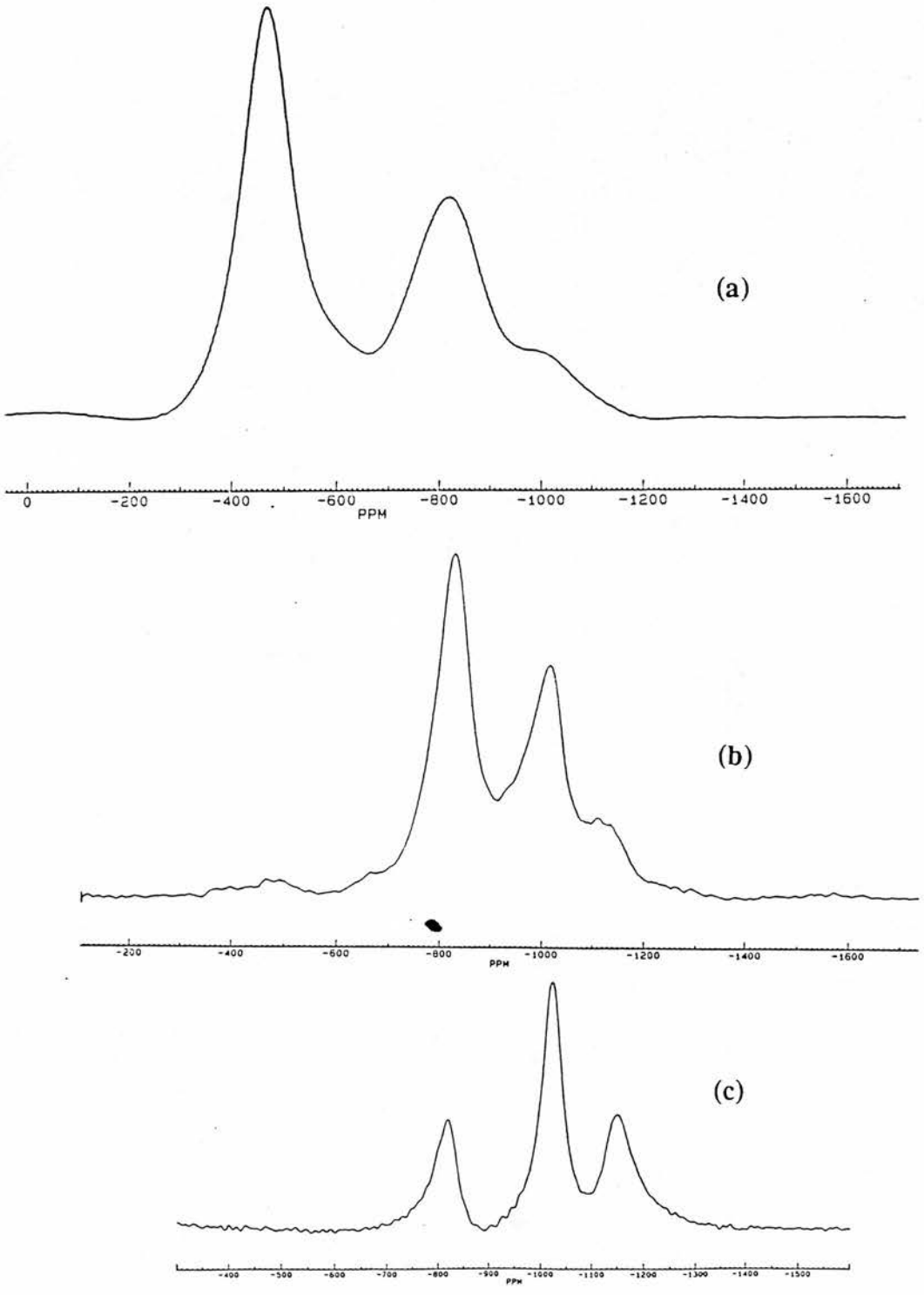

Fig. 2.4. ^{93}Nb NMR spectra of $(NbCl_5)_2$ in MeOH at 293K in the following concentrations: (a) 1.65 mol dm^{-3}, (b) 0.5 mol dm^{-3}, (c) 0.05 mol dm^{-3}.

spectrum of the 1.65 mol dm^{-3} solution consisted of a single broad peak from -400 to -900ppm. However upon heating and subsequent cooling the spectrum converted into the spectrum shown in Fig.2.4 (a). A possible explanation for this observed change is that the initial high viscosity of the solution at 293K limits diffusion of MeOH to the $NbCl_5$ so that less substituted species (including $(NbCl_3(OMe)_2)_2$) are observed and thus a broad single peak is observed. On warming, the viscosity decreases allowing for unhindered diffusion, $(NbCl_3(OMe)_2)_2$ disproportionates via eq.2.3 and on cooling the spectrum shown in Fig. 2.4(a) is observed. It is apparent that, like the $CsNbCl_6$ solutions, as the concentration of $(NbCl_5)_2$ in MeOH decreases, the degree of OMe substitution per Nb (V) atom increases.

Table 2.5 also gives ^{93}Nb NMR data for the corresponding species observed when $(NbCl_5)_2$ is dissolved in the higher alcohols, ROH, R=Et and ^{i}Pr. It is apparent that as the steric bulk of R increases the degree of substitution decreases.

2.3.3 Degree of Substitution

By taking the relative proportions of substituted species given in Table 2.5, it is possible to rank the solutions in increasing degree of OR substitution. This ranking is shown in Fig. 2.5, where M ROH = mol dm^{-3} of $(NbCl_5)_2$ in ROH

Fig. 2.5

1.65M MeOH — 0.5M MeOH ,0.25M MeOH — 0.05M MeOH

0.5M EtOH, 0.25M EtOH — 0.05M EtOH

0.5M $Pr^{i}OH$

Increasing Degree of OR Substitution →

Fig. 2.5 shows that for a given alcohol, as the concentration of $(NbCl_5)_2$ decreases, the degree of OMe substitution increases.

Table 2.6 shows the number of alcohol molecules per Nb(V) atom at given concentrations of $(NbCl_5)_2$ in alcohol. Thus if the degree of OR substitution was purely dependent upon the number of alcohol molecules available, then one would expect to see not only an increasing degree of OR substitution as the concentration of $(NbCl_5)_2$ decreases, but

Table 2.6

	Number of Alcohol Molecules/Nb(V) Atom at Given Concentrations of $(NbCl_5)_2$ in Various Alcohols		
Concentration (mol dm^{-3})	MeOH	EtOH	Pr^iOH
1.65	8	5.2	4
0.5	24.7	17.1	13.1
0.25	49.4	34.2	26.1
0.05	247	171	131

also that the overall ranking of the solutions in increasing degree of OR substitution would be as shown in Fig. 2.6.

Fig. 2.6

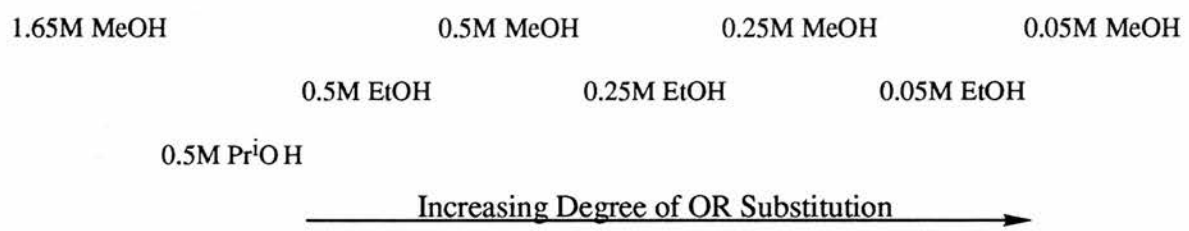

This overall ranking is not seen (see Fig. 2.5), the MeOH solutions have a far higher degree of OR substitution compared to the EtOH and Pr^iOH solutions than can be accounted for purely by the number of alcohol molecules per Nb (V) atom. It seems unlikely that steric factors are causing this lower degree of OR substitution for the EtOH and Pr^iOH as Et is not that much bigger a ligand than Me. It seems far more probable that the increased degree of OR substitution per Nb(V) atom in MeOH solutions, compared to the other alcohols, is due to the pKa's of the alcohols.

The standard pK_a values for the aqueous alcohols at 298K are MeOH = 15.09, EtOH = 15.93 and Pr^iOH = 17.1[34] and so as R decreases in size, the acidity of ROH increases. Thus Pr^iOH and EtOH are far weaker acids than MeOH and so are less inclined to react like an acid

with $(NbCl_5)_2$ and protonate the bound Cl^- to produce HCl gas and a bound OR group. Hence, MeOH is far more likely to undergo substitution and protonation reactions with $(NbCl_5)_2$ than EtOH and Pr^iOH and produces solutions with a higher than expected degree of OR substitution. This means that the degree of OR substitution is dependent upon two factors: (i) the ratio of alcohol molecules to Nb(V) centres: and (ii) the pKa of the alcohol.

2.3.4 HCl Concentration

Finally, Table 2.6 shows that at 1.65 mol dm^{-3} $(NbCl_5)_2$ in MeOH, the ratio of MeOH:Nb is 8:1. This is greater than the 5:1 MeOH:Nb ratio observed when $(NbCl_5)_2$ was dissolved in benzene, yet the degree of OMe substitution in benzene was greater (100% $NbCl_2(OMe)_3)_2$ formation). This is a surprising result as one would have expected the 8:1 MeOH:Nb solution to produce a greater degree of OMe substitution than the 5:1 MeOH:Nb solution. However, it can be explained by the solubility of HCl in alcohols and benzene.

HCl gas is far less soluble in benzene than in alcohols.[35] This means that in alcohol solutions, at a given ratio of ROH:Nb, there is a far greater molarity of HCl present than in the corresponding benzene solutions. Therefore, in alcohol solutions, there is a greater chance of rechlorinating niobium chloroalkoxide species and so the equilibrium mixture of species will contain a greater percentage of molecules with a lower degree of alkoxide substitution than would be expected from the benzene experiments.

That this back reaction of chlorination occurs has been graphically shown by the following experiment. A 0.0175 mol dm^{-3} solution of $(Nb(OMe)_5)_2$ in toluene was prepared and split into parts. Varying amounts of HCl gas were then bubbled through the solutions (at a flow rate of ~1.5ml/second) and the ^{93}Nb spectra run. When 3.5 equivalents of HCl had been bubbled through the solutions, $(NbCl_2(OMe)_3)_2$ and $(NbCl(OMe)_4)_2$ were the only species present, in a 85:15 ratio. After 10 equivalents of HCl has passed through the solution, only $(NbCl_2(OMe)_3)_2$ was present. Thus the quantity of HCl dissolved in a solution of niobium chloroalkoxides can also affect the degree of alkoxide substitution.

2.4 Conclusions

In summary, this work shows that ^{93}Nb NMR can be used to identify the $NbCl_{5-x}(OMe)_x$ series of molecules and distinguish between the dimeric and monomeric species. It also confirms Kolditz and Schönherr's report that only $(NbCl_2(OMe)_3)_2$ is formed in non-polar solvents on adding excess (5 fold) MeOH to $(NbCl_5)_2$ and indicates that $(NbCl_3(OMe)_2)_2$ appears to be unstable, disproportionating to $(NbCl_4(OMe))_2$ and $(NbCl_2(OMe)_3)_2$. In neat ROH, ^{93}Nb N.M.R. has shown that the reaction does not go by eq.(2.1) where x=2, 3 as previously believed but that a mixture of chloroalkoxides is present whose composition is strongly dependent on the total Nb concentration.

References

1. L.L. Hench and J.K. West, *Chem. Rev.,* 1990, **90**, 22.

2a. M. Sayer and K. Sreenivas, *Science,* 1990, **247**, 1056.

2b. M. Nabavi, S. Doeuff, C. Sanchez and J. Livage, *Mat. Sci. Eng.,* 1989, **3**, 203.

3. G. Rob Lee and Joe A. Crayston, *J. Mat. Chem.* , 1991, **1**,381.

4. L.G Hubert-Pfalzgraf, M.Postel and J.G.Riess, "Comprehensive Coordination Chemistry" ed. G.Wilkinson, Pergamon, 1987, Vol.3, p 585-698.

5. C.Sanchez, J. Livage, M. Henry and F. Babonneau, *J. Non-Cryst. Solids,* 1988, **100**, 65.

6. C. Alquier, M.T. Vandenborne and M. Henry, *J. Non-Cryst. Solids,* 1986, **79**, 383.

7a. M. Schönherr and L. Kolditz, *Z. Chem.,* 1970, **10**, 72.

7b. V.C. Gibson, T.P. Kee, A. Shaw, *Polyhedron*, 1988, **7**, 2217.

8. R.K. Harris and B.E. Mann, "NMR and the Periodic Table", Academic Press, London, 1978, p. 208.

9. R.G. Kidd and H.G. Spinney, *Inorg. Chem.,* 1973, **12**, 1967.

10. L.G. Hubert-Pfalzgraf, J.G. Reiss, A.A.Pinkerton, *Inorg. Chem.*, 1978, **17**, 663.

11. D.C. Bradley, W. Wardlaw and B.N. Chakravarty, *J. Chem. Soc.,* 1956, 2381

12. L.G. Hubert-Pfalzgraf, J.G. Riess, *Inorg. Chem.*, 1975, **14**, 2854.

13. J.G. Riess, L.G. Pfalzgraf, *Bull. Soc. Chim.*, 1968, 2401.

14. J.G. Riess, L.G. Pfalzgraf, *Bull. Soc. Chim.*, 1968, 4348.

15. D.C. Bradley, C.E. Holloway, *J. Chem. Soc.(A)*, 1968, 219.

16. C.E. Holloway, *J. Coord. Chem.*, 1972, **1**, 253.

17. J. Mason, *Polyhedron*, 1989, **8**, 1657.

18. R.Gut, H.Buser, E.Schmid, *Helv. Chim. Acta*, 1965, **48**, 878.

19. D.L. Kepert, R.S. Nyholm, *J. Chem. Soc.*, 1965, 2871.

20. C. Chavant, J.C.Dora, Y.Jeannin, G.Constant, R.Morancho, *Acta. Cryst.,* 1975, **31B**, 1828.

21. A.Merbach, J.C.Bunzli, *Helv. Chim. Acta*, 1971, **54**, 2543.

22. L.G. Hubert-Pfalzgraf, J.G. Riess, *J. de Chim. Phys.*, 1973, **70**, 646.

23. D.C. Bradley, *Coord. Chem. Rev.*, 1967, 299.

24. J.J. Dechter, "Progress in Inorganic Chemistry", ed S.J. Lippard, J. Wiley and Sons, Chichester, 1985, p393.

25. D. Rehder, *Magn. Res. Rev.*, 1984, **9**, 125.

26. J.S. Griffith, L.E. Orgel, *Trans. Faraday Soc.*, 1957, **53**, 601.

27. D.D. Devore, J.D. Lichtenhan, F. Takusagawa, E.A. Maatta, *J. Am. Chem. Soc.*, 1987, **109**, 7408.

28. W. Priebsch, D. Rehder, *Inorg. Chem.*, 1985, **24**, 3058.

29. V.P. Tarasov, V.I. Privalov, Y.U. Buslaev, *Mol. Phys.*, 1978, **35**,1047.

30. T. Vladimoff, E.R. Malinowski, *J.Chem. Phys.*, 1967, **46**, 1830.

31. B.F. Speilvogel, J.M. Purser, *J. Am. Chem. Soc.*, 1971, **93**, 4418.

32. E.R. Malinowski, *J. Am. Chem. Soc.*, 1969, **91**, 4701.

33. R.G.Kidd, H.G. Spinney, *J. Am. Chem. Soc.*, 1973, **95**, 88.

34. S.G. Wilkinson, "Comprehensive Organic Chemistry" Vol.1, Eds D. Barton, W.D. Ollis, Pergamon, 1979, p584.

35. "Handbook of Chemistry and Physics", Vol. 56, ed R.C. Weast, C.R.C. Press, Cleveland, 1975, pB67-160.

Chapter 3

Gelation Studies of Niobium Chloroalkoxides

3.1 Introduction

In this chapter, the factors affecting the gelation rate of the niobium chloroalkoxide sols are examined and discussed. Within the sol-gel processed systems being examined in this thesis, a precursor solution (sol) of a colloidal suspension of solid particles e.g. metal alkoxides, is hydrolysed and undergoes condensation reactions (two partially hydrolysed molecules linking together and liberating ROH or H_2O). Upon condensation the hydrolysed molecules first form oligomers, that is a molecule that is neither a monomer or a polymer but of intermediate size, and then polymers.[1] In non-aqueous solutions e.g.alcohol/water, the solubility of the solid phase formed by the condensation reactions is so limited that the condensation reactions are virtually irreversible and thus the bonds formed between the oligomers are random – they cannot be converted to an equilibrium configuration and so generally lead to the formation of fractal polymeric clusters. A fractal mass is a species whose mass (m) increases with its radius where m is proportional to r^d and $d<3$ (and is known as the fractal dimension).[1] The polymeric clusters undergo gelation, that is they grow until they are so large that they impinge on one another, at which point the clusters link together to form a network. When this network spans the whole of the sol, the gelation point is said to have been reached and a gel formed. A gel is defined as consisting of continuous solid and fluid phases of colloidal dimensions, and can be visualised as having a sponge like structure – it is possible to traverse the whole of the gel either by taking a purely fluid route through the "holes" or a purely solid route through the polymer network. If the gel thus formed is bigger than a few millimetres then it is called a monolith. Upon drying the gel shrinks due to capillary pressure producing stress upon the gel, and a xerogel is formed. Most gels so formed are amorphous, even after drying, but often crystallise upon high temperature heating (sintering).[1]

The purpose of using the sol gel method was to create thin films of Nb_2O_5 and if possible, thick monolithic films and compare their electrochemical properties.

3.1.1 General Mechanisms

In general, transition metal alkoxides are very reactive towards water and other nucleophiles. This is due to the alkoxo groups acting as hard π donors and stabilizing the metals in their highest oxidation state and thus making the metal more susceptible to nucleophilic attack. Compared with $Si(OR)_4$, the most commonly used type of precursor, whose hydrolysis and gelation is very well studied, the transition metal alkoxides are different in a number of ways:[1]

1) their lower electronegativity causes them to be more electrophilic and hence more reactive towards hydrolysis and condensation;

2) they generally have several stable coordinations, thus allowing them to undergo olation, oxolation, alkoxy bridging and other nucleophilic association mechanisms.

The rapid kinetics of nucleophilic reactions has meant studies of hydrolysis and condensation of transition metal alkoxides are far more difficult than for $Si(OR)_4$ and hence much less is actually known about the specific pathways. However, it is believed that the basic pathway for the hydrolysis and condensation reactions of transition metal alkoxides, in the absence of catalysts, is via nucleophilic substitution. This consists of nucleophilic addition via an associative mechanism, followed by proton transfer from the attacking nucleophile to one of the other bound ligands and removal of the protonated species.[2-5] Whilst transition metal chloroalkoxides are not as well studied as transition metal alkoxides, it is believed that they undergo the same types of reactions.

Thus the following reactions may occur;

Hydrolysis

$$H_2O + MOR \rightarrow MOH + ROH \qquad (3.1)$$

Alcolation

$$ROH + MOH \rightarrow MOR + H_2O \qquad (3.2)$$

Chlorination

$$HCl + MOH \rightarrow MCl + H_2O \qquad (3.3)$$

Oxolation

$$MOH + MOH \rightarrow MOM + H_2O \qquad (3.4)$$

Alcoxolation

$$MOR + MOH \rightarrow MOM + ROH \qquad (3.5)$$

Chloroxolation

$$MCl + MOH \rightarrow MOM + HCl \qquad (3.6)$$

Olation

$$MOH + MX \rightarrow MO(H)M + X \qquad (3.7)$$

where X is H_2O or ROH.

Thus the thermodynamics of hydrolysis, alcoxolation and oxolation, etc. are governed by the strength of the entering nucleophile, electrophilicity of the metal and the partial charge and stability of the leaving group.[2] The kinetics are governed by the extent of coordinative unsaturation, the ability to transfer protons and the molecular complexity of the metal chloroalkoxides ie. the number of metal atoms per molecule.[2] These factors will be discussed in more detail later, with special reference to niobium chloroalkoxides.

Unfortunately there appear to be very few papers dealing with the hydrolysis and gelation of niobium chloroalkoxides and alkoxides, and those that exist are full of contradictions, simplifications and errors.[4,6-8] Alquier et al[6] stated that on addition of water to 0.3 mol dm^{-3} solutions of niobium chloroalkoxides in the respective alcohol, a hydrolysis and gelation reaction occurs giving a white amorphous gel. They proposed that the following reaction occurred;

$$NbCl_5 \xrightarrow{ROH} NbCl_2(OR)_3 + 3HCl \xrightarrow{H_2O} NbCl_2(OH)_3 \qquad (3.8)$$

They further proposed that owing to the strong coordination properties of the OH groups, the molecule $NbCl_2(OH)_3$ was not stable as a monomer and underwent olation to form a colloidal gel containing chlorine/chloride. However Sanchez et al[4] believed that $NbCl_2(OH)_3$ was the final gel product. Finally Alquier et al noted that the rate of gelation of the hydrolysed chloroalkoxide solution depended upon the size of the alcohol. It increased as the alkyl chain increased, thus gelation ranged from seconds with Pr^iOH, through a few hours with EtOH to several days with MeOH. This was, at first, reiterated by Sanchez et al [4] and then contradicted in a later paper by the same group.[8] In this latter paper they state, "....the reactivity of metal

alkoxides decreases when the length of the alkyl chain increases." As these and other points seemed rather confusing, gelation studies of our own were undertaken.

Results and Discussion

3.2 Gelation Rates of $(NbX_5)_2$ Species (X=Halide, Alkoxide)

A number of solutions of various $(NbX_5)_2$ species were made and reacted with demineralised H_2O, 1.0 or 10.8 mol dm^{-3} HCl. The time taken for the complete hydrolysis and condensation reaction was noted (see section 9.3 for the method of determining gel time), and a summary of this data is given in Table 3.1 (H_2O addition) and Table 3.2 (10.8 mol dm^{-3} acid addition).

Table 3.1 shows that for all of the solutions, when reacted with water, the reaction time for hydrolysis and condensation was 5 seconds or less, regardless of X or concentration of $(NbX_5)_2$. This implies that hydrolysis is very fast (ie order of seconds) regardless of the type of ligand bound to the niobium .

Table 3.2 shows the affect of adding 10.8 mol dm^{-3} HCl to the solutions. Addition of 1.0 mol dm^{-3} HCl to the niobium solutions did not affect the gelation times noted in Table 3.1, however addition of 10.8 mol dm^{-3} HCl causes the gelation times to increase. Because the results in Table 3.1 show that hydrolysis is fast this increase in the observed gelation times must be due to the inhibition of the condensation reactions by chlorination back reactions (eq.3.3). This will prove to be important in later discussions on mechanisms for observed gelation rates.

From these observations it appears that the statement by Sanchez et al [4] that "$NbCl_5$ is more rapidly hydrolysed than $Nb(OR)_5$" does not appear fully justified (in this and other statements by this group, "hydrolyse" encompasses the terms "hydrolysis and condensation/gelation"). Furthermore, it is evident that $(NbCl_2(OMe)_3)_2$ reacts as fast as its parent molecules $(Nb(OMe)_5)_2$ and $(NbCl_5)_2$. Similarly, whether the alkoxide is a dimer (acetonitrile solutions) or a mixed monomer/dimer system (alcohol solutions) does not appear to affect the rate of reaction.

Table 3.1

Nb precursor	Gelation Times (secs) for Various Niobium Sol Mixtures with H_2O.[a]				
	Acetonitrile[b] (0.002/1.0)	MeOH[b] (0.002/0.1/1.0)	EtOH[b] (0.002/0.1/1.0)	Pr^iOH[b] (0.002/0.1)	Solid[c]
$(NbCl_5)_2$	1[d]/1				1
$(Nb(OMe)_5)_2$	1[d]	1/1/5			5
$(Nb(OEt)_5)_2$	1[d]		1/1/1		2
$(Nb(OPr^i)_5)_2$	1[d]			1/1	2
$(NbCl_2(OMe)_3)_2$	1[d]				5

(a). Gelation times (see section 9.3) shown are in the corresponding order to the concentrations (see (b)).

(b). Figures in parentheses are the concentrations in mol dm^{-3}. H_2O:Nb ratios are 2778, 103 and 28 for the 0.002, 0.1 and 1.0 mol dm^{-3} solutions respectively.

(c). H_2O:Nb ratio is 25.

(d). Time taken for white liquid to form. After 20 seconds flocculation occurred.

Table 3.2

Nb precursor	Gelation Times for Various Niobium Sol Mixtures with 10.8 mol dm^{-3} HCl.[a]			
	Acetonitrile[b] (0.002)	MeOH[b] (0.1/1.0)	Pr^iOH[b] (0.1/0.1)	Solid[c]
$(NbCl_5)_2$	3 days			2 hours
$(Nb(OMe)_5)_2$	3 days	1.5 days/5 mins.		
$(Nb(OEt)_5)_2$	3 days		1.5 days/5 mins.	
$(Nb(OPr^i)_5)_2$	3 days			

(a). Gelation times (see section 9.3) shown are in the corresponding order to the concentrations (see (b)).

(b). Figures in parentheses are the concentrations in mol dm^{-3}. H_2O:Nb ratios are 2778, 103 and 28 for the 0.002, 0.1 and 1.0 mol dm^{-3} solutions respectively.

(c). H_2O:Nb ratio is 25.

3.3 Gelation Rates of $(NbCl_5)_2$ in Alcohols

Mixing equal volumes of demineralised H_2O with 0.35 mol dm^{-3} solutions of $(NbCl_5)_2$ in ROH (where R=Me, Et, Pr^i), H_2O:Nb = 80:1, at ambient temperature and pressure appeared to verify the rate of gelation observations of Alquier et al.[6] The Pr^iOH solution formed a white liquid within seconds and a solid gel within minutes. The EtOH solution formed a gel within 2 hours and the MeOH solution took 24 hours. However these gelation times, ie. seconds for Pr^iOH solutions etc, are a simplification. The rate of gelation is as dependent upon the concentration of niobium (and hence the type of $NbCl_{5-x}(OR)_x$ species) in the solution as it is upon the type of alcohol.

Fig. 3.1(a) shows a graph of the gelation times for 0.5 mol dm^{-3} solutions of $(NbCl_5)_2$ in ROH (R=Me,Et,Pr^i) with demineralised water. Fig. 3.1(b) shows a graph of gelation times for 0.5, 0.125 and 0.0875 mol dm^{-3} solutions of $(NbCl)_5)_2$ in EtOH with distilled water. Fig. 3.1(a) clearly shows that for a given concentration of niobium, the gel times increase as the size of the alcohol decreases. Similarly, Fig. 3.1(b) shows that as the concentration of niobium decreases, the gel times increase. Furthermore, both these figures show that there is an optimum H_2O:Nb ratio for each solution to minimise the gel time.

As can be seen in Figs. 3.1(a) and (b) addition of demineralised water gives a slightly different optimum H_2O:Nb ratio compared to distilled water, but no other differences were observed. Repeating the experiment shown in Fig. 3.1(b) with MeOH as the solvent alcohol (and demineralised water) gave similar plots but at longer gel times. However when Pr^iOH was used even the 0.05 mol dm^{-3} $(NbCl_5)_2$ solutions gelled within seconds. In general, whereas both the EtOH and MeOH solutions formed homogeneous gels, the Pr^iOH solutions did not undergo homogeneous gelation but formed flakes and lumps and finally an inhomogeneous gel.

It is interesting to note that the gelation experiment was repeated with 0.5 mol dm^{-3} solutions of $(NbCl_5)_2$ in ROH (R=Me,Et) but, after the addition of demineralised water and mixing, the solutions were stoppered. None of these solutions formed a gel, even after 2 months. This is presumably because the system is not allowed to lose substituted ligands to the atmosphere and so alcolation and chlorination take place in increased amounts, as back

Fig. 3.1 (a)

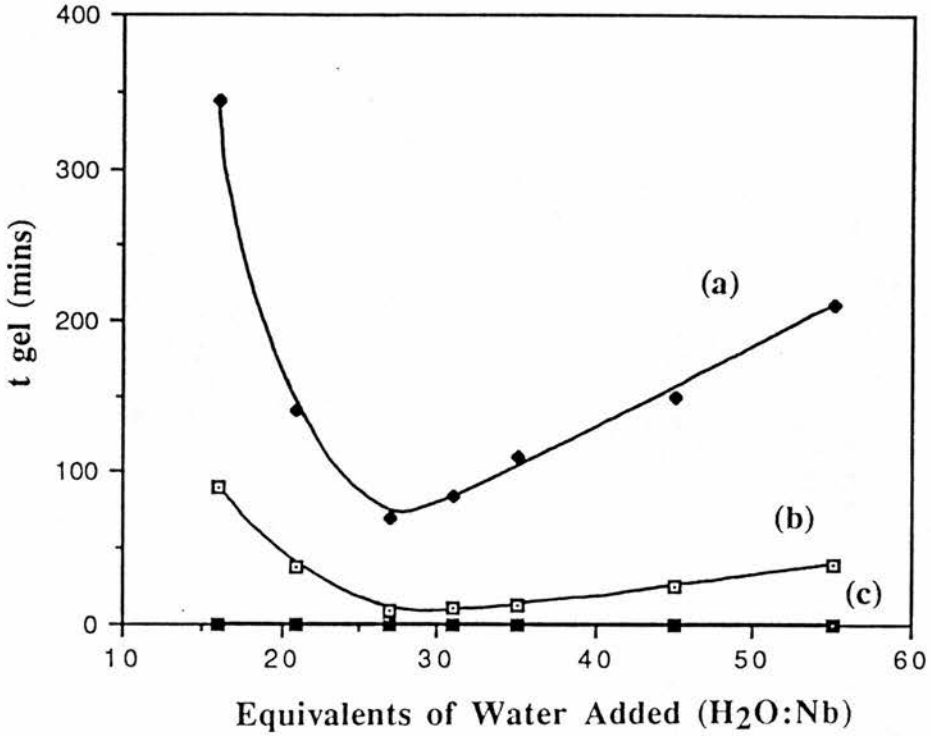

Fig.3.1(a). Gelation time (t gel, mins) vs equivalents of demineralised water (H_2O:Nb) added for 0.5 mol dm^{-3} solutions of $(NbCl_5)_2$ in ROH where (a) R = Me, (b) R = Et , (c) R = Pr^i.

Fig 3.1 (b)

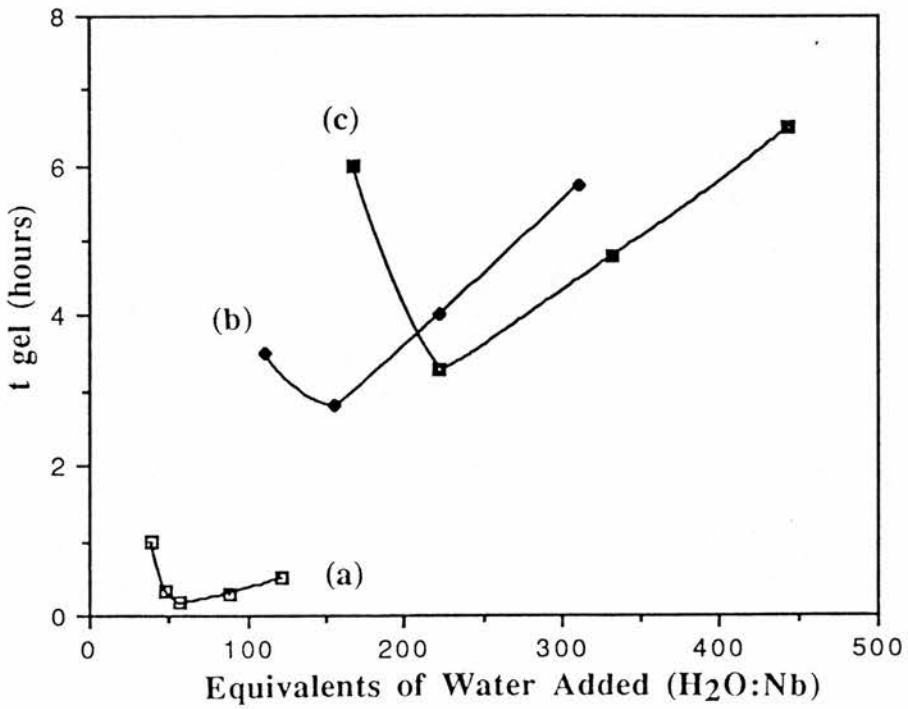

Fig. 3.1(b). Gelation times (t gel, hours) vs equivalents of distilled water (H_2O:Nb) added for (a) 0.5, (b) 0.125 and (c) 0.0875 mol dm^{-3} solutions of $(NbCl_5)_2$ in EtOH.

reactions, to reform the niobium chloroalkoxides and break down any hydrolysis oligomers formed.

Fig 3.2 shows the percentage weight loss of the sol/gels as a function of time for various niobium chloroalkoxide solutions. This shows (as might be expected) that weight loss increases as the concentration of niobium decreases for a given alcohol, and that at a given concentration of niobium the rate of weight loss is dependent upon the boiling point of the alcohol, thus MeOH, with the lowest boiling point, loses weight at a faster rate than the EtOH and Pr^iOH. Finally, no effect is observed on the weight loss rates due to crack formation which occurs in the gels after gelation (t_g).

3.3.1 Hydrolysis and Gelation Products

Alquier et al[6] had $NbCl_2(OH)_3$ as the final product of niobium chloroalkoxide hydrolysis and that this olated to form a gel, whilst Sanchez et al[4] thought $NbCl_2(OH)_3$ was the final gelation product. However it has already been shown that in alcohol solution the niobium chloroalkoxides do not exist purely as $NbCl_2(OR)_3$ as Alquier had thought but as a mixture of $NbCl_{5-x}(OR)_x$ monomer adducts or dimer species (x=1,2,3,4,5 dependent upon concentration). It seemed improbable that $Nb(OR)_5$ would hydrolyse to $NbCl_2(OH)_3$ rather than hydrated Nb_2O_5. Furthermore, if $NbCl_{5-x}(OR)_x$ (x =1 to 4) could be substituted by oxygen-bearing ligands to $Nb(OR)_5$ then there appears to be no reason why $NbCl_{5-x}(OR)_x$ should not also hydrolyse to hydrated Nb_2O_5. Because of these doubts the hydrolysis and gelation products of a number of hydrolysis reactions were analysed.

In order to ascertain whether the chlorine remained bound to the niobium, the gelation products of the hydrolysis reaction were comprehensively analysed. For this analysis, solutions of 0.5 mol dm^{-3} $(NbCl_5)_2$ in ROH were used, as the ^{93}Nb NMR studies had shown them to contain $NbCl_{5-x}(OR)_x$ (x = 1 to 4) as well as $Nb(OR)_5$ and thus it would be possible to ascertain whether, upon gelation, $NbCl_{5-x}(OR)_x$ had hydrolysed fully or not. Solutions of $(NbCl_5)_2$ in Pr^iOH, EtOH, and ethylene glycol were added to a large excess (100 equivalents) of demineralised water and left for 6 hours to gel. The gels were then washed and submitted to three drying processes:-(a) room temperature drying to give a cracked glass; (b) oven drying at

Fig. 3.2

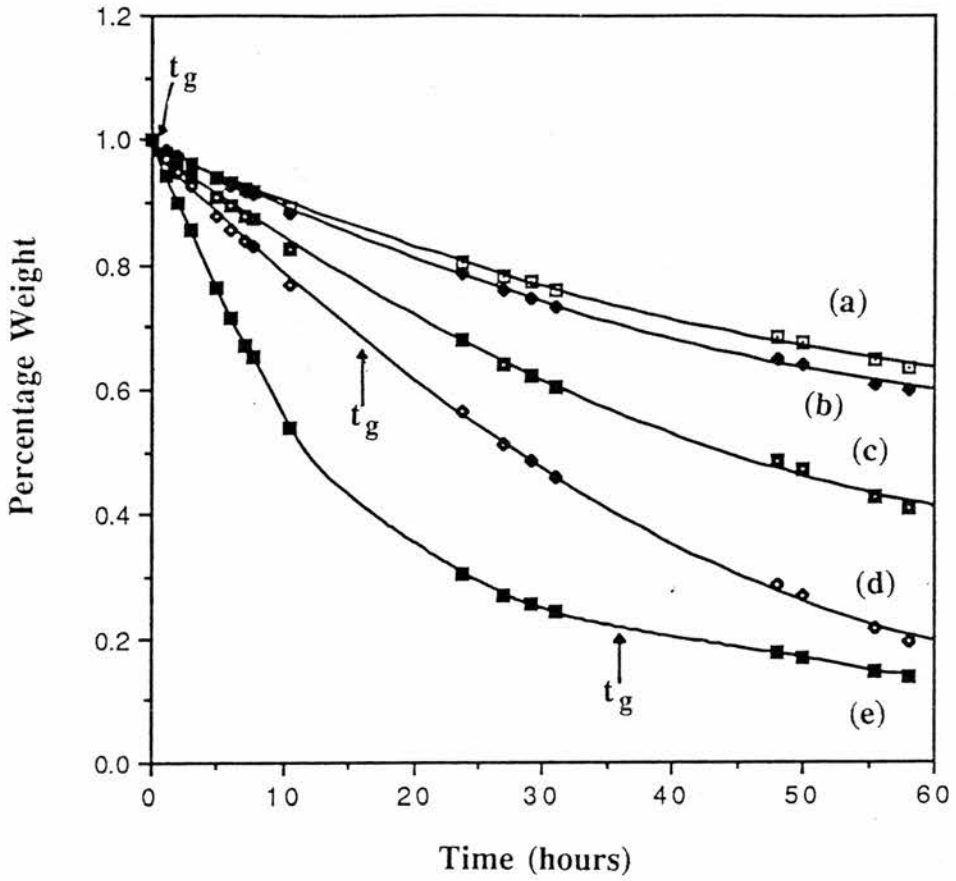

Fig. 3.2 Graph showing percentage weight loss of the sols/gels due to drying as a function of time. Sol/gel weight (expressed as percentage of original sol weight) vs time for X mol dm^{-3} solutions of $(NbCl_5)_2$ in ROH, where (a) X=0.5, R=Pr^i; (b) X=0.5, R=Et; (c) X=0.2, R=Et; (d) X=0.05, R=Et; (e) X=0.05, R=Me. The points t_g indicate the gelation time of the various sols.

150°C for 18 hours to give a powder; (c) as (b) but then followed by heating to 900°C over 4 hours.

EDAX and Cl^- analysis[9] upon the 150°C dried gels and EDAX upon the room temperature dried gels confirmed that the resulting gel was hydrated amorphous Nb_2O_5; no evidence could be found for remaining Nb–Cl bonds after hydrolysis. Thus hydrated Nb_2O_5 is the hydrolysis and gelation product of the $NbCl_{5-x}(OR)_x$ series, not $NbCl_2(OH)_3$ and the hydrolysis proceeds as follows:-

$$NbCl_{5-x}(OR)_x + 5H_2O \rightarrow {}^1/_2Nb_2O_5 + xROH + (5-x)HCl \qquad (3.9)$$

CO_2 pore analysis (267K) on the room temperature dried niobium oxide showed that the dried gels had no meso-porous or significant micro-porous volume (2.0 m^2g^{-1}). This implies a dense glass-like structure.

3.3.2 Attempted ^{93}Nb NMR Studies

In an attempt to characterise the hydrolysis products formed prior to gelation, the hydrolysis reaction was observed by ^{93}Nb NMR. Thus, 0.5 mol dm^{-3} solutions of $(NbCl_5)_2$ in MeOH and EtOH were placed in NMR tubes, water added (H_2O:Nb of 27:1) and the ^{93}Nb NMR spectra immediately run. However no signal was ever observed. This could be due to one or more of the following reasons, causing excessive broadening of the signal: (i) addition of water allows for a large increase in spin relaxation of the ^{93}Nb nuclei due to the increased interaction of the ^{93}Nb with the electric and magnetic fields associated with the dipole of the H_2O molecules; (ii) the niobium chloroalkoxide species react quickly to form a number of oligomeric structures (cf. ^{29}Si NMR of TEOS and TMOS hydrolysis[10]) prior to gelation but these species are very unsymmetrical giving a high electric field gradient at the nucleus; (iii) the niobium chloroalkoxides are continuously undergoing hydrolysis, alcoxolation, oxolation etc with rapid exchange between these species on the NMR time scale.

To try and resolve the problem of a lack of signal, a 0.05 mol dm^{-3} of $(NbCl_5)_2$ in MeOH solution was reacted with varying ratios of H_2O and the ^{93}Nb spectra run immediately.

It was observed that addition of water to the solution (H_2O:Nb 2.5:1, 7.5:1, 30:1) does indeed cause the increased spin relaxation of ^{93}Nb. In these systems, in order to obtain a resonance signal, the recycle delay pulse (τ_o) had to be decreased from 500ms to 200ms. As τ_o is usually ~5 times the spin relaxation time, it implies the relaxation rate drops from the order of 100ms to 40ms. Furthermore, on going from 2.5:1 to 30:1 H_2O:Nb a broad peak between -700ppm and -1600ppm was observed that replaced the precursor species resonances (-825ppm, -1020ppm and -1150ppm). This broad peak is featureless except for two maxima at ~-1070ppm and ~-1290ppm. It is unknown whether this broad peak is due to either the fast reaction of the niobium species present, the production of unsymmetrical oligomers, or both. This is in sharp contrast to Si and Al alkoxides where the hydrolysis reaction and products have been followed by ^{29}Si and ^{27}Al NMR.[10-12] However, these hydrolysis reactions are up to 5 orders of magnitude slower.[1] The two maxima observed at ~-1070ppm and ~-1290ppm imply that there are at least two types of hydrolysis products formed rather than the single $NbCl_2(OH)_3$ species as proposed by Alquier et al.[6]

3.4. Mechanism To Explain The Observed Gelation Rates

Fig. 3.3 shows the plot of $[Nb]^{-1}$ ([Nb] = niobium concentration) vs gel time (hours) for 0.5, 0.125, 0.0875 and 0.050 mol dm^{-3} solutions of $(NbCl_5)_2$ in EtOH upon addition of various equivalents of distilled water. The general increase observed in gel time on decreasing niobium concentration is predicted by the Flory model of polymerization[13] (see Appendix 1) where the gel time, $t_g = mC_o^{-1}$ (m is a constant and C_o is the initial niobium concentration) and is to be expected because the more dilute the niobium species, the longer it takes for a colloidal network to be formed. However, in Fig. 3.3 the least squares fit is only 87%, which implies that other factors are also contributing to the gelation rate within a given alcohol.

Thus there are two questions that require further answers: (i) Why for a given concentration, does the gelation rate increase as the size of the alcohol increases? (ii) Within a given alcohol solution, what factors other than concentration are also contributing to the gelation rate?

Fig. 3.3

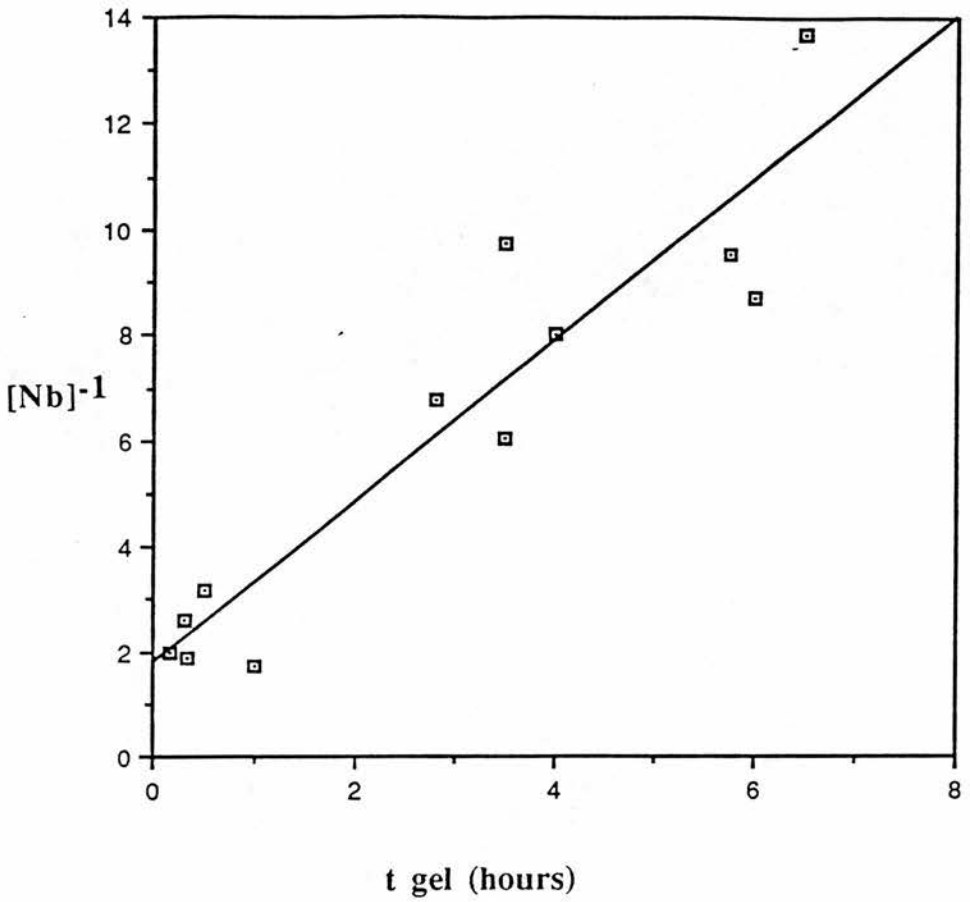

Fig. 3.3. $[Nb]^{-1}$ ([Nb] = niobium concentration) vs gelation time (t gel, hours) for 0.5, 0.125, 0.0875 and 0.050 mol dm^{-3} solutions of $(NbCl_5)_2$ in EtOH upon addition of various equivalents of distilled water.

On a general level there are a number of factors believed to affect the hydrolysis and condensation rates of metal chloroalkoxides containing different bound alkoxy species – the strength of the entering nucleophile, the electrophilicity of the metal, the partial charge and stability of the leaving groups, the degree of coordinative unsaturation and the molecular complexity of the precursor species. In many cases, it is a complex interplay of these factors which produces the trend observed, and sections 3.4.1 to 3.4.5 will discuss the relative merits of each of these factors. However pH studies (in section 3.4.4) on the gelling niobium chloroalkoxide solutions indicate that the concentration of Cl^- within the solution and the pKa of the alcohol are important factors.

3.4.1 Partial Charge Model

Using the partial charge model developed by Livage[2,4] it is possible to calculate the partial charge upon the atoms within a given molecule. The equations governing this model are given below:

$$\mathbf{X} = ({}_i\Sigma\rho_i\{x_i^o\}^{1/2})({}_i\Sigma\rho_i\{x_i^o\}^{-1/2})^{-1} \qquad (3.10)$$

$$\delta_i = (\mathbf{X}-x_i^o)(K\{x_i^o\}^{1/2})^{-1} \qquad (3.11)$$

where $\mathbf{X}$ is the mean electronegativity of the molecule, x_i^o is the electronegativity of the neutral atom, k=1.36 in the Pauling's units,ρ_i is the stoichiometry of the i^{th} atom and δ_i is the partial charge of the atom. There are two ways of calculating the partial charge on the metal in a compound $M(OR)_x$. Either to break the molecule up into its component atoms and then apply the formulas given in the eq(3.10) and eq(3.11), to give δ(M), or to break the molecule into neutral metal and ligands, apply eq(3.10) and eq(3.11) to the component atoms of each of the ligands to obtain the mean electronegativity for each of the ligands, then reapply eq(3.10) and eq(3.11) to the metal and ligands to obtain δ(M) and δ(OR). Although the 2 methods give slightly differing values of δ(M), they give the same trends.

Livage et al[2,4] claim that the use of the Partial Charge Model can predict the hydrolysis and condensation rates of precursor species. When applied to very general trends, and when

the calculated differences between the partial charges found on the metal atoms are *large* (>0.1), the Partial Charge Model appears to work. For example in the system $M(OEt)_x$, where M= Si → Ti, Livage et al [2] found that δ(M) changed from +0.32 for Si, to +0.63 for Ti. This was used to explain the faster hydrolysis and condensation rates of transition metals over Si. At pH 7, Ti has a hydrolysis rate [14-16] of $K_h=10^{-3}M^{-1}s^{-1}$ and a condensation rate,[16] $K_c=30M^{-1}s^{-1}$, compared with a condensation rate for Si [18,19] of $K_c=10^{-4}M^{-1}s^{-1}$ and hydrolysis rate,[20-22] $K_h=5 \times 10^{-9} M^{-1}s^{-1}$.

However, when the Partial Charge Model is applied to more specific systems where the difference in the calculated partial charges for varying species is *small*, eg niobium chloroalkoxides series, one has to be careful as to what conclusions can be drawn. Table 3.3 shows the partial charge, δ(X), of Nb, bound ligands and potential leaving groups of a variety of niobium species, calculated by use of the second method described above.

Livage et al [2] proposed that the most positively charged ligand is the best leaving group and from this proposal a number of observations can be made from the data given in Table 3.3. These observations are not consistent with the observed experimental data as shown in Table 3.1:-

1) For both $NbCl_2(OR)_3$ and $Nb(OR)_5$ species, as the size of the alcohol increases, the calculated partial charge on niobium decreases by up to 0.1, implying a slower rate of attack by H_2O upon the metal as the alcohol size increases.

2)The difference in the calculated partial charge for the leaving group δ(HOR) in $NbCl_2(OR)_2(HOR)OH$ as R is changed from Me to Pr^i is less than 0.015. Livage et al [2] claimed that this minor increase in δ(HOR) was the reason for the increase in gelation time on going from Pr^i to Me solutions.

3)Upon formation of $Nb(OR)_5.H_2O$ and $Nb(OR)_4(HOR)OH$ species, δ(HOR) is indeed the most positively charged ligand and hence the best leaving group, but the difference in replacing HOMe by $HOPr^i$ is almost zero.

4)Livage et al[4] claimed that in the $NbCl_2(OR)_3.H_2O$ system, as HOR is the best leaving group, this explained why the chloride ligands remained unhydrolysed.

Table 3.3

	Partial Charges (δ) on Component Groups of Niobium Species[a]						
Molecule	δNb	δOR	δH_2O	δHOR	δOH	δCl	δHCl
$NbOR_5.H_2O$	0.429 0.404 0.392	-0.066 -0.057 -0.053	-0.100 -0.120 -0.129				
$NbOR_4.HOR.OH$	0.439 0.416 0.405	-0.057 -0.047 -0.042		-0.035 -0.035 -0.035	-0.175 -0.193 -0.201		
$NbCl_2OR_3.H_2O$	0.526 0.510 0.503	0.013 0.030 0.038	0.023 -0.022 -0.041			-0.271 -0.282 -0.287	
$NbCl.HCl.OR_3.OH$	0.504 0.488 0.481	-0.005 0.012 0.020			-0.126 -0.138 -0.143	-0.286 -0.298 -0.303	-0.077 -0.089 -0.095
$NbCl_2OR_2.HOR.OH$	0.538 0.523 0.517	0.022 0.041 0.049		0.045 0.053 0.057	-0.100 -0.111 -0.116	-0.263 -0.273 -0.278	
$NbOH_3Cl_2.H_2O$	0.593		0.030		-0.058	-0.224	
$NbOH_4Cl.HCl$	0.570				-0.0.76	-0.240	-0.026
$NbOR_5$	0.409 0.380 0.301	-0.082 -0.076 -0.073					
$NbCl_2OR_3$	0.421 0.413 0.396	-0.072 -0.050 -0.050				-0.104 -0.111 -0.124	

(a). For molecules containing OR ligands the order of data is R = Me, Et then Pr^i. Thus the top number is for R = Me and the bottom number for R = Pr^i.

As can be seen from observations 1-3, one has to be careful how one treats the trends thus shown. If 1), 2) and 3) are taken together, then the implication is that as the size of the alcohol increases, the rate of hydrolysis decreases. If only 2) and 3) are examined, and the fact that the differences in δ(HOR) are small is ignored, then it would appear that as the size of the alcohol increased, the rate of hydrolysis increases. Neither of these conclusions is supported by the experiments shown in Table 3.1. The only conclusion which is supported by the experimental facts, is that 2) and 3) show that the differences in δ(HOR) on going from Me to Pr^i are negligible and thus the gelation rates should be equal. However this conclusion is contradicted by observation 1.

Similarly if 4) was a correct proposal, then the species $Nb(OH)_3Cl_2$ would be formed. Table 3.3 shows that for the $Nb(OH)_3Cl_2.H_2O/Nb(OH)_4Cl(HCl)$ system, H_2O has a more positive partial charge than HCl implying that further hydrolysis does not take place – this appears to confirm Livage's proposal in 4). Yet we have shown that the chlorine ligands are hydrolysed and the final product is $Nb_2O_5.(H_2O)_x$.

Thus it is obvious that the Partial Charge Model fails to fit or predict the experimentally obtained gelation observations for the individual precursors. It is felt that the reason for this is that the model is not a powerful enough algorithm to correctly calculate the partial charges on the metal and ligands and so it is incorrect to use the very small differences in partial charges that it predicts, to propose specific mechanisms or reasons for differing reaction rates. This is not the first time the Partial Charge Model has broken down as a predictive tool. It predicts alcoxolation should be the favoured condensation reaction between partially hydrolysed coordinatively saturated silicates, yet ^{29}Si NMR investigations reveal oxolation, rather than alcoxolation is favoured.[1] Finally it should be pointed out that it has proved impossible to reproduce the set of partial charge figures quoted by Livage et al.[2,4] Application of either of the two methods used to calculate δ(M) failed to give the values of δ(M) or δ(ligand) found by Livage. For example, Livage gives δ(M) for $Nb(OEt)_5$ as +0.53. By the first method, δ(M) was found to be +0.46 and by the second, +0.38. However the general trends of the partial charges quoted by Livage et al were matched by the partial charges shown in Table 3.3.

3.4.2 Coordinative Unsaturation and Oligomerization

As the transition state of the hydrolysis reaction is believed to proceed via an associative intermediate, a coordinatively unsaturated metal atom should form this intermediate faster than a similar metal atom that was coordinatively saturated. Likewise the degree of oligomerization (molecular complexity) also plays a crucial role – bridging alkoxy groups are more stable towards hydrolysis than terminal alkoxy ligands and associated solvent molecules. Hence $Zr(OPr^n)_4$ dissolved in Pr^nOH is monomeric and hydrolysis results in rapid precipitation, whereas when it is dissolved in cyclohexane it is oligomeric and controlled hydrolysis occurs to give a homogeneous gel.[23] However, it does not seem likely that these two factors greatly influence the observed difference in gelation rates of the niobium chloroalkoxides – although the degree of coordination unsaturation is unknown (niobium (V) species are known to exist with coordination numbers from 4-9, with 6 being by far the most prevalent[24]), there is no evidence to suggest that the niobium is in any state other than coordinatively saturated (ie 6 coordinate). Likewise, whilst the degree of oligomerization of the niobium chloroalkoxides in alcohol solution is not known, the degree of dimerization of the pentaalkoxides is known. Bradley et al [25] showed by ebullioscopic measurement that 34% of $Nb(OMe)_5$, 52% of $Nb(OEt)_5$ and 29% of $Nb(OPr^i)_5$ exist as dimers in solutions of their parent alcohols. Because Table 3.1 shows that $Nb(OR)_5/(Nb(OR)_5)_2$ in alcohol generally reacts as fast as $(Nb(OR)_5)_2$ in acetonitrile, this tends to imply that oligomerization is not a factor that affects the rate of hydrolysis and gelation in this system.

3.4.3 Steric Factors

In titanium alkoxide systems, it has been shown that increasing alkyl chain length leads to slower gelation kinetics. Thus upon addition of water to $Ti(OR)_4$, when R = Et,Pr^i,Pr^n, rapid precipitation occurs[14,15,17] yet when R =Bu^n or Am^t, stable sols are formed.[26,27] It is suggested that this is due to a difference in the condensation products – the larger the size of R, the smaller the oligomer.[1] Again though, this is not believed to play an important role in niobium chloroalkoxide gelation as the opposite is observed.

3.4.4 HCl Concentration

It was found that upon addition of water to the niobium chloroalkoxide (R=Me and Et) solutions (the solution then being vigorously stirred for 30 seconds), the pH of the solutions dropped for the first 120 seconds and then remained reasonably constant, implying fast initial hydrolysis and slow condensation. Collecting pH data on the solutions as they gelled allows the proton concentration and hence the chloride ion concentration [Cl^-] to be calculated as it is assumed that the protons present are due to HCl. Fig. 3.4 shows a plot of chloride to niobium ratio ([Cl^-][Nb]$^{-1}$) vs gel time for three $(NbCl_5)_2$ solutions in EtOH (0.5, 0.125 and 0.0875 mol dm^{-3}) with varying amounts of water added (plots for the MeOH solutions are not shown due to the experimental problems in measuring the large t_g). Thus in each of the linear plots shown the EtOH to niobium ratio remains constant (ie obtained from the initial niobium concentration in the EtOH solution, see section 9.2), but the chloride concentration:niobium concentration varies as different amounts of water are added. The total niobium concentration decreases as water is added and was calculated by assuming that Xml of EtOH and Yml of H_2O mix to give a solution of volume (X+Y)ml. It is evident from Fig. 3.4 that for a given EtOH to niobium ratio, increasing the chloride to niobium ratio linearly increases the gel time. The explanation for this is that at higher chloride to niobium ratios, chlorination of partially and fully hydrolysed niobium oligomers (eq's 3.1, 3.2 and 3.3 where R^2 =H and OR^1 = Cl^-) occurs at a greater rate, slowing the rate of hydrolysis and oligomerization.

The fact that gel times differ from seconds in Pr^iOH solutions to tens of hours in MeOH solutions at a given [Cl^-]:[Nb] and similar alcohol to niobium ratio, implies that alcolation (eq. 3.2) is also occurring in these hydrolysing solutions – the difference in observed gel times for different alcohols must be due to the different propensity to alcolate, ie their pKa's. The standard pK_a values for the alcohols are MeOH = 15.09, EtOH = 15.93 and Pr^iOH = 17.1[28] and so as R decreases in size, the acidity of ROH increases, hence MeOH is far more likely to alcolate hydrolysed niobium species and slow the gelation rate than is Pr^iOH. Why alcolation (eq. 3.2) should be observed in the hydrolysing niobium chloroalkoxide solutions but not be observed in hydrolysing solutions of $(NbX_5)_2$ (section3.2), is not

Fig. 3.4

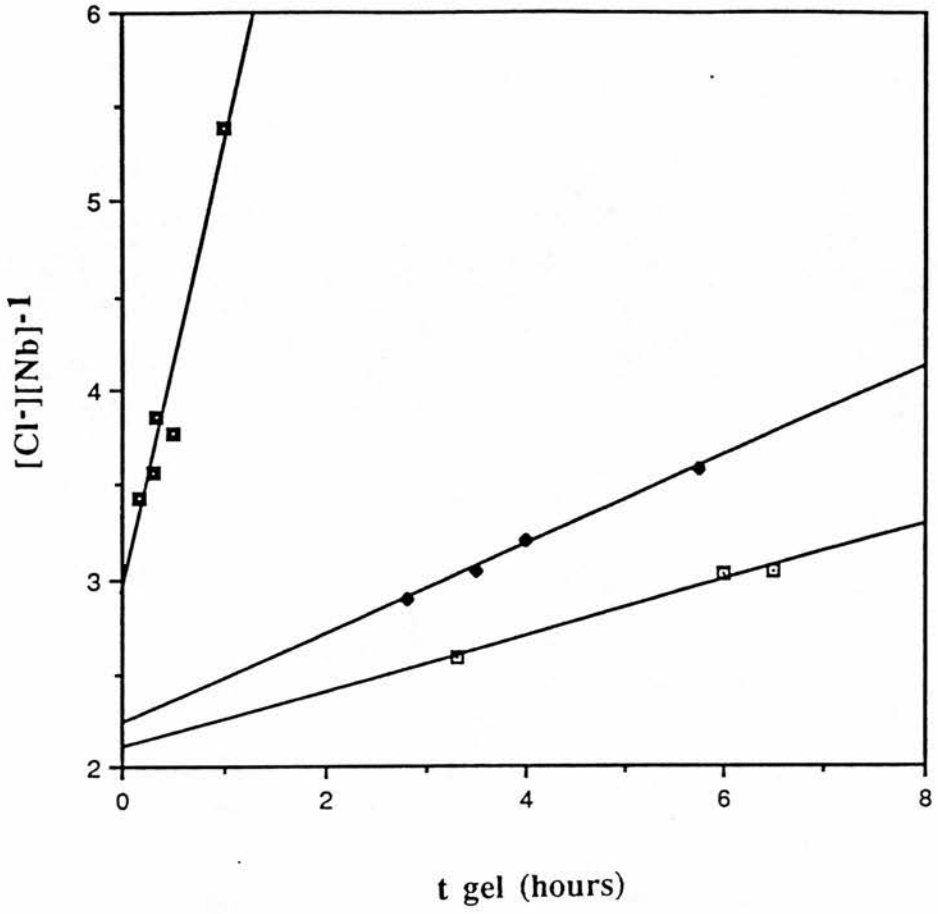

Fig. 3.4. Ratio of chloride ion to niobium ion ($[Cl^-][Nb]^{-1}$) vs gelation time (t gel, hours) for X mol dm^{-3} solutions of $(NbCl_5)_2$ in EtOH where (a) X = 0.5; (b) X = 0.125 ; (c) X = 0.0875.

apparent, but it may be that alcolation requires preprotonation of bound hydroxide groups before substitution and the niobium chloroalkoxide solutions can readily supply protons.

A number of attempts have been made to fit the observed data to theoretically derived rate equations, taking into account chlorination and alcolation as well as the different types of condensation reactions, however no match was made. It is felt that whilst the experimental data can serve as a base for a qualitative explanation, it has not been developed far enough to enable a quantitative explanation to be proposed. Future work should concentrate on the kinetics of individual steps of the hydrolysis and condensation reactions of model species, ie $(NbX_5)_2$ where X = halide and alkoxide.

3.4.5 Summary of The Mechanisms of Observed Gelation Rates

The observed trend that the rate of gelation decreases as the concentration of niobium in a given alcohol decreases (see Fig. 3.1(b)) has been shown to be due to the dilution of niobium species making it harder to form a colloidal network. For a given alcohol and concentration varying the H_2O:Nb ratio gives an optimum H_2O:Nb ratio with a minimum gel time (see Fig. 3.1(b)). The dependence of the gel time with the H_2O:Nb is due to the ratio of chloride ion concentration to the niobium concentration; as the ratio increases, the rate of chlorination increases, slowing the hydrolysis of the niobium species. Finally, the observed trend that the rate of gelation increases as the size of the alcohol increases, for a given concentration of niobium, is believed to be due to the increase in pKa values with increasing size of the alcohols. This means that the smaller the alcohol, the greater the alcolation occurring and thus the slower the hydrolysis of the niobium species.

3.5 The Effect of Different Acids on Gelation Rates

It is well known that acid or base catalysts influence both the hydrolysis and gelation rates and structure of the condensed product.[1] In order to compare possible catalysts for the gelation of the niobium chloroalkoxide solutions, 0.5 and 0.2 mol dm^{-3} solutions of $(NbCl_5)_2$ in EtOH were mixed in equal volumes (H_2O:Nb, 55:1 and 137:1 respectively) with various reagents and the time taken to gel noted. The results are given in Table 3.4.

The standard mechanism for acid catalysis of hydrolysis and condensation,[1] is one of protonation of a partially negatively charged ligand (OR in the example shown below), enhancing hydrolysis reaction kinetics by producing a good leaving group;

$$M\text{-}OR + H_3O^+ \longrightarrow M^{+}\!\!\leftarrow\!\!-\!-:\overset{H}{\underset{|}{O}}R + H_2O \qquad (3.12)$$

Table 3.4

Gelation Study of 0.2 and 0.5 mol dm^{-3} $(NbCl_5)_2$ in Ethanol with Various Acids and Base				
acid/base conc.	gelation time 0.4 M Nb	gelation time 1.0 M Nb	Type of Gel Formed	Gel formed upon Atmospheric Drying
2M HCl	>20 mins	~15 mins	white, homogeneous	white monolith,uncracked
2M H_3PO_4	~5 mins	~3 mins	white, homogeneous	white monolith, cracked
1M H_2SO_4	5 secs	1 sec	white, "swirled"	cracked yellow glass
2M NaOH	5 secs	1 sec	white, "swirled"	cracked yellow glass

In basic solutions, strong nucleophiles are produced via deprotonation of hydroxo ligands and thus hydrolysis and condensation reaction kinetics are enhanced;

$$L\text{-}OH + :B \rightarrow L\text{-}O^- + BH^+ \qquad (3.14)$$

So it is to be expected that H_3PO_4 is not as strong a catalyst as H_2SO_4, as it is a weaker acid and thus supplies less H^+. However these mechanisms do not take into account the affect of the anions present. HCl is as strong an acid as H_2SO_4 and certainly stronger than H_3PO_4, thus its poor catalytic properties are due to the Cl^- anion which increases the rate of rechlorination of the niobium. As this is a back reaction, the gelation rate is slowed.

Analyses of H_2SO_4 catalysed gels (0.5 mol dm^{-3} solutions of $(NbCl_5)_2$ in MeOH, EtOH, and ethylene glycol added to a large excess (100 equivalents) of 0.01 mol dm^{-3} H_2SO_4 and left for 6 hours to gel, washed and dried as in section 3.3.2, revealed that all the gels formed showed identical analytical properties to those found for the gels formed by the

hydrolysis of 0.5 mol dm^{-3} solutions of $(NbCl_5)_2$ in Pr^iOH, EtOH, and ethylene glycol, except that: (i) EDAX revealed that sulfur was still present within the gels; (ii) FTIR spectroscopy revealed the presence of SO_4^{2-} within the gels. As the washing had extracted all the Cl^- within the gels, it appears that for SO_4^{2-} to be present, it must still be bound to the gel. This could occur either as SO_4^{2-} acting as a strong network former, attacking the Nb and remaining bound (both inter and intramolecularly) as a ligand or that it acts to join oligomers through hydrogen bonding:-

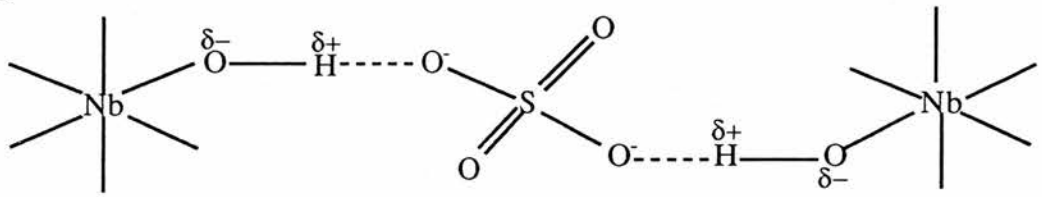

It seems probable that the SO_4^{2-} found within the washed gels is due to SO_4^{2-} actually bound to the niobium as a ligand rather than being bound by hydrogen bonding, since Cl^- could also act as a hydrogen bonded bridge for oligomers and this is removed by the washing process. If SO_4^{2-} is acting as a strong network former, then it should catalyse the hydrolysis and condensation reactions. To test this 0.5 and 0.05 mol dm^{-3} solutions of $(NbCl_5)_2$ in EtOH were added to equal volumes of solutions of H_2SO_4 and Na_2SO_4, and the time taken to form a gel noted. Fig.3.5 shows a graph of gel time vs SO_4^{2-} concentration, and from this it is apparent that Na_2SO_4 is as good as, if not a better catalyst than H_2SO_4. Although Na_2SO_4 cannot protonate Cl or OR to produce good leaving groups, it can react to form NaCl (which is far less soluble in alcohols than HCl[29] and thus lowers the rate of rechlorination of the hydrolysed species) and NaOEt (which reacts with water to form ethanol and sodium hydroxide – a powerful hydrolysis catalyst) and so the gelation rates are not that different to H_2SO_4.

At 0.5/1.0 mol dm^{-3} SO_4^{2-}, the catalytic properties reach a maximum, and at greater molarities of SO_4^{2-} the gelation time drops. This is traditionally ascribed to protonation of hydroxo ligands on partially hydrolysed species allowing the back reactions of alcolation and chlorination to proceed faster. However this cannot be the case for Na_2SO_4, and it may be that an excess of SO_4^{2-} inhibits the hydrogen bonding between oligomers thus slowing gel formation:

Fig. 3.5

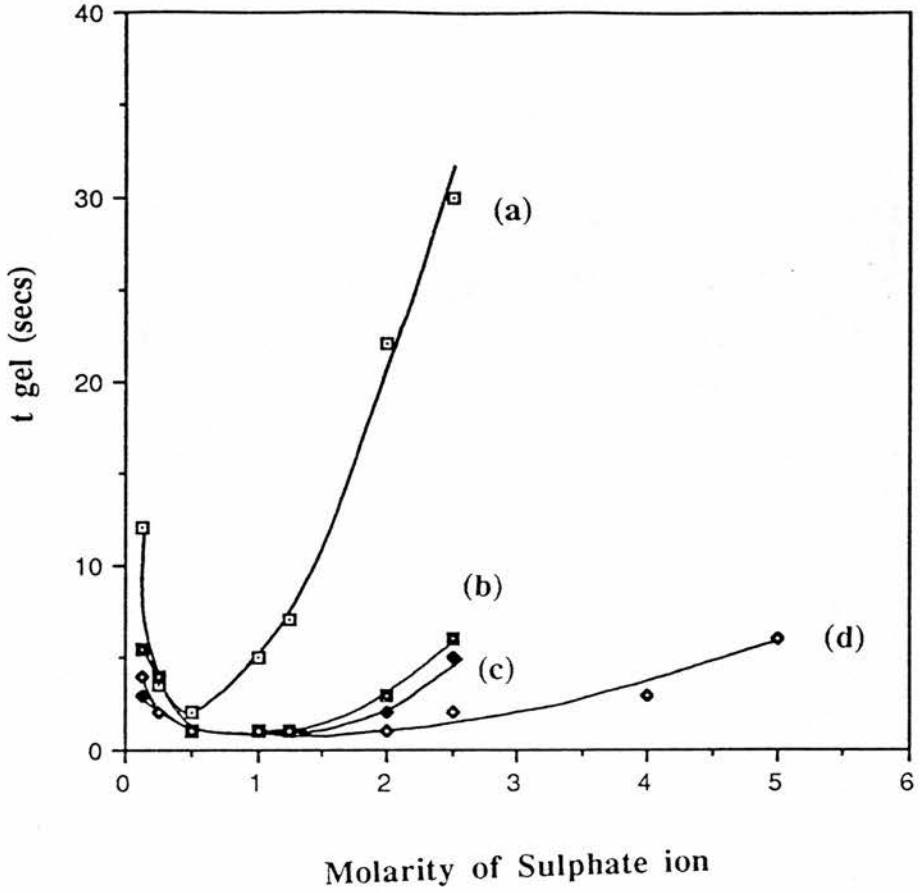

Fig. 3.5 Gelation time (t gel, seconds) vs molarity of SO_4^{2-} solution when equal volumes of M_2SO_4 solution and X mol dm^{-3} $(NbCl_5)_2$ in EtOH are mixed. (a) M = H, X = 0.2; (b) M = Na, X = 0.2; (c) M = Na, X = 0.5; (d) M = H, X = 0.5.

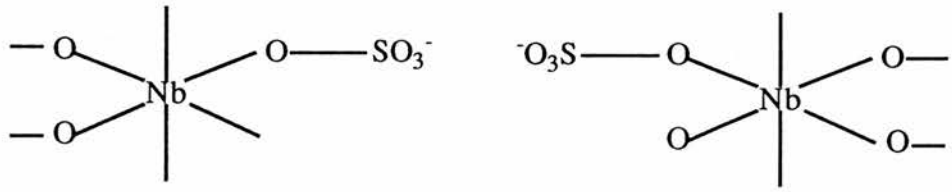

Because of the very fast gelation time of the niobium chloroethoxide solutions in the presence of sulphuric acid, it was possible, by the use of an acid catalyst such as sulphuric acid, to create films of soft hydrated niobium oxide gel for use as an electrode. This process is discussed in more detail in the next chapter.

3.6 Conclusions

The products and mechanisms for the hydrolysis and gelation of niobium chloroalkoxide solutions have been investigated. We have shown that the product of hydrolysis and gelation is hydrated Nb_2O_5 rather than $NbCl_2(OH)_3$ as previously proposed. We have also shown that the mechanism for hydrolysis and gelation can be qualitatively explained in terms of the concentration of the niobium species, the ratio of chloride ions present to niobium and the pKa's of the alcohols. Thus the observed trend that the rate of gelation decreases as the concentration of niobium in a given alcohol decreases is due to the dilution of niobium species making it harder to form a colloidal network. Secondly, the apparent dependence of the gel time with H_2O:Nb is in fact due to the ratio of free chloride ion concentration to the niobium concentration. As the H_2O:Nb ratio increases, the rate of chlorination increases, slowing the hydrolysis of the niobium species. Thirdly, the observed trend that the rate of gelation increases as the size of the alcohol increases is due to the increase in pKa values with increasing size of the alcohols. This means that the smaller the alcohol, the greater the alcolation occurring and thus the slower the hydrolysis of the niobium species. Finally, the catalytic properties of H_2SO_4 and Na_2SO_4 have been examined and indicate that SO_4^{2-} is a powerful network former which increases the rate of hydrolysis and gelation of niobium chloroalkoxide solutions.

References

1. C.J. Brinker, G.W. Scherer,"Sol-Gel Science", Academic Press, 1990.
2. J. Livage, M. Henry, C. Sanchez, "Sol-Gel Chemistry of Transition Metal Oxides" in *Progress in Solid State Chem.*, 1988,**18**, p259-342.
3. J. Livage, M. Henry, "Ultra Structure Processing of Advanced Ceramics", Eds J.D.Mackenzie, D.R. Ulrich, Wiley, New York, 1988 ,p183.
4. C. Sanchez, J. Livage, M. Henry, F. Babonneau, *J. Non-Cryst. Solids*, 1988, **100**, 65.
5. D.C. Bradley, *Coord. Chem. Rev.*, 1967, **2**, 299.
6. C. Alquier, M.T. Vandenborne, M. Henry, *J. Non-Cryst. Solids*, 1986, **79**, 383.
7. B. Morosin, P.S. Peercy, *Chem. Phys. Lett.*, 1976, **40**, 263.
8. P. Griesmor, G. Papin, C. Sanchez, J. Livage, *Chem. Mater.*, 1991, **3**, 335.
9. A.I. Vogel "Textbook of Quantitative Inorganic Analysis", Longman, 1971.
10. L.W. Kelts, N.J. Armstrong, "Better Ceramics Through Chem. III", eds C.J. Brinker, D. E. Clark, D. R. Ulrich, Mat. Res. Soc. Pittsburgh, 1988, p519.
11. A.G. Williams, L.V. Interante,"Better Ceramics Through Chem. I", eds C.J. Brinker, D. E. Clark, D. R. Ulrich, North Holland, N.Y.,1984, p151.
12. C.V. Edney, R.A. Condrate Sr., W.B. Crandell, M.E. Washburn, *Mat. Lett.*, 1987, **5**, 463.
13. D.H. Solomon, "Step Growth Polymerization", Vol. 3, ed. D.H. Solomon, Marcel Dekker, New York, 1972, p7.
14. E.A. Barringer, H.K. Bowen, *Langmuir*, 1985, **1**, 414.
15. E.A. Barringer, H.K. Bowen, *Langmuir*, 1985, **1**, 420.
16. B.J. Inglebrethsen, E. Matjevic, *J. Colloid Interface Sci.*, 1984, **100**, 1.
17. R.W. Hartel, K.A. Berglurd,"Better Ceramics Through Chem. II", eds C.J. Brinker, D. E. Clark, D. R. Ulrich, Mat. Res. Soc. Pittsburgh, 1986, p633.
18. M.F. Bechtold, W. Mahler, R.A. Schunn, *J. Polym. Sci. Polym. Ed.*, 1980, **18**, 2823.
19. R.W. Adams, E. Bishop, R.L. Martin, G. Winter., *Aust. J. Chem.*, 1966, **19**, 207.

20. R.A. Assink, B.D. Kay, *J. Non-Cryst. Solids*, 1988, **99**, 359.

21. B.D. Kay, R.A. Assink, *J. Non-Cryst. Solids*, 1988, **104**, 112.

22. G. Orcel, L. Hench, *J. Non-Cryst. Solids*, 1986, **79**, 177.

23. D. Kundi, D.Ganguli, *J. Mater. Sci. Lett.*, 1986, **5**, 293.

24. F.A. Cotton, G. Wilkinson, "Advanced Inorganic Chemistry", J. Wiley, Chichester, 1988, p788.

25. D.C. Bradley, B.N. Chakravarty, W. Wardlaw, *J. Chem. Soc.*,1956, 2381.

26. T. Boyd, *J. Polym. Sci.*, 1951, **7**, 591.

27. N.M.S. Culliane, J. Chard, G.F.Price, B.B. Millward, G. Langlois, *J. Appl. Chem.*, 1951, **1**, 400.

28. S.G. Wilkinson, "Comprehensive Organic Chemistry" Vol.1, eds D. Barton, W.D. Ollis, Pergamon, 1979, p584.

29. "Handbook of Chemistry and Physics", Vol. 56, ed R.C. Weast, C.R.C. Press, Cleveland, 1975, pB67-160.

Chapter 4

Techniques for Film Formation of Nb_2O_5

Introduction

4.0 Drying - Shrinkage and Cracking

The process of drying a porous material can be divided into four stages:[1]

(1) the constant rate period, (2) the critical point, (3) the first falling rate period, (4) second falling rate period. These are described below and shown graphically in Fig. 4.1.

(1) The Constant Rate Period (CRP)

The body shrinks by the volume of liquid lost through evaporation. In alcohol/water gels, the alcohol evaporates preferentially from the pores, leading to a concentration gradient of alcohol in water. This gradient creates osmotic forces which induce the inter-diffusion of the liquids within the gel. The liquid/ vapour interface remains at the exterior surface of the gel network, and so, in order to decrease in size, the gel network is "drawn" into the liquid by capillary and osmotic forces. However, whilst the solid surfaces of the gel come together, electrostatic repulsion, hydration forces and solvent structure resist contraction of the gel and so, in an attempt to allow the surfaces to move apart, more pore liquid diffuses from the interior to the exterior and is lost by evaporation. This cycle continues until the critical point:-

(2) Critical Point

When the critical point is reached, shrinkage of the gel stops and cracking is most likely to occur, the reason for this being that during the CRP the capillary tension developed in the liquid as it evaporates is countered by the contraction of the gel. This keeps stress on the gel to a minimum and the radii of the liquid menisci at the surface larger than the pore radii. However the gel cannot carry on shrinking indefinitely, because it stiffens as it shrinks. This causes the stress within the gel to rise and the radii of the menisci at the surface to shrink since interior liquid is lost by evaporation and the lost volume is not fully countered by a decrease in gel volume. At the critical point the radii of the menisci become equal to that of the pore radii , the

CRP ends and the liquid recedes into the gel. The tension in a liquid (P) is related to the radius of curvature (r) of the meniscus by:[1]

$$P = -2\gamma(r)^{-1} \qquad (4.1)$$

where γ is the liquid /vapour interfacial energy.

This means that for gels with small pores, the stresses upon the network, whilst the liquid recedes into the gel, can exceed the strength of the network. Pressure gradients develop through the thickness of the gel, such that the gel is more compressed at the exterior than the interior and thus the strain causes cracking.

(3) First Falling Rate Period (FRP1)

The liquid recedes into the interior of the gel, creating air filled pores near the surface. A continuous liquid film on the pore walls supports flow to the exterior from the interior so the evaporation continues from the surface of the body.

(4) Second Falling Rate Period (FRP2)

Liquid is trapped in pockets inside the gel, drying can only proceed by evaporation of the liquid within the body and diffusion of the vapour to the outside.

Fig. 4.1

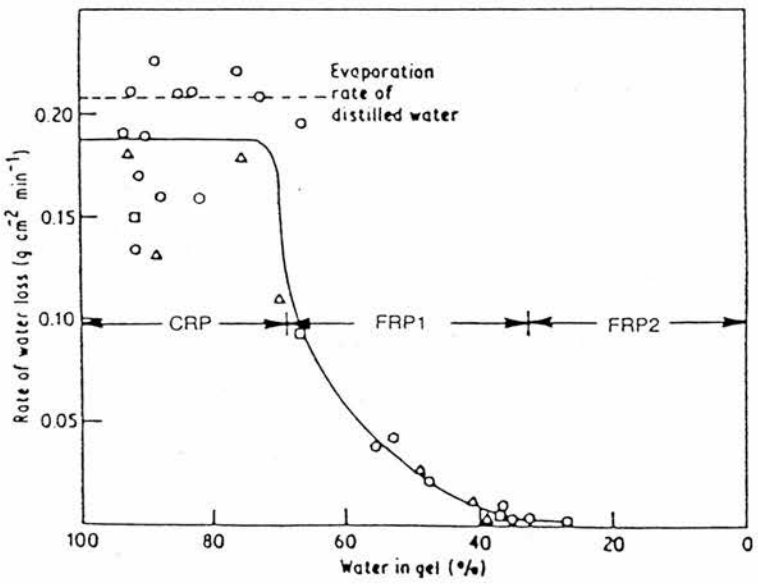

Fig. 4.1 Rate of water loss from alumina gel vs water content of gel for various initial thicknesses (o 7.5;○3.9;□1.8;Δ 0.8 mm) showing the CRP, FRP1 and FRP2 stages. Taken from ref.(1) p455.

4.1 Avoiding Fracture

4.1.1 Thin Film Production

It is well known that sol-gel cast thin films (thickness<0.5μm), upon drying, form crackless ceramics. The explanation for this fascinating observation is that the energy that drives crack growth in a solid comes from the relief of stress in a volume proportional to the size of the original flaw, whereas the energy invested in growing the crack is proportional to the surface area created, thus in thin films the surface to volume ratio becomes a barrier to the growth of the crack. Thouless [2] has shown (for the system shown in Fig. 4.2) that the energy release rate (G) for such flaws is approximately proportional to the thickness of the film (L) ie. G~L (when R/a =1). The stress intensity (K) at the tip of the crack is given by;

$$K \alpha G^{1/2} \alpha L^{1/2} \qquad (4.2)$$

Therefore as $L \rightarrow 0$, K inevitably falls below the critical stress intensity of the material K_c, and it appears that this point is reached at ~1μm for most films. Thus films less than 1μm thick do not crack upon drying. A commonly used technique to form such films is that of spin coating.

Bornside et al[3] divide the technique of spin coating into 4 stages; deposition, spin up , spin off, and evaporation (see Fig. 4.3) although evaporation also occurs during the other three stages. An excess of liquid is applied to the substrate surface during the deposition stage. In the spin up stage, this liquid flows radially outward, and then during the spin off, leaves as droplets. The rate of removal of excess liquid decreases as the film thins, due to the increased flow resistance and an increased viscosity due to the concentration of non-volatile components. During the final stage, evaporation is the primary mechanism of thinning. Spin coating has the advantage of producing uniformly thick films during spin off. It was felt that it would not be hard to produce films of Nb_2O_5 of <0.5μm thickness for use in electrochemical experiments, by application of a spin coating technique, and this indeed proved to be the case.

4.1.2 Thick Film Processing Techniques

Traditionally to make thicker crack-free films a number of methods have been employed. Firstly, multiple 0.5μm layers may be built up on top of each other by, for example, spin coating. Secondly, thick films may be created as one layer and then dried on a moving belt

Fig. 4.2

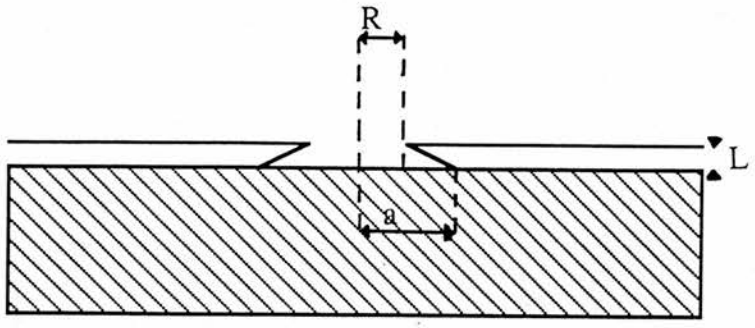

Pin hole of radius, R, in film extends to radius, a, along interface. Film thickness, L, is much less than the thickness of the substrate. The flaw propagates by peeling (a grows, R fixed).

Fig 4.3

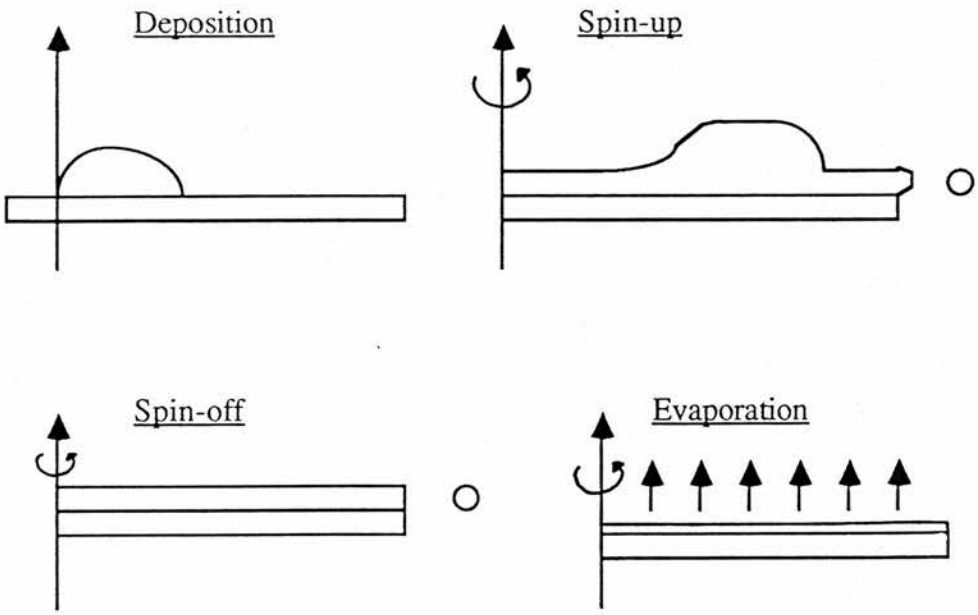

Stages of the spin-coating process

with a stream of air flowing in the opposite direction to the belt. The air is saturated with the same solvent used to prepare the gel.[4] This reduces capillary forces and hence differential shrinkage and cracking. However both these methods are expensive and lead to films which are prone to cracking. Thirdly, use of supercritical drying, whereby the thick films are subjected to temperatures and pressures above the critical temperature and pressure of the pore liquid. This has been successfully used on many alkoxide systems (Al, Ti, Ni, Fe, Mg, Zr).[5-7] Here there is no liquid vapour interface and no capillary pressure, and so drying proceeds without cracking to form an aerogel. However the aerogels collapse upon immersion in a liquid.

4.1.3 Chemical Additives

Chemical additives can be used to hinder crack propagation within gels and can be divided into three types:

a) Surfactants, that are added to the pore liquid to reduce interfacial energy and thus decrease capillary stress. They have been shown to reduce cracking in alkoxide derived gels.[8]

b)Drying control chemical additives (DCCA), such as formamide, added to the precursor solvent, which produce larger and more uniform pore size and hence reduce capillary stress. However formamide is difficult to remove from the gel and often causes bloating and subsequent cracking.[9-14]

c)"Plasticizers" such as glycerol,[15] which when added to the precursor solvent reduce capillary pressure and are not evaporated, but are retained in the gel, even in the smallest pores, and provide sufficient compliance (rubberiness) to prevent fracture. Similar work has been done by Schmidt[16] on silicon systems and Schlichting[17] on metal alkoxides, where the plasticizer was incorporated onto the metal and remained unhydrolysed during drying, allowing for a rubbery film to form intact.

This chapter describes the methods investigated in order to be able to form both thick and thin films of Nb_2O_5 for use in electrochemical studies. These include the use of spin coating techniques to form crack-free thin films of Nb_2O_5 as well as the investigation of a number of different chemical additives to ascertain whether they could cause the crack-free drying of niobium oxide monoliths and thick films.

4.2 Spin Coating

4.2.1 Thin Films of Nb_2O_5

Thin films of Nb_2O_5 were produced by applying 50µl drops of 0.05 mol dm^{-3} solution of $(NbCl_5)_2$ in EtOH to 5 x 1 x 0.3 cm ITO glass electrodes. The electrodes were then spun at 2000 rpm for 2 minutes and finally dried at 393K for 2 hours. SEM revealed that the films produced were of the order of 0.1µm thick and crackless, and hence could be used in the electrochemical experiments. Measurements of film weight gave film densities in the region of 3.9-4.1 g cm^{-3}. This is close to the density of pure Nb_2O_5 powder (4.47 g cm^{-3}) and indicates a very high Nb_2O_5 composition in a dense and glass-like film. CO_2 pore analysis (267K) showed the films had no significant microporous structure.

4.2.2 Thick Films of Nb_2O_5

Having successfully created thin films of Nb_2O_5, we attempted to form thick (~5µm) uniform films of Nb_2O_5 in order to increase the optical densities. In order to create uniform films of 5 µm thickness, reproducibly, 50µm drops of 0.5 mol dm^{-3} solution of $(NbCl_5)_2$ in EtOH were applied to 5 x 1 x 0.3 cm ITO glass electrodes and spun at 1250 rpm for 3 seconds. The electrodes were then immediately placed in 1 mol dm^{-3} H_2SO_4 for 1 minute for complete hydrolysis and gelation. The thickness of the films was measured by both SEM and micrometer methods. Because of the short spin time, the spin coating had only progressed to the spin off stage and a residual ridge of ca. 10-15µm thickness was observed at the very edges of the film. These edges were stripped off and the exposed ITO glass coated with silicone grease, to give a thick (5 µm) Nb_2O_5 film for use in the electrochemical experiments.

Upon drying of these thick films (5-10 µm) at room temperature it was found that substantial cracking and peeling occurred, pulling the film from the electrode. Electron microscopy revealed that the gels had suffered shrinkage and cracking to give isolated islands of *ca.*10 µm in diameter. It is known that such shrinkage in dried sol-gel processed films is caused by capillary stresses due to surface tension. Thus, although it was possible to create

5μm thick films of soft hydrated niobium oxide, they dried within a few hours to form a cracked gel. Because of the lack of durability of the thick films the use of chemical additives was investigated. It was hoped that these additives might aid the formation of more durable thick niobium oxide or niobium oxide like films, that would not crack upon drying.

4.3 Potential Chemical Additives

4.3.1 Ethylene Glycol

Alquier et al[18] claimed that using ethylene glycol as the substituting alcohol gave 2 reactions upon addition to $NbCl_5$:- an intramolecular reaction to give a bidentate glycerol ligand (X):

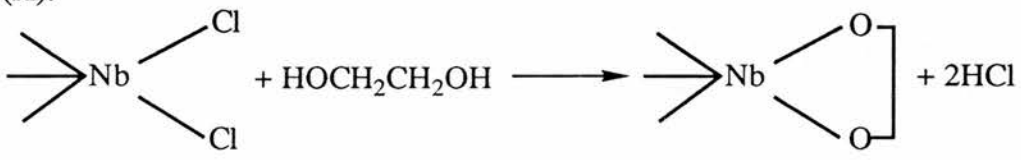

(4.3)

(X)

and an intermolecular reaction (crosslinking):

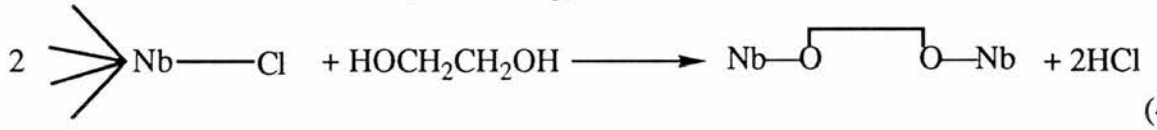

(4.4)

They stated that eq(4.4) would occur without the addition of water, giving a mixed mineral organic polymer, but that crosslinking via X would only occur if water was present, by the following reaction;

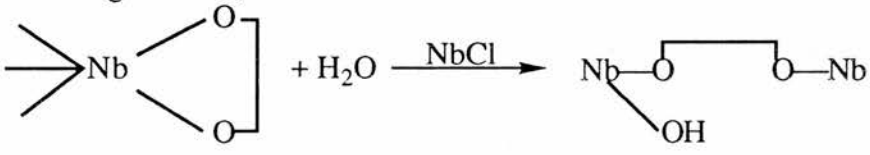

(4.5)

In both cases they further claimed that the gels formed upon hydrolysis led to monoliths formed through crosslinking reactions. If this was the case then ethylene glycol was acting as a plasticizer, forming a more compliant, but more strongly crosslinked gel which dried without cracking and would be ideal for film formation. To investigate these claims a 0.5 mol dm^{-3} solution of $(NbCl_5)_2$ in ethylene glycol was prepared, reacted with various molar equivalents of water and dried as both film and monolith at three different temperatures. The results are shown in Table 4.1

Table 4.1

Gelation Products of 0.5 mol dm^{-3} $(NbCl_5)_2$ in Ethylene Glycol, dried as Monoliths (M) and Films (F) at the Specified Temperature			
Ratio H_2O: Nb	product at t=75 mins F,M 293K	product at t=2 weeks F,M 293K	product at t=1 hour F, 313 and 333 K
0:1	white liquid	cracked glass	cracked glass
10:1	white viscous liquid	cracked glass	cracked glass
32:1	white gel	cracked glass	cracked glass

Actual gelation time for the 32:1 H_2O:Nb solution is ~ 75 mins. Immersion of the 10:1 H_2O: Nb ratio films in 1.0 mol dm^{-3} sulphuric acid caused immediate gelation, however the films formed were uneven and "stringy" and dried at 293K to give cracked glasses. Similarly, addition of 1.0 mol dm^{-3} hydrochloric acid to the 10:1 H_2O: Nb ratio monolith solutions also gave cracked glasses upon drying at 293K.

It would appear from our work that niobium chloroethyleneglycoxides do not hydrolyse and gel to give uncracked monoliths. Our analysis of the gels showed that, upon addition of water, the ethylene glycol is hydrolysed off to give hydrated niobium oxide (see section 3.3.2), rather than the intermolecular bonded species claimed by Alquier et al[18] in eq(4.5). The hydrolysis to niobium oxide is not surprising as it is observed for the other alcohols as well. Thus, it seems that alcolation via intermolecular bonding during hydrolysis, as proposed by Alquier et al, to give a crosslinked monolith is unlikely. These gels were checked for electrochemical activity (see chapter 5).

4.3.2 Diacids

As ethylene glycol had not proved successful as a plasticizer and anti-cracking agent, it was felt that the addition of a chelating group, such as a CO_2^- group, which would remain bound to the niobium after hydrolysis might work. It was hoped that the diacids would bind via CO_2^- groups to form intermolecular species like those claimed for ethylene glycol. They might also act as DCCA's and produce a more uniform pore size, as the diacids would be able

to hydrogen bond across the diameters of the pores, thus regulating size and producing a counter force to drying tension. Unfortunately this did not prove to be the case.

Two diacids were tried: adipic acid $(CH_2CH_2\ COOH)_2$ and 1-10 decanedicarboxylic acid. Saturated solutions of both acids in water and 50/50 water/ethanol were prepared and mixed with 0.5 and 0.2 mol dm^{-3} solutions of $(NbCl_5)_2$ in ethanol in a 10:1 ratio H_2O:Nb to give films and monoliths. However, in all cases, drying at 293K gave cracked films after ~6 hours and broken glass monoliths after two weeks.

4.3.3 Bis-cyclopentadienylniobium (V) chloride ($NbCl_3Cp_2$)

The literature was searched to try and find a niobium compound which contained nonhydrolysable groups. These nonhydrolysable groups might act as bound plasticizers and reduce capillary pressure and perhaps produce a more uniform pore size. The only compound which appeared to have this property was $NbCl_3Cp_2$, which Wilkinson and Birmingham claimed[19] reacted with water to form $NbCl_2Cp_2OH$. If this was indeed the case then the cyclopentadiene groups had the potential of acting as bound plasticizers. However, upon reacting 0.5ml aliquots of a saturated green/brown solution of $NbCl_3Cp_2$ in methanol (~0.05 mol dm^{-3}) with 0.5ml volumes of H_2O, 1 mol dm^{-3} H_2SO_4, and 0.1 mol dm^{-3} NaOH only cracked solids were formed. Both the H_2O and NaOH mixtures gave a yellow solution which, when left for 72 hours, gave a cracked yellow/brown "mud". The acid solution immediately gave a gel which also gave a cracked yellow/brown "mud" after 72 hours at room temperature. Reacting the $NbCl_3Cp_2$ solid with excess water gave a white precipitate after 72 hours.

4.3.4 Miscellaneous Chemical Modifications

The use of amides, such as formamide and DMF, as drying control agents [9-14] could not be overlooked and so three solutions of 1.25 mol dm^{-3} $(NbCl_5)_2$ in formamide, methyl formamide and dimethylformamide were prepared. Likewise, the possibility that the lowering of the quantity and type of solvent in the gel might aid crack-free monolith formation, led to the preparation of solid $(Nb(OPr^i)_5)_2$ and $(NbCl_5)_2$, 6 and 3 mol dm^{-3} $(Nb(OEt)_5)_2$ in EtOH and pure liquid $(Nb(OEt)_5)_2$ and $Nb(OPr^i)_4Acac$. The lowering of the quantity of solvent would

hopefully produce denser gels that would not undergo as great a shrinkage as the ones formed previously, and thus not be subjected to as great a drying stress.

These nine systems were then reacted with i) 5 eq. of H_2O and ii) 5 eq. H_2O + $^1/_4$ eq. formamide, stirred vigorously for 5 seconds and allowed to gel. After drying at room temperature for 2 weeks all had formed cracked glasses. The inability to form uncracked monoliths by reducing the quantity and type of solvent implies that even if denser gels were formed, the attached ligands did not, in any way, increase the size and uniformity of the pore radii and so the stresses felt at the critical point of drying still pulled the gels apart. The failure of the amide solutions to form crackfree monoliths is surprising and harder to explain. They either did not modify the pores enough or it is possible that the lab air was too moist as the crackfree silica gel monoliths processed with DMF cracked on exposure to water vapour.[11,12] These amide processed gels would have warranted further investigation had it not been for the success of other systems.

4.4 Use of Organically Modified Silanes

4.4.1 Mixed Silicone/NbO Gels

Over the past few years research has been conducted into the properties of a new group of silanes- ORMOSILS, ie.Organically Modified Silanes, which have a non hydrolysable organic group attached to the silicon. This non-hydrolysable group is very important in the drying properties of the gels derived from these materials because it acts as a bound plasticizer. "Glymo", 3-(glycidyloxypropyl)trimethoxysilane (see below) is an example.

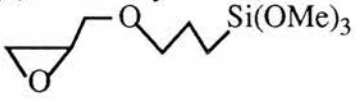

(4.6)

Glymo has been developed by Schmidt et al[16] for the production of new contact lens materials[20] and membranes on porous supports.[21] Work done by our group has shown that durable, porous, inorganic/organic coatings can be prepared by spin coating, dip coating, or painting methods with glymo.[22] The hydrolysis and condensation of glymo occurs in methanol/water solutions, is catalysed by acids and gives, on drying, gels which are not strictly glasses but rather a type of polymer (silicone).

If excess water is added during hydrolysis then the reaction is;

$$RSi(OMe)_3 + H_2O \rightarrow RSi(OH)_3 + 3MeOH \quad (4.7)$$

$$RSi(OH)_3 \rightarrow (RSiO_{1.5})_n + 1.5H_2O \quad (4.8)$$

Research on glymo hydrolysis[22] has shown that the non hydrolysable epoxide group acts as a drying control agent in that it reduces surface tension stresses within the pores, by increasing pore size and by ensuring an even distribution of pores and pore radii throughout the condensing gel enabling thick coatings to be made which were crackfree and highly durable. This work also showed that the optimum temperature for hydrolysis and condensation is 353K. Higher temperatures lead to bubbles of MeOH and H_2O vapour trapped in the polymer; lower temperatures lead to longer heating times for full gelation.

Orgaz and Rawson[23] have shown it is possible to create mixed SiO/MO_x glasses for M = Co, Cu, Cr. Likewise, Schmidt et al [24] have prepared Fe and V containing ormosil gels. Thus it seemed possible that if glymo and the niobium chloroalkoxides could be mixed together and then hydrolysed they might form a mixed, crosslinked polymer of the type;

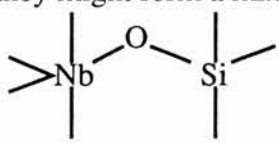

(4.9)

This copolymer would hopefully have the crackfree properties of the glymo coupled with the electrochromic properties of the niobium oxide. Initial experiments were conducted to see if mixed hydrolysis would work using 0.35 mol dm^{-3} solutions of $(NbCl_5)_2$ in 80%MeOH/20%^{i}PrOH (NbClOR) mixed with various quantities of glymo, water, methanol and phosphoric acid and dried at 293K or 353K. The results are summarized in Table 4.2.

Table 4.2 shows that the normal hydrolysis of glymo, requiring a MeOH/water mixture, due to glymo's immiscibility with water, was not required since the alcohol in the $NbCl_5$ solution acts as a solubility enhancer. In addition, the phosphoric acid catalyst was unnecessary since HCl is present in the $NbCl_5$ solution. It was decided to do a detailed survey of the types of gels formed, depending upon the Nb:Si:H_2O molar ratios, in order to find the tolerances of the system. In this series of experiments 0.25 mol dm^{-3} and 0.5 mol dm^{-3} $(NbCl_5)_2$ solutions in ethanol were mixed with glymo and water, heated for 18 hours at 353K

Table 4.2

NbClOR ml	H_2O ml	H_3PO_4 ml	MeOH ml	Glymo ml	353K	Gel Description, at specified time after mixing
1	1	0.04	0.16	4		3 days clear hard polymer
1	3 to 10	0.08	0.16	4		3 days clear viscous liquid
1	1 to 10	0.04	0.16	4	✔	2 to 4 hrs clear yellow elastic polymer
1	1			4		3 days clear colourless polymer
1	3 to 10			4		3 days viscous clear liquid
1	1 to 10			4	✔	2 to 4 hrs clear yellow elastic polymer
1	1	0.04		1 to 2	✔	1 hr clear yellow elastic polymer
1	1	0.04		0.5	✔	0.5 hr cracked white polymer

and the resulting polymer examined. The initial percentage moles of Nb, Si and water were calculated and the type of polymer plotted on a 3 way graph shown in Fig. 4.4.

It is clear from Fig. 4.4 that 3 main zones exist:-

i) Nb>Si leading to clusters of niobium oxide within a Si-O polymer which resemble a sand and glue mixture;

ii)Si>Nb forming clear crack free polymers;

iii)Nb/Si~1 leading to clear but bubbled and cracked polymers.

The Nb>Si polymers were undesirable since flaws caused by the niobium oxide clusters lead to cracking of the polymers. Likewise Si>Nb did not appear promising as SiO_2 is not an electrochromic material. Ideally we required a Nb/Si~1 ratio which produced bubble and crack free polymers. Furthermore, the stoichiometry of hydrolysis requires that at least 80% of the molar species had to be water for complete hydrolysis to be assured. As the bubbling implied that the reactants had been heated too hard, the experiment was repeated at the lower temperatures of 343K and 323K, using a 0.25 mol dm^{-3} $(NbCl_5)_2$ solution in ethanol, mixed

Fig. 4.4

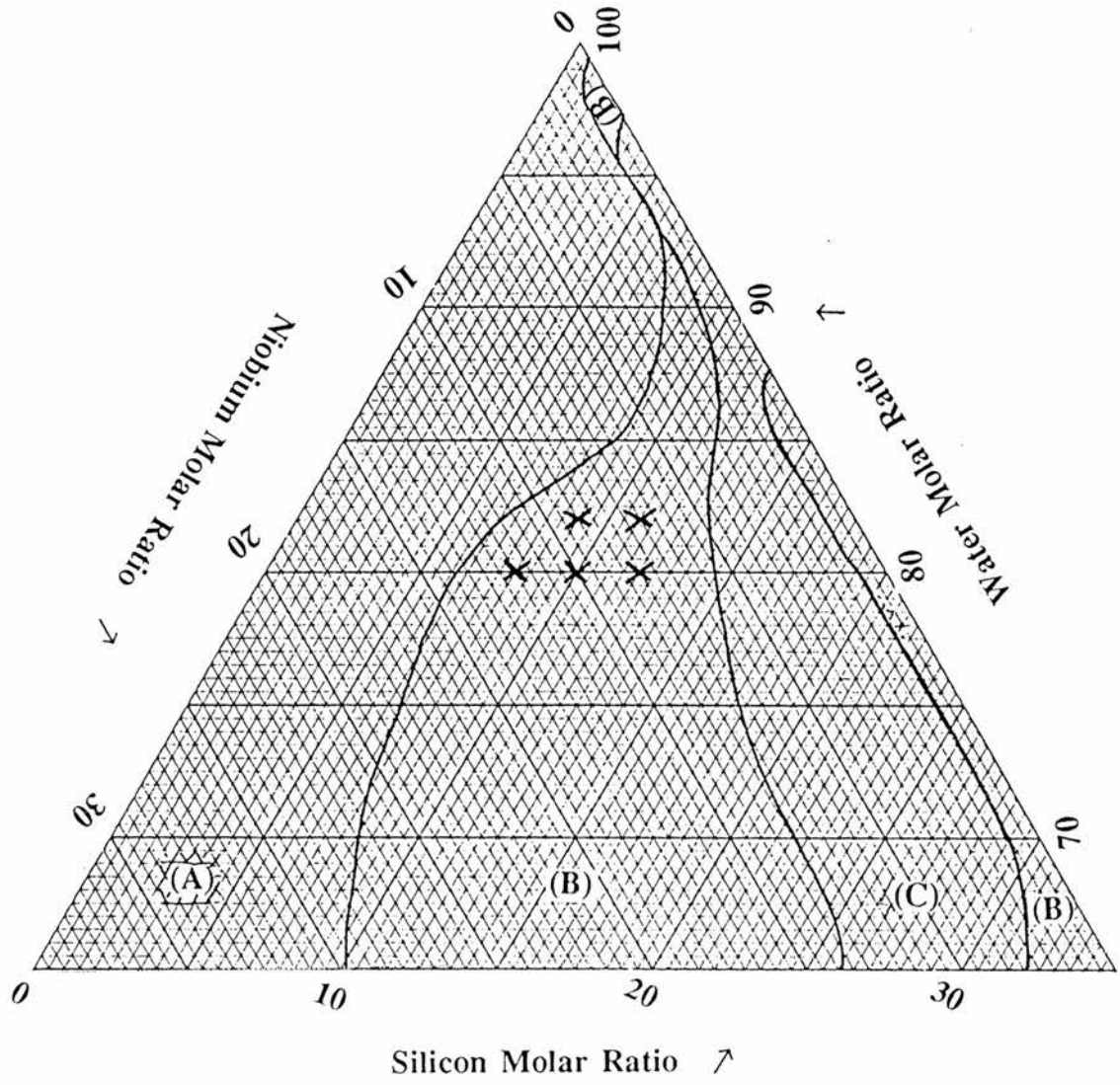

Fig. 4.4 Three way plot of initial niobium, silicon and water molar ratios and the type of polymer formed (A, B or C) after 18 hours at 353K. (A) is clusters of niobium oxide in polymer; (B) is clear hard gel, but cracked or bubbled; (C) clear hard gel.

with H_2O and glymo at the percentage molarities marked (by **X**) on Fig. 4.4. This time though both monoliths and hand dipped films were prepared.

All the samples in the flasks at 343K contained bubbles whilst the samples in the flasks at 323K went cloudy after a week. A possible explanation for this is that at the lower temperatures, glymo fails to fully hydrolyse and continues to do so once removed from the oven. Thus hydrolysis, due to trapped H_2O and atmospheric moisture, could cause local expansion in the gel and hence flaws. If these flaws were small enough it is possible for them to scatter light. However all the films with a Nb percentage molarity < 10% were uncracked and none went cloudy. The FTIR data for the 9:9:82 polymer, shows that full hydrolysis has occurred since no Si-OR peaks (at 850-750 cm^{-1} and 1460 cm^{-1}), no Nb-OR peaks (at 580 cm^{-1}) nor any peaks due to free alcohol are observed.

Mixed silicone/NbO polymer electrodes were obtained by mixing the required volumes of niobium chloroethoxide solutions, glymo and water, and then spreading a 6µl drop of the resulting solution onto 2 cm^2 of an ITO glass electrode and heating in the oven. A variety of temperatures higher than 323K and two different molarities of $(NbCl_5)_2$ in EtOH were used to find the tolerances for drying without cracking for the 9:9:82 and 8:12:80 systems. It was hoped to produce electrodes which would prove resilient to electrochemical cycling in organic solvents. Table 4.3 contains a summary of these results.

Table 4.3

mole ratio Nb:Si:H_2O	$(NbCl_5)_2$ molarity mol dm^{-3}	oven temperature K	Heating time (hr)	Cracked film ?
9:9:82	0.2	335	24	
9:9:82	0.5	335	24	✔
9:9:82	0.2	338	18	✔
9:9:82	0.2	353	18	✔
8:12:80	0.2	335	24	
8:12:80	0.5	335	24	✔
8:12:80	0.2	338	18	
8:12:80	0.2	353	18	

The films produced were ca. 20μm thick. Thus, to form uncracked films, it would appear that low heating temperatures are required, as well as a low molarity of $NbCl_5$ in EtOH. CO_2 pore analysis (267K) on these mixed NbO/silicone films showed them to be microporous, having a micropore volume of $0.053cm^3g^{-1}$ and a micropore area of $142m^2g^{-1}$. This is slightly lower than glymo films which were found to have a micropore volume of $0.086cm^3g^{-1}$ and a micropore area of $192m^2g^{-1}$. The glymo films and the mixed films have very similar modal pore diameters of 1.56nm and 1.50nm respectively. The uncracked mixed NbO/silicone films were tested for electrochromic properties and the results are discussed in chapter 5.

4.4.2 Composite Systems

As a final possible solution to the problem of thick niobium oxide films cracking upon drying, the possibility of producing a composite electrode was investigated. The hydrated Nb_2O_5 gel is porous and so it seemed likely that glymo, or a glymo/niobium alkoxide solution could be diffused into the Nb_2O_5 via the gel's pores and hydrolysed to form an interlocking framework. This flexible polymer framework would hopefully relieve the stress on the niobium oxide during drying to give a crack free film and yet still allow ion insertion into the niobium oxide to form a bronze.

Thick niobium oxide films were prepared and then these soft films were dipped in either a glymo/MeOH/ water mixture or a 5:13:82 Nb:Si:water mixture or a 9:9:82 Nb:Si:water mixture and spun again to remove excess second coating and then heated at 353K for 3 hours. Whilst the 9:9:82 second coated films always cracked and peeled even when heated at 315K, application of both the glymo/MeOH/ water and 5:13:82 Nb:Si:water mixtures produced uncracked composite films, which were tested for electrochromic properties (see chapter 5).

EDAX of the uncracked films showed that for the glymo and 5:13:82 mixture composites, Si had diffused all the way through the hydrated niobium oxide. The reason as to why the 9:9:82 films always cracked is unclear, but it could be due to the fact that this second coating failed to fully diffuse through the original gel film and hence the soft niobium oxide pulled away from the ITO upon drying. SEM of the films showed that they were ~5μm thick

Fig. 4.5

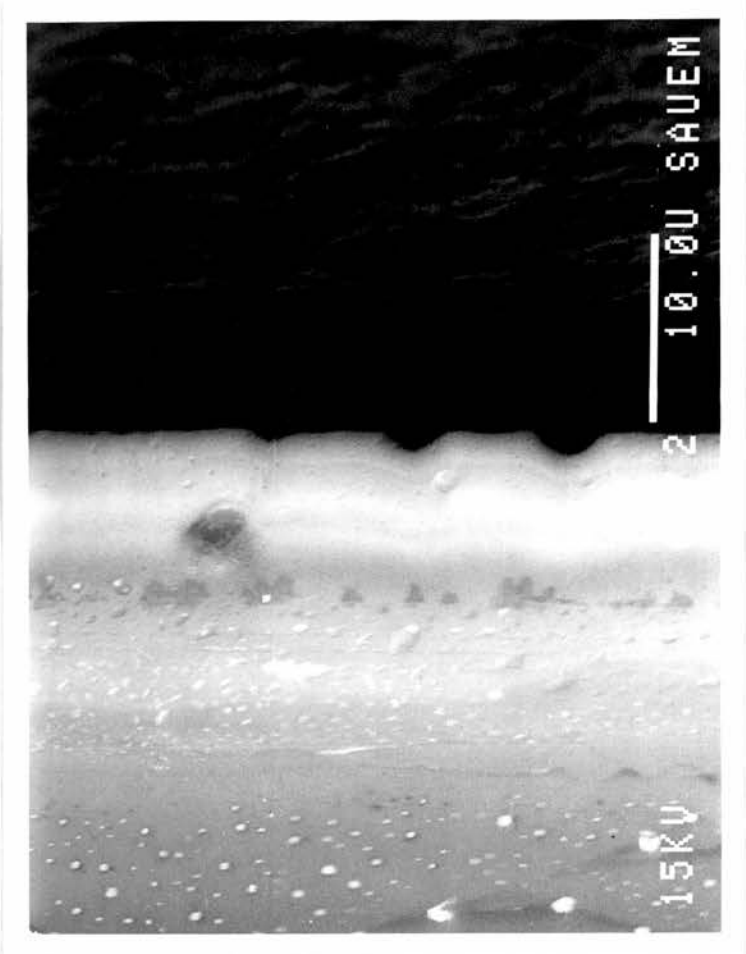

Fig. 4.5. SEM picture of the 5:13:82 composite film, edge on.

and a SEM picture of a 5:13:82 composite film, edge on, is shown in Fig.4.5. Both types of second coating were uncracked after 2 weeks at room temperature but after 4 weeks had cracked and peeled.

It would seem therefore that the overcoat layer of glymo composite did indeed reduce the drying stresses and give rise to a longer lived thick film. During drying the role of the glymo may be one or more of the following:-

(1) it provides flexibility during the drying process thus preventing large capillary forces from cracking the material;(2) the epoxide chains on the silicon may act as a hydrophobic barrier, forming less porous pore walls and thus trapping H_2O in the metal oxide and hence slowing the drying process;(3) It may act as a pore size regulator, creating more uniform pore sizes and hence lowering the cracking stress. Pore analysis on the mixed NbO/silicone films showed that they retained glymo gel's characteristics rather than niobium oxide, ie. they did not dry to give a nonmicroporous glass but a microporous gel. It seems reasonable to assume that the overcoat layer imparts this characteristic to the soft niobium oxide film and that the composite film dries to give a microporous gel, rather than a dense cracked glass. The diffusion data in chapter five tends to support this view.

4.5 Conclusions

It has been shown that it is possible to create uncracked 0.1μm thick films of Nb_2O_5 which have a high density and are not microporous for electrochemical testing. It is also possible to produce thicker, 5μm films, however these films are soft gels and crack within 4 hours on drying at 293K. More durable thick films can be prepared which do not crack immediately on drying at 293K by the application of a second Nb/silicone composite coating. This second coat retains the drying characteristics of its silicone component and produces microporous films. The Nb/silicone composite coating may also be applied to form thick durable microporous films it its own right. Furthermore, the use of chemical additives such as ethylene glycol and diacids to form crackfree films of Nb_2O_5 has been investigated but they were found not to hinder crack propagation.

References

1. "Sol-Gel Science", Eds C.J. Brinker, G.W. Scherer, Academic Press, 1990.
2. M.D. Thoules, *Acta. Metall.*, 1988, **36**, 3131.
3. D.E Bornside, C.W. Macosko, L.E. Scriven, *J. Imaging Tech.*, 1987, **13**, 122.
4. R.M. Guppy, A. Atkinson, "The Cracking Behaviour Of Sol-Gel Films", presented at Special Ceramics 9, Imperial College, London, 18-20 Dec. 1990.
5. S.S. Teichner in "Aerosols", ed J. Fricke, (Springer-Verlog, N.Y., 1986), p22-30.
6. S.S. Teichner, G.A. Nicholson, M.A. Vicarini, G.E.E. Gardis, *Adv. Colloid Interface Sci.*, 1976, **5**, 245.
7. H.D.Gesser, P.C. Goswami, *Chem. Rev.*, 1989, **89**, 765.
8. J. Zarzycki, M. Prassas, J. Pholippou, *J. Mater. Sci.*, 1982, **17**, 3371.
9. S.H.Wang, L.L. Hench,Better Ceramics Through Chem. I", eds C.J.Brinker, D. E. Clark, D. R. Ulrich, North Holland, N.Y.,1984, p71.
10. L.L. Hench, G. Orcel, "Better Ceramics Through Chem. I", eds C.J. Brinker, D.E. Clark, D. R. Ulrich, North Holland, N.Y.,1984, p79.
11. T. Adachi, S. Sakka, *J. Mater. Sci.*, 1987, **22**, 4407.
12. T. Adachi, S. Sakka, *J. Non-Cryst. Solids*, 1988, **99**, 118.
13. A.H. Boonstra, T.N.n. Bernards, J.J.T. Smits, *J. Non-Cryst. Solids*, 1989, **109**, 141.
14. L. Hench, G.Orcel, J.L. Nogues, "Better Ceramics Through Chem. III", eds C.J. Brinker, D. E. Clark, D. R. Ulrich, Mat. Res. Soc. Pittsburgh, 1988, p35.
15. S.M. Wolfrum, *J. Mater. Sci. Lett.*, 1987, **6**, 706.
16. H. Schmidt, G. Rinn, R. Nass, D. Sporn, "Better Ceramics Through Chem. III", eds C.J. Brinker, D. E. Clark, D. R. Ulrich, Mat. Res. Soc. Pittsburgh, 1988, p743.
17. J. Schlichting, *J. Non-Cryst. Solids*, 1984, **63**, 173.
18. C. Alquier, M.T. Vandenborne, M. Henry, *J. Non-Cryst. Solids*, 1986, **79**, 383.
19. G. Wilkinson, J.M. Birmingham, *J. Chem. Soc.*, 1954, 4281.
20. G. Phillipp, H. Schmidt, *J. Non-Cryst. Solids*, 1984, **63**, 283.
21. A. Kaiser, H.K. Schmidt, *J. Non-Cryst. Solids*, 1984, **63**, 261.

22. N. Young, J.A. Crayston, manuscript in preparation.

23. F. Orgaz, H. Rawson, *J. Non-Cryst. Solids*,1986, **82**, 378.

24. F. Hutter, H. Schmidt, H. Scholze, *J. Non-Cryst. Solids*, 1986, **82**, 373.

Chapter 5

Electrochromic Properties of Nb_2O_5 Films

5.0 Introduction

An electrochromic material is one in which a visible absorption band can be introduced reversibly by the passage of current through the material, or by application of an electric field. These materials are of interest for display devices.[1] A major requirement of an electrochromic material is that it exhibits mixed conduction, ie. both electronic and ionic conductivity. Typically a metal redox centre is generated by injecting electrons, and for charge neutrality to be preserved cations must be allowed into the material. Since it is usually the movement of ions which is rate-limiting, materials with fast ion conduction at room temperature are desired (usually with H^+, Li^+ or Na^+ ions).[2] Often such materials are amorphous and of low density so as to provide an open framework for rapid ionic diffusion. Amorphous materials also have the advantages of flexibility of composition, high concentrations of vacancies for ionic motion and generally are more easily prepared as the thin coatings necessary for display devices. Materials which have been investigated include WO_3,[3] Prussian Blue,[4] and organic molecules such as alkyl viologens.[5]

Whilst WO_3 has been extensively studied, other oxides, such as Nb_2O_5 have received much less attention. Thin Nb_2O_5 films have been prepared by thermal[6] (500 ^oC) or anodic[7] oxidation of the metal, and by oxidation of sputtered NbN_x.[8] Unfortunately the metal oxidation routes preclude the use of the electrochromic films in most display devices where the metal oxide is sandwiched between optically transparent electrodes; however, they can be used in reflectance mode. Finally, it is also possible to sputter Nb_2O_5 thin films.[9]

This chapter describes the properties of three new types of electrochromic Nb_2O_5 films obtained using the sol-gel method. The different procedures used to form these films are detailed in chapter 3. Sol-gel processing has the advantages of control of porosity and structure, convenience and the ability to coat large objects with adherent films.[10,11] The sol-gel method has already been successfully employed in the synthesis of V_2O_5, TiO_2[12] and WO_3[13]

electrochromic devices. However, the sol-gel process can only be used to make crack-free films of thickness ≤ 0.5 μm. Typical electrochromic efficiencies are 10 mC cm^{-2} for V_2O_5, corresponding to an optical density of ca 0.5 in a film of thickness 0.5μm.[12] For greater display densities a method for producing thick (5 μm), crack-free electrochromic films with fast response times would be desirable. This chapter reports the electrochromic properties of both thin film Nb_2O_5 electrodes and of thick-film Nb_2O_5 electrodes and the stabilisation of the latter by overcoating with a silicone based gel to give a more durable composite electrode. This composite is related to the organically modified ceramics or silicates (ORMOCERS or ORMOSILS) introduced by Schmidt et al.[14]

Results and Discussion

5.1Thick (>0.5μm) Films

5.1.1 Preparation of Nb_2O_5 Films

Nb_2O_5 films were prepared by the spin coating method onto ITO optically transparent electrodes of 1 mol dm^{-3} $NbCl_5$/EtOH solution which was subsequently hydrolysed in acid. The $NbCl_5$/EtOH solution has been shown to contain chiefly $NbCl_{5-x}(OEt)_x$ type species. Thus the hydrolysis follows:-

$$NbCl_x(OEt)_{5-x} + 5H_2O \rightarrow {}^1/_2Nb_2O_5 + (5-x)\,EtOH + xHCl \qquad (5.1)$$

X-Ray diffraction, EDAX (energy dispersive analysis by X rays), Cl^- and Nb analysis confirmed that the resulting film was hydrated amorphous Nb_2O_5.

Upon drying of these thick films (5-10 μm) at room temperature it was found that substantial cracking and peeling occurred, pulling the film from the electrode. Electron microscopy revealed that the gels had suffered shrinkage and cracking to give isolated islands of *ca.*10 μm in diameter (Fig. 5.1(a)). It is known that such shrinkage in dried sol-gel processed films is caused by capillary stresses due to surface tension.[10] For this reason the soft hydrated amorphous Nb_2O_5 films proved unstable to potential cycling in cells containing

Fig 5.1(a)

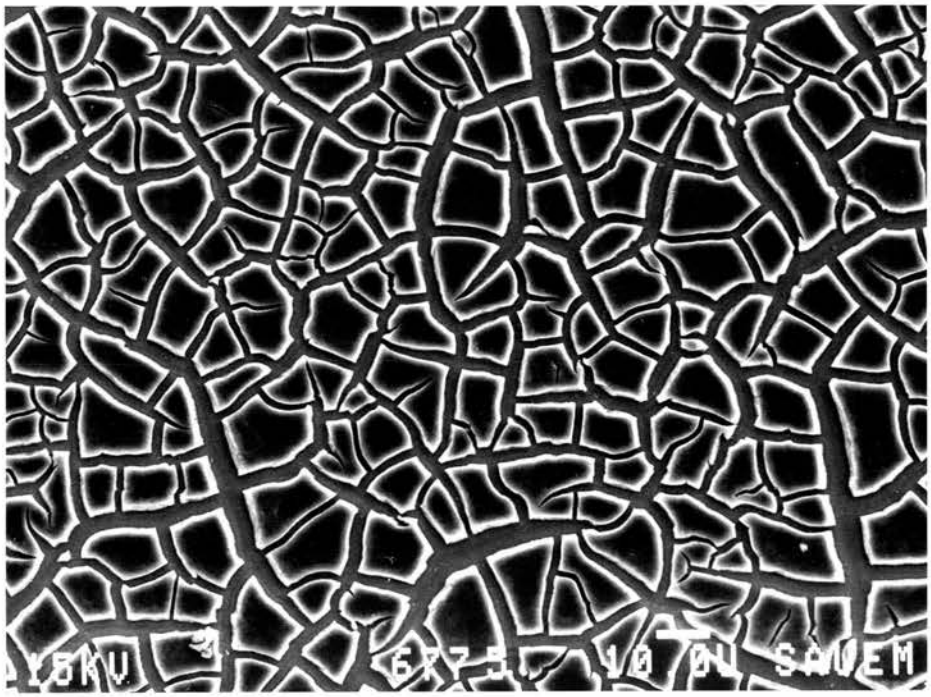

Fig 5.1(b)

Fig. 5.1. SEM photographs of (a) thick $Nb_2O_5.xH_2O$ film after drying at 293K for 4 hours; (b) thick $Nb_2O_5.xH_2O$ film after failure during electrochemical potential cycling (5 cycles) in 0.5 $LiClO_4$/MeCN.

non-aqueous solvent. SEM (scanning electron microscopy) upon cycled films that failed (Fig 5.1(b)) shows a similar set of cracking and islands of about 10 μm diameter to those found in the dried films. The films proved to be a little more stable when 1.0 mol dm^{-3} H_2SO_4 (aq) was used as the solvent/electrolyte.

In order to increase the longevity of the electrochromic films, several modifications of the procedure were attempted. (a) Using the method of Alquier et al[15], 0.5 mol dm^{-3} $(NbCl_5)_2$ in ethylene glycol was used as the sol precursor to gelation. While electrochromic films were produced with this method, their durability was actually less than that of the $Nb_2O_5.xH_2O$ films described above. These films are described in section 5.7. (b) Mixed NbO/silicone gels were produced by the addition of the trialkoxysilane, 3-glycidoxypropyltrimethoxysilane ("glymo") to the niobium chloroalkoxide precursor, (where the Si/Nb molar ratio ~1) followed by hydrolysis. No electrochromic response was observed for any of these films, however the microelectrode properties of some of these films are described in section 5.8. (c) Finally the composite system, described below, gave more robust electrochemically active films.

5.1.2 Preparation of Nb_2O_5 Films With Glymo Composite

A full range of composite molar ratios were tested for the second coating, as were spinning speeds and times; however, most of the films thus produced failed for a number of reasons:- reproducibility, film cracking and loss of electrochromic properties.

The thick Nb_2O_5 films previously described were prepared, excess water was gently blown off and while this film was still moist, the second coating of $Nb:Si:H_2O$ of 5:13:82 mol ratio solution was applied by dipping the electrode in the solution, spinning for 3 secs at 1250 rpm and dried at 60 °C for 3 hours. These films showed significantly greater durability in non-aqueous solvents but broke up on immersion in water/acid. The films were rougher in morphology (Fig. 5.2(a)) than the uncoated Nb_2O_5 films. EDAX revealed that the Si in the second coating had penetrated throughout the full 5 μm thickness of the film, thus we prefer to describe the electrode as a composite rather than a heterogeneous 2-layer structure. Electrochemical failure was accompanied by the same type of microcracking as in the uncoated

Fig. 5.2(a)

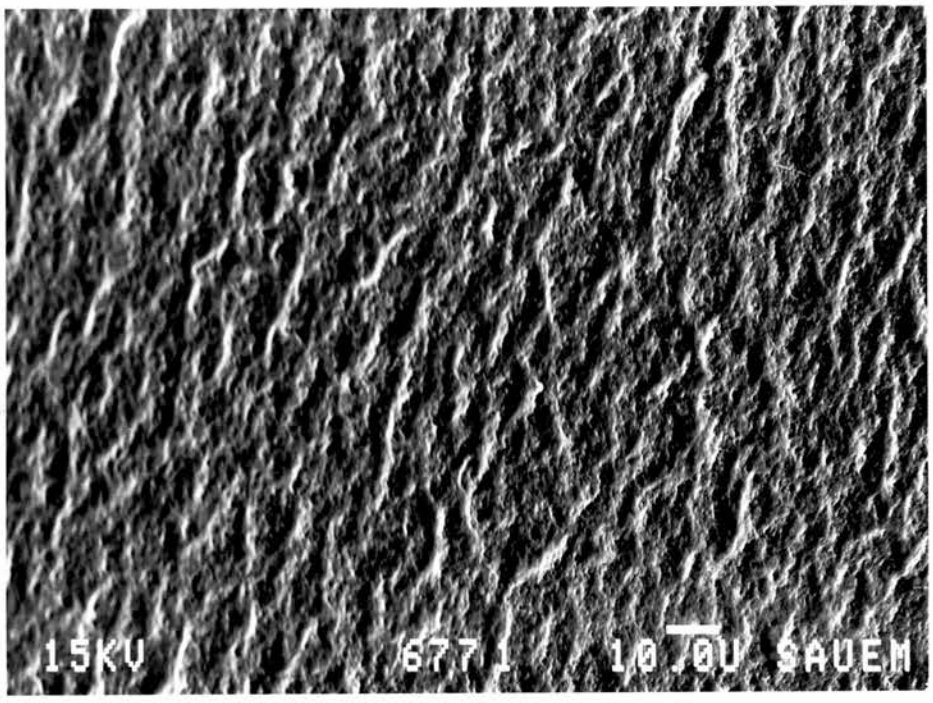

Fig. 5.2(b)

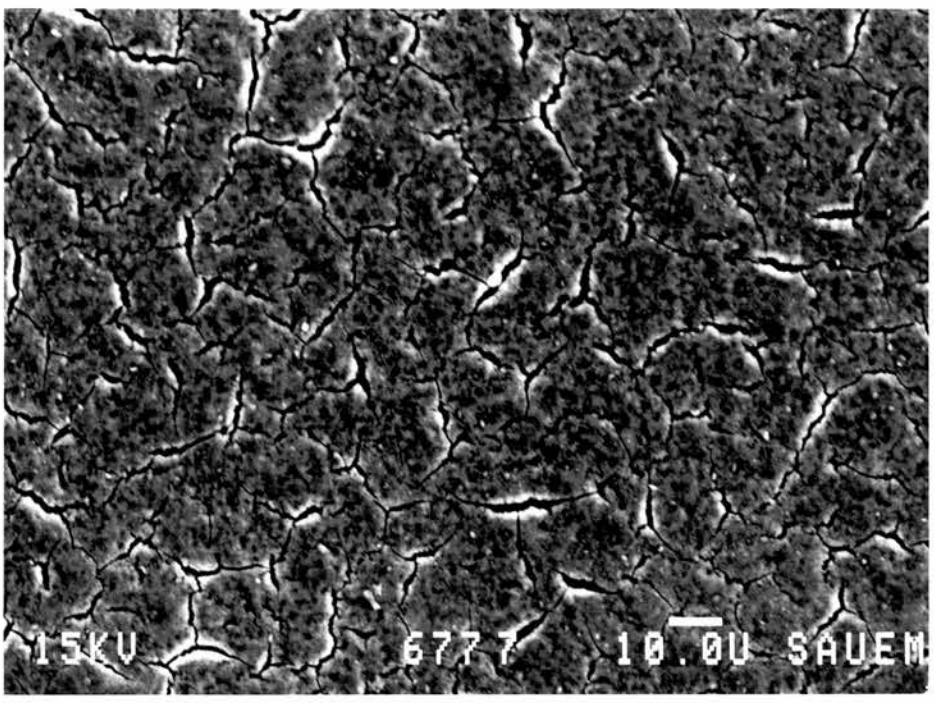

Fig. 5.2. SEM photographs of (a) composite film after drying at 293K for 4 hours; (b) composite film after failure during electrochemical potential cycling (30 cycles) in 0.5 $LiClO_4$/MeCN.

Fig 5.3

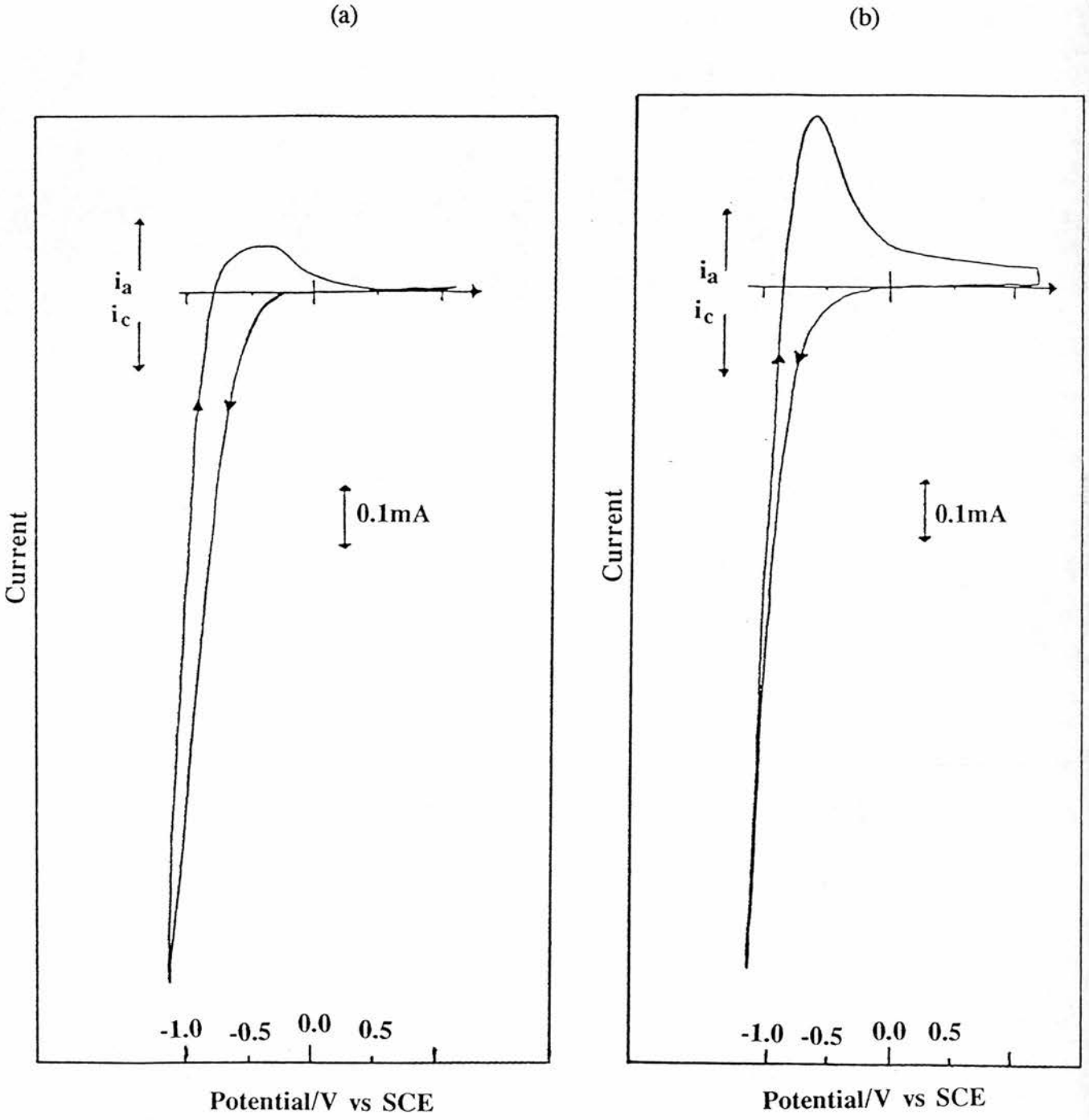

Fig. 5.3. Cyclic voltammetry (100 mVs^{-1}) of: (a)thick Nb_2O_5 film in 0.5 mol dm^{-3} $LiClO_4$/MeCN; (b) composite Nb_2O_5/silicone electrode. The cross indicates zero current and potential.

Nb_2O_5 films (Fig. 5.2(b)). This type of microcracking was also observed in the films if they were left for 4 weeks at room temperature to dry.

5.1.3 Cyclic Voltammetry

Cyclic voltammograms (CV's) run at 100mV/s of both the coated and uncoated films on ITO electrodes in 0.5 mol dm^{-3} $LiClO_4$/ MeCN are shown in Figs. 5.3(a) and (b). The potential range covers the potentials controlling the colouration and bleaching processes. The onset of the blue colouration is observed when the potential reaches -0.4V. Both CV's exhibit a very large cathodic current at potentials less than -0.4V but this is presumably partly due to H_2 evolution, at either the ITO/Nb_2O_5.xH_2O interface or at Nb (IV) sites within the electrode, rather than colouration current and is discussed later. On the reverse sweep an anodic peak is observed at -0.5V associated with the bleaching of the electrode. The CV's shown in Fig. 5.3 are characteristic of Nb_2O_5 undergoing electrochromic reactions.[6-8] Roughly 50% of the composite electrodes required 2-3 cycles of "breaking in" or "conditioning" before maximum contrast was observed between the bleached and coloured absorption. This is a common phenomenon seen in electrochromic films due to the solvent opening of the pores. SEM showed no apparent morphological differences between the composite electrodes which required breaking in and those which did not. However, the composite sol has to diffuse through the pores and undergo gelation within them. This would give rise to smaller pore sizes and presumably some partly closed pores which would require breaking in. Similar CVs are observed for the uncoated Nb_2O_5 films in 1.0 mol dm^{-3} H_2SO_4(aq); however, the coated films are unstable in aqueous media.

The optical absorption changes on colouration of the thick Nb_2O_5 films in 1.0 mol dm^{-3} H_2SO_4 at -0.875V (Fig. 5.4) are dominated by the broad structureless band which peaks at $\lambda >$ 800nm. In 0.5 mol dm^{-3} $LiClO_4$/MeCN, at -0.80V, both the coated and uncoated films gave similar spectra to that shown in Fig. 5.4. Under the model proposed by Faughnan and Crandall[16] this absorption is associated with Nb-bronze formation:-

Fig. 5.4

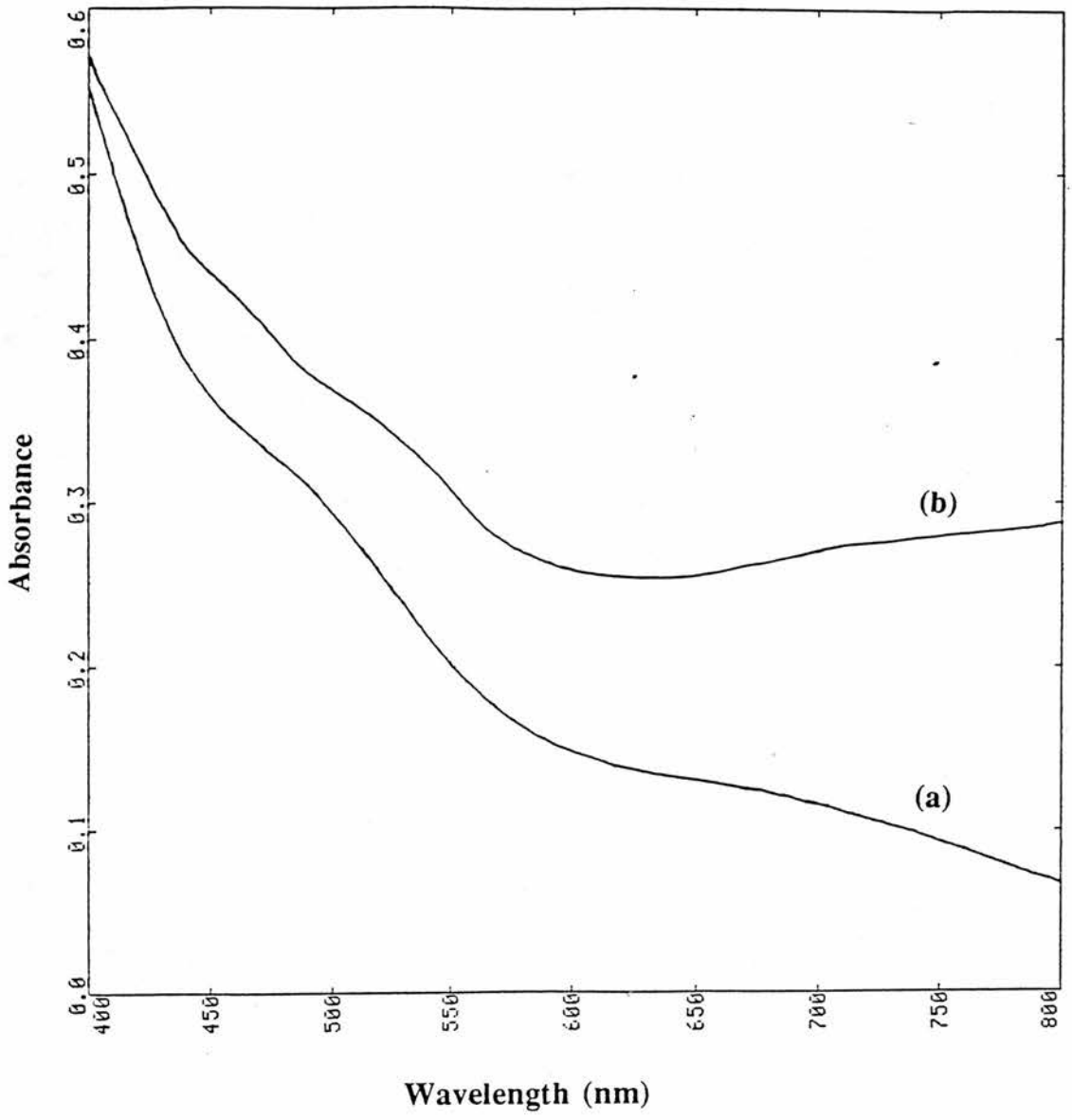

Fig. 5.4. UV-visible changes in Nb_2O_5/ITO absorbance in (a) the bleached state (0V vs SCE) and (b) the coloured state (-0.875V vs SCE). Medium: 1.0 mol dm^{-3} H_2SO_4, film thickness 5μm.

$$xM^+ + xe^- + Nb_2O_5 \rightleftharpoons M_xNb_2O_5 \qquad (5.2)$$

white blue Nb-bronze

M^+ can be H^+, Li^+, Na^+, and so on.

Simultaneous injection of electrons and cations is necessary to maintain charge neutrality. The Nb-bronze can be written as $(Nb^{IV}OM)_x(Nb_{2-x}{}^{V}O_{5-x})$, and thus the colouration comes from a photon-induced electronic transition between the Nb^{IV} and the Nb^{V}.[8] Whether the colour front associated with the Nb-bronze formation moves from the electrolyte/electrode interface to the electrode/ITO interface[16] or in the opposite direction, as suggested by Deb,[17] is as yet unclear. The reaction is related to the same process observed in crystalline Nb-bronzes.[18] The kinetics of interconversion between bleached and coloured states is described below.

5.1.4 Durability

For the uncoated Nb_2O_5 films the absorbance maximum of the coloured state (-0.875V) decays very rapidly with the number of cycles (100mV/s) as shown in Fig. 5.5, whilst simultaneously the background absorbance of the bleached state increases, possibly as a result of incomplete bleaching, or more likely due to the increased light scattering properties of the cracked film. The two states become indistinguishable after only 4 cycles, and the electrode suffers the dramatic peeling referred to earlier (Fig. 5.1(b)).

As noted earlier, different behaviour is observed for the glymo Nb_2O_5 composite film (Fig. 5.5). Here, there is often the rise in absorbance of the coloured state to reach a maximum at about the third cycle (breaking in) followed by a steady decay. Alternatively a steady decay from the initial absorbance maximum on the first cycle is observed. For both cases after prolonged cycling (30 cycles, typically) the two states are indistinguishable and the electrode is deemed to have failed. Visually, at this point, only the outer edges of the electrode have been observed to retain any of the blue bronze formation. The morphology of the film suggests cracking and peeling (Fig. 5.2(b)) in a similar way to that of the uncoated electrode.

We propose two possible mechanisms for the rapid failure of these films:- (i) peeling due to H_2 evolution on the cathodic sweep; (ii) rapid dehydration of the hydrated oxide layer

Fig. 5.5

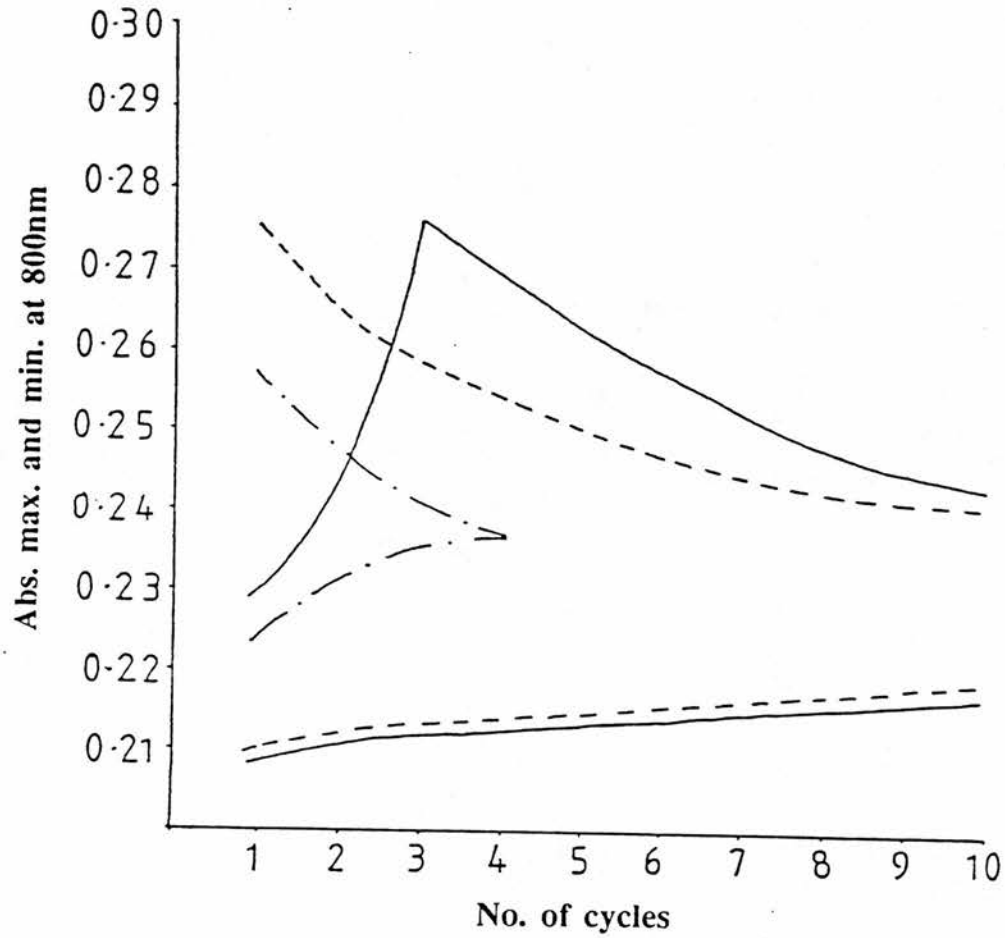

Fig 5.5. Durability of the electrochromic response: dependence of the absorbance at 800nm in the coloured state (upper traces) and the bleached state (lower traces) as a function of cycles: pure Nb_2O_5 electrode (— · — ·); composite electrode (— sample 1; - - - sample 2). (Media: Nb_2O_5, 1 mol dm^{-3} H_2SO_4; composite, 0.5 mol dm^{-3} $LiClO_4$/MeCN)

either by H_2O diffusion into the non-aqueous solvent, or H_2O binding as water of hydration to the Li^+ ions cycling in and out of the film. It is interesting to note that uncycled Nb_2O_5 films left in MeCN for a few hours will, upon removal, show similar cracking patterns to those shown in Fig. 5.1 lending credence to (ii). Those left in sulphuric acid tended to peel in large area pieces from the ITO, implying that here dehydration of the oxide film was not so much of a problem as the formation of a water layer between the film and the ITO.

That the composite dramatically increases cycling lifetime can thus be explained. If mechanism (i) is operating then the composite may be slowing down the diffusion of H^+ or the more "elastic" nature of the film spreads the stress caused by H_2 evolution more evenly and thus slows cracking. If mechanism (ii) is operating then the composite may be serving as a barrier to H_2O/MeCN exchange and dehydration. If this is so then it may be possible to eliminate film failure during cycling by the predrying of the films at a reduced drying rate. This is achieved by drying the films in a stream of air saturated with the solvent used in the sol and is commonly used in industry.

5.2 Kinetics of Thick Nb_2O_5 Electrochromic Films In $LiClO_4$/MeCN

The kinetics of colouration and bleaching (in 0.5 mol dm^{-3} $LiClO_4$/MeCN) may be studied by stepping the potential between the bleached state (0V vs SCE) and the coloured state (-0.8V vs SCE) and back, whilst monitoring the time-dependence of the current (chronoamperometry) and the absorbance at 800nm (chronoabsorptiometry). Chronoamperometric results for the Nb_2O_5 and the Nb_2O_5/silicone composite electrodes (Fig 5.6 and 5.7(a)) revealed that for both electrodes the full cycle is complete in ca. 40 secs. In each case the bleaching current decays considerably faster than the colouration current. Furthermore the colouration charge (area under the i-t curve) is much larger than the bleaching charge. This has been observed in a number of electrochromic systems[8,9] and appears to be due to hydrogen evolution on the cathodic potential excursion. Due to the high initial electronic resistance of the bleached composite film the colouration current rise time of the composite is very sluggish. In addition, chronoabsorptiometric data is shown for the composite electrode (Fig. 5.7(b)). The coulombic efficiency (η) for electrodes is given as:[19]

Fig 5.6

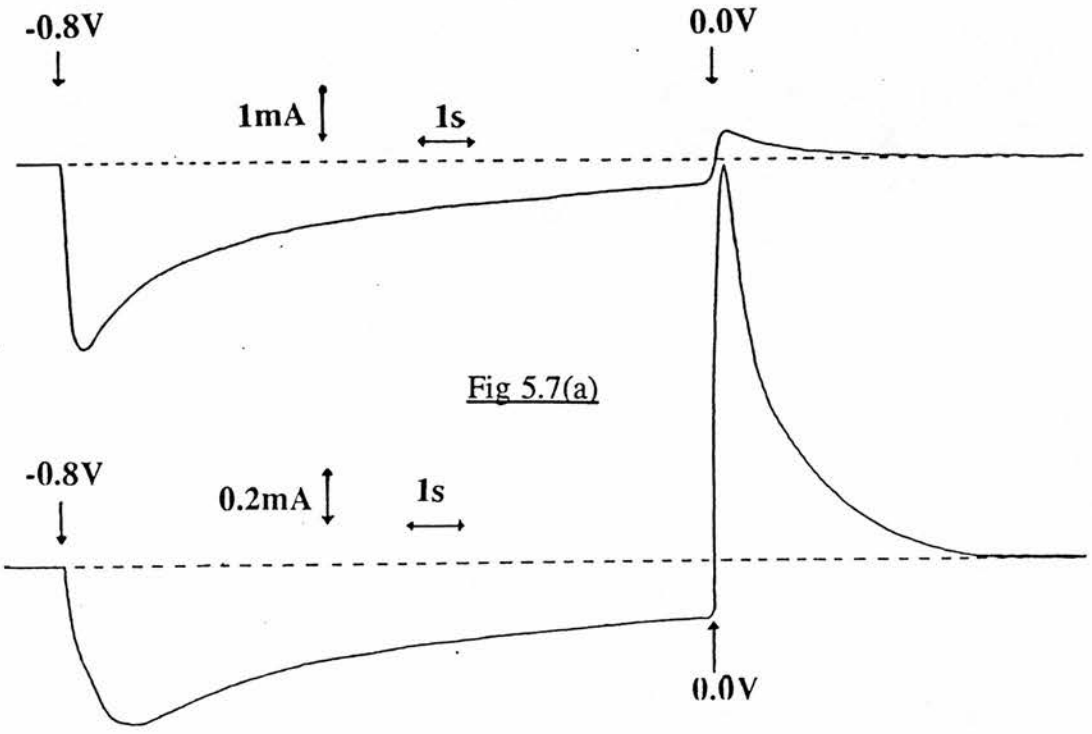

Fig 5.7(a)

Fig 5.7(b)

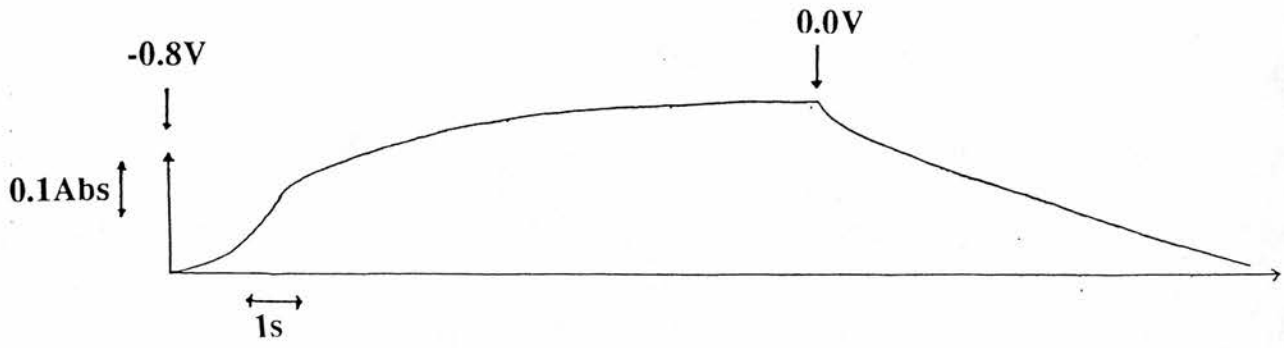

Fig 5.6 and 5.7(a). Current-time curve for Nb_2O_5 and composite electrodes respectively, on stepping the potential from 0V to -0.8V (vs SCE) and back to 0V. Fig. 5.7 (b), chronoabsorptiometric curve (800nm) for the composite electrode. Medium: 0.5 mol dm^{-3} $LiClO_4$/MeCN.

$$\eta = \frac{\Delta OD \times A}{Q} \qquad (5.3)$$

ΔOD = difference in opt. density between bleached and coloured states

A = area of electrode (cm^2)

Q = total charge passed during colouration

Typically, for the composite electrode of $\Delta OD = 0.05$, the charge passed during colouration is ~4.9 mC. Thus the electrochromic efficiency for these 0.6cm^2 electrodes is 6 $cm^2\ C^{-1}$. This value is comparable to the ca. 10 $cm^2\ C^{-1}$ reported earlier for sputtered Nb_2O_5,[20] but lower than the 25 cm^2C^{-1} value reported for Nb_2O_5 (at 620nm) obtained via the oxidation of sputtered NbN_x.[8]

5.2.1 Colouration Kinetics

Application of a large overvoltage, as the colouration potential, during chronoamperometry experiments ensures that the reactant centres at the film interface are consumed rapidly. Thus, film charge propagation (ie. diffusion of M^+ within the film) rather than interfacial kinetics (ie. M^+ injection at the film/electrolyte interface) is the rate determining step.[16,21,22] Because at short times the depletion of reactant centres has not reached the outer interface of the the film, semi-infinite diffusion prevails and thus the Cottrell equation applies:[8,21,23]

$$i(t) = \frac{nFAD^{1/2}C}{\pi^{1/2}\ t^{1/2}} = \frac{Q_{tot}D^{1/2}}{d\ t^{1/2}}, \quad t \leq \frac{d^2}{D}, \qquad (5.4)$$

Where Q_{tot} is the total charge passed during the colouration step (in C), t is the time taken (sec), A is the macroscopic area of the film (cm^2), F is the Faraday constant, C is the concentration of reactant sites (mol cm^{-3}) and d is the thickness of the film (cm). Thus the diffusion coefficient (D_{M+}) may be obtained from the slope of the i vs $t^{-1/2}$ graphs and plots

Fig. 5.8(a)

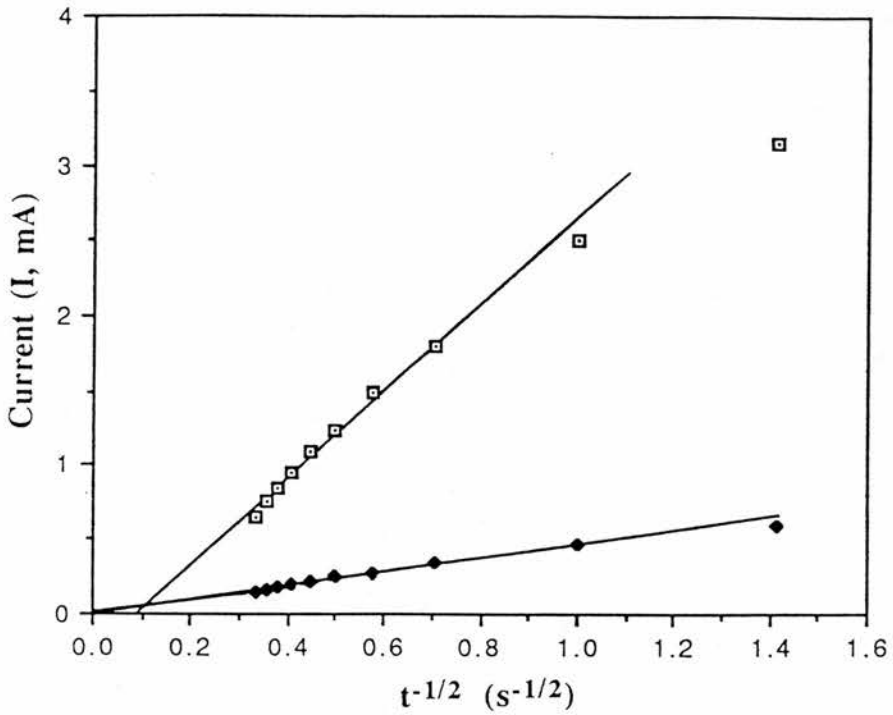

Fig 5.8(b)

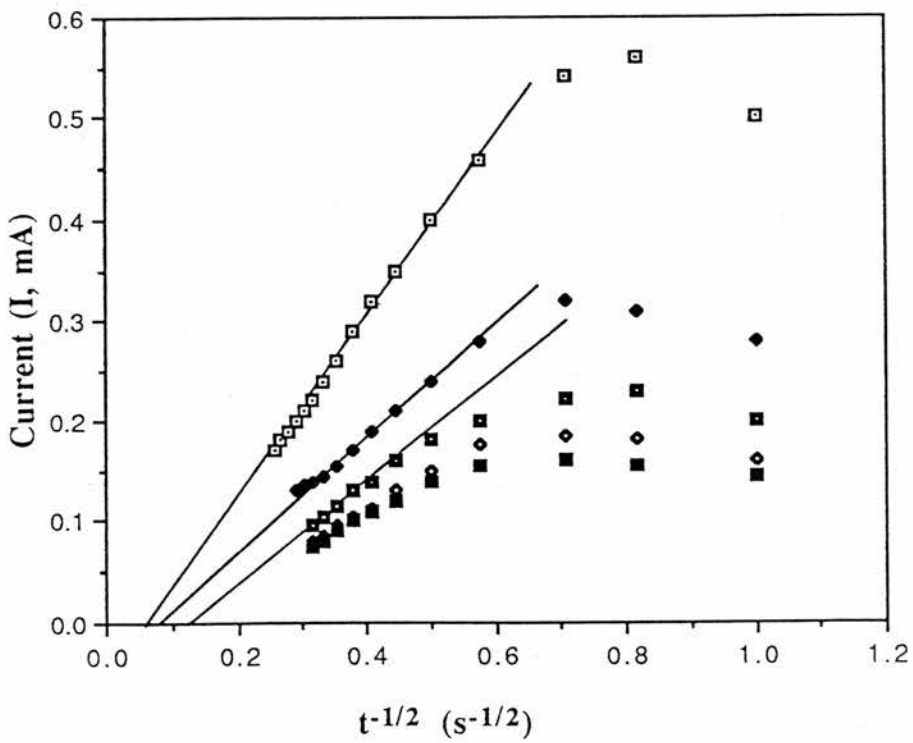

Fig. 5.8. Typical current vs $t^{-1/2}$ plots for the colouration current transients of pure Nb_2O_5 (a) and composite electrodes (b).

should extrapolate to the origin. At longer times ($t \geq \frac{d^2}{D}$) the finite nature of the reactant reservoir results in lower currents.[21,23] Figs 5.8(a) and (b) show for both the Nb_2O_5 and the composite films, respectively, that the decaying part of colouration current-time curve follows a $t^{-1/2}$ dependence. For the composite electrode, during the initial few seconds when the colouration current rise-time is sluggish due to high initial resistance (causing an uncompensated "iR" drop), the curve deviates from this $t^{-1/2}$ dependence. Furthermore, the plot for the composite electrode (Fig. 5.8(b)) intercepts the negative current axis at infinite times. This reflects lower than expected current values due to the resistance of the electrode[21] and has been observed in other systems using ITO electrodes.[8] For each of the two types of electrode the derived diffusion coefficients (Table 5.1) are independent of the particular cycle taken. These diffusion coefficients imply that diffusion is slightly slower in the composite than in the pure Nb_2O_5 film. A possible explanation for the slower diffusion rate in the composite is that the silicone layer has diffused and gelled in the very same pores and grain boundaries that the M^+ is trying to move through. The fact that the diffusion coefficients for both types of film are of the same order of magnitude would imply that the application of the overcoat layer has created a film which is microporous and similar to the microporous structure of the soft pure Nb_2O_5 gel.

The order of magnitude of these results compared with similar systems (Table 5.1), suggest that the diffusing species is H^+, not Li^+. Although both the acetonitrile and $LiClO_4$ had been thoroughly dried, the films themselves could act as good proton sources, having water and sulphuric acid trapped within their pores. The claim that protons are the dominant diffusing species, responsible for the observed colour change was confirmed by cycling the composite electrodes in a 0.1 mol dm^{-3} solution of tetra butyl ammonium hexafluorophosphate in acetonitrile. As the tetra butyl ammonium ions are too large to form Nb-bronzes, no electrochromic behaviour would be expected to be seen. However, upon cycling both a colour change and a CV typical of electrochromic Nb_2O_5 were observed, implying that protons trapped within the film pores were inserting into the Nb_2O_5 reactant centres to form $H_xNb_2O_5$.

Table 5.1

Diffusion Coefficient	Film Composition	
Our work D_{M^+} (cm^2s^{-1})	Pure Nb_2O_5 Films (5μm) $(2.04 \pm 0.36) \times 10^{-8}$	Composite Film (5μm) $(1.43 \pm 0.31) \times 10^{-8}$
Our work D_{M^+} (cm^2s^{-1})	0.1μm Nb_2O_5 Films, (M=H) $(1.38 \pm 0.47) \times 10^{-13}$	0.1μm Nb_2O_5 Films, (M=Li) $(9.87 \pm 0.32) \times 10^{-15}$
D_{H^+} (cm^2s^{-1})	Sputtered Nb_2O_5[a] 1.5×10^{-8}	Amorphous WO_3[b] 1.9×10^{-8}
D_{Li^+} (cm^2s^{-1})	WO_3[b] 1.9×10^{-9}	Amorphous WO_3[c] 5×10^{-10}
D_{Li^+} (cm^2s^{-1})	50:50 $Li_2O/Nb_2)_5$[d] 3.4×10^{-10}	40:35:25 $Li_2O/WO_3/Nb_2O_5$[d] 3.6×10^{-9}

(a) is reference 8.

(b) is reference 24.

(c) is reference 25.

(d) is reference 9.

Furthermore, if part of the chronoamperometric current observed in Fig. 5.8(b) is due to Li^+ diffusion, the following equation would now apply:

$$i \propto (aD_{H^+} + bD_{Li^+})^{1/2} t^{-1/2} \qquad (5.5)$$

where a and b are the mole fraction of $H^+$and Li^+ respectively

As D_{H^+} is between one and two orders of magnitude greater than D_{Li^+} (see Table 5.1) the presence of even small amounts of H^+ would cause D_{H^+} to dominate the observed slope of i vs $t^{-1/2}$ graph. Thus Li^+ diffusion can be ruled out as an observed mechanism. This also explains the observed difference between the colouration charge and the bleach charge ie. the difference is due to H_2 evolution. If the colouration current had been due to Li^+ diffusion then there should be no observed difference between these charges as the reduction of Li^+ to Li occurs at -3.04V (NHE), well below the colouration potential applied.

Absorbance-time transients for the composite electrode may be analysed by assuming that the absorbance (OD) is proportional to the charge passed.[8] Thus by integrating eq.(5.3) we obtain :-

$$OD = \frac{2\eta S t^{1/2}}{A} + OD_0 \qquad (5.6)$$

where η is the electrochromic efficiency, S is the slope of I ($t^{-1/2}$) graph, A is the macroscopic area of the electrode and OD_0 is the value of OD at t=0. However, plotting OD vs $t^{1/2}$ (Fig. 5.9) gives a sigmoidal plot similar to that obtained for sputtered films.[8] The sigmoidal dependence is probably due to hydrogen evolution. Hydrogen evolution has been observed in amorphous Nb_2O_5[8] and Li_2O/Nb_2O_5 films,[9] $Sr_{0.95}NbO_{3-\delta}$ films[26] and crystalline Nb_2O_5 films[27] held at potentials less than -0.3V (vs SCE). Manoharan and Goodenough[26] have shown that in the $Sr_{0.95}NbO_{3-\delta}$ system, there occurs not only a Nb(V)->Nb(IV) reduction (similar to eq(4.2)), but also a hydrogen evolution reaction of the following type occurs:

$$Nb^{IV}OH + H^+ + e^- \rightarrow Nb^{V}O + H_2 \qquad (5.7)$$

This reaction is facilitated by the mixed Nb^V/Nb^{IV} valence that occurs throughout the film. Thus absorbance (OD) is no longer proportional to the charge passed, as part of the charge flow is used to oxidise coloured reactant centres back to Nb^V, as shown in the following reaction:

$$H_xNb_2O_5 + xH^+ + e^- \rightarrow Nb_2O_5 + xH_2 \qquad (5.8)$$

Between t=1 and t=5 secs Fig. 5.9 appears to follow a linear dependence. Calculations using eq(5.6) and the values of S obtained from the earlier i vs $t^{-1/2}$ plots give values of η between 3 cm^2C^{-1} and 7 cm^2C^{-1} which are close to the value of 6 cm^2C^{-1} obtained earlier. This implies that, initially, absorbance is proportional to the charge passed and that H_2 evolution does not occur until a reasonable quantity of Nb^{IV} sites are present.

Thus H_2 evolution could cause the composite films to slowly break up and this could only be circumvented by the removal of the H_2SO_4 catalysed formation phase of the film production (to remove the H^+ within the film), followed by complete drying of the film.

Fig. 5.9

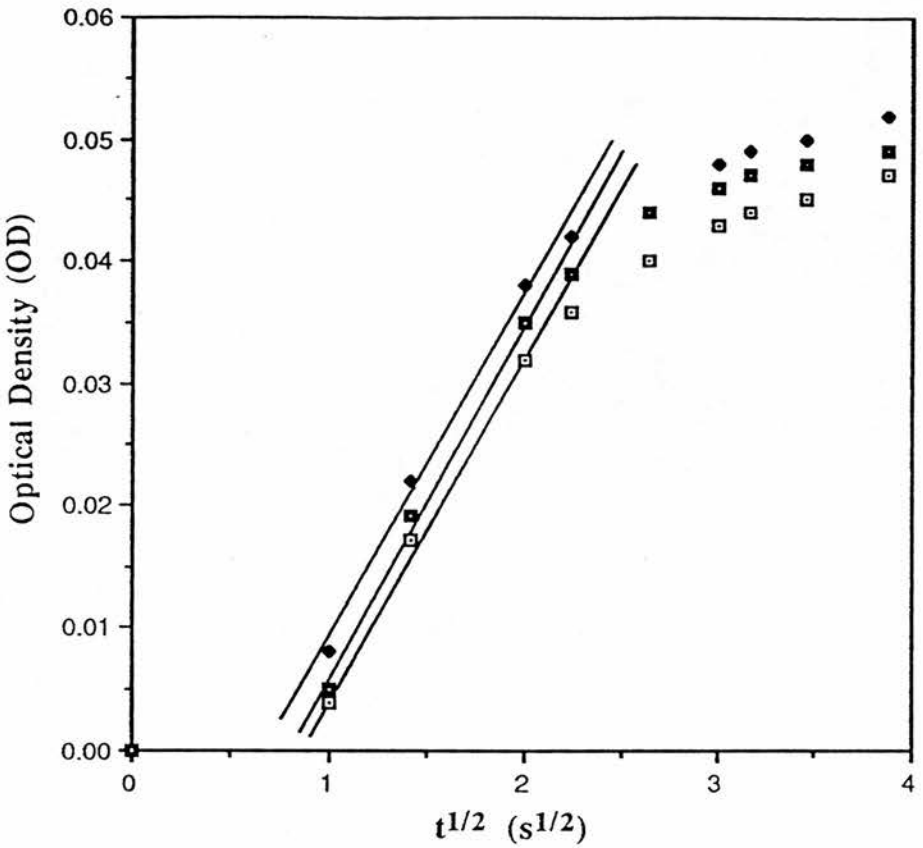

Fig. 5.9. Typical optical density vs $t^{1/2}$ plots for the colouration current transients of the composite electrodes .

5.2.2 Kinetics of Bleaching

According to Faughnan et al[28] bleaching of WO_3 films is determined by the migration of cations through an electric field developed across the electrochromic film and thus the current is not limited by any interfacial barriers and is expected to decay as $t^{-3/4}$ (rather than $t^{-1/2}$ as in the diffusional model). However, log(i) vs log(t) plots for bleaching of our uncoated and composite coated films did not show this or any other simple dependence for either the uncoated Nb_2O_5 or for the composite film. The reason for this became apparent when ln(i) vs t graphs were plotted – a linear dependence was observed. This is due to the cell geometry, – as the spacing between the working and counter electrodes was ~1mm, a thin layer cell had been inadvertently set up.

In thin layer cells, the amount of electrolyte between the electrodes is finite and thus steep concentration gradients are set up between the electrodes when a potential is applied (unlike bulk solutions where the concentration can be considered constant) and this gives a characteristic $i \alpha e^{-kt}$ dependence.[29] During the colouration cycle the diffusion of the protons into the film reactant sites is slow compared to the diffusion of the electrolyte in between the plates and is thus the rate determining step. However, during bleaching the diffusion of the charge out of the film is fast and hence the diffusion of the electrolyte between the plates is the rate determining step.

In order to observe the bleaching diffusion within the film, the geometry of the cell was changed so that the working and counter electrodes were separated by ~4cm, thus ensuring a constant concentration of electrolyte between the electrodes. However, log(i) vs log(t) plots for bleaching of the uncoated and composite coated films (see Fig.5.10) did not show a $t^{-3/4}$ dependence but a $t^{-1.2}$ dependence. The reason for this dependence is not clear but it has been seen in other systems. Machida et al[9] and Lemons et al[30] observed a $t^{-1.2}$ dependence for the bleaching current in $58WO_3.42Nb_2O_5$ and $W_9Nb_8O_{47-x}$ films respectively but could offer no explanation. It is however apparent that the diffusion of H^+ out of niobium oxide films is much faster than diffusion into them.

Again, assuming the absorbance (OD) is proportional to the charge passed, $\log(OD-OD_0)$ vs log(t) plots might help in explaining the observed $t^{-1.2}$ dependence of i,

Fig. 5.10

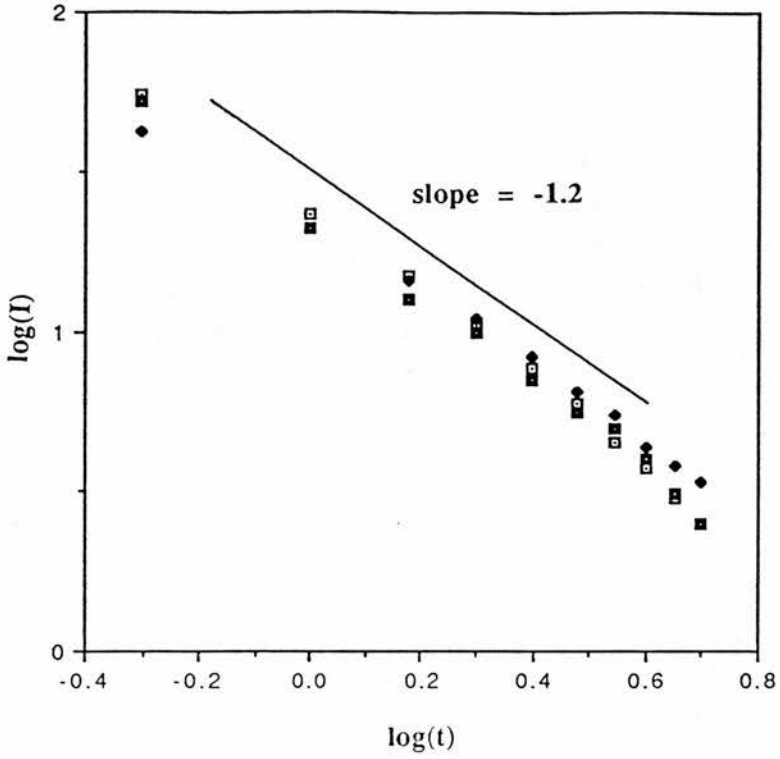

Fig 5.10. Log(i) vs log(t) plots for the bleaching current transients of the composite electrode.

Fig 5.11

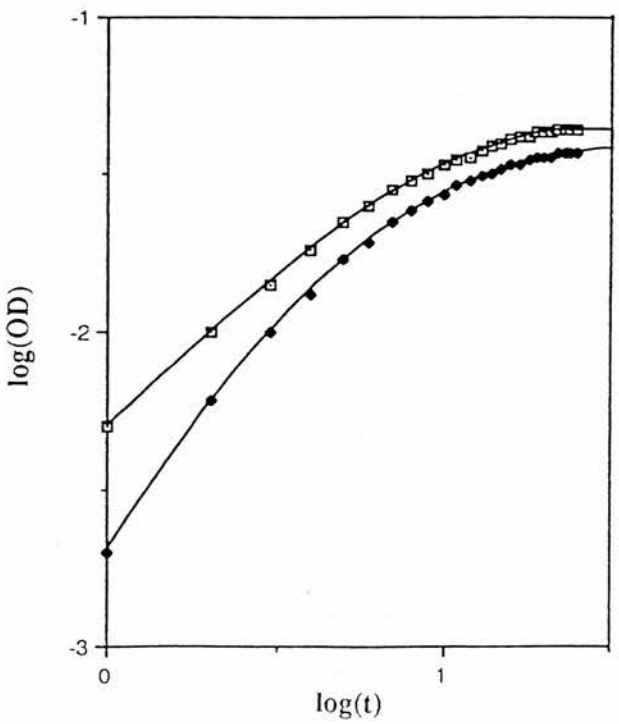

Fig. 5.11. Log(OD) vs log(t) plots for the bleaching current transients of the composite electrode.

however as Fig. 5.11 shows log(OD-OD_o) vs log(t) plots for the composite do not reflect any simple relationship and must await a better model.

5.3 Thin (0.1μm) Films of Nb_2O_5

5.3.1 Preparation of Thin (0.1μm) Films of Nb_2O_5

Thin films of Nb_2O_5 were produced by applying 50μl drops of 0.05 mol dm^{-3} solution of $(NbCl_5)_2$ in EtOH to 5 x 1 x 0.3 cm ITO glass electrodes. The electrodes were then spun at 2000 rpm for 2 minutes and finally dried at 393K for 2 hours. SEM revealed the films to be of the order of 0.1μm thickness and all the films thus produced were crackfree, and hence could be used in the electrochemical experiments. Measurements of film weight gave film densities in the region of 3.9-4.1 g cm^{-3}. This is close to the density of pure Nb_2O_5 powder (4.47 g cm^{-3}) and indicates a very high Nb_2O_5 composition in a dense and glass like film.

5.3.2 Cyclic Voltammetry

Cyclic Voltammograms (CV's) of the films in 1.0 mol dm^{-3} H_2SO_4 and 0.5 mol dm^{-3} $LiClO_4$ in acetonitrile are shown in Figures 5.12 (a) and (b) respectively. Unlike the thick films, the cathodic current onset potential of the thin films is -0.5→-0.6V rather than ~-0.25V. Furthermore, H_2 evolution is not observed in acid solutions until cathodic sweep potentials of less than -1.0V are applied, where upon a corresponding hydrogen oxidation peak is observed at -0.23V on the anodic sweep (see Fig.5.12(c)). Another difference between the films is that the thin films do not give a blue colour upon charge injection but a brown colour, regardless of cation. Figs. 5.13(a) and (b) show the optical absorption changes on colouration of the thin films, held at -0.8V for 30 seconds. Applying -0.8V to ITO glass electrode blanks gives no absorbance change (see Fig. 5.13(c)) confirming that the brown colour observed is due to the Nb_2O_5 rather than the ITO. Machida et al[31] found that the colour of rapidly quenched glasses in the LiO_2-WO_3-Nb_2O_5 system varied from blue to brown with increasing Nb_2O_5 content, so it appears that the brown colouration colour is a property of Nb_2O_5 glasses. This may be a property of the closeness of packing of the niobium reactant sites. Our thick films and the sputtered films[8] are less dense and so discrete Nb(IV) sites occur which give rise to the

Fig. 5.12

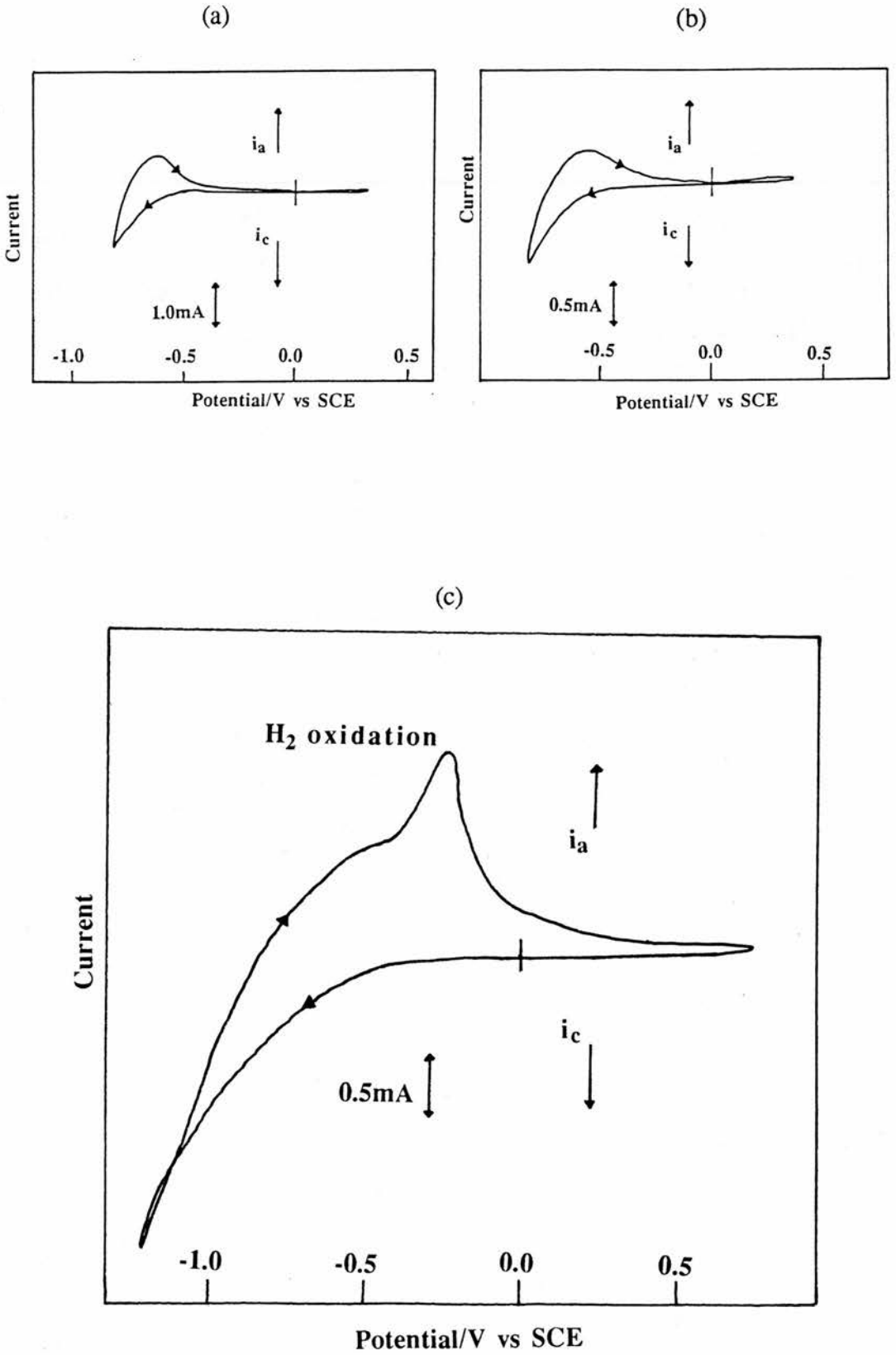

Fig. 5.12. Cyclic voltammetry (100 mVs^{-1}) of the thin Nb_2O_5films in (a) and (c) 1.0 mol dm^{-3} H_2SO_4 and (b) 0.5 mol dm^{-3} $LiClO_4$/MeCN.

Fig. 5.13(a)

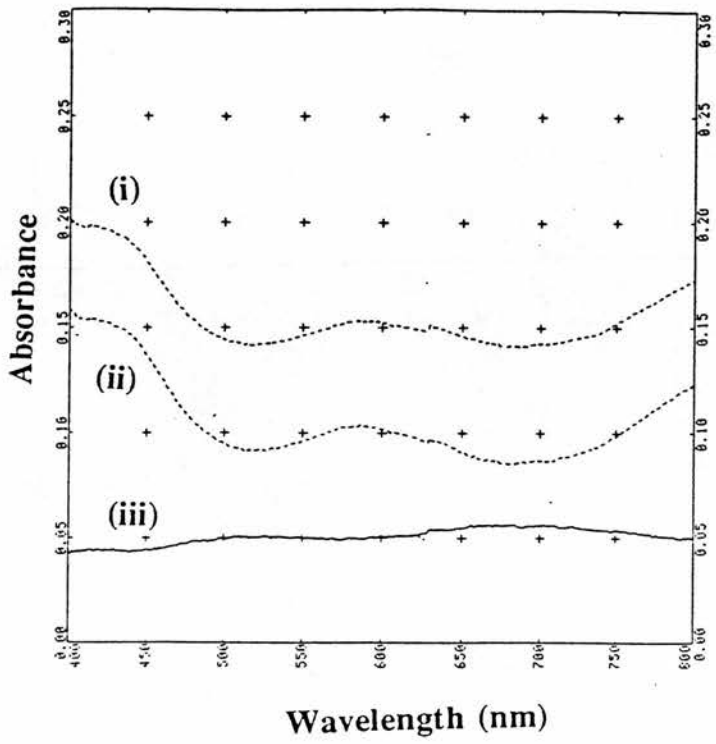

Fig. 5.13(b)

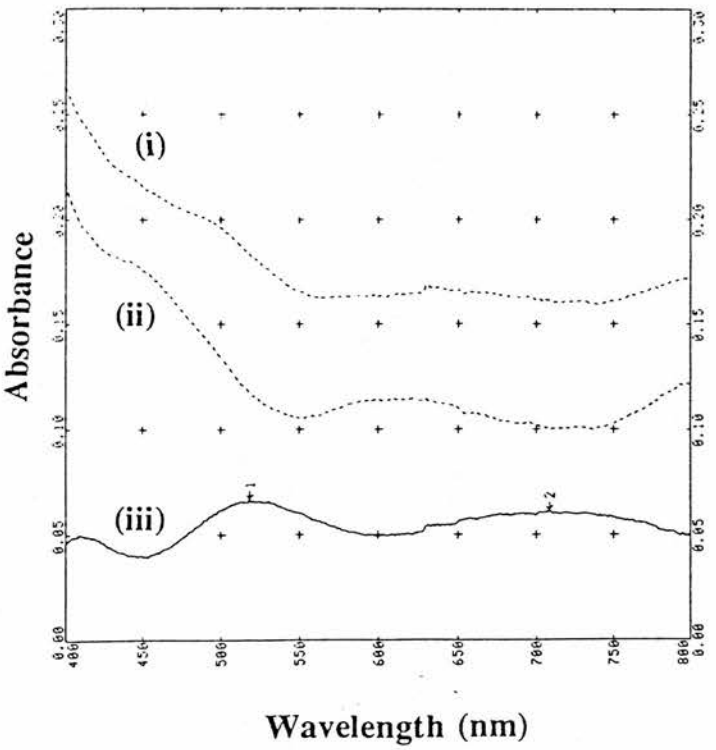

Fig. 5.13. UV-Vis spectral changes in Nb_2O_5/ITO films (0.1μm thick) in (a) 1.0 mol dm^{-3} H_2SO_4 and (b) 0.5 $LiClO_4$/MeCN where (i) is the coloured state, (ii) is the bleached state and (iii) is the difference between (i) and (ii).

Fig. 5.13(c)

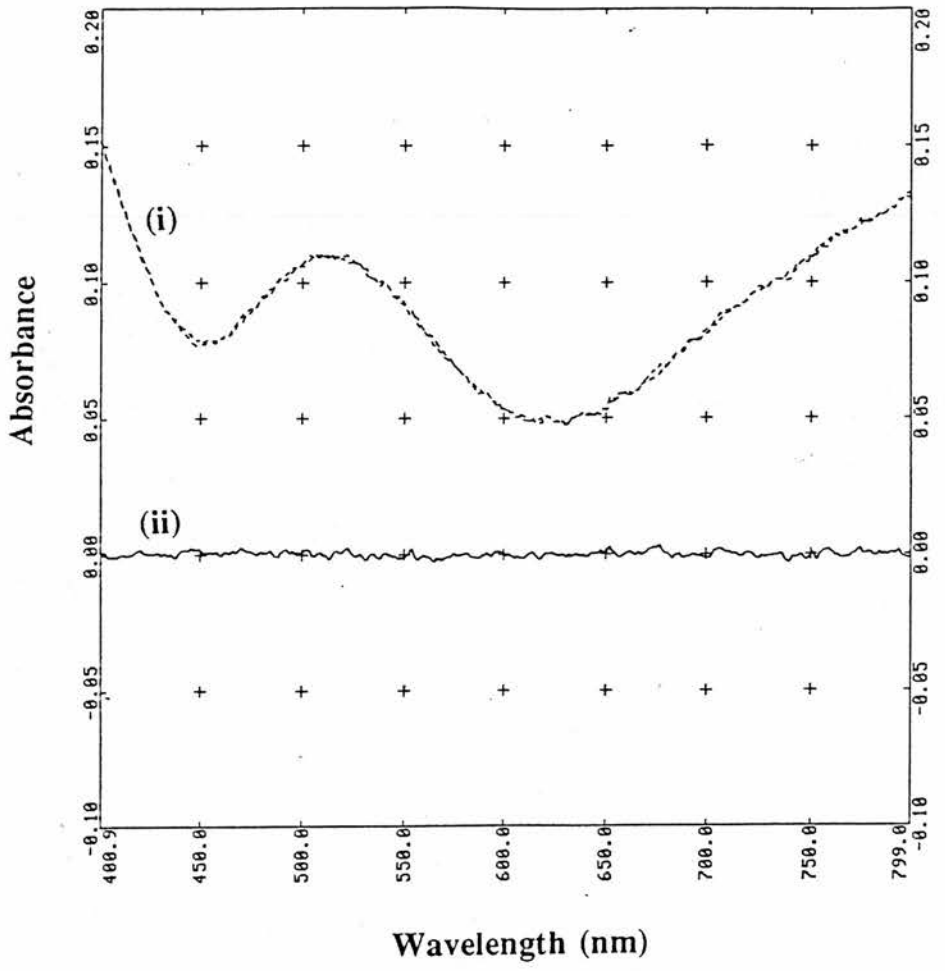

Fig. 5.13(c). UV-Vis spectral changes in ITO glass electrode in 1.0 mol dm^{-3} H_2SO_4, where (i) is the UV-Vis spectra of the ITO glass at 0V and after 90 seconds at -0.80V and (ii) is the difference between the 0V and -0.8V spectra.

characteristic blue colour of niobium (IV). Alternatively, in the dense Nb_2O_5 glasses the reactant sites may be close enough to allow electron orbital overlap to give a metal type band and a change in the colour observed. Fig. 5.13(c) shows the visible spectrum of ITO glass. The variation in optical absorbance with wavelength is an interference pattern, and is characteristic of a 20Ω/square thick ITO film.[32]

5.3.3 Durability

The durability of the thin films was far greater than that of the thick films. In either solvent, the films were cycled for ~250 cycles without failure, although there was some degree of optical density loss. Extrapolation of these losses indicates that the films would fail at ~10^3 cycles. The lack of hydrogen evolution and the well-dried nature of the films are evidently large factors in their durability. The long term failure of the films is perhaps due to formation of a solvent layer between the films and the ITO.

5.4 Kinetics of Nb_2O_5 Thin Films in Acid and $LiClO_4$/MeCN

5.4.1 Colouration Kinetics

The kinetics of colouration and bleaching were studied by stepping the potential between 0V and -0.8V and making chronoamperometric and chronoabsorptiometric (700 nm) measurements. The films were well behaved, exhibiting no initial "iR" drop (unlike the composite films), and negligible difference in the colouration and the bleaching charges. Figures 5.14(a) and (b) show the i vs $t^{-1/2}$ graphs of the films in acid and $LiClO_4$/MeCN solutions respectively. It is apparent that they are linear plots and thus allow for the calculation of the diffusion coefficients (eq (5.4)). Taking the concentration of reactant sites to be proportional to the density of the films[9,16,24] gives a reactant site concentration of 0.0150 mols/cm^3. Table 5.1 gives the diffusion coefficients for both systems. Whilst they are rather small compared to other systems (see Table 5.1), they do show an expected two orders of magnitude difference between the two types of cation. The very low diffusion coefficients can be explained by the dense glass morphology which CO_2 absorbance pore analysis has shown to have very few pores (and presumably large tortuosity).

Fig. 5.14(a)

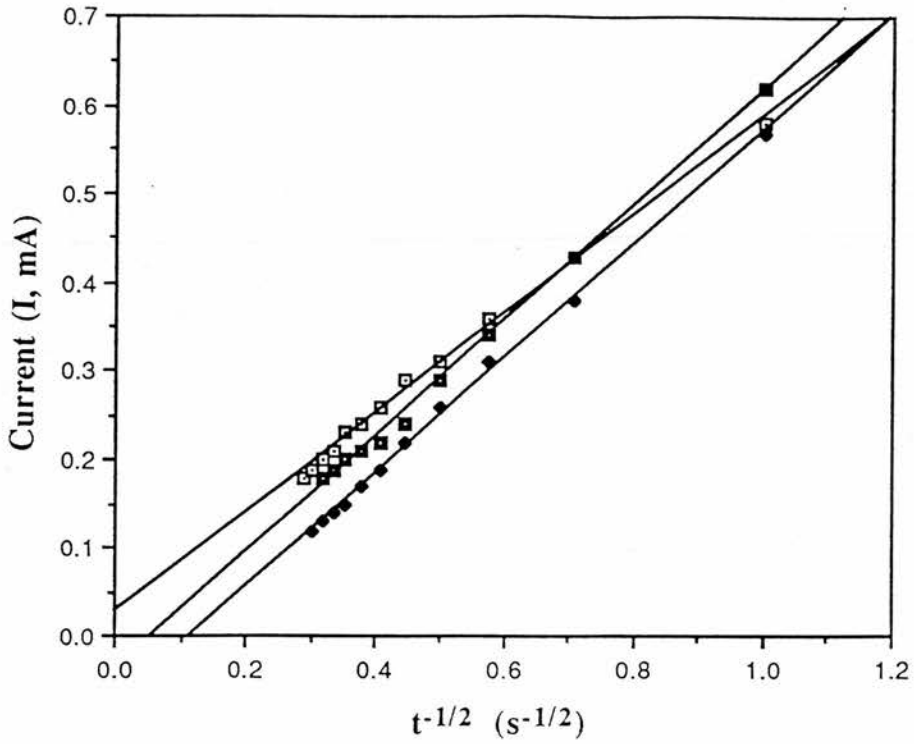

Fig. 5.14(b)

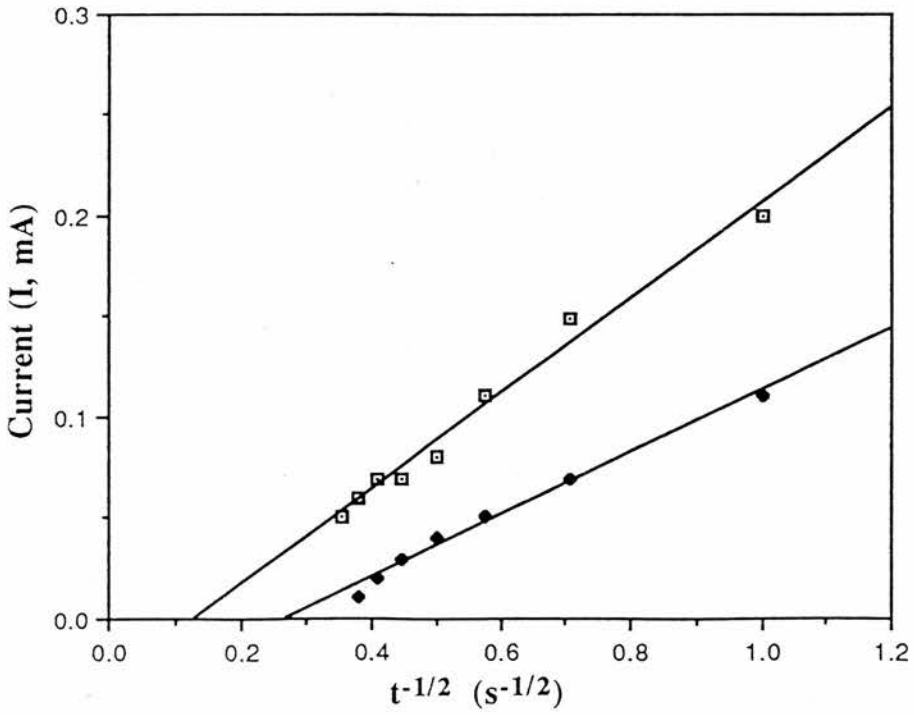

Fig. 5.14. Typical i vs $t^{-1/2}$ plots for the thin Nb_2O_5 films in (a) 1.0 mol dm^{-3} H_2SO_4 and (b) 0.5 $LiClO_4$/MeCN.

Fig. 5.15(a)

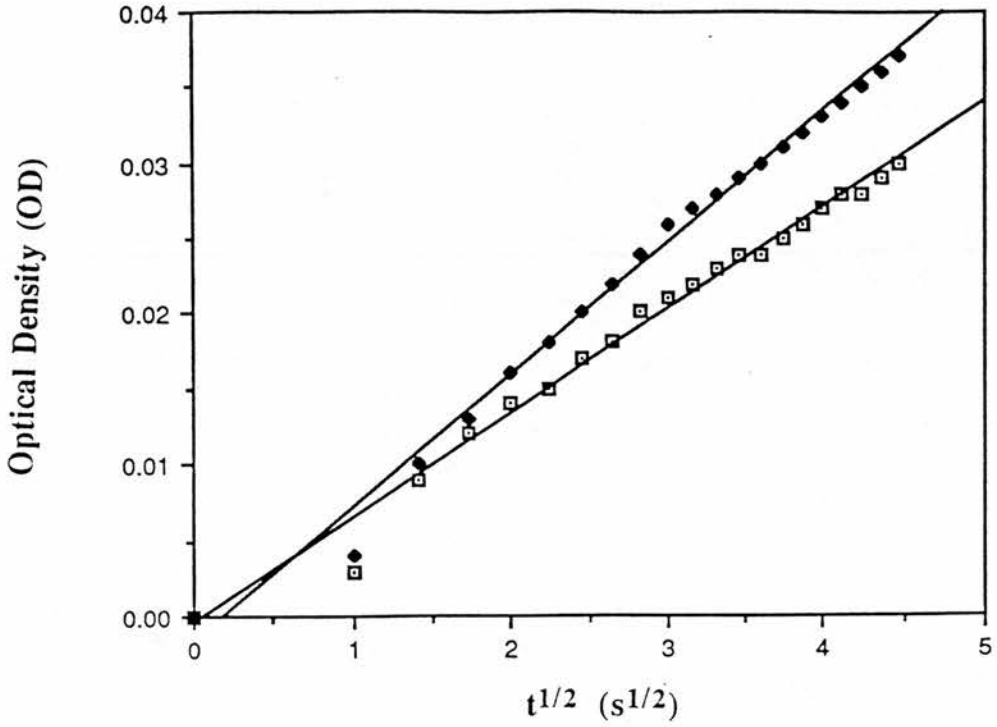

Fig 5.15(b)

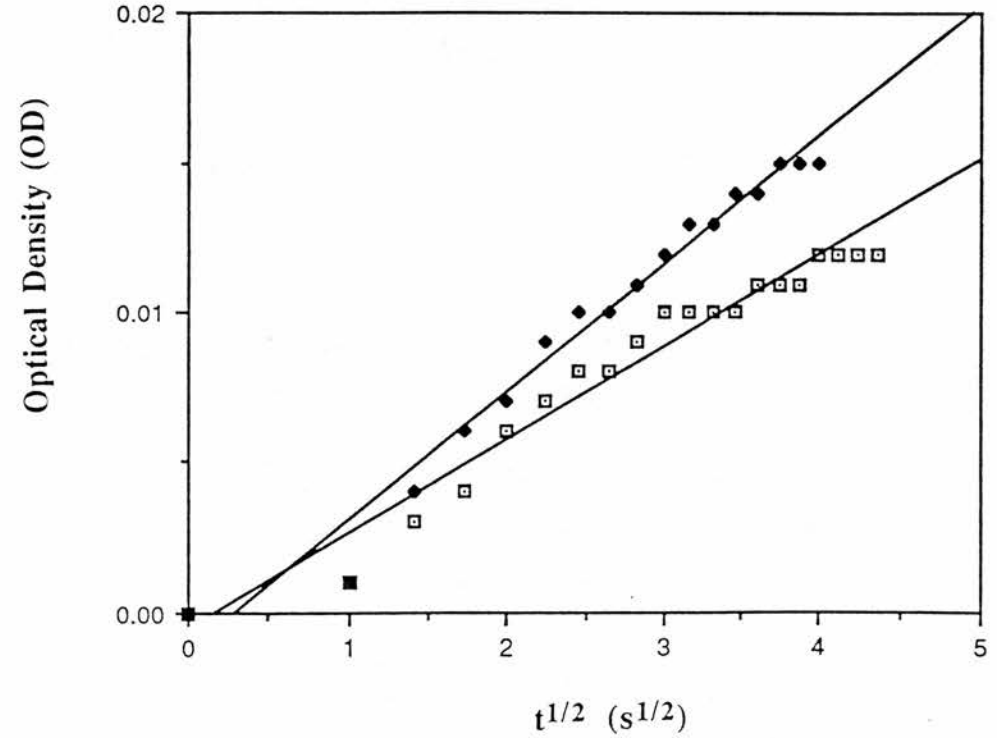

Fig. 5.15. Typical OD vs $t^{1/2}$ plots for the thin Nb_2O_5 films in (a) 1.0 mol dm^{-3} H_2SO_4 and (b) 0.5 $LiClO_4$/MeCN.

Figs.5.15(a) and (b) show the OD (700nm) vs $t^{1/2}$ plots of the films in acid and $LiClO_4$/MeCN solutions respectively. Apart from an initial sluggishness during the first second they exhibit the predicted $t^{1/2}$ dependence (see eq(5.24)). Calculations of the electrochromic efficiency from the slopes of the OD vs $t^{1/2}$ graphs gives efficiencies of 13.5 cm^2C^{-1} and 24 cm^2C^{-1} for the films in acid and $LiClO_4$/MeCN solutions respectively. These compare very favourably with the previously reported values of between 10 and 25 cm^2C^{-1} for Nb_2O_5.[8,19] Use of eq(5.3) gives electrochromic efficiencies of 11 cm^2C^{-1} and 15 cm^2C^{-1} for the films in acid and $LiClO_4$/MeCN solutions respectively.

5.4.2 Kinetics of Bleaching

Like the thick films reported in section 5.23, the diffusion of charge out of the film is much faster than that of insertion and does not appear to obey any easily explained relationship. A plot of log(i) vs log(t) for the electrodes when separated by 4 cm, gives a -1.2 dependence (as observed before for the thick films) and a log(OD) vs log(t) shows no simple relationship.

5.5 A.C. Impedance Measurements

A.C. impedance measurements analyse a reaction at equilibrium, i.e. at open circuit potential, with no net current flow. The a.c. excitation is generally small (<5 mV peak to peak) and is varied over a wide range of frequencies. When the a.c. signal is first impressed, a time dependent diffusion layer is created. As no net current flows, a steady state is set up after a few cycles.[29,33] Generally under these conditions, most electrode systems can be thought of having an "equivalent circuit" of the type shown in Fig. 5.16.

Fig.5.16

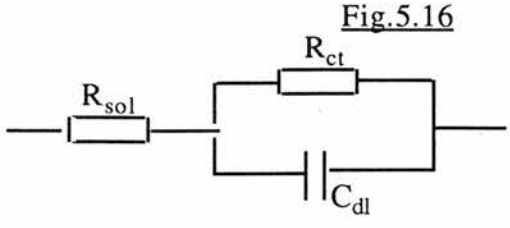

where C_{dl} is the double layer capacitance of the electrode, R_{ct} is the charge transfer resistance due to ionic conductivity and R_{sol} is the solution resistance between the reference

electrode and the working electrode.[29,33] By Ohm's Law, the current, I, passing through a resistor, R, at an applied voltage, E, is given as:

$$I = ER^{-1} \qquad (5.9)$$

Likewise the current through a capacitor, C, (a.c. only, as d.c. current is not passed by a capacitor) is given by:

$$I = i\,\omega CE \qquad (5.10)$$

where ω is the angular frequency ($\omega = 2\pi f$) and $i = (-1)^{1/2}$. Thus for a circuit containing both resistance and capacitance, the current may be defined as:

$$I = EZ^{-1} \qquad (5.11)$$

where Z is the complex impedance of the circuit. The impedance of the capacitance is imaginary due to the 90° difference in phase angle between the sinusoidal current and the voltage. Therefore, the impedance of the circuit contains both real (Z') and imaginary (Z") terms and is called the complex impedance (Z^*), where:

$$Z^* = Z' - iZ'' \qquad (5.12)$$

Thus the "equivalent circuit" shown in Fig.4.16 has a complex impedance of:[29]

$$Z^* = R_{sol} + R_{ct}(1 + R_{ct}i\omega C_{dl})^{-1} \qquad (5.13)$$

Similarly the complex admittance, A^*, of a circuit can be defined as $(Z^*)^{-1}$ and the complex capacitance, C^*, as $(A^*)\omega^{-1}$. Both of these terms have real (Z' and A') and imaginary (Z" and A") components, respectively. Thus complex impedance, admittance and capacitance (Argand plane) plots can be formed upon varying the applied a.c. voltage frequency.

A complex impedance plot for the circuit given in Fig.5.16 is shown in Fig. 5.17. Fig.5.17 shows that this plot is a semicircle:

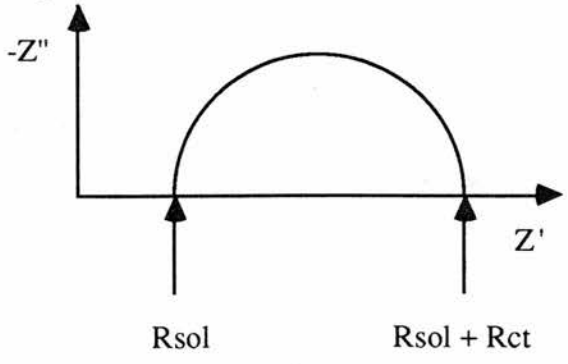

Fig 5.17

Fig. 5.18(a)

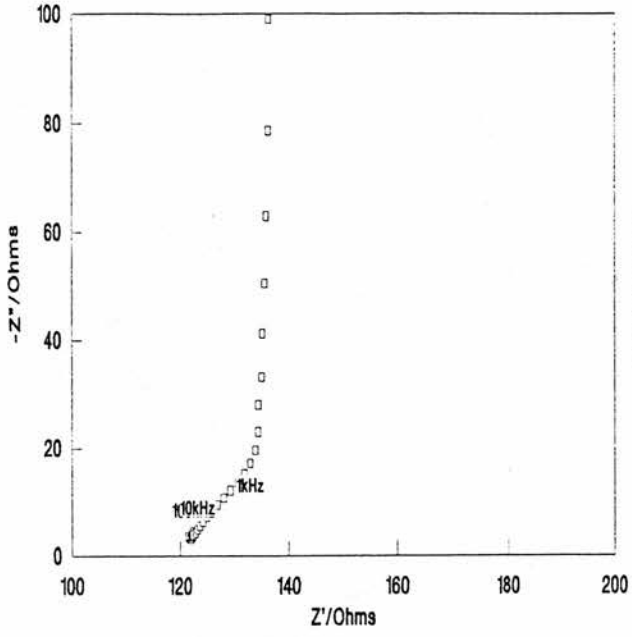

Fig. 5.18(b)

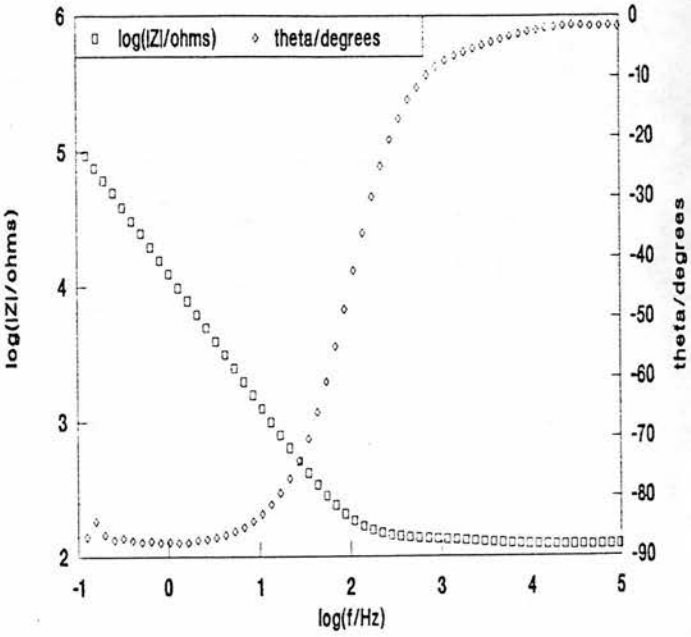

Fig. 5.18(c)

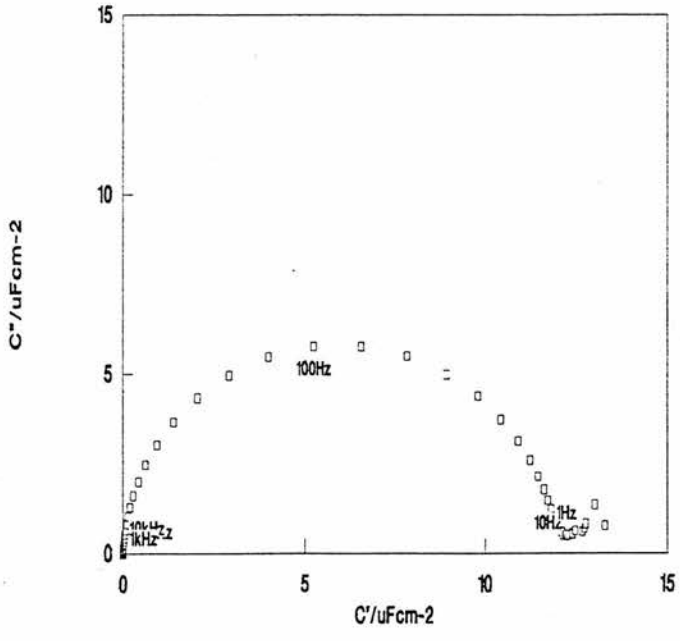

Fig. 5.18. (a) Nyquist, (b) Bode and (c) complex capacitance plots for ITO glass electrode in 1.0 mol dm^{-3} H_2SO_4 at -0.424V vs SCE.; a.c. amplitude 10 mV.

At low frequencies the complex impedance is purely resistive because the reactance of the capacitor is very high, and so $Z^* = R_{sol} + R_{ct}$. As the frequency increases, the capacitor's reactance decreases and it passes increasing current, giving rise to the semicircular plot. At very high frequencies the resistance of the parallel combination (C_{dl} and R_{ct}) decreases to zero and only the series resistance of the solution (R_{sol}) is observed.

Fig. 5.18(a) shows the complex impedance plot for an ITO glass electrode in 1.0 mol dm^{-3} H_2SO_4 at the open ciruit voltage of -0.424V vs SCE. The film does not show the semi circle plot characteristic of the double layer charging circuit described in Fig. 5.16. Figs. 5.18 (b) and (c) show respectively, the Bode plot and complex capacitance plots for the film. The Bode plot (Fig. 5.18(b)) shows that the electrical behaviour of the film changes from capacitive at low frequencies to resistive at high frequencies, with a transition region at ca. 100 Hz in which the impedance magnitude slope changes from -1 to zero and the phase angle tends to zero. The complex capacitance (Fig.5.18(c)) shows a single low frequency semicircle. Extrapolation of this semicircle plot to the real axis at low frequencies gives a film double layer capacitance of 12 $\mu F\ cm^{-2}$.

These plots are characteristic of a distributed resistance due to the ITO substrate.[34] In effect the electrode can be represented as a distributed resistive network which is connected via the impedance of the ITO film to the distributed resistance of the electrolyte solution. The equivalent circuit of the ITO electrode is shown in Fig.5.19.

Fig.5.19

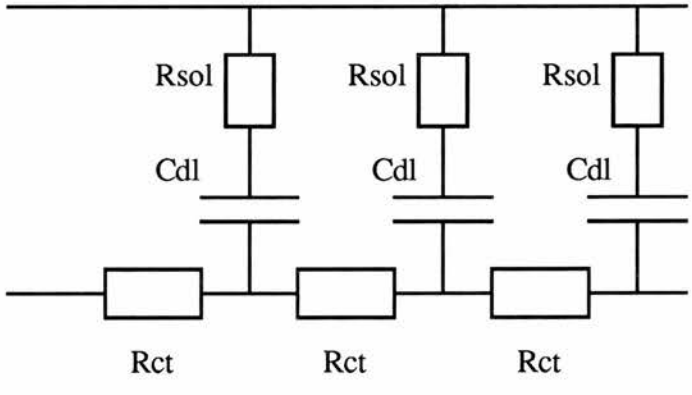

Fig 5.20(a)

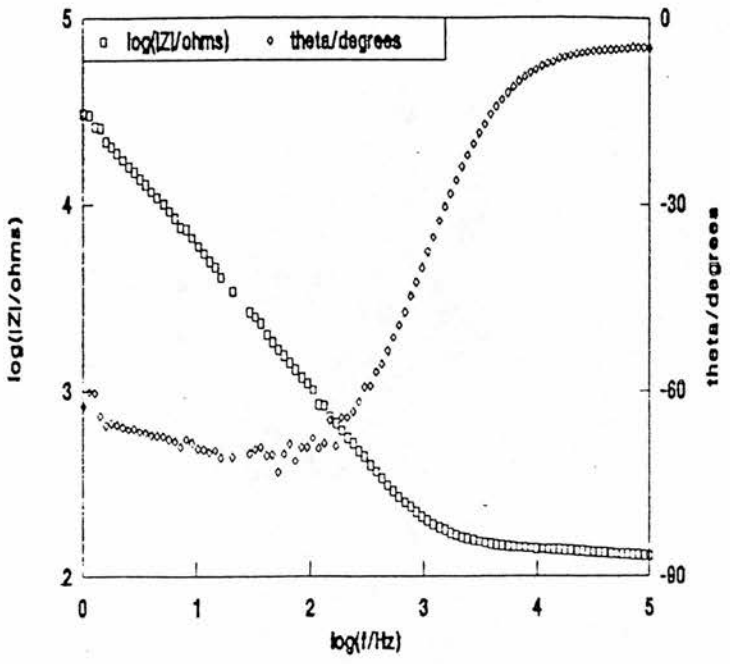

Fig. 5.20(b)

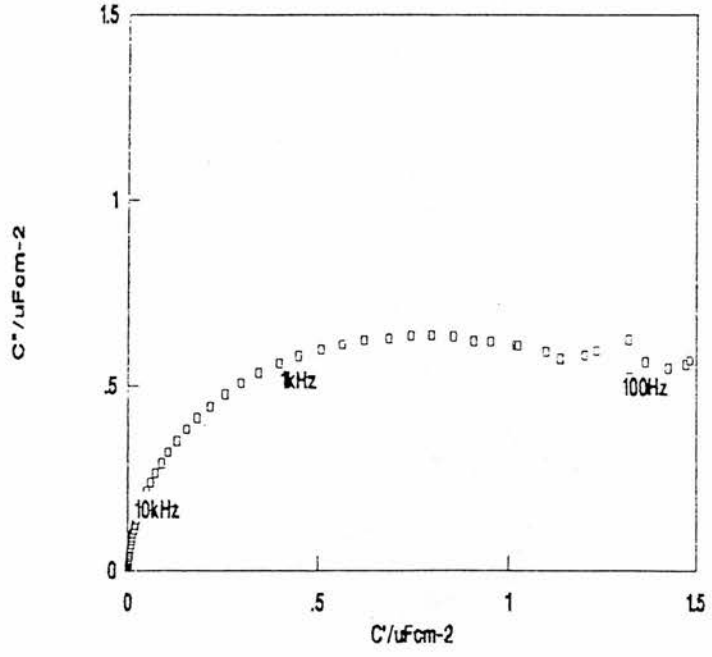

Fig. 5.20. (a) Bode and (b) complex capacitance plots for 0.1μm thick Nb_2O_5 film on ITO glass electrode in 1.0 mol dm^{-3} H_2SO_4 at -0.203V vs SCE.; a.c. amplitude 10 mV.

Such an equivalent circuit explains why the Bode plot shows that at low frequency the impedance evolves from almost purely capacitive behaviour to purely resistive behaviour, with a transition region of mixed (distributed) character during which the phase angle tends to zero and the slope of the log(Z) curve changes from -1 to -0.5 to 0. The ITO film's double layer capacitance is between that expected for a smooth nonporous surface (~1 $\mu F\ cm^{-2}$) and that observed for porous polymers (~1 $mF\ cm^{-1}$)[34] implying that it has a very high degree of surface roughness.

Figs 20 (a) and (b) show the Bode plot and complex capacitance plots of the thin Nb_2O_5 films on ITO glass electrodes at the open circuit voltage of -0.203V vs SCE in 1.0 mol dm^{-3} H_2SO_4. They are very similar to the ITO glass electrode plots in Figs. 18 (b) and (c) but with two notable differences. In the Bode plot at low frequencies the electrode behaviour is no longer purely capacitive. This is due to the Nb_2O_5 film having a very large charge transfer resistance, and is consistent with the observation that the diffusion of the protons in the film is very slow. Secondly, in the complex capacitance plot the extrapolation of the semicircle plot to the real axis at low frequencies gives a double layer film capacitance of 1.2 $\mu F\ cm^{-2}$. This implies a smooth non-porous electrode surface and is consistent with the CO_2 absorbance pore size analysis data. This means that, in effect, the electrode can be represented as a distributed resistive ITO network which is connected via the impedance of the Nb_2O_5 film to the distributed resistance of the electrolyte solution. The equivalent circuit of the Nb_2O_5-coated ITO electrode is shown in Fig.5.21

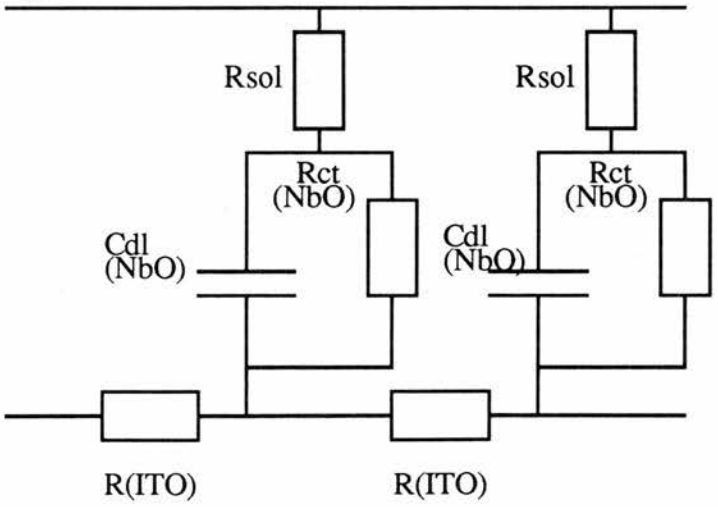

Fig.5.21

The impedance measurements were repeated at -0.8V but no difference in the film characteristics were observed. That the open circuit voltage for the Nb^{V}/Nb^{IV} redox occurs at -0.203V rather than the -0.6V (vs SCE) observed on the cyclic voltammogram can be explained by kinetic limitations on the large current measurement. Although the $Nb^{V} \rightarrow Nb^{IV}$ reduction is fast, the proton diffusion into the film is slow and requires a larger overpotential to be observed.

5.6 Galvanostatic Intermittent Titration Technique

The galvanostatic intermittent titration technique (GITT) was developed by Weppener and Huggins[35] and consists of applying a constant current (I) to the cell, whilst measuring the cell voltage. The current causes a constant concentration gradient through the electrode film at the phase boundary with the electrolyte. In order to maintain this concentration gradient, the applied cell voltage varies with time. Upon interruption of the applied current, the composition of the film becomes homogeneous again by the diffusion of the injected mobile species, causing the cell voltage to drift to a new steady state value E_e corresponding to a new activity of the injected species in the sample, as a result of the change of the stoichiometry (x) caused by the coulometric titration.[36] The advantage of this technique over chronoamperometry is that the measurements are taken at open circuit, and thus the film's resistance does not affect the results.

GITT was applied to the thin films (on ITO glass) in 1.0 mol dm^{-3} H_2SO_4 and the data analysed. The change in stoichiometry (x) is expressed as:[36]

$$x = ItM_B(Z_a m_B F)^{-1} \qquad (5.14)$$

where I, t, M_B, Z_a,m_B, F are, respectively, the constant current pulse, duration of the pulse, molecular weight of Nb_2O_5, valence of H^+, the mass of the oxide, and Faraday's constant. This enables a plot of E_e vs x to be obtained. Furthermore the potential is expressed as;[36]

$$E(t) = 2V(dE_e/dx)I^2(t/\pi D)^{1/2}(FAZ_a)^{-1} \qquad (5.15)$$

where V, A, dE_e/dx, D are, respectively, the molar volume, the surface area, the slope of the open circuit voltage vs the change in stoichiometry, and the diffusion coefficient of H^+. Thus a plot of E(t) vs $t^{1/2}$ should give a linear plot from which the diffusion coefficient at a given

charge density is obtained. However, upon plotting E(t) vs $t^{1/2}$ for the Nb_2O_5 films, no linear plot was observed. Furthermore log(E) vs log(t) plots did not show a simple relationship. This is perhaps due to the distributive resistance effects of the film but has not been confirmed.

5.7 Ethylene Glycol Gel Electrodes

As Chapter 3 indicated, a number of thick Nb_2O_5 films were made from ethylene glycol solutions of $NbCl_5$. A 0.5 mol dm^{-3} solution of $(NbCl_5)_2$ was made, mixed with water in a 10:1 H_2O:Nb ratio and spread onto ITO glass. The electrodes were then left for 4 days at room temperature until they had formed soft white gel films on the electrodes. Using a 0.5 mol dm^{-3} $LiClO_4$ solution in acetonitrile, cyclic voltammetry and chronoamperometry experiments were conducted on the films. The films gave CV's of the type shown in Fig.5.3. All the films gave very little bronze formation, only a slight blue colour was ever observed and then mainly around the edges of the film.Film failure occurred after 3 cycles, when the films broke up. The low electrochromic response of the films can be explained by considering the effect of the expelled ethylene glycol upon the gel. Because of its low vapour pressure it will not evaporate, but is retained in the smallest pores, limiting access to the these pores, which hinders diffusion of M^+.[10]

5.8 Microelectrodes

In a normal large surface area electrode, oxidation or reduction of the species in the electrolyte, causes a build up of oxidised (or reduced) species at the electrode surface as the diffusion from the surface layer of the electrode/electrolyte is slower than the production of oxidised (or reduced) species. This is due to the large area electrode having a perpendicular concentration flux to the electrode surface (see fig 5.22(a)). This build up gives rise to the characteristic oxidation and reduction peaks, which for ferrocene give the CV trace shown in Fig. 5.22(b).

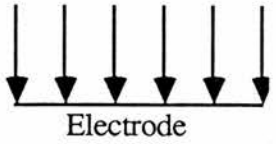

Fig.5.22(a)

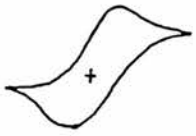

Fig.5.22(b)

For these large surface area electrodes, the anodic peak current is defined as;[37]

$$i_p=(2.69x10^5)n^{3/2}AD^{1/2}v^{1/2}C \qquad (5.16)$$

where n=number of electrons, F = Faraday constant=96500Cmol^{-1}, A = area of electrode, D = diffusion rate, v = scan rate of CV, C = conc. of redox active species.

However, with microelectrodes only a tiny fraction of the electrode surface is accessible, the rest of the electrode being covered in an impervious layer. These very small, often circular areas of naked electrode, have a hemispherical diffusion flux (see Fig. 5.23(a)).

Fig.5.23(a)

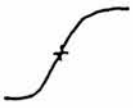

Fig 5.23(b)

Thus, by analogy, they have a greater edge to area ratio than the normal large electrode, giving rise to an expansion of the diffusion layer and to faster diffusion. This means that oxidised (or reduced) species do not build up at the electrode surface, and are not present in large quantities upon cycling to a reducing (or oxidising) voltage. Thus they give rise to hysteresis-free CV plots (as shown in Fig.5.23(b)). When the electrode current is controlled by a hemispherical diffusion process, the limiting plateau current (i_l) is given by:[37]

$$i_l=4nFDCrN \qquad (5.17)$$

where r = radius of electrodes, N =number of electrodes/cm^2, n = number of electrons, F = Faraday constant, A = area of electrode (1cm^2), D = diffusion rate, C = conc. of redox active species. Thus it is possible to calculate the number of microelectrodes/cm^2.

5.8.1 Mixed Silicone/NbO Polymer Electrodes

A set of mixed uncracked silicone/NbO polymers electrodes were obtained by mixing the required volumes of 0.2 mol dm^{-3} $(NbCl_5)_2$ in EtOH , glymo and water, spreading a 6µl drop of the resulting solution on 2 cm^2 of an ITO glass electrode and heating in the oven (see section 9.5.5 for detailed preparation). They are effectively electrodes made solely from the composite type coating.

Because glymo films break up when immersed in water, non-aqueous anhydrous solvents were used for the electrochemical experiments. None of the films showed any electrochemistry or electrochromism when CV's were run in a 0.5 mol dm^{-3} $LiClO_4$ solution in acetonitrile. When the CV's were run in a 0.1mol dm^{-3} TBAHFP and 1.37 x 10^{-3}mol dm^{-3} ferrocene solution in AN, the electrodes gave steady state currents which could be due to hemispherical diffusion through micropores. The typical current for the NbO/silicone films was a factor of 20 times lower than that for similar sized bare ITO glass electrodes, showing the blocking nature of the silicone film.

5.9 Conclusions

In conclusion, we have shown that it is possible to make large area thick-film displays from sol-gel processed Nb_2O_5, but that these cells are extremely unstable to cycling and thus their durability is limited. It is possible to create more durable cells by the application of a mixed NbO/silicone second coating.This coating does not appear to detract greatly from the electrochromic properties of the Nb_2O_5 films, as these composite films show similar H^+ colouration diffusion properties to the uncoated film and similar coulombic efficiencies to earlier reported Nb_2O_5 films.[21] This would indicate that the durability of thick sol-gel processed films can be increased without the loss of their electrochromic properties i.e. coulombic efficiencies and response times are similar to those of Nb_2O_5 films created by sputtering techniques.

We have also shown that it is possible to create thin Nb_2O_5 films, by sol-gel processing, that are extremely durable. These films have a dense glass like structure and exhibit excellent coulombic efficiencies.

References

1. M. Green and K. Kang, *Displays*, (October 1988), 166.
2. W.A. England, M.G. Cross, A. Hamnett, P.J. Wiseman and J.B. Goodenough, *Solid State Ionics*, 1980, **1**, 231.
3. B. Reichman and A.J. Bard, *J. Electrochem. Soc.*, 1979, **126**, 583.
4. K. Itaya and I. Uchida, *Acc. Chem. Res.*, 1986, **19**, 162.
5. R.E. Malpas and A.J. Bard, *Analyt. Chem.*, 1980, **52**, 109.
6. B. Reichman and A.J. Bard, *J. Electrochem. Soc.*, 1980, **127**, 241.
7. (a) S. Rigo, J. Siejka, *Solid State Commun.*, 1974, **15**, 259; (b) T. Hurless, H. Bentzen and S. Homkjol, *Electrochim. Acta*, 1987, **32**, 1613; (c) R.M. Toresi and F.C. Nant, *Electrochim. Acta*, 1988, **33**, 1015; (d) C.K. Dyer and J.S.L. Leach, *J. Electrochem. Soc.*, 1978, **125**, 23.
8. R. Cabanel, J. Chaussy, J. Mazuer, G. De la Bouglise, J.C. Jubert, G. Barral and C. Montella, *J. Electrochem. Soc.*, 1990, **137**, 1444.
9. N. Machida, M. Tatsumisaga and T. Minami, *J. Electrochem. Soc.*, 1986, **133**, 1963.
10. C.J. Brinker and G. Scherer, "Sol-gel Science", Academic Press, New York, 1989.
11. J. Livage, *Prog. Solid State Chem.*, 1988, **18**, 259.
12. M. Nabari, S. Doeff, C. Sanchez and J. Livage, *Mater. Sci. Eng.*, 1989, **133**, 203.
13. (a) A. Chemseddine, R. Monneau and J. Livage, *Solid State Ionics*, 1983, **5**, 357; (b) C. Sanchez, J. Livage, M. Henry and F. Babonneau, *J. Non-Cryst. Solids*, 1988, **100**, 65: (c) O. Kamaguchi, D. Tonihisa, H. Kawabata and K. Shimizer, *J. Am. Ceram. Soc.*, 1987, **70**, C94; (d) K. Yamanaka, *J. Appl. Phys.*, 1981, **20**, L307.
14. H. Schmidt, *Inorganic and Organometallic Polymers* ACS Symp. Series 360 Washington DC, 1988, Ch. 27, p. 333.
15. C. Alquier, M.T. Vandenborne and M. Henry, *J. Non-Cryst. Solids*, 1986, **79**, 383.
16. R.S. Crandall and B.W. Faughnan, *Appl. Phys. Lett.*, 1976, **28**, 95.
17. S.K. Deb "*Proceedings of the Symposium on Electrochromic Materials*" Eds. M.K. Carpenter, D.A. Corrigan, The Electrochem. Soc. Vol 90-2, Philadelphia, 1990, p3.
18. R.J. Cava, D.W. Murphy and S.M. Zahurak, *J. Electrochem. Soc.*, 1983, **130**, 2345.

19. W.C. Dautrmont-Smith, *Displays*, 1982, **3**, 3.

20. R.D. Rauh and S.F. Cogan, *Solid State Ionics*, 1988, **28-30**, 1707.

21. A.R. Hillman, "Electrochemical Science and Technology of Polymers", ed. R. G. Linford, Elsevier Appl. Sci., London, 1987, p103+.

22. P. Audebert, P. Griesmar, C. Sanchez, *J. Mater. Chem.*,1991, **1**, 699.

23. R.W. Murray, "*Electroanalytical Chemistry*",1985, p191.

24. S.K. Mohapatra, *J. Electrochem. Soc.*, 1978, **125**, 284.

25. J. Nagai, T. Kamimori, *Jpn. J. Appl. Phy.*, 1983, **22**, 681.

26. R. Manoharan, J.B. Goodenough, *J. Electrochem. Soc.*, 1990, **137**, 910.

27. M.A.B. Gomes, L.O. de S. Bulhoes, S.C. de Castro, A.J. Damiao, *J. Electrochem. Soc.*, 1990, **137**, 3067.

28. B.W. Faughnan, R.S. Crandall and M.A. Lampert, *Appl. Phys. Lett.*, 1975, **27**, 275.

29. Southampton Electrochemistry Group, "Instrumental Methods in Electrochemistry", Ellis Horwood, London, 1990, p251-282.

30. R.A. Lemon, G.D. Boyd, J.C. Phillips, J.P. Remeika, E.G. Spencer, *Solid State Commun.*, 1979, **30**, 73.

31. N. Machida, I. Sakono, M. Tatsumisago, T. Minami, *Chem. Lett.*, 1985, **46**, 1501.

32. N. Winograd, "Laboratory Techniques in Electroanalytical Chemistry," eds. P.T. Kissinger, W.R. Heineman, Dekker, New York, 1984, p. 326.

33. A.R. West, "Solid State Chemistry and its Applications", J. Wiley and Sons, London, 1984, p482-489.

34. M. Kalaji, L.M. Peter, *J. Chem. Soc. Farady Trans.*, 1991, **87**, 853.

35. W. Weppner, R.A. Huggins, *J. Electrochem. Soc.*, 1977, **124**,1569.

36. M.A.B. Gomes, L.O. De Sousa Bulhoes, *Electrochim. Acta*, 1990, **35**, 765.

37. R.M. Penner, N.S. Lewis, *Chem. and Ind.*, 1991, 788.

38. T. Kowhnat, D.E. Boblitz, *J. Am. Chem. Soc.*, 1960, **82**, 584.

Chapter 6

The Electrochemistry of Niobium Precursor Compounds

6.0 Introduction

Prior to the electrodeposition experiments, the electrochemistry of the niobium precursor compounds used in the electrodeposition experiments was investigated. The electrochemistry experiments can be split into two categories, aqueous and non-aqueous systems. Previous investigations of the non aqueous electrochemistry of niobium(V) have been complicated by the well-known hydrolytic instability of early transition metal halides.[1-4] $NbCl_5$ is readily hydrolysed to $NbOCl_3$ and HCl, for example. Clear characterization of the species present in the electrolyte solution under the conditions of the electrolysis is thus essential. Use of ^{93}Nb NMR offers the perfect tool for in situ characterization of the solutions prior to an electrochemical investigation of these species. We investigated the cyclic voltammetry of a number of niobium species:- $CsNbCl_6$, $(NbCl_5)_2$, $NbCl_5.AN$, (AN = CH_3CN), $NbOCl_3$, and $(Nb(OR)_5)_2$, (R = Me, Et, ^iPr) in non-aqueous solvents. Likewise the aqueous cyclic voltammetry of $(NbCl_5)_2$ and $K_7HNb_6O_{19}.13H_2O$.

Results and Discussion

6.1 Non-Aqueous Electrochemistry

6.1.1 $(NbCl_5)_2$ in Acetonitrile

^{93}Nb NMR of $(NbCl_5)_2$ added to warm (315K) anhydrous acetonitrile gives a peak at -55ppm (FWHM 500Hz) and is indicative of the monomer adduct, $NbCl_5.AN$.[5] The cyclic voltammogram of a 0.05 mol dm^{-3} solution of $NbCl_5.AN$ at 293K is shown in Fig. 6.1 and consists of five reduction waves and an oxidation wave (6) observed on the reverse scan. A summary of the redox potentials observed by us is given in Table 6.1. Kirk et al[6] assigned the reduction waves to the following reactions:

Fig. 6.1

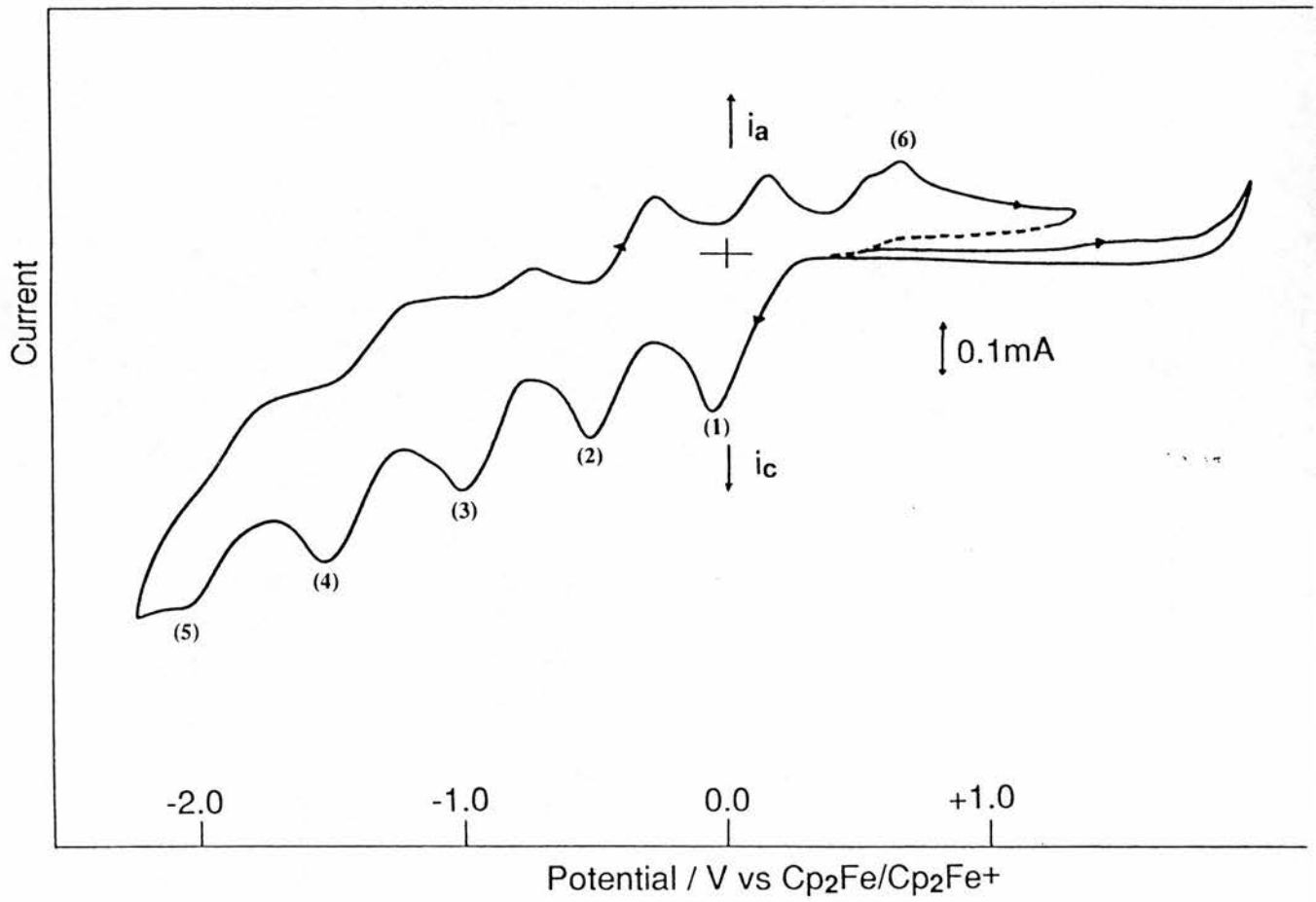

Fig. 6.1. CV (scan rate 100 mV/s) of 0.05 mol dm^{-3} solution of $NbCl_5$.AN in acetonitrile

Table 6.1

	Summary of the Redox Potentials of $(NbCl_5)_2$ in Acetonitrile at 293K.[a]		
Redox Couple	$E_{p,c}$ (V)	$E_{p,a}$ (V)	$E_{p,1/2}$ (V)
Wave 1	-0.06	0.16	0.05
wave 2	-0.53	-0.26	-0.40
wave 3	-1.03	-0.74	-0.89
wave 4	-1.56	-1.21	-1.39
wave 5	-2.09	-1.75	-1.92

(a) vs Cp_2Fe/Cp_2Fe^+ $E_{1/2}$

Table 6.2

	Summary of Nb^V--->Nb^{IV} Cyclic Voltammetric Data Obtained for Various Niobium Compounds and Solvents at 293K				
Species	Solvent	$E_{p,c}$,[a] V	$E_{p,a}$,[a] V	$E_{1/2}$,[a] V	$E_{p,c}$,[a] V
Nb_2Cl_{10}	DMF	-0.48	-0.40	-0.44	
$NbCl_5$.AN	AN	-0.06	0.16	0.05	0.13[b]
$CsNbCl_6$	AN	-0.25	-0.10	-0.18	-0.29[c]
$NbOCl_3.(AN)_2$	AN	-1.50	-1.20	-1.35	
$NbOCl_3$	DMF	-1.10	-0.80	-0.95	-1.15[d]

(a) vs Cp_2Fe/Cp_2Fe^+ $E_{1/2}$

(b) Originally vs N.H.E. at T=278K. Cp_2Fe/Cp_2Fe^+ $E_{1/2}$ = 0.400V vs N.H.E. (ref.3).

(c) Originally vs N.H.E. (ref. 3).

(d) Originally vs Saturated Cadmium Amalgam Electrode (SCAdE). Cp_2Fe/Cp_2Fe^+ $E_{1/2}$ = 1.05V vs SCAdE. (ref. 4).

wave 1 $NbCl_5.AN + e^- \rightarrow [NbCl_5.AN]^-$ (6.1)

wave 2 $[NbCl_6]^- + e^- \rightarrow [NbCl_6]^{2-}$ (6.2)

wave 3 $NbCl_4.AN_2 + e^- \rightarrow [NbCl_4.AN_2]^-$ (6.3)

wave 4 $[NbCl_5.AN]^- + e^- \rightarrow [NbCl_5.AN]^{2-}$ (6.4)

wave 5 $[NbCl_6]^{2-} + e^- \rightarrow [NbCl_6]^{3-}$ (6.5)

wave 6 $NbCl_4.AN_2 - e^- \rightarrow [NbCl_4.AN_2]^+$ (6.6)

They further proposed that the redox couple associated with wave 1 is characteristic of an ec reaction with the following mechanism:

$NbCl_5.AN + e^- \rightarrow [NbCl_5.AN]^-$ (6.7)

$[NbCl_5.AN]^- + NbCl_5.AN \rightarrow NbCl_4.AN_2 + [NbCl_6]^-$ (6.8)

We conducted variable scan-rate studies on the redox couple associated with wave 1. This showed that an ec reaction was occurring. The evidence for the ec reaction is based on the following criteria:[7] (i) $I_{p,a}/I_{p,c} < 1$,but tends to 1 as scan rate (ν) increases. (ii) $I_{p,c}/\nu^{1}/_{2}$ decreases by 0.2V from $\nu = 20$ mV s^{-1} to 800 mV s^{-1}. (iii) $E_{p,c}$ is positive of the value for the reversible case. This confirms the proposal[6] regarding the formation of $NbCl_4.AN_2$ and $[NbCl_6]^-$ in eq.(6.8). Using Nicholson and Shain's method,[7] the rate constant (k) for eq.(6.8) is calculated to be $k = 1.97 \pm 0.08$ s^{-1}.

Likewise, our variable scan-rate studies show that the larger than expected ΔE_p (approximately 200mV at a scan rate of 100mVs^{-1}) for each of the redox couples associated with waves 3, 4, 5 is due to an ec reaction. This is because the Nb(III) species formed on the cathodic scan are unstable on the time scale of cyclic voltammetry.[6] The further oxidation peak (wave 6) observed at +0.66V does not have an observable reduction peak associated with it at low scan rates (0-100mV s^{-1}). However, at high scan rates (200-800mV s^{-1}) a reduction peak is observed at +0.54 V. Bursten et al[3] have shown that eq(6.6) has an anodic peak ($E_{p,a}$) at +0.66V vs Cp_2Fe/Cp_2Fe^+, and a cathodic peak ($E_{p,c}$) at 0.60V which is only observed at high scan-rates (500mV s^{-1}), matching that observed for wave 6. Thus it appears that the peak at +0.66V is due to the oxidation of $NbCl_4.AN_2$ (eq.(6.6)). Variable scan rate studies indicate that the shoulder observed at 0.56V on the anodic sweep is due to the oxidation of a species

formed by an ec reaction at the redox couple associated with wave 2, however the exact nature of this species is not yet known.

6.1.2 $(NbCl_5)_2$ in DMF

Cyclic voltammetry of the 10 mmol dm^{-3} solution of $(NbCl_5)_2$ in DMF reveals a reversible reduction at -0.48 V vs Cp_2Fe/Cp_2Fe^+ (see Table 6.2). Microelectrode chronamperometry on the $(NbCl_5)_2$ dimer at -0.5 V showed a $1e^-$ process (n=1.006) and a very slow diffusion rate, $D = 4.03 \times 10^{-7} cm^2 s^{-1}$ (cf $[NbCl_6]^-$ $D = 0.8 \times 10^{-5}$ $cm^2 s^{-1}$).[6] This implies that for the dimer, each Nb undergoes a $^1/_2$ e reduction process or that only one Nb is reduced fully to Nb(IV), to give a mixed Nb^{IV}/Nb^V dimer. The reason for the slow diffusion rate (ferrocene is 100 times faster) is puzzling, but perhaps can be partly explained by the bulkiness of the dimer.

6.1.3 $CsNbCl_6$ in Acetonitrile

The position of the $[NbCl_6]^-$ redox couple ($E_{1/2}$=-0.18V, see Table 6.2) was found to be in agreement with that seen by Bursten et al[3] and Kirk et al[6] and is close to that observed for $(NbCl_5)_2$. This is to be expected, as both are octahedral $NbCl_6$ units. Upon cycling the 0.02 mol dm^{-3} solution around the redox potential, a purple film of highly insoluble Cs_2NbCl_6 forms.

6.1.4 $Nb(OR)_5)_2$ in DMF or Acetonitrile (R = Me, Et, ^{i}Pr)

No redox couples were observed for any of the niobium alkoxides, although $(Nb(OEt)_5)_2$ does show a broad irreversible reduction peak at -1.30V in DMF. This is assigned to a Nb(V) $\rightarrow$ Nb(IV) reduction due to the formation of the characteristic blue colour of Nb(IV) upon electrolysis of the solution at -1.35V. Unfortunately, the compound produced was too unstable to be analysed.

6.2 $(NbCl_5)_2$ in Wet Solvents

6.2.1 $NbOCl_3$ Formation

Water impurities, or deliberate addition of water to dissolved $NbCl_5$ leads ultimately to a Nb_2O_5 gel. However, controlled addition of 2 equivalents of water to $(NbCl_5)_2$ dissolved in organic solvent gave, upon ultrasonication for 1 hour, $NbOCl_3.(AN)_2$ in acetonitrile or $NbOCl_3$ in DMF. This was confirmed by ^{93}Nb NMR, $NbOCl_3.(AN)_2$ having a peak at -498ppm (FWHM~850Hz) and $NbOCl_3$ in DMF having a peak at -500ppm (FWHM~1200Hz).[5] More water than is stoichiometrically necessary must be added to force the complete hydrolysis to $NbOCl_3$ otherwise the partial hydrolysis occurs as shown in eq.(6.9):

$$(NbCl_5)_2 + H_2O \rightleftharpoons NbOCl_3 + [NbCl_6]^- + 2H^+ + Cl^- \qquad (6.9)$$

The redox couples for 0.02 mol dm^{-3} solutions of $NbOCl_3.(AN)_2$ and $NbOCl_3$ are given in Table 6.2. Microelectrode chronoamperometry on the $NbOCl_3.(AN)_2$ reduction at -1.5V gave n = 1.198 and D = 3.098 x 10^{-5} cm^{-2} s^{-1}. In DMF, $NbOCl_3$ reduction at -1.1V gave n = 1.304 and D = 1.426 x 10^{-5} cm^{-2} s^{-1}. Variable scan rate studies on these two redox couples show that there is a catalytic reaction occurring (ie regeneration of starting species). The evidence for the catalytic reaction is based on the following criteria:[7] (i) $I_{p,a}/I_{p,c} << 1$. (ii) $I_{p,c}/\nu^1/_2$ decreases markedly (by 50%) on increasing ν from 10-1000 mV s^{-1}. Precisely what this catalytic mechanism is, is not clear at the moment; however, one mechanism that seems likely is that the excess water present immediately oxidises any Nb^{IV} formed back up to Nb^V. After correcting for the use of different reference electrodes our data confirms Sherman and Archer's belief[4] that their observed reduction at -1.15V vs Cp_2Fe/Cp_2Fe^+ for $(NbCl_5)_2$ in wet DMF was in fact due to $NbOCl_3$ rather than $NbCl_5$. When they generated large amounts of blue Nb(IV) by the reduction of $NbOCl_3$ they observed that its blue colour and ESR signal faded over time, and from this they postulated that Nb^{IV} disproportionated to a diamagnetic Nb^V/Nb^{III} dimer species of the form:

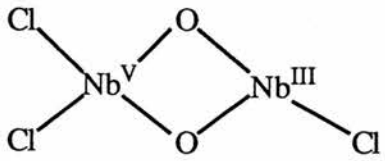

We have not been able to verify that this dimer species is formed because no oxidation peak has ever been observed for this species. However, because excess water is still present in these solutions, there exists a second possible reason for the loss of Nb^{IV}. The water will be free to react with any species formed by the electrochemical reduction. Nb^{IV} species in organic solvents are notoriously moisture sensitive[8,9] and so it seems possible that the Nb^{IV} is being oxidised back to Nb^{V} by excess water rather than disproportionating by the following type of reaction:

$$[NbOCl_3]^- + [H_3O]^+ \rightarrow NbOCl_3 + H_2O + {}^1/_2H_2 \qquad (6.10)$$

6.3 Aqueous Electrochemistry

6.3.1 $(NbCl_5)_2$ in Conc. HCl

The 0.1 mol dm^{-3} solutions of $(NbCl_5)_2$ in conc. HCl showed two reduction peaks at E_{pc}= -0.50V and -0.76V (vs SCE) (see Fig.6.2) and confirm the $E_{1/2}$ values reported by McCullough and Meites.[10,11] They assigned the peak at -0.50V to the $2e^-$ reduction of the Nb(V) dimer species, $[(NbOCl_4)_2]^{2-}$, to a Nb(IV) dimer species. Our variable scan rate and limited scan range studies show that the corresponding oxidation peak is observed at -0.30V. The second reduction peak they assigned to a $2e^-$ reduction of the Nb(IV) dimer to a mixed Nb(IV)/Nb(II) dimer species. This mixed dimer species then disproportionates to a Nb(III) dimer. The shoulder observed at -0.1V on the anodic sweep is only observed at low scan rates (<500mVs^{-1}). McCullough and Meites[10,11] found that the Nb(IV) dimer species could disproportionate into a mixed Nb(V)/Nb(III) dimer, thus the observed peak at -0.1V may be due to the $2e^-$ oxidation of this mixed oxidation state dimer.

6.3.2 "Amorphous" $K_7HNb_6O_{19}.13H_2O$ in 0.1 Mol dm^{-3} KOH

No redox couples were observed for this compound in the -1.0V to +0.7V electrochemical window available.

Fig. 6.2

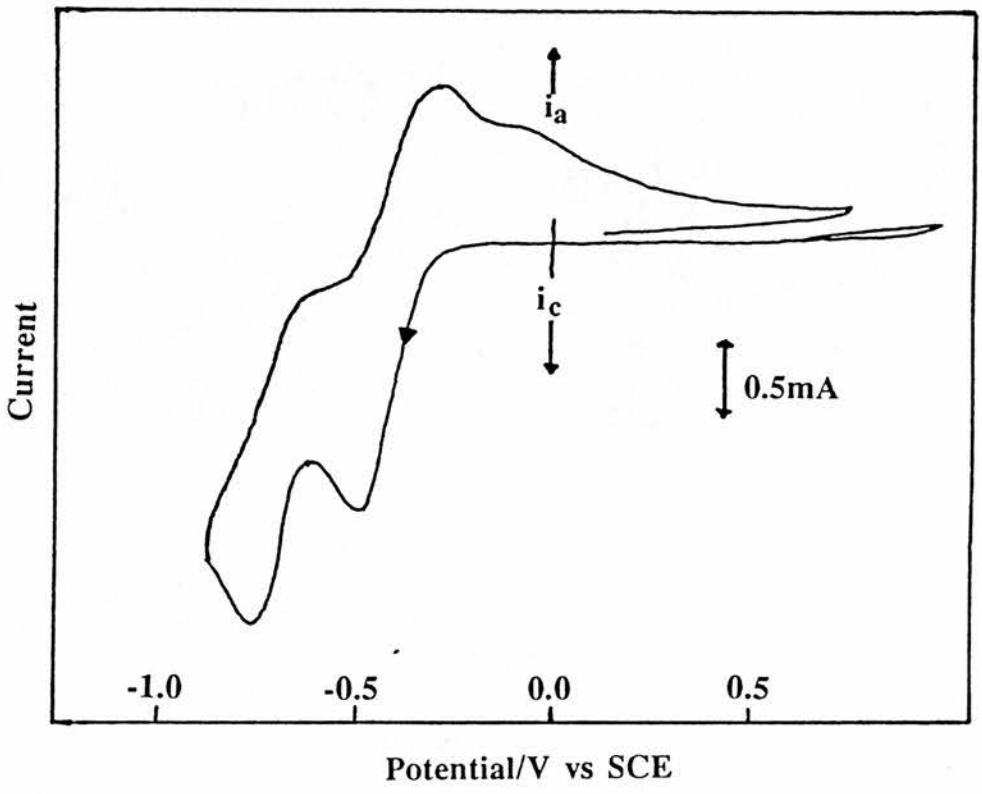

Fig. 6.2. CV (scan rate of 100 mV/s) of 0.1 mol dm^{-3} solution of $(NbCl_5)_2$ in conc. HCl.

References

1. R. Gut, *Helv. Chim. Acta*, 1960, **43**, 830.
2. V.Gutmann and M.Michlanayr, *Monactsch. Chem.*, 1968, **99** , 326.
3. B.E. Bursten, M.R. Green, V.Katovic, J.R. Kirk and D. Lightner Jr., *Inorg. Chem.*, 1986, **25**, 831.
4. L.R.Sherman and V.S. Archer, *Analytical Chem.*, 1970,**42** ,1356.
5. R.G.Kidd and H.G.Spinney, *Inorg. Chem.*, 1973, **12**, 1967.
6. J.R. Kirk, D. Page, M. Prazak, V. Katovic, *Inorg. Chem.*, 1988, **27**, 1956.
7. Southampton Electrochemistry Group," Instrumental Methods in Electrochemistry", Ellis-Horwood, Chichester, 1985, p 193-196.
8. D.A.Miller and R.D. Bereman, *Coord. Chem. Rev.*, 1972/3, **9**, 107.
9. L.G. Hubert-Pfalzgraf, M.Postel and J.G.Riess," Comprehensive Coordination Chemistry" ed G. Wilkinson, Pergamon,1987, vol.3, p 585-698.
10. J.G. McCullough, L. Meites, *J. Electroanal. Chem.*, 1967, **18**, 123.
11. J.G. McCullough, L. Meites, *J. Electroanal. Chem.*, 1968, **19**, 111.

Chapter 7

Electrochemical Deposition of Niobium Oxide

7.0 Introduction

Electrochemical deposition of ceramic metal oxide films can, like sol-gel processing (SGP), offer the advantages of low temperature processing, high purity and controlled microstructure. However, unlike SGP it also offers the possibility of forming crystalline rather than amorphous low temperature processed films.[1]

Much work has been done developing techniques to electrodeposit metal oxide films, mainly from aqueous solution using a redox change technique, whereby a metal is oxidised or reduced at the electrode surface by a fixed applied potential. The pH of the solution is adjusted so that whilst the initial oxidation state is stable, the new oxidation state readily undergoes hydrolysis to a metal hydroxide or oxide. This metal hydroxide/oxide is insoluble and forms a film on the electrode.

Some of the first research done using this technique was that by Tench and Warren[2] who successfully electrodeposited oxide and hydroxide films (up to 1μm thick) of copper, nickel, cobalt, iron and manganese from aqueous metal salt solutions (pH 6.5-7.5). These films were shown to have some interesting properties: thus the nickel oxy-hydroxide films showed electrochromic properties whilst the crystalline Cu_2O films exhibited p-type semiconducting behaviour when under illumination. Since then the technique has blossomed with much work being directed at the formation of the YBaCuO superconductors,[3] and lead/thallium oxide films.[1,4-7] Upon codeposition of Tl_2O_3 and PbO_2 Sakkai et al[4] obtained a new compound, $Pb_8Tl_5O_{24}$ which had a cubic fluorite type structure, whilst Thanos and Wabner[7] were able to grow lead dioxide anodes (for use as dimensionally stable electrodes), and by varying the electrodeposition temperature vary the content of β-PbO_2 relative to α-PbO_2. Switzer[1,5] prepared films of Tl_2O_3 on n-silicon to give a heterojunction

photoelectrochemical solar cell of 11% efficiency with 75.3 $mWcm^{-2}$ natural sunlight, as well as mixed Pb/Tl oxide films with a superlattice structure.[6]

Recently attention has turned to 2nd and 3rd row transition metal oxide electrodeposition because of their electrochromic and catalytic properties. Here potential cycling, rather than the earlier fixed applied potential method is used as this favours the formation of porous, hydrated metal oxide coatings.[8] Thus, IrO_x,[9] WO_3, MoO_3 and mixed WO_3/MoO_3 films[10] have been prepared and their electrochromic properties investigated, whilst Kulesza and Faulkner[11] prepared mixed covalent tungsten (VI,V) oxide films and examined their electrocatalytic properties.

Use of organic solvents for electrodeposition of metal oxides has not received as much attention as that of the aqueous systems and in general has been limited to the electrodeposition of pure metals which could subsequently be converted to oxides. YBaCu metal films have been deposited on cubic zirconia substrates from DMSO[12,13] at very negative potentials (-2.5V→-5V vs Ag/Ag^+) and sintered at 900°C to form YBaCuO superconductors, with a zero resistance at 91K. However, use of a mixed H_2O/DMSO solvent allows for the direct electrodeposition of YBaCuO films[14] at less negative potentials (-1.4V→-2.0V vs Ag/Ag^+) than that required for the deposition of YBaCu metal films. This favourable shift in the deposition potentials is attributed to the deposition of the oxide/hydroxide with the subsequent evolution of H_2. Thus although hydrogen evolution in this solvent system is observed at -2.0V, the metal ions in solution acts as hydrogen evolution promoters and react as follows:

$$M^{x+} + xH_2O + xe^- \rightarrow M(OH)_x + {}^x/_2H_2 \qquad (7.1)$$

Use of electrodeposition to form metal oxides, specifically niobium oxide seemed a natural extension of the work already done in investigating film formation techniques for preparing Nb_2O_5 electrodes. Niobium metal has been electrodeposited from molten salts in alkali metals,[15-17] or pure liquid halogens[18] and also from propylene carbonate and acetonitrile using $LiNbF_6$.[19] However, other than work done on the anodisation of niobium metal to niobium oxide[20] there appeared to be no methods for the direct electrodeposition of niobium oxide. Some factors contributing to the difficulty in electrodepositing Nb (and Nb_2O_5) appear to be a very negative reduction potential (which leads to interference by H_2 evolution in

aqueous systems), the tendency of niobium species to form electrochemically inactive species when reacted with O_2 or H_2O and the ability to form stable cluster compounds at low valence states.[19]

We decided to attempt to circumvent these problems by combining SGP with electrodeposition. Niobium species are known to be stable in aqueous and non-aqueous systems, but pH manipulation of these systems causes a hydrated Nb_2O_5 gel to form. Therefore, electrochemical generation of either ^-OH or H^+ in these solutions should, in theory, cause the electrodeposition of niobium oxide films, and it was this method of electrodeposition that we investigated.

Results and Discussion

7.1 Non-Aqueous Systems

NbX_5 precursors (X=OR,Cl etc) in organic solvents are very moisture sensitive, readily forming insoluble Nb_2O_5. Therefore, in order to electrodeposit Nb_2O_5 from organic solvents containing NbX_5, H_2O or ^-OH have to be generated electrochemically. Two methods for the electrochemical generation of H_2O or ^-OH were investigated.

7.1.1 Superoxide Generation

Constant potential electrolysis of non-aqueous solutions (AN, DMF, DMSO) containing 0.0025 mol dm^{-3} niobium precursor ($(NbCl_5)_2$, $(Nb(OEt)_5)_2$, and $(Nb(OPr^i)_5)_2$), O_2 and electrolyte (0.1 mol dm^{-3} tetrabutylammonium (TBA) hexafluorophosphate or TBA dihydrogen phosphate) were undertaken in an attempt to form films of Nb_2O_5. The reasoning behind these experiments was as follows. Oxygen readily undergoes a one electron reduction to form the superoxide ion:[21]

$$O_2 + e^- \rightleftharpoons O_2^- \qquad (7.2)$$

This can then undergo a second irreversible reduction (E_{pc} = -1.8V), with the product species reacting with solvent or electrolyte:[21,22]

$$O_2^- + e^- \rightarrow O_2^{2-} \qquad (7.3)$$

$$O_2^{2-} + \text{solv-H} \rightarrow HO_2^- + \text{solv} \qquad (7.4)$$

$$HO_2^- + \text{solv-H} \rightarrow H_2O_2 + \text{solv} \qquad (7.5)$$

where solv-H is a proton source (often the tetra butyl ammonium ion). H_2O_2 is known to react with $NbCl_5$ to give Nb_2O_5 gels, so it was hoped that the production of H_2O_2 at the electrode surface (via H^+ abstraction either from TBA or $H_2PO_4^-$) might give rise to a Nb_2O_5 film formation. Likewise the production of HO_2^- might lead to Nb_2O_5 via the following type of reaction:

$$10HO_2^- + 2Nb(X)_5 \rightarrow Nb(OH)_5 + 10X^- + 5O_2 \qquad (7.6)$$

However, regardless of solvent (AN, DMF), working electrode (Au, Pt, C), niobium precursor or period of electrolysis, no Nb_2O_5 film was ever observed when the solutions were electrolysed at -1.85→ -2.0V (vs SCE). The reason for this failure is not clear, but it is probable that the superoxide and its products were reacting with the solvent and electrolyte rather than the niobium precursors. Evidence for this belief is found when the electrolysis was done using the Au electrode. Upon electrolysis, small dendritic needles of a white compound were formed. SEM EDAX analysis revealed that this compound contained no metals. This implies the formation of an insoluble carbon species. That this was only observed on the Au electrode is ascribed to the fact that Au is the best generator of the superoxide ion.[21,22]

DMSO is extremely hard to dry[23] and, although redistilled over CaH_2, upon addition of $(NbCl_5)_2$ the solutions in DMSO became clear and gave CV's characteristic of $NbOCl_3$ formation (see section 6.2.1) implying the presence of water. Superoxide reacts in the following manner with water:[22]

$$2O_2^- + H_2O \rightleftharpoons O_2 + HO_2^- + {}^-OH \quad (k=0.91\text{x}10^9) \qquad (7.7)$$

Thus by electrolysing the solutions at -1.1V (vs SCE) it was hoped to generate ^-OH which would react with the $NbOCl_3$ to give Nb_2O_5. The failure to form Nb_2O_5 can be ascribed to the stability of $NbOCl_3$[19] and the neutralisation of ^-OH by H^+ generated in the formation of $NbOCl_3$.

7.1.2 Reduction of Tertiary Alcohols

Lund et al[24,25] have shown that tertiary alcohols can undergo a two electron reduction of the following type:

$$ROH + 2e^- + H^+ \rightarrow RH + {}^-OH \qquad (7.8)$$

This reaction occurs in anhydrous DMF (0.1 mol dm^{-3} TBA electrolyte), on a mercury electrode and at very negative potentials, usually less than -2.4V vs SCE. The generation of ^-OH in a solution containing niobium precursor species should instigate a sol-gel reaction and formation of a Nb_2O_5 film, and this does indeed occur.

Two tertiary alcohols were investigated – Triphenyl methanol (TPM, $(C_6H_5)_3COH$, $E_{1/2}$ = -2.81V[24]) and 9-Fluorenemethanol (9F, $(C_6H_4)_2C(CH_3)OH$, $E_{1/2}$ = -2.47V[24]). 0.1 mol dm^{-3} solutions of TPM and 9F in anhydrous DMF containing 0.1 mol dm^{-3} TBAHFP and 0.0025 mol dm^{-3} $(Nb(OEt)_5)_2$ were electrolysed at -2.90V and -2.50V respectively for between 3 and 16 hours. This produced yellow/white air stable films around the mercury drop. SEM EDAX analysis indicated the sole presence of niobium, and the absence of mercury. FTIR spectra confirmed that these films were Nb_2O_5. Figs. 7.1 (a) and (b) show SEM pictures of one of these coatings. Fig. 7(a) shows how the film followed the circular contours of the Hg drop.

Although this was a successful technique for the electrodeposition of Nb_2O_5 films, the very negative potentials excluded the possibility of forming films on more convenient electrodes (eg C) and the cost of the alcohols (9F costs £9.10g^{-1}) would prove prohibitive for the widespread use of this technique to generate Nb_2O_5 films. Because of these problems no further investigations of this approach were undertaken.

7.2 Aqueous Systems

Niobium (V) precursor compounds eg $Nb(OR)_5$ are notoriously moisture sensitive and readily form insoluble hydrated Nb_2O_5 upon addition of water. A literature search revealed only one instance of a soluble aqueous system being formed – the addition of $(NbCl_5)_2$ to conc. HCl.[26] Similarly most niobate systems are insoluble except for $K_7HNb_6O_{19}.13H_2O$ which is sparingly soluble in strong alkali.[27,28] Both these systems are pH sensitive – increase the pH of the HCl solution from -1 to -0.85 and a Nb_2O_5 gel forms. Likewise, lowering the pH of the alkali solution causes $K_7HNb_6O_{19}.13H_2O$ to undergoes hydrolysis to form

Fig 7.1 (a)

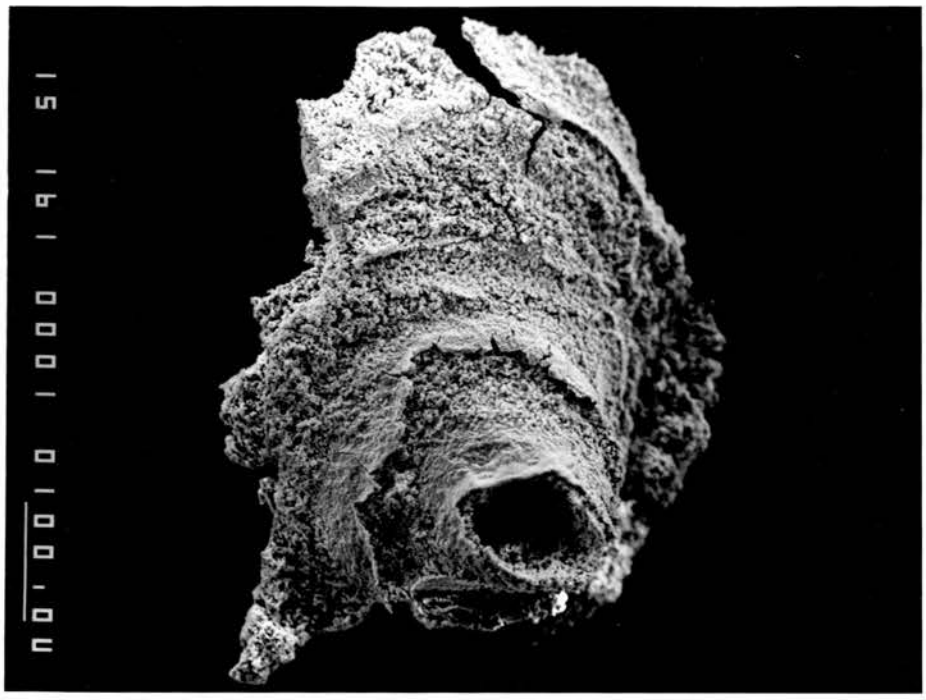

Fig. 7.1 (b)

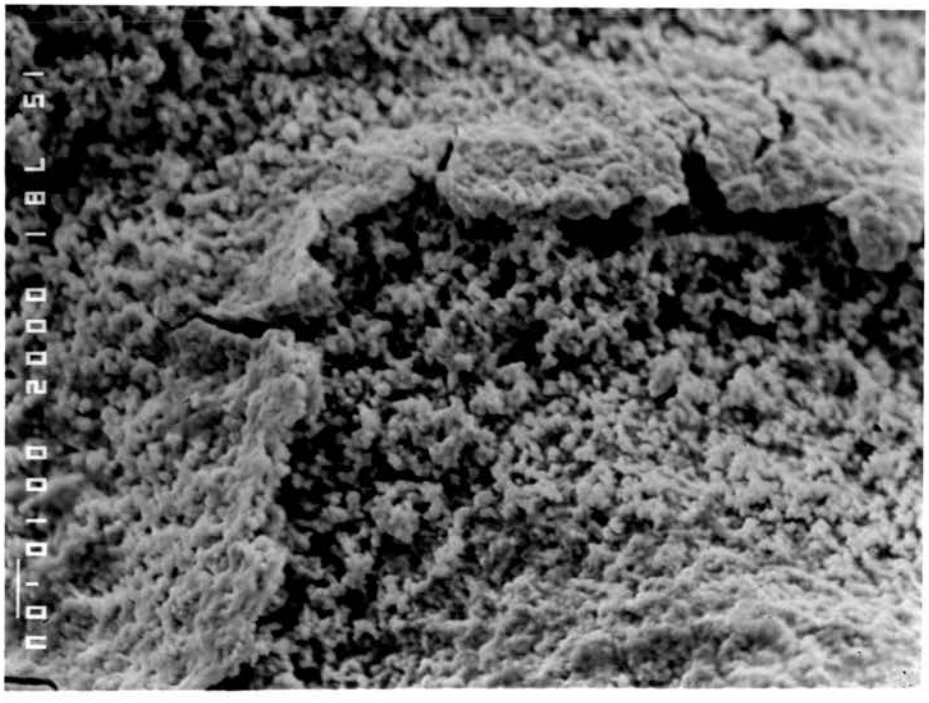

Fig 7.1. SEM picture of Nb_2O_5 film produced by the reduction of triphenyl methanol (a) and at higher magnification (b).

$H_6Nb_6O_{18}$ which dissociates irreversibly to form Nb_2O_5 and water.[29,30] As both H^+ and ^-OH can be generated electrochemically from H_2O, we tried to electrodeposit niobium oxide films from these aqueous systems.

7.2.1 $K_7HNb_6O_{19}$ in 0.1 mol dm^{-3} KOH

0.0019 mol dm^{-3} solutions of "amorphous" $K_7HNb_6O_{19}$ (see section 9.6.6) in 0.1 mol dm^{-3} KOH were electrolysed at between +1.60V and +1.95V for 1 to 23 hours. At these voltages water undergoes the following oxidation:

$$H_2O \rightarrow 2H^+ + {}^1/_2O_2 + 2e^- \qquad (7.9)$$

The protons generated neutralise the base, lowering the pH and electrodepositing a non-uniformly thick (~0.1mm) white film on the platinum electrode. X-ray Powder Diffraction analysis of this film proved that it is amorphous. FTIR analysis indicates a mixture of Nb_6O_{19}/Nb_2O_5 units.

The CV's of these films, obtained in 1.0 mol dm^{-3} H_2SO_4, are characteristic of electrochromic behaviour (see Fig. 7.2). The non-uniformity of the film is believed to be due to the slow formation of large O_2 bubbles, which pull bits of the film off. In order to further characterise these films a method of suppressing the O_2 bubble formation would be needed as well as a technique for electrodepositing the film onto an ITO electrode rather than Pt, so that chronoabsorptiometric techniques could be applied.

7.2.2 $(NbCl_5)_2$ in Conc. HCl

Electrolysing a 0.1 mol dm^{-3} solution of $(NbCl_5)_2$ in conc. (10.8 mol dm^{-3}) HCl at -0.5V (Pt electrode) or -1.0V (C electrode) reduces water by the following reaction:

$$H_2O + e^- \rightarrow {}^-OH + {}^1/_2H_2 \qquad (7.10)$$

The production of ^-OH increases the pH of the solution, and precipitates Nb_2O_5, rather than forming a film on the working electrode. This is surprising in view of the success in forming a film with $K_7HNb_6O_{19}$ upon pH manipulation. However, it was noted that H_2 evolution was accompanied by a large and very fast formation of small H_2 bubbles on the electrode surface which were rapidly lost to the solution. Thus it appears that any film formed is immediately

Fig. 7.2

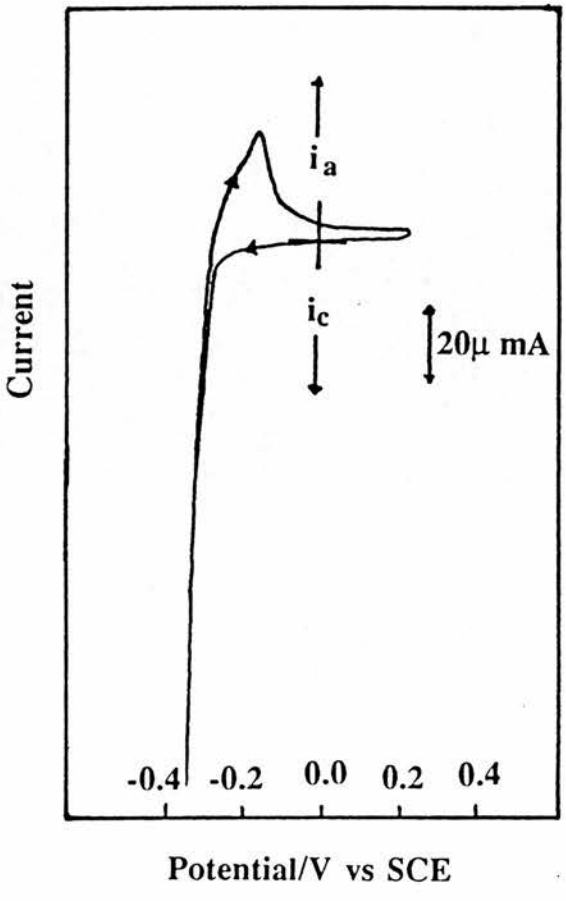

Fig. 7.2. CV (scan rate of 100 mV/s) of $K_7HNb_6O_{19}$ derived film in 1.0 mol dm^{-3} H_2SO_4.

pulled off by the "scouring" action of the H_2 bubbles, giving the observed precipitate. The Nb_2O_5, upon washing and subsequent drying at 150°C, gave FTIR's similar to those found for the niobium chloroalkoxide gels described in chapter 3 and shown in Fig. 9.1(a) and (c).

7.3. Mixed Organic/Aqueous Systems

Due to the unexpected and favourable shift in deposition potentials for the deposition of YBaCuO films in mixed organic/aqueous systems,[14] we felt we should examine this type of system for the case of niobium. 1.08 ml of conc. HCl was added to 10 ml of 0.1 mol dm^{-3} $(NbCl_5)_2$ in AN or DMF ($Nb:H_2O$ = 1:20). CV's of these solutions gave evidence for the formation of $NbOCl_3$ species and cycling around the Nb(V)/Nb(IV) redox potential gave a blue coloured solution but no film formation. Electrolysing at -1.20V (vs SCE) gave H_2 gas and a Nb_2O_5 precipitate (similar to that found in 7.2.2), but no film.

7.4 Conclusions

Electrodeposition of niobium oxide from a number of aqueous and non-aqueous solvent systems, via sol-gel processing techniques, has been attempted by the electrochemical pH manipulation of the solutions. Two methods have been shown to work. These techniques rely upon the electrochemical generation of protons and hydroxide ions. In nonaqueous systems containing niobium alkoxides, the hydroxide ions are generated by the two electron reduction of tertiary alcohols and react with the niobium precursor to give a film of niobium oxide. In aqueous systems containing a niobate, protons are generated by the electrochemical oxidation of water; this lowers the pH, destabilises the niobate sol and forms a film of mixed niobate and niobium oxide. Further work needs to be targeted at producing reproducible and uniform films.

References

1. J.A. Switzer, *Am. Ceram. Soc. Bull.*, 1987, **66**, 1521.
2. D. Tench, L.F. Warren, *J. Electrochem. Soc.*, 1983, **130**, 869.
3. P. Slezak, A Wieckowski, *J. Electrochem. Soc.*, 1991, **138**, 1039.
4. M. Sakai, T. Sekine, Y. Yamazaki, *J. Electrochem. Soc.*, 1983, **130**, 1631.
5. J.A. Switzer, *J. Electrochem. Soc.*, 1986, **133**, 722.
6. J. A. Switzer, *Science*, 1990, **247**, 444.
7. J.C.G. Thomas, D.W. Wabner, *J. Electroanal. Chem.*, 1985, **182**, 25.
8. L.D. Burke, E.J.M. O'Sullivan, *J. Electroanal. Chem.*, 1981, **117**, 155.
9. T. Yoshino, N. Baba, H. Masuda, K. Arai, "Proceedings of the Symposium on Electrochromic Materials" Eds. M.K. Carpenter, D.A. Corrigan, The Electrochem. Soc. Vol 90-2, Philadelphia, 1990, p89.
10. L.H. Dao, A. Guerfi, M.T. Nguyen, K.Arai, "Proceedings of the Symposium on Electrochromic Materials" Eds. M.K. Carpenter, D.A. Corrigan, The Electrochem. Soc. Vol 90-2, Philadelphia, 1990, p30.
11. P.J. Kulesza, L.R. Faulkner, *J. Am. Chem. Soc.*, 1988, **110**, 4905.
12. M. Maxfield, H. Eckhardt, Z. Iqbal, F. Reidinger, R.H. Baughman, *Appl. Phys. Lett.*, 1989, **54**, 1932.
13. R.N. Bhattacharya, R. Noufi, L.L. Roybal, R.K. Ahrenkiel, *J. Electrochem. Soc.*, 1991, **138**, 1643.
14. H. Minoura, K. Naruto, H. Takano, E. Haseo, T. Suguira, Y. Ueno, T. Endo, *Chem. Lett.*, 1991, 379.
15. U. Cohen, *J. Electrochem. Soc.*, 1981, **128**, 731.
16. G.P. Capsimalis, E.S. Chen, R. E. Paterson, I. Ahmad, *J. Appl. Electrochem.*, 1987, **17**, 253.
17. Q. Zhiyu, T. Pierre, *J. Appl. Electrochem.*, 1985, **15**, 259.
18. R.M. Rose, D.R. Sodoway, U.S. Patents No. 4,517,253 (1985).
19. N.S. Chong, J.L. Anderson, M.L. Norton, *J. Electrochem. Soc.*, 1989, **136**, 1245.

20. M.A. Biason Gomes, S. Onofre, S. Juanto, L.O. de S. Bulhoes, *J. Appl. Electrochem.*, 1991, **21**, 1023.

21. D.T.Sawyer, E.J. Narni, "Oxygen and Oxy Radicals in Chemistry and Biology", Academic Press, 1981, p15-44.

22. D.T. Sawyer, J.S. Valentine, *Acc. Chem. Res.*, 1981, **14**, 393.

23. D.R. Burfield, R.H. Smithers, *J.Org. Chem.*, 1978, **43**, 3966.

24. H. Lund, H. Doupeux, M.A. Michel, G. Mousset, J. Simonet, *Electrochim Acta*, 1974, **19**, 629.

25. M.A. Michel, G. Mousset, J. Simonet, H. Lund, *Electrochim Acta*, 1974, **19**, 629.

26. L.G. Hubert-Pfalzgraf, M. Postel, J.G. Riess, "Comprehensive Coordination Chemistry" eds G. Wilkinson, R.D. Gillard, J.A. McCleverty, Pergamon, Oxford, 1987, p585+.

27. D.J. Edlund, R.J. Saxton, D.K. Lyon, R.G. Finke, *Organometallics*, 1988, **7**, 1692.

28. F. Fairbrother, "The Chemistry of Niobium and Tantalum", Elsevier, London, 1967, p37.

29. G. Jander, D. Ertel, *J. Inorg. Nucl. Chem.*, 1960, **14**, (a) 71, (b) 77, (c) 85.

30. I. Lindqvist, *Arkiv Kemi*, 1952, **5**, 47. *Chem. Abs.* , 1953, **47**, 7284.

Chapter 8

Novel Chemistry of Nb(V) Compounds

8.0 Introduction

During the course of the research done for this thesis, a number of unexpected reactions were observed. These reactions are not part of the main thrust of the thesis, however it is felt that they are interesting enough to warrant inclusion within the thesis.

Results and Discussion

8.1 Chemical Reduction by Ferrocene of Nb (V)

Use of ferrocene ($FeCp_2$) as an internal standard for electrochemical experiments had interesting consequences. When added to the $CsNbCl_6$ solution (0.020 mol dm^{-3}) in acetonitrile, a purple solid (identical to the film formed in the $NbCl_6^-/NbCl_6^{2-}$ redox) immediately precipitated out, and the solution became a blue-green colour. The following reaction is proposed:-

$$2CsNbCl_6 + Cp_2Fe \rightarrow Cs_2NbCl_{6\,(s)} + Cp_2Fe^+NbCl_6^- \qquad (8.1)$$

The purple precipitate has been shown to be Cs_2NbCl_6. The IR spectum of the blue/black solid recovered from the blue solution identifies it as $FeCp_2NbCl_6$. Likewise, the UV/Vis data of the blue solution (Table 8.1) confirms the presence of Cp_2Fe^+ [λ_{max} /nm (relative intensity): 360(11), 615(1)][1] and $[NbCl_6]^-$ [247 (80), 293 (112), 324(sh)][2] in solution. That ferrocene should reduce $CsNbCl_6$ is surprising as the Nb^V/Nb^{IV} reduction is at -0.25 V vs Cp_2Fe/Cp_2Fe^+; however, it is assumed that the precipitation of Cs_2NbCl_6 acts as a driving force for this reaction. There appears to be no reason why the full range of the M_2NbCl_6 compounds (M= Gp I metal) cannot be prepared by this method and it certainly offers many advantages over a number of previous methods that often involved fusing of the materials at high temperatures.[3]

Table 8.1

Summary of UV/Vis Data Obtained For $NbCl_6^-$ and Ferricenium (nm)[a]						
Species	Solvent	$NbCl_6^-$			Ferricenium ion	
$CsNbCl_6$	AN	243.0 (80)	293.6 (115)	sh323.1		
$Cs_2NbCl_{6(s)} + Cp_2FeNbCl_6$	AN	244.6 (80)	293.0 (112)	sh324.1	361.3 (12)	616.8 (1)
$Cp_2FeNbCl_6$ redissolved	AN	245.6 (80)	292.9 (122)	sh325.0	361.4 (11)	616.4 (1)
$Cp_2^*Fe + Nb_2Cl_{10}$	DMF		292.2	sh324.0		778.4

(a) Figures in parentheses are the relative intensities of the peaks.

On addition of ferrocene to a 0.01 mol dm^{-3} solution of $(NbCl_5)_2$ in acetonitrile (AN), the yellow solution became blue. When the molarity of the $(NbCl_5)_2$ was increased to 0.25 mol dm^{-3}, a black/blue precipitate was formed which analysed as $FeCp_2NbCl_6$ (see chapter nine, section 9.8.2). Futhermore, the UV/Vis spectrum of the redissolved precipitate (Table 8.1) confirms the presence of both ferricenium and $[NbCl_6]^-$ chromophores. The following reaction is therefore proposed:

$$Cp_2Fe + 2\ NbCl_5 \xrightarrow{AN} Cp_2FeNbCl_{6\ (s)} + NbCl_4(AN)_2 \qquad (8.2)$$

A similar reaction has been observed for other redox systems, such as hexafluorometallates[4,5] and hexachlorometallates.[6] When ferrocene is added to $(NbCl_5)_2$ in DMF no reaction takes place, as the ferrocene is not a strong enough reducing agent ($E_{1/2}$ for $(NbCl_5)_2$ is -0.44V vs ferrocene). However, when decamethylferrocene ($E_{1/2}$ -0.47V vs ferrocene) is added, a blue/green solution is formed which shows the characteristic ferricenium peaks and one of the $[NbCl_6]^-$ peaks in the UV/Vis spectra (Table 8.1). The other $[NbCl_6]^-$ peak is obscured by the absorption of DMF in this region. Finally, note that $NbCl_4(AN)_2$, the other product of equation (8.2) was not isolated. However, evidence for its formation is observed by cyclic voltammetry. Upon addition of ferrocene to solutions of $NbCl_5$.AN in acetonitrile, the anodic peak at +0.66 V due to reoxidation of $NbCl_4(AN)_2$ increases in height.

Due to the very low solubility of $Cp_2FeNbCl_6$ in solvents such as acetonitrile, THF, DMF etc it proved impossible to obtain ^{93}Nb solution NMR of the compound. However it did prove possible to obtain ^{93}Nb solid powder NMR spectra of $Cp_2FeNbCl_6$ and this is described in the next section.

8.1.1 Solid State NMR

When a molecule is placed in a magnetic field, the shielding electrons around the nuclei are not spherically distributed and so the shielding is anisotropic. Thus the shielding observed (σ) on the proton or carbon nuclei in chloroform, for instance, will be different when the molecular symmetry axis of the molecule is perpendicular and when it is parallel to the applied field B_0 (see Fig. 8.1).

Fig. 8.1

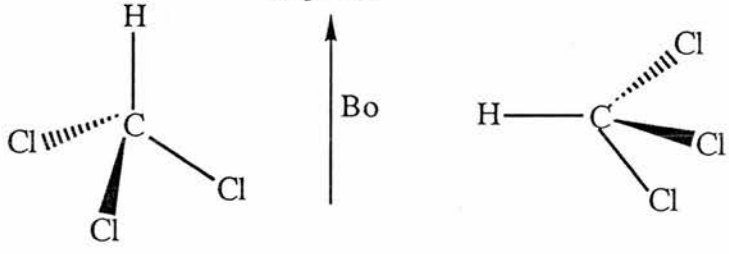

In general, for an axially symmetric molecule, the effective shielding in the direction of B_0, when the molecular axis is at an angle θ to B_0 is;

$$\sigma_{zz} = {}^1/_3(\sigma_{//} + \sigma_{\perp}) + {}^1/_3(3\cos^2\theta - 1)(\sigma_{//} - \sigma_{\perp}) \qquad (8.3)$$

Thus for a microcrystalline material, with all values of θ allowed at random, 3 types of spectra can be observed, as shown in Fig. 8.2.

Fig. 8.2

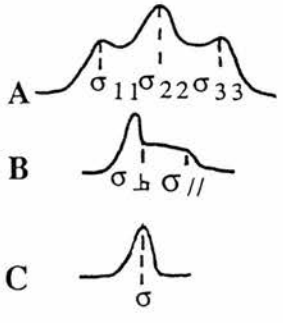

where A is the general case, B an axially symmetric case, C an isotropic case (σ = isotropic average = ${}^1/_3(\sigma_{//} + 2\sigma_{\perp})$).[7]

Fig. 8.3

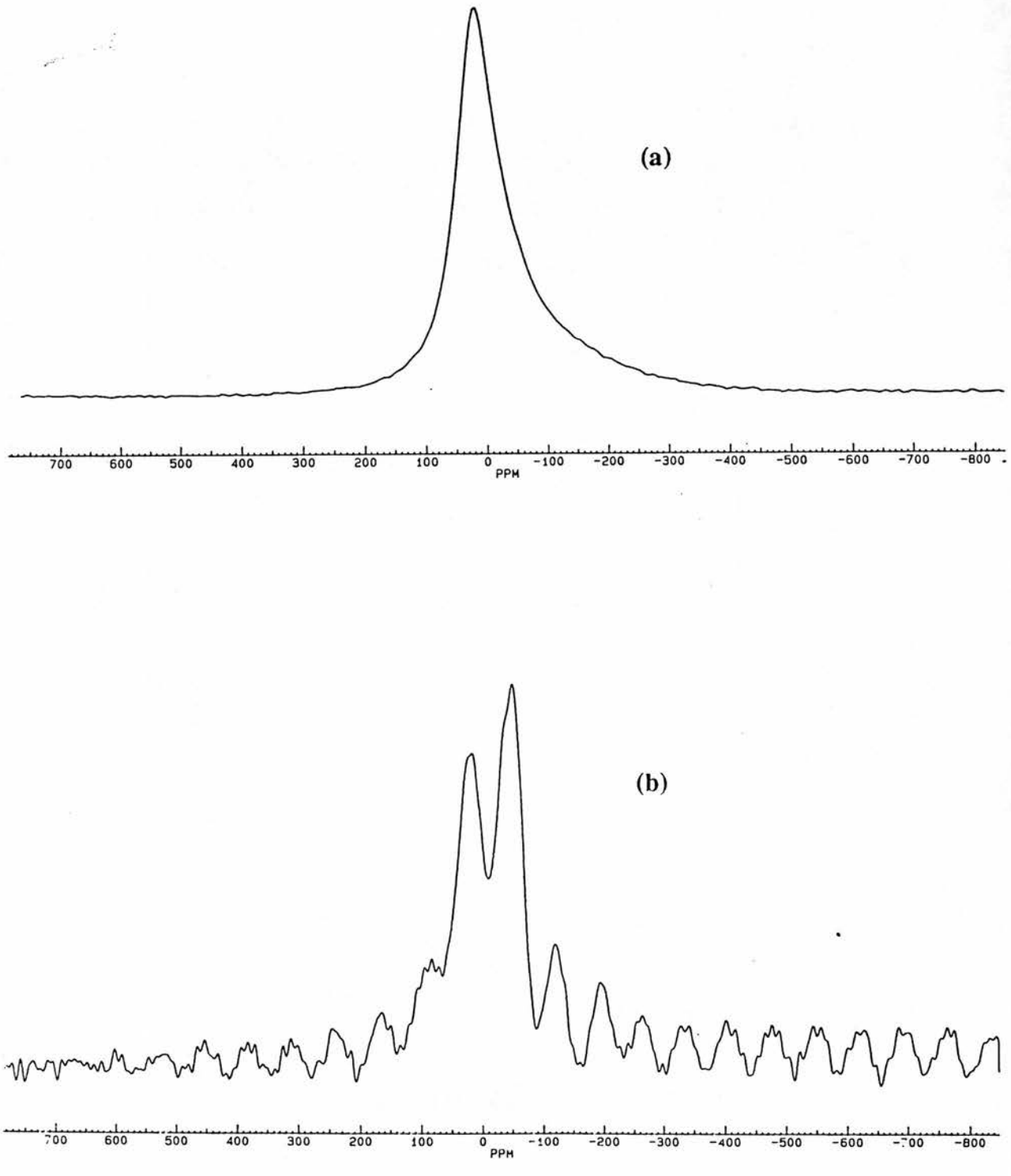

Fig. 8.3. ^{93}Nb Spectra of solid $Cp_2FeNbCl_6$: (a) static; (b) spun at 8 kHz.

The $Cp_2FeNbCl_6$ ^{93}Nb NMR static spectrum was run and gave a peak at 20ppm (FWHM ~10 kHz) which is shown in Fig. 8.3(a) (reference compound $CsNbCl_6$ powder, spun at 5kHz, FWHM of 400 Hz). The peak shape is a predominantly isotropic case with a small amount of axial symmetry. Unfortunately, it has proved impossible to quantify the degree of anisotropy, the reason being that the molecule does not have appreciable assymmetry parameters and so the spectrum is dominated by 2nd order quadrupolar broadening. This quadrupolar broadening makes it difficult to assign "edges" (ie σ_{11} and σ_{33}) and hence σ values. Confirmation that quadrupolar broadening was dominating the spectrum came from applying the method of Oldfield et al [8,9] – the sample was spun at various speeds at the magic angle. This caused the spectrum to change from a single peak to a complex sideband pattern (see Fig. 8.3(b)) due to quadrupole satellite interactions which reach a maximum at ~8kHz. This implies that the breadth of the static peak (of ~10kHz) consists mainly of a ~8kHz contribution due to quadrupole broadening.

That $Cp_2FeNbCl_6$ has a high degree of symmetry is not surprising, as $[NbCl_6]^-$ is an octahedral ion. [10-12] However, the small amount of axial symmetry in the static spectrum implies that there is some degree of either lengthening or shortening of the Nb-Cl bonds along the axis of the $[NbCl_6]^-$ unit. This is not unexpected as it has been found from other studies of crystals of $[NbCl_6]^-$ ions with large organic cations (eg. $(PPh_4)^+$)[13] that the cation can distort the octahedral symmetry of the $[NbCl_6]^-$ unit.

As ferricenium is an ESR active species, saturated solutions (mmol dm^{-3}) of $Cp_2FeNbCl_6$ were made up and the ESR spectra taken, see Table 8.2. Likewise small amounts of 1,1'-dimethylferrocene and decamethylferrocene were reacted with the $NbCl_5$ in acetonitrile to give green precipitates which were then examined by ESR spectroscopy (see Table 8.2). The redox potentials of these two ferrocene compounds are -0.047 V per methyl group attatched vs that of ferrocene.[14] Thus the $E^{o'}$ for 1,1'-dimethylferrocene occurs at -0.094V and the $E^{o'}$ for decamethylferrocene at -0.47V vs ferrocene and both should be able to reduce the $NbCl_5$ in acetonitrile. No signal was seen for acetonitrile solutions at low temperature, or for the THF or MeOH solutions at room temperature. If the ESR active species was due to trace amounts of Nb^{IV} we should expect to see a 10 line spectrum, g=1.95, line width <a> = 200G.[15,16]

(Photoreduced solutions of 0.5 mol dm^{-3} $(NbCl_5)_2$ in ROH give deep blue/purple coloured solutions. The ESR spectrum (293K) of the reduced solution, when R=Pr^i consists of 10 lines, g=1.96 and ΔH=200G). However, in all cases, except for $Cp_2FeNbCl_6$ in a MeOH glass, only one line was ever observed, thus confirming that Nb^{IV} was <u>not</u> present. The ESR spectrum of $Cp_2Fe[NbCl_6]$ in a MeOH glass consists of two lines (see Table 8.2), one at g=1.815 and a second line at g=4.24. This is consistent with the $g_\perp$ and $g_{//}$ values of ferricinium.[17,18] Whether this is $Cp_2FeNbCl_6$ or $Cp_2FeNbCl_{6-x}(OMe)_x$ in MeOH is not yet known. Thus it appears that the ESR active species is indeed the ferricenium species and this makes the spectra in acetonitrile the first observed room temperature spectra of ferricenium and its methyl derivatives.

Table 8.2

Summary of ESR Data Obtained for $FeCp_2NbCl_6$ and Its Derivatives				
Species	Solvent	Temperature (K)	g	$\Delta H(G)^c$
$Cp_2FeNbCl_6$	Acetonitrile	293	1.992	60
$Cp_2FeNbCl_6$	THF	106	1.988	100
$Cp_2FeNbCl_6$	Methanol	139	1.815 4.24	275 35
$Cp_2'FeNbCl_6$ [a]	Acetonitrile	293	1.933	135
$Cp_2^*FeNbCl_6$ [b]	Acetonitrile	293	1.918	170
$Cp_2^*FeNbCl_6$ [b]	THF	106	1.991	95
$Cp_2^*FeNbCl_6$ [b]	Methanol	139	1.815	330

(a) $Cp_2'FeNbCl_6$ is dimethylferricenium niobiumhexachloride

(b) $Cp_2^*FeNbCl_6$ is decamethylferricenium niobiumhexachloride

(c) ΔH is the peak splitting value.

8.1.2 Conclusions

Although ferrocene makes an excellent internal reference for electrochemistry in organic solvents, care has to be taken to avoid irreversible chemical reduction. Thus ferrocene may readily reduce $[NbCl_6]^-$ to $[NbCl_6]^{2-}$ with the formation of Cs_2NbCl_6 as well as $Cp_2FeNbCl_6$

acetonitrile (but not DMF), $Cp_2FeNbCl_6$ shows the first ever recorded room temperature ESR of the ferricenium ion.

8.2 Hydrolysis of Acetonitrile

During the early ^{93}Nb NMR research upon the $NbCl_{5-x}(OR)_x$ series, $(NbCl_5)_2$ was dissolved in acetonitrile (0.05 mol dm^{-3}), and 1 to 5 equivalents of MeOH were added in an attempt to generate the species $[NbCl_{5-x}(OR)_x.AN]$ in situ. After two days, it was observed that crystals had formed. Elemental analysis and FTIR confirmed that these crystals were NH_4Cl.

This observation led to two conclusions:

i) the commercially dried "anhydrous" acetonitrile, was not completely anhydrous, and thus in subsequent experiments redistilled acetonitrile was used;

ii) the acetonitrile was being hydrolysed to NH_4Cl.

The latter is surprising as nitriles are generally resistant to hydrolysis, eg.the rate of hydrolysis is of the order of $10^{-6}M^{-1}s^{-1}$ for OH^- catalysed hydrolysis[19] or boiling with conc. H_2SO_4.[20]

8.2.1 Turnover

The production of NH_4Cl as crystals meant that the degree of hydrolysis could be quantified, as ammonium chloride is only very sparingly soluble in acetonitrile. The number of moles of ammonium chloride produced would indicate whether the reaction was a catalytic one or not – if the value of the turnover (T) (T= number of moles of ammonium chloride/ number of moles of Nb) exceeded 1, then the reaction would be catalytic. To measure the turnover, known quantities of water were added to 0.05 mol dm^{-3} solutions of $(NbCl_5)_2$ in acetonitrile with 3 equivalents of MeOH and left for 3 days. The ammonium chloride crystals formed were washed with cold acetonitrile, dried and weighed. It was found that the turnover reached a maximum at a value of 1, for two or more equivalents of water. Addition of further MeOH or water to solutions with a turnover of 1 did not cause further production of NH_4Cl. This means that the reaction is not catalytic.

The reaction was repeated with 1 to 4 equivalents of water, but this time no MeOH was added. None of the reactions produced ammonium chloride, however GCMS on the solutions did show trace quantities of acetamide were present. ^{93}Nb NMR of the solutions gave a single peak at -495ppm, indicative of $Nb(OH)Cl_4.AN/Nb(OH)Cl_3.(AN)_2$ species, and this was generally formed within minutes of addition of H_2O.

8.2.2 NMR Studies of Reactants and Products

In order to elucidate a mechanism for the hydrolysis, a series of NMR studies were undertaken. The studies had to be done in deuterated acetonitrile as the addition of water to solutions of $(NbCl_5)_2$ in non coordinating solvents caused the immediate precipitation of Nb_2O_5. 0.1 mol dm^{-3} solutions of $NbCl_5.AN$ and 0.05 mol dm^{-3} solutions of $NbCl_5.BN$ (BN = phenyl acetonitrile) were prepared. To these solutions were then added either (i) 2 or 3 equivalents of H_2O (ii) 3 equivalents of MeOH and 2 equivalents of H_2O. Varying nuclei NMR spectra were then run on these solutions to follow the reactions occurring.

In all the $NbCl_5.AN$ cases it was observed that the CD_3CN exchanged with the bound CH_3CN to give a large free CH_3CN peak at 2.0ppm in the ^1H spectra. Likewise, for both sets of niobium chloride adduct solutions which only had H_2O added, no hydrolysis of the nitrile was observed, only the hydrolysis of the $NbCl_5$ to the $Nb(OH)Cl_4$ species.

Upon addition of 3 equivalents of MeOH and 2 equivalents of H_2O to solutions of $NbCl_5.AN$, many other species were observed. A summary of the NMR spectra and the assigned species is shown in Table 8.3.

These NMR studies of the $NbCl_5.AN/H_2O/MeOH$ system confirmed a number of points:
i) the reactions proceeded over about 3 days, but after this further reactions occured only very slowly;
ii) that it is CD_3CN being hydrolysed, rather than N_2;
iii) that a turnover of 1 is observed for the 2 eq H_2O + 3 eq MeOH systems – this is obtained from the integrals of the ^1H signals in the product mixture for methyl ethanoate (35), acetic acid (1) and free CH_3CN (36). As the only CH_3CN added was that bound in a 1:1 ratio with $NbCl_5$

Table 8.3

	Species Observed[a]				
NMR	$MeOC(O)CD_3$	NH_4Cl	$CD_3C(O)OH$	$NbCL_4OMe.AN$	$NbCL_4OH.AN$
^1H	3.675	5.50 6.20 6.88 (1) (1) (1)[b]	Broad 9-10	4.20	
^2D	2.15			2.35	2.35
^{13}C [f]	51.0 171.3 18.4 septet		19.1 178.6 septet	59.9 [e]	[e]
^{14}N		-356 [c] quintet			
^{93}Nb				-560 [d]	-495

(a) MeOH observed at 3.45ppm in ^1H and 49.85 in ^{13}C NMR spectra.

(b) J_{NH} = 53.5Hz, total peak area no more than 4 % of CH_3CN peak area. Figures in parentheses are relative peak areas.

(c) J_{NH} = 54Hz.

(d) Decreases to ~ 70% of overall Nb species after 4 days.

(e) Shoulder between 1 and 3 ppm due to CD_3.

(f) Proton decoupled and DEPT spectra.

the ratio of hydrolysis products to Nb is 1:1 and thus confirms the turnover observed by the gravimetric analysis of the ammonium chloride.

The reaction of $NbCl_5.BN$ with 3 eq MeOH and 2 eq H_2O produced the hydrolysis products of acetonitrile, and a turnover of ~ 0.8. This was unexpected as it was assumed the system would give the hydrolysis products of phenyl acetonitrile (ie. methyl benzyloate ($MeOC(O)CH_2C_6H_5$) and phenyl acetic acid), rather than methyl ethanoate and acetic acid.

The fact that the total number of moles of methyl ethanoate and acetic acid produced was equal to the number of moles of ammonium chloride produced suggests two possible mechanisms:- metal catalysed hydrolysis of bound nitriles; and the Pinner synthesis. Of the two the Pinner synthesis is favoured for the reasons discussed below.

8.2.3 Possible Mechanisms:

(A) Metal Catalysed Hydrolysis of Bound Nitriles

Although nitriles are quite resistant to hydrolysis, a number of metal cations are known to catalyse hydrolysis. Thus the hydrolysis of nitriles is catalysed by Co(III),[19] Rh(III),[21] Ru(III),[22,23] and Ir(III)[24] where the nitriles are coordinated to the metal, and by Cu^{2+}, Ni^{2+}, Zn^{2+}, where the nitrile function is covalently linked to the metal coordinating functionalities.[24,25] In all cases the nitrile is hydrated to the corresponding amide. Thus it is plausible that the bound acetonitrile was being hydrolysed to acetamide, and then further reacting to form ammonium chloride and methyl ethanoate, by the type of reaction shown in Fig. 8.4.

Fig. 8.4

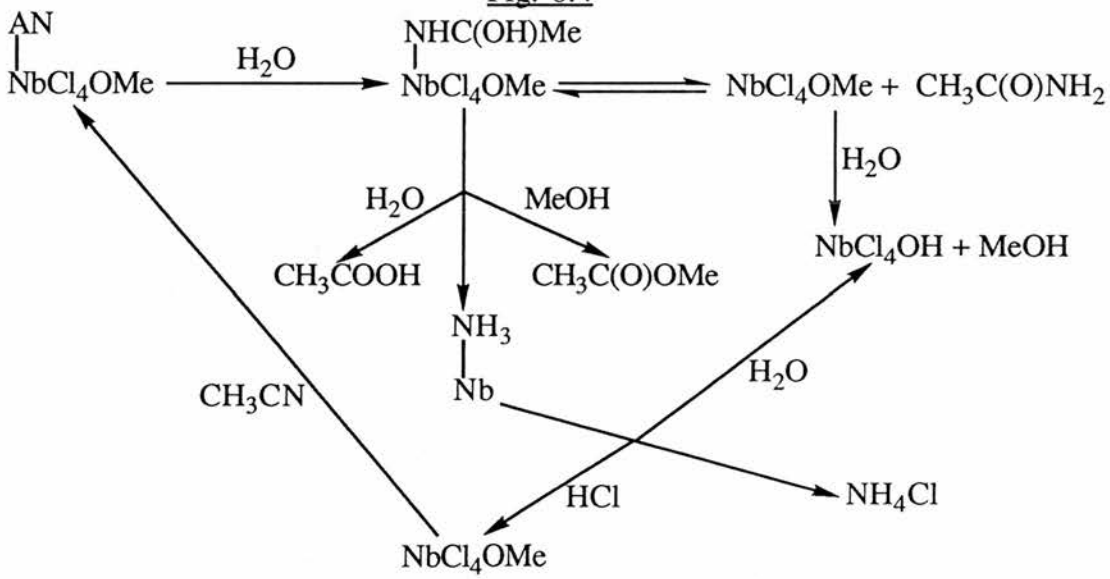

This mechanism would give an explanation as to why hydrolysis was only observed when MeOH was added to the system:- since $NbOCl_3/NbOHCl_4$ is formed within minutes of addition of water to $NbCl_5$.AN, and as it is not a catalyst for hydrolysis its formation precludes the possible hydrolysis catalysis as there is no $NbCl_5$.AN present to catalyse the reaction. Whereas ^{93}Nb NMR shows that $NbCl_4(OMe)$.AN exists in equilibrium with $NbOCl_3$ in $MeOH/H_2O$ systems and can thus by its presence, catalyse the hydrolysis of bound acetonitrile.

However, a number of questions were left unanswered by this mechanism. Firstly, if $NbCl_4(OMe)$.AN does catalyse the hydrolysis of bound acetonitrile, why does the reaction

stop at a turnover of 1? Surely it should carry on catalysing the reaction? Secondly, the formation of acetamide is never observed. Thirdly, the addition of 3 eq. of MeOH and 2 eq. of H_2O to $NbCl_5$.BN did not give the formation of methyl benzyloate, but rather the formation of methyl ethanoate. If the reaction was occurring by hydrolysis of bound nitriles, the production of benzylamide or methyl benzyloate would be expected, as Mukaiyama et al [26] have shown that a mixture of $TiCl_4/H_2O$ in a 1/2 ratio will hydrolyse benzonitrile to benzamide in a 90% yield. This was never seen. Because no free phenyl acetonitrile was ever observed, the exchange of bound benzylnitrile with deuterated acetonitrile solvent can be ruled out, thus impling that unbound deuterated acetonitrile was being hydrolysed.

(B) The Pinner Synthesis

The Pinner Synthesis is an important organic reaction for the production of imidates from nitriles and is also used as an alternative to the direct (base catalysed) hydrolysis of nitriles to give esters and carboxylic acids. The reaction proceeds by the route given in eq. 8.4-eq 8.6:[20]

$$R^1C{\equiv}N \xrightarrow{H^+} R^1\overset{+}{C}{=}NH \qquad (8.4)$$

$$R^1\overset{+}{C}{=}NH + R^2OH \longrightarrow R^1C(OR^2){=}\overset{+}{N}H_2 \qquad (8.5)$$

$$R^1C(OR^2){=}\overset{+}{N}H_2 + H_2O \longrightarrow R^1C(O)OR^2 + \overset{+}{N}H_4 \qquad (8.6)$$

(X)

Typically HCl is used as the catalyst and a primary or secondary alcohol as the alcolating agent. The formation of the alkoxy iminium ion (X) usually takes between 12 and 72 hours depending on R_1 and R_2. [27-30] Hydration of the alkoxy iminium ion takes place instantaneously. Since attack by H_2O on the protonated nitrile is very slow and rarely observed, the water may be present throughout the reaction or added after the formation of X.[20]

Thus, this synthesis fits the experimental observations far better than the metal catalysed hydrolysis of bound nitriles. The reaction time is of the correct order. The fact that acetamide is not observed is to be expected and although X (methoxy methyl imidate hydrochloride R_1 and R_2 = Me) is not observed in the NMR spectra,[31] this is also to be expected as it is unstable in

the presence of H_2O and decomposes to methyl ethanoate. It also explains why no reaction with the bound phenyl acetonitrile was observed – MeOH and H_2O were reacting with the $NbCl_5$.BN to release HCl which then catalysed the alcolation of the solvent CD_3CN to give methyl ethanoate. Finally the non catalytic property of the reaction, with a turnover of only 1, is now explainable – all the protons generated in this system come from the reaction of Nb-Cl bonds with ROH (where R =H or Me). This reaction yields only 1 proton and the species $NbCl_4(OMe)$.AN or $NbCl_4(OH)$.AN. These latter two species exist in equilibrium together and, under the reactions conditions observed, do not undergo further substitution and proton release. Therefore the single proton consumed by eqs.8.4-6 (the protonation of the nitrile) is formed by the single substitution of each Nb molecule and thus only a turnover of 1 is observed.

8.2.3 Conclusions

The formation of ammonium chloride in acetonitrile solutions containing $NbCl_5$, MeOH and H_2O is due to the release of protons which catalyse the alcolation of acetonitrile, by the Pinner Synthesis. The formation of the protons occurs when the $NbCl_5$ is substituted by ROH. This highlights the need for dry solvents in niobium (V) chemistry, and the unexpected reactions that can occur.

References

1. M. Rosenblum, "Chemistry of Iron Group Metallocenes" Part 1, Wiley, 1975, p40.
2. C.Furlani, E. Zinato, *Z. anorg. allg. Chem.*, 1967, **351**, 210.
3. D.A.Miller and R.D. Bereman, *Coord. Chem. Rev.*, 1972/3, **9**, 107.
4. G.A. Heath, G.t. Hefter, T.w. Boyle, C.D.Desjardin, D.W.A. Sharp, *J. Fluorine Chem.*, 1978, **11**, 399.
5. K. Moock, L. Twowsky, K. Seppelt, *J. Fluorine Chem.*, 1987, **37**, 253.
6. G.A. Heath, K.H.Moock, D.W.A. Sharp, L.J. Yellowlees, *J. Chem. Soc., Chem. Comm.*, 1985 150.
7. "Multi Nuclear Magnetic Resonance in Liquids and Solids, Chemical Applications" Eds. P. Granger, R.K. Harris, Ch. 15 (R.K. Harris), p269-291. NATO ASI Series C Vol. 322, Kluwer Acad. Pub. Dordrecht, Netherlands, 1990.
8. E. Oldfield, R.A. Kinsey, B. Mantez, T. Ray, K.A. Smith, *J. Chem. Soc. Chem. Comm.*, 1982, 254.
9. M.D. Meadows, K.A. Smith, R.A. Kinsey,T.M. Rothgeb, R.P. Skarjune, E. Oldfield, Proc. Natl. Acad. Sci. USA, 1982, **79**, 1351.
10. D.M. Adams, J. Chatt, J.M. Davidson, *J. Chem. Soc.* (A), 1963, 2184.
11. K.W. Bagnell, D. Brown, *J. Chem. Soc.* (B), 1964, 3021.
12. W. van Bronswyk, R.J.H. Clark, L. Maresca, *Inorg. Chem.*, 1969, **8**, 1395.
13. R. Dubgen, U. Muller, F. Weller, K. Dehnicke, *Z. anorg. allg. Chem.*, 1980, **471**, 89.
14. A.J.Deeming, "Comprehensive Organometallic Chemistry" ed G.Wilkinson, Pergamon, 1982, vol. 4, p480.
15. D.P.Johnson and R.D.Bereman, *J. Inorg. and Nuc. Chem.*, 1972, **34**, 679.
16. P.G. Rasmussen, H.A. Kuska and C.H.Brubaker Jr. ,*Inorg. Chem.*, 1965, **4**, 343.
17. R.Pris and A.R.Karswagen, *J.Organomet. Chem.*,1970, **25**, C74.
18. D.M.Duggan and D.N.Hendrickson, *Inorg. Chem.*, 1975, **14**, 955.
20. D.A. Buckingham, F.R. Keene, A.M. Sargeson, *J. Am. Chem. Soc.*, 1973, **95**, 5649.

21. I.O. Sutherland , "Comprehensive Organic Chemistry" Vol. 2, Eds D. Barton, W.D. Ollis, Pergamon, Oxford, p869-957.

22. N.J. Curtis, A.M. Sargeson, *J. Am. Chem. Soc.*, 1984, **106**, 625.

23. A.W. Zanella, P.C. Ford, *J. Chem. Soc. Chem. Comm.*, 1974, 795.

24. A.W. Zanella, P.C. Ford, *Inorg. Chem.*, 1975, **14**, 42.

25. P.F.B. Barnard, *J. Chem. Soc.* (A), 1969, 2140.

26. R. Breslow, R. Fairweather, J. Keana, *J. Am. Chem. Soc.*, 1967, **89**, 2135.

27. T. Mukaiyoma, K Kamio, S. Kobayoshi, H. Takei, *Chem. Lett.*, 1973, 357.

28. R. E. Allan, E. L. Schumann, W. C. Day, M. G. Van Comper Jr., *J. Am .Chem. Soc.*,1958, **80**, 591.

29. R. Rodger, D.G. Neilson, *Chem. Rev.*, 1961, **61**, 179.

30. R. Rodger, D.G. Neilson, *J. Chem. Soc.*,1959, 688.

31. L. Weintraub, S.R. Oles, R. Kalish, *J. Org. Chem.*, 1968, **33**, 1671.

32. H.G. Viehe, H. Bohme, "Advances in Organic Chemistry" Vol. 9, Wiley, 1974, part 1,p 42-77, (expected ^{14}N NMR in the range of -160 to -200ppm, ^{1}H NMR R_1 ~2.6ppm, R_2 ~ 4.4) .

Chapter 9

Experimental

9.1. General

All preparative reactions were done under N_2 and in dry glassware (at 293K except where noted), and **unless specifically noted all solvents, regardless of grade, were redistilled over Na, 3Å molecular sieves or CaH_2.** ^{93}Nb NMR (coupled) were run on a Bruker MSL 500 spectrometer (τ_0=~500ms, τ_1=5-20ms), and ^1H NMR on AM300 or WP80 spectrometer. FTIR spectra were obtained on a Perkin Elmer 1710 spectrometer, and Raman spectra on a Spex 1403 interfaced to a DM1B computer with Coherent Radiation Innova 90-6 Ar^+ laser excitation at 514.5 nm, power < 100 mW at the sample (spectroscopic data are within $\pm$ 1 cm^{-1}). Mass spectroscopy was obtained on an INCOS GCMS spectrometer. X ray powder diffraction was run on a Stoe Stadi-P using Cu $k_{\alpha 1}$ radiation. SEM (Scanning electron microscopy) was performed on a Jeol JSM 35CF (15keV) with scanning EDAX (energy dispersive analysis by X-rays) attachment at the Gatty Marine Laboratory.

9.2.Chapter 2, General

For in situ generation of $(NbCl_{5-x}(OMe)_x)_2$ species in aromatic solvents, $(NbCl_5)_2$ (99%+ Aldrich), was suspended in benzene or toluene (Aldrich reagent grade dried by Na and 4Å molecular sieves) and controlled equivalents of methanol (spectroscopic grade, Aldrich) added. For in situ generation of $(NbCl_{5-x}(OR)_x)_2$ species in alcohols, weighed amounts of $(NbCl_5)_2$ (99%+ Aldrich) were dissolved in the required alcohol (spectroscopic grade, Aldrich) to give the specified molarity. For in situ generation of $[NbCl_{6-x}(OR)_x]^-$ species, weighed amounts of $CsNbCl_6$ (standard preparation,[1] see section 9.2.1) were dissolved in methanol (spectroscopic grade, Aldrich) to give the specified molarity. For rechlorination experiments HCl gas (Aldrich) was used.

9.2.1 $CsNbCl_6$ Preparation[1]

A thionyl chloride solution (6ml)(Aldrich, 99+%) of $(NbCl_5)_2$ (1.5g) was added to CsCl (1g)(Fisons, 99.5%) in ICl (2ml)(Hopkin and Williams, 99%) and left for 2 hours. $CsNbCl_6$ precipitated out and was washed with thionyl chloride and vacuum dried over P_2O_5. IR 335 (s)(ν_3, t_{iu}) cm^{-1}; Raman: 367 (overtone 732) (ν_1, a_{1g}), 285 (ν_2,E_g) cm^{-1}, 180 (ν_6, t_{2u}) cm^{-1} [cf. Nakamoto[2] IR 333 (ν_3) cm^{-1}, Raman 368 (ν_1) cm^{-1}, 288 (ν_2) cm^{-1}, 183 (ν_6) cm^{-1}. X ray powder diffraction confirmed that the product was $CsNbCl_6$ but also that some CsCl remained.

To confirm our assignments of in situ generated species we isolated and characterized by ^1H NMR, FTIR and mass spectroscopy $(NbCl_4(OMe))_2$, $(NbCl_2(OMe)_3)_2$ and $(Nb(OMe)_5)_2$ prior to redissolution in deuterated toluene (Na dried, Aldrich) and anhydrous acetonitrile (AN)(Aldrich) and ^{93}Nb and ^1H NMR spectra being run (see Section 2.1.1). Elemental analysis of the compounds described in sections 9.2.3-9.2.6 never quite matched the theoretical composition of these species. The reason for this is that the uni- and tri-methoxide substituted compounds described are labile d^0 species, and ^1H and ^{93}Nb NMR reveal that even after purification each $NbCl_{5-x}(OMe)_x$ species (x=1,3,4) exists in equilibrium with small amounts of the other species, so that typically the compound is only ~93% pure.

9.2.2 $(Nb(OMe)_5)_2$

$(Nb(OMe)_5)_2$ was prepared by the method of Bradley et al.[3] 8.1g $(NbCl_5)_2$ was suspended in 50ml of toluene, 7ml MeOH (excess) added and anhydrous NH_3 gas (Aldrich) blown through. The solution was filtered under N_2 and rotary evaporated to give a white crystalline solid. It was used without further purification. Elemental Analysis calculated for $(Nb(OMe)_5)_2$: C, 24.19; H, 6.05. Found: C, 23.81; H, 5.97. FTIR (cm^{-1}) 1150 (w), 1106 (vs), 1030 (m) (ν CO); 850 (mw) (ν Nb-O-Nb); 555 (νNb-O).[cf Schonherr and Kolditz[4] :$Nb(OMe)_5$ 1110cm^{-1} (νCO); 555cm^{-1} (νNb-O).]. Raman (cm^{-1}) 552 (s); 534, 474 (m); 439, 378, 343, 288, 230, 198 (w), assignments can be made by comparison with the assignments of Nb_2Cl_{10}.[5] Mass.Spectra : m/z 465 $(Nb_2(OMe)_9)^+$ fragmentation pattern identical to that given by Preiss[6] and Reiss et al[7] for $Nb_2(OMe)_{10}$. ^1H NMR see Table 2.2. Results are identical with those found by other authors[7-10] in that we see, at 220K, 3 peaks due to ax:eq:br

OMe's in the ratio 2:2:1. At 238K they coalesce to 2 peaks; ax/eq:br OMe's in the ratio of 4:1 and finally at 310K a single peak .

$(Nb(OEt)_5)_2$ (Aldrich 99%) and $(Nb(O^iPr)_5)_2$ (standard preparation by the method of Bradley and Holloway[10] similar to that described for $(Nb(OMe)_5)_2$) were also used. Confirmation by ^1H NMR. $(Nb(OEt)_5)_2$ ^1H NMR (293K) 4.45ppm (broad), 2H (CH_2); 1.35ppm triplet, 3H, (CH_3). $(Nb(O^iPr)_5)_2$ ^1H NMR (293K) 4.65ppm (broad), 1H, (CH); 1.25ppm doublet, 6H, (CH_3). These spectra match those found by Bradley and Holloway[10] for $(Nb(OEt)_5)_2$ and $(Nb(O^iPr)_5)_2$.

9.2.3 $(NbCl_2(OMe)_3)_2$

$(NbCl_2(OMe)_3)_2$ was prepared by the following method: 8.1g of $(NbCl_5)_2$ was suspended in 50ml of toluene, and 6.06ml of MeOH were added (0.15 moles). The solution was stirred for one day, and then the excess MeOH and toluene evaporated until a saturated solution formed. After the addition of 3 ml of petroleum ether (40-60), the solution was allowed to crystallize at -10°C. The crystals were filtered and washed with cold toluene. FTIR (cm^{-1}) 1600 (mw); 1150 (w) 1075 (s) (vCO); 980 (s) ; 570 (w) (vNb-O). (cf Schonherr and Kolditz,[4] $(NbCl_2(OMe)_3)_2$: 1080cm^{-1} (vCO) , 575cm^{-1} (vNb-O).) Mass Spec. m/z 221 $(NbCl(OMe)_3)^+$, same fragmentation pattern as for $NbCl_2(OMe)_3$ found by Preiss.[6] ^1H NMR when dissolved in deuterated toluene at low temperatures gave a complex set of lines. However, although the 3 groups of peaks are solvent shifted, they matched those found for $(NbCl_2(OMe)_3)_2$ in CD_2Cl_2.[11]

9.2.4 $(NbCl_4(OMe))_2$

$(NbCl_4(OMe))_2$ was prepared by the following method: 8.1g of $NbCl_5$ was suspended in 50ml of toluene, and 1.22ml of MeOH added. Upon stirring for one day, $(NbCl_4(OMe))_2$ precipitates out, and was filtered, and reprecipitated from benzene. FTIR (cm^{-1}) 1600 (ms); 1100(mw) 1056(s) 1020 (sh) (vCO); 980 (s) 850 (m) 780(w); 595 (vNb-O). (cf Schonherr and Kolditz [4] $NbCl_4(OMe)$ 1055cm^{-1} (vCO) , 595cm^{-1} (vNb-O).) Mass spec.m/z 264/266 $(NbCl_4(OMe))^+$, 213 $(NbCl_3CH_3)^+$, 210 $(NbCl_3C)^+$, 198 $(NbCl_3)^+$.

Characterization of Monomer Adducts

9.2.5 $NbCl_4(OMe).AN$

When $(NbCl_4(OMe))_2$ is dissolved in acetonitrile (AN) two peaks are observed at -495ppm (full width at half maximum = FWHM = 1kHz) and -560ppm (FWHM 1.5kHz). The latter is shifted upfield from the dimer (-495ppm) by the appropriate amount for a monomeric niobium acetonitrile adduct.[12] This acetonitrile adduct is isolated by removal of excess solvent to give an orange solid. The IR spectrum showed shifted acetonitrile stretches at 2325cm^{-1} (δCH_3 + νC-C) and 2296cm^{-1} (νC=N) [cf. $NbCl_5.AN$[11,13] 2308cm^{-1} and (δCH_3 + νC-C) and 2283cm^{-1} (νC=N), Free AN 2298cm^{-1} (δCH_3 + νC-C) and 2254cm^{-1} (νC=N)], a shifted (νCO) of 1153cm^{-1} (m) and 1075cm^{-1} (s) as well as peaks at 1020cm^{-1} (m) and 780cm^{-1}. The orange $NbCl_4(OMe).AN$ in deuterated toluene gave two new peaks (3.90ppm and 2.35ppm) in the low temperature ^1H spectrum in a 1:1 ratio and a new peak was observed at -550ppm in the ^{93}Nb spectrum. The ^1H peaks can be assigned to NbOMe (3.90ppm) and Nb.NCMe (2.35ppm)[14] confirming that it is $NbCl_4(OMe).AN$.

9.2.6 $NbCl_2(OMe)_3.AN$

When $(NbCl_2(OMe)_3)_2$ is dissolved in acetonitrile it gives a single peak at -850ppm (FWHM 10.5KHz) in the ^{93}Nb spectra. Removal of the acetonitrile solvent gives a yellow solid whose FTIR shows shifted acetonitrile stretches at 2313cm^{-1} (δCH_3 +νC-C) and 2285cm^{-1} (νC=N) as well as peaks at 1090cm^{-1} broad(s) (νCO) 1000 cm^{-1} (s), 860cm^{-1} broad (m) and 560cm^{-1} (νNb-O). This implies the formation of some monomer adduct $NbCl_2(OMe)_3.AN$. When the adduct is dissolved in deuterated toluene it gives rise to a complex pattern of peaks in the low temperature ^1H NMR spectrum. Apart from a peak at 2.35ppm (Nb-NCMe) it has proved impossible to assign the peaks and hence confirm the adduct formation by ^1H NMR.

Methoxide Precursors for the Generation of $[NbCl_{6-x}(OMe]_x^-$ Species

9.2.7 NaOMe

The standard preparation in Vogel was followed.[15] 13.6g of sodium (Fisons, 99.8%+) cut into small pieces were placed into a 1 litre flask with a condenser and separating funnel (with calcium chloride guard tubes). The flask was placed in an acetonitrile/N_2 bath and 200ml of anhydrous methanol added. After the reaction had moderated a further 200ml of methanol was added and the flask slowly removed from the acetonitrile/N_2 bath to facilitate the production of NaOMe. Upon visual confirmation of the reaction completion, the solution was refluxed on a water bath for $^1/_2$ hour to ensure completion. The solution was then rotary evaporated to give white, water sensitive NaOMe. FTIR matched that in Aldrich Library[16a] for NaOMe.

9.2.8 Tetrabutyl ammonium methoxide (TBAOMe)

TBAOMe was prepared in the following manner. 5.4g of NaOMe in 50ml of a 50/50 CH_2Cl_2/MeOH mixture was added to a solution of 32.3g tetrabutyl ammonium bromide (Aldrich, 99%) in 50ml CH_2Cl_2 (Aldrich, lab grade, redistilled over sodium benzophenone) and a further 400ml of CH_2Cl_2 added. NaBr precipitated out upon cooling at -10°C. The solution was filtered and upon rotary evaporation gave white TBAOMe. This was then twice recrystallized from acetonitrile and dried in solution over 3Å molecular sieves (BDH, activated at 500°C for 12 hours) as well as vacuum dried in the solid state over P_2O_5. However ^1H NMR of the solid in deuterated toluene revealed the presence of free methanol (3.50ppm) implying that our attmpts at drying the TBAOMe had failed. ^1H NMR, TBAOMe, 1.00ppm (triplet, 3H) (CH_3); 1.40ppm (multiplet, 2H) and 1.60ppm (2H) (2 x CH_2); 3.30ppm (2H) (CH_2-N^+): MeOH 3.50ppm (3H) (CH_3), 4.85ppm (broad, ~1H) (OH). FTIR matches that of TBABr with additional peak at 1650cm^{-1}(m).[16a]

9.2.9 Errors

It is evident from Table 1.1 that all the ^{93}Nb chemical shift data quoted in this thesis has an error of $\pm$ 7ppm. This is an experimentally derived error margin, because due to the paucity

of ^{93}Nb NMR data, there does not appear to be a standard error associated with ^{93}Nb chemical shift positions. This initially caused some problem in being able to assign peaks to given species. However, it was not difficult to quantify this error experimentally.

Within a given solvent there are three possible areas of error:- (i) instrumental, associated with the failure to correctly pick out the peak maximum; (ii) temperature dependence causing variation in the peak position; (iii) concentration dependence, also causing the peak position to shift. Instrumental error can be discounted, as although ^{93}Nb NMR peaks often have line widths (FWHM) of the order of 10KHz, the peak maximum is well defined. Even if it were not, a broad flat peak maximum of 250Hz would only have an associated error of $\pm$ 1ppm (122.4Hz = 1ppm).

Temperature dependence was measured by cooling a solution of $(NbCl_4(OMe))_2$ in toluene (~0.1 mol dm^{-3}) and measuring the associated chemical shift. As the temperature dropped, the observed peak shifted to lower frequencies. This shift was linear down to 245 K. At 295K the observed peak position was -500ppm; at 270K the position was -509.5ppm; at 245K the position was -519ppm and finally at 225K the peak position was -521ppm. Although the NMR laboratory temperature is not constant from day to day, its variation is between ~296K and 286K. This implies a maximum possible lower frequency shift, due to temperature dependence, of 5ppm.

The concentration dependence at 295K was easily measured by preparing samples of $(Nb(OMe)_5)_2$ in toluene at various concentrations and measuring the change in the ^{93}Nb NMR peak position. Three concentrations were prepared; 0.05, 0.005, and 0.0005 mol dm^{-3} and these solutions gave the following chemical shifts; -1156ppm, -1146ppm, -1140ppm, respectively. Thus the concentration dependence is in opposition to the temperature dependence – as the concentration decreases, the peak position shifts to higher frequencies. As most of the ^{93}Nb spectra were obtained from solutions with concentrations of Nb of between 0.05 and 0.005 mol dm^{-3}, this gives a maximum higher frequency shift of ~10ppm.

Overall, therefore,there is an error band of 15ppm or $\pm$7ppm from the median position. Thus the ^{93}Nb chemical shift positions quoted in Table 2.1 are median positions with an associated possible error of $\pm$7ppm.

9.3. Chapter 3, General

Demineralised water was used for all the gelation studies, except the pH studies when distilled water was added. Addition of demineralised water gives a slightly different optimum H_2O:Nb ratio compared to distilled water (for example, 0.5 mol dm^{-3} $(NbCl_5)_2$ in EtOH has an minimum gel time of 5 mins at H_2O:Nb ratio of 55:1 for distilled water and 27:1 for demineralised water), but no other differences were observed. All gelation reactions were done in unsealed 12 ml, 2.0 cm diameter, sample bottles (washed and dried) at 293K. At the gel point, viscosity increases as a step function (see Fig. 9.1). In the absence of viscosity measurements, the large increase in viscosity upon gelation enables the gel times to be measured as the time taken, after addition of water, to form a continuous gel network through out the sample that could support its own weight when the sample bottle is turned on its side. The pH studies were run on a Radiometer SAM 90 Sample Station with a VIT 90 video Titrator and Orion 8103 Ross Combination pH electrode, which was standardised beforehand.

9.3.1 Gelation of $(NbX_5)_2$ Species

$(NbCl_5)_2$ and $(Nb(OEt)_5)_2$ were obtained from Aldrich (99%+). $(Nb(OMe)_5)_2$, $(Nb(OPr^i)_5)_2$, and $(NbCl_2(OMe)_3)_2$ were prepared as before (sections 9.2.2 and 9.2.3). 0.002, 0.1 and 1.0 mol dm^{-3} solutions of these compounds were then prepared in acetonitrile (Aldrich, anhydrous), MeOH, EtOH and Pr^iOH (all Aldrich, spectroscopic grade). 2 ml water or 3 ml conc. HCl (Aldrich, lab grade) (2778 H_2O equivalents) were added to the 0.002 mol dm^{-3} solutions (10 ml). 1.75 ml water or 2.625 ml conc. HCl (103 H_2O equivalents) were added to the 0.1 mol dm^{-3} solutions (10 ml). 2.5 ml water or 3.75 ml conc. HCl (28 H_2O equivalents) were added to the 1.0 mol dm^{-3} solutions (5 ml). Upon addition of water or acid all the solutions were mixed thoroughly. The gel time for each of the solutions was noted.

9.3.2 Gelation of $(NbCl_5)_2$ in Alcohols

0.5, and 0.05 mol dm^{-3} solutions of $(NbCl_5)_2$ in MeOH, EtOH and Pr^iOH (Aldrich, spectroscopic grade) were prepared as in section 9.2 and 2 ml quantities of the solutions were reacted with between 16 and 670 equivalents of water. The gel times were noted. Similarly

Fig. 9.1

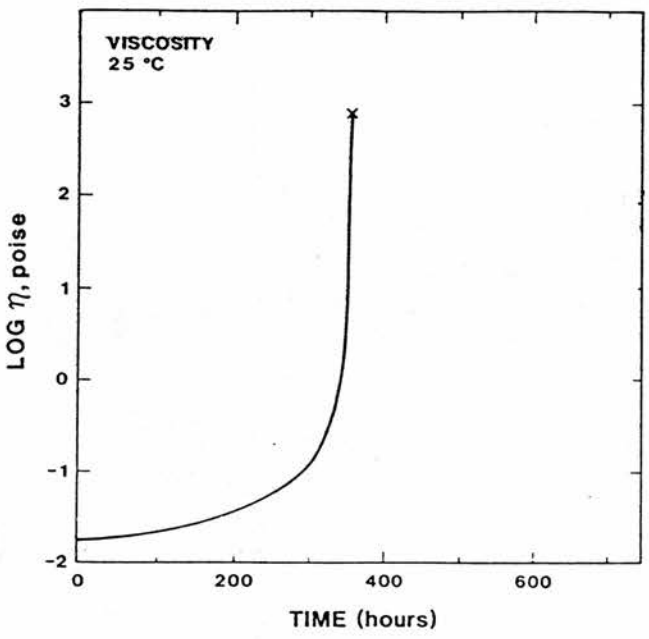

Fig. 9.1. Log (viscosity) vs time for 382.0g $Si(OEt)_4$, 33.0g H_2O and 83.4g EtOH. HCl catalysed (mole ratio of HCl to $Si(OEt)_4$ is 0.01). Cross indicates gel point. Taken from ref 16(b), p204.

0.5, 0.125, 0.0875 and 0.05 mol dm^{-3} solutions of $(NbCl_5)_2$ in MeOH and EtOH were prepared and 2 ml quantities reacted with between 16 and 670 equivalents of distilled water and the gel times noted.

9.3.3 Characterisation of Hydrolysis and Gelation Products

0.05 mol dm^{-3} solutions of $(NbCl_5)_2$ in Pr^iOH, EtOH, and ethylene glycol were added to a large excess (100 equivalents) of demineralised water and left for 6 hours to gel. The gels were then washed and decanted from demineralised water until the decanted water was no longer acidic. This was done to remove any HCl trapped in the gel, formed by the hydrolysis of the Nb-Cl bonds in $NbCl_{5-x}(OR)_x$. The washed gels were then submitted to three drying processes:-(a) room temperature drying to give a cracked glass; (b) oven drying at 150°C for 18 hours to give a powder; (c) as (b) but then followed by heating to 900°C over 4 hours.

EDAX and Cl^- analysis[17] upon the 150°C dried gels and EDAX upon the gels dried at 293K confirmed that the resulting gel was hydrated amorphous Nb_2O_5; no evidence could be found for remaining Nb–Cl bonds after hydrolysis. Regardless of the parent alcohol all the gels showed the same analytical properties. The Raman spectra of the room temperature dried gels contain bands due to the ROH group, for example EtO ν(CO) at 1090 cm^{-1}. Weak bands below 1000 cm^{-1} (932, 760, 465 cm^{-1}) were observed and correspond, respectively, to the ν_1, ν_2 and ν_5 stretching regions of Nb_2O_5.[18] No bands due to Nb-Cl stretching vibrations (100-200cm^{-1} and 350-450cm^{-1}) were observed. The FTIR spectra of the gels, after drying at 150°C, showed that the majority of ROH and RO^- had been removed, by the hydrolysis reaction and subsequent drying, as peaks characteristic of the particular ROH were missing and only broad peaks characteristic of metal oxides were observed. Fig. 9.2(a) shows a typical spectrum of an EtOH gel after 150°C drying compared to hydrated Nb_2O_5 aged at 200°C (Fig. 9.2(b)) and room temperature (Fig. 9.2(c)).[19] The very broad band (600-700 cm^{-1}) observed is due to antisymmetric Nb-O stretching in the distorted NbO_6 octahedra.[18] The shoulder at ca 900 cm^{-1} may be assigned to ν(Nb=O). Three weak bands observed at 1180, 1120 and 1050 cm^{-1} correspond to bands claimed to be diagnostic of ageing of Nb oxide precipitates.[19] Specifically, the 1180 and 1050 cm^{-1} bands are due to the Nb-(OH)-Nb group.[19] After heating

Fig. 9.2

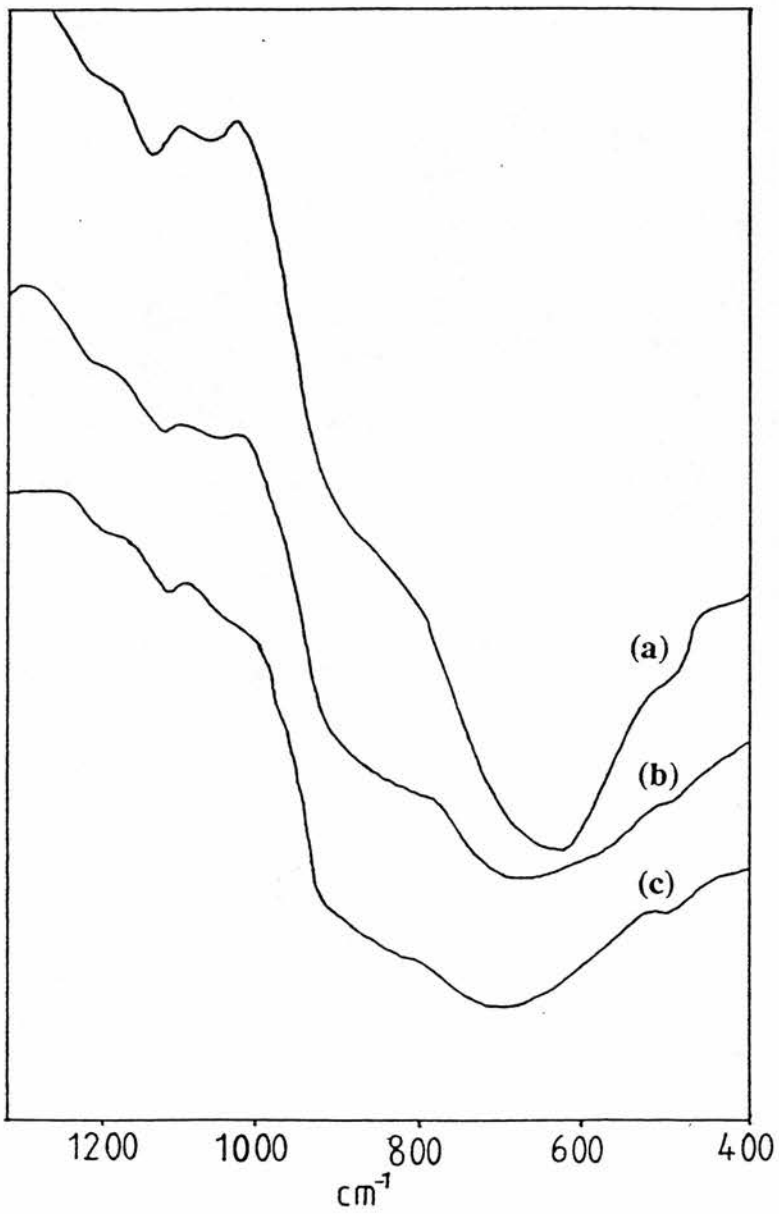

Fig. 9.2. Typical FTIR spectra of an EtOH gel after (a) 150°C drying compared to (b) hydrated Nb_2O_5 aged at 200°C and (c) room temperature.[19]

the gels to 900°C the Raman spectrum is identical to that of H-Nb_2O_5 [18] [Raman bands in cm^{-1}: ν_1 region 991(s), 896(m); ν_2 region 674(s), 625(s); ν_5 region (T_{2g}) 548(mw), 470(m), 350(w); ν_6 region (T_{2u}) 260(s), 240(s)]. Thus hydrated Nb_2O_5 is the hydrolysis product of the $NbCl_{5-x}(OR)_x$ series.

Identical procedures were run on 0.05 mol dm^{-3} solutions of $(NbCl_5)_2$ in MeOH, EtOH, and ethylene glycol which were added to a large excess of 0.01 mol dm^{-3} H_2SO_4 (100 equivalents of water) and left to gel for 6 hours. The washed and dried gels are very similar to the non acid catalysed gels. SEM EDAX showed that the washed gels still contained sulfur. The FTIR spectrum of the 150°C is identical to those of the non acid catalysed gels except that the peak at 1120 cm^{-1} is hidden by an SO_4^{2-} peak at 1135cm^{-1}. The Raman spectrum of the gels heated at 900°C is identical to that of H-Nb_2O_5.[18]

9.3.4 pH Studies

0.5, 0.125, 0.0875 and 0.05 mol dm^{-3} solutions of $(NbCl_5)_2$ in MeOH and EtOH were prepared and 0.5 ml quantities placed in 3ml sample bottles. These sample bottles were placed in 12 ml sample bottles containing water, to give a minature water bath. This ensured that during hydrolysis the temperature of the solution remained at 298K $\pm$3K. Between 40 and 670 equivalents of water were added to the samples which were stirred vigorously for 30 seconds and the pH was then monitored.

9.4. Chapter 4, General

For alcohol solutions of $(NbCl_5)_2$ weighed amounts of $(NbCl_5)_2$ (99%+ Aldrich) were dissolved in the required alcohol (spectroscopic grade, Aldrich) to give the specified molarity, and sonicated for 5 minutes. Gelation studies were done with the same experimental apparatus and procedures as outlined in section 9.3. Unless otherwise stated in chapter 4 or below, film formation entailed spreading a 50µl drop of solution over 6 cm^2 of washed and dried microscope slide. CO_2 absorbance pore analysis was run by Dr. Steve Jones, British Gas, R. and D. Div., Wharf Lane, Solihull, B91 2JW on a Digisorb 2600, and the Dubinin-Astakhov theory applied for data reduction.[20,21]

9.4.1 Spin Coating of Thin Films of Nb_2O_5

In an attempt to create thin films of <0.5μm thickness, initially 50μl and 100μl drops of 0.5 mol dm^{-3} solution of $(NbCl_5)_2$ in EtOH were applied to 5 x 1 x 0.3 cm ITO glass electrodes and spun at 2000 rpm for between 2 and 17 minutes. They were then subjected to three different temperatures (293K, 353K, 393K) for two hours. SEM revealed that the films were of the order of 1μm thickness and that the films were cracked and peeled. However, the experiment was successfully repeated using 50μl drops of 0.05 mol dm^{-3} solutions of $(NbCl_5)_2$ in EtOH, with the films being spun at 2000 rpm for 2 minutes followed by drying at 393K for two hours. SEM revealed that the films produced were of the order of 0.1μm thick and crack-free, and hence could be used in the electrochemical experiments. CO_2 absorbance pore analysis revealed the films to be non-porous solids.

9.4.2 Thick Films of Nb_2O_5

Having successfully created thin films of Nb_2O_5, we attempted to form thick (~5μm) uniform films of Nb_2O_5 in order to compare the optical densities. It had been found that upon dipping microscope slides into 0.5 mol dm^{-3} solutions of $(NbCl_5)_2$ in ethanol, ethylene glycol or isopropanol, and then into 1.0 mol dm^{-3} H_2SO_4, immediate hydrolysis and gelation occurred to give a film of hydrated Nb_2O_5. Repeating this with a 0.5 mol dm^{-3} solution of $(NbCl_5)_2$ in methanol did not give immediate gelation. Use of EtOH solutions gave the most homogeneous gel coating. However the process of hand dip coating did not produce uniform thickness films. In order to create an even and uniform thick film, 50μl drops of 0.5 mol dm^{-3} solution of $(NbCl_5)_2$ in EtOH were applied to 5 x 1 x 0.3 cm ITO glass elctrodes and spun at speeds from 500 to 2000 rpm for 1 to 10 seconds. The electrodes were then immediately placed in 1.0 mol dm^{-3} H_2SO_4 for 1 minute for complete hydrolysis and gelation. The thickness of the films was then measured by SEM and micrometer. It was found that uniform films of 5μm thickness were reproducibly formed when the electrode was spun at 1250 rpm for 3 seconds. However, because of the short spin time, the spin coating had only progressed to the spin off stage and a residual ridge of ca. 10-15μm thickness was observed at the very

edges of the film. These edges were stripped off and the exposed ITO glass coated with silicone grease to give a thick (5 μm) Nb_2O_5 film for use in the electrochemical experiments.

Chemical Additives

9.4.3 Diacids

Two diacids were tried: adipic acid $(CH_2CH_2COOH)_2$ (Aldrich, 99+%) and 1,10-decanedicarboxylic acid (Aldrich, 99%). Saturated solutions of both acids in water and 50/50 water/ethanol were prepared and mixed with 0.5 and 0.2 mol dm^{-3} solutions of $(NbCl_5)_2$ in ethanol in a 10:1 ratio H_2O:Nb. Into both solutions were immediately dipped microscope slides to give films, the remainder of the solutions also being left to gel (at 293K). For the adipic acid solutions, no acid catalysed gelation was observed, the gelation taking 90 minutes for the 0.5 mol dm^{-3} $(NbCl_5)_2$ solution in EtOH mixed with the adipic acid saturated solution in water. Upon addition of 1,10-decanedicarboxylic acid solution to the niobium chloroethoxide solutions, a grainy white gel precipitated out over 1 minute. In all cases, drying at 293K gave cracked films after ~ 6 hours and eventually broken glass monoliths.

9.4.4 Bis-cyclopentadienylniobium (V) chloride ($NbCl_3Cp_2$)

The literature preparation of Wilkinson and Birmingham[22] was followed:

4.05g of $(NbCl_5)_2$ was suspended (under N_2) in 30ml dichloromethane (Aldrich, HPLC grade, redistilled over sodium benzophenone) and 15ml of 2.0 mol dm^{-3} sodium cyclopentadienylide in THF (Aldrich) was added with vigorous stirring and ice cooling. After 3 hours a brown "slush" formed which gave, upon Soxhlet extraction with dichloromethane (under N_2/HCl atmosphere) and cooling, red/brown crystals of $NbCl_3Cp_2$. If HCl gas is not bubbled through the dichloromethane, then black $NbCl_2Cp_2$ forms. Mass spec.: 293/5/7 $NbCl_2Cp_2^+$; 258, $NbClCp_2^+$; 228/229/31 $NbCl_2Cp^+$. FTIR 1180 cm^{-1}(w), 1170 cm^{-1}(w), 1140 cm^{-1} (w) 1095 cm^{-1} (w), 1040 cm^{-1} (w), 1020 cm^{-1} (m), 960 cm^{-1} (m), 935 cm^{-1} (s), 865 cm^{-1} (s), 750 cm^{-1} (s) – matches that found by Wilkinson.[22] A saturated solution of $NbCl_3Cp_2$ in methanol (~0.05 mol dm^{-3}) was prepared and gave a green/brown coloured solution. This solution was then reacted water, acid and base (see section 4.3.3).

9.4.5 Miscellaneous Chemical Modifiers

1.25 mol dm^{-3} solutions of $(NbCl_5)_2$ in formamide (Aldich), methyl formamide (Aldrich,) and dimethylformamide (Aldrich, HPLC grade) were prepared as in section 9.2. Preparation of solid $(Nb(OPr^i)_5)_2$, $(NbCl_5)_2$, 6 and 3 mol dm^{-3} solutions of $(Nb(OEt)_5)_2$ in EtOH and pure liquid $(Nb(OEt)_5)_2$ was as before, see sections 9.2 and 9.2.2. $Nb(OPr^i)_4Acac$ was prepared by the addition of acetylacetone (BDH) and $(Nb(OPr^i)_5)_2$ in a 1:4 ratio and sonication for 1 hour to give an orange liquid, $Nb(OPr^i)_4Acac$.[23] ^1H NMR (293K): 1.10, 1.20ppm,12H (CH_3, OPr^i); 1.35, 1.45ppm, 12H (CH_3, OPr^i); 1.65ppm, 6H (CH_3, acac); 5.20ppm, 2H (CH, OPr^i), 5.45ppm, 1H (CH, acac), 5.75 broad, 2H (CH, OPr^i). FTIR (cm^{-1}): 3100(s) and 3070 (m); 1580 (s) and 1530 (s); 1450 br (mw); 1360 (s); 1300 (m); 1160 (m); 1100 (s); 1000 doublet (s); 930- (w); 880 (m); 800 br (m); 685 (m); 610 (w).

9.4.6 3-(Glycidyloxypropyl)trimethoxysilane "Glymo"

Glymo was obtained from Aldrich (96%, ^1H NMR confirmed that there were no major or assignable impurities present). Glymo gels/polymers are formed by the hydrolyis reaction of the following species at 353K for 1 hour: 4.1 ml glymo, 1.0 ml H_2O, 0.5 ml MeOH(miscibility agent) and 0.05 ml H_3PO_4 (catalyst). The gels formed are clear and "plastic" in nature. FTIR reveals that the methoxide groups have been fully hydrolysed:

Glymo, FTIR (cm^{-1}): 2840, 2940 (s) (OMe, epoxide); 1900, 1730 (w); 1480 br (s), 1440, 1420 (m); 1395 (w), 1340 (s) (OMe); 1260 (s) (SiOMe); 1200 (vs) (epoxide); 1100 br. (vs) (SiOMe, ROR); 905 (s) (epoxide); 870 br. (vs), 740 (s) (SiOMe); 700, 680, 640 (w); 440(s).[24]

Glymo Gel FTIR (cm^{-1}): 2840, 2940 (s) (epoxide); 1650(m); 1420 (m); 1200 (vs) (epoxide); 1060-20 br (vs) (δSi-O-Si); 700 (m) (νSi-O-Si); 590 (w) (δO-Si-O).[24]

9.4.7 Mixed NbO/Silicone Gels

Mixed silicone/NbO gels were created by mixing 0.25 mol dm^{-3} and 0.5 mol dm^{-3} $(NbCl_5)_2$ solutions in EtOH with glymo and water, in sample bottles, placing in an oven for 18

hours at 353K and the resulting polymers examined. Different initial Nb:Si:H_2O molar ratios were used to find the tolerences of the system.

A second set of experiments was run using 0.25 mol dm^{-3} $(NbCl_5)_2$ solution in ethanol and mixing with H_2O and glymo at the following Nb:Si:H_2O percentage molarities:- 7:11:82, 9:9:82, 8:12:80, 10:10:80, 12:8:80. This time though both monoliths and hand dipped films were prepared and 2 types of heating were used: (a) 343K for 18hours and (b) 298K for 25 minutes, ramp the temperature to 323K over 25 minutes and hold for 18 hours. All the films with a Nb percentage molarity < 10% were uncracked and none went cloudy. FTIR data for a typical mixed NbO/silicone 9:9:82 mol ratio film is given here:

9:9:82 Mixed NbO/Silicone Film FTIR (cm^{-1}): 3200 (s) (H_2O); 2840, 2940 (s) (epoxide); 1650 (ms); 1420 (w); 1200 (s) (epoxide); 1120 (s) (ROR); 1060 br (s) (δSi-O-Si); 840 br (s); 750 (m); 700 (m) (νSi-O-Si); 650 br (m); 590 (w) (δO-Si-O). Although it is hard to be definitive in the assignment of the broad band between 900-600 cm^{-1} in the films (characteristic of Nb-O, see section 9.3.3), it is clear that full hydrolysis has occurred – there are no Si-OR peaks at 850-750 cm^{-1} and 1460nm; no Nb-OR at 580nm nor any trace of free alcohol.

9.4.8 Mixed NbO/Silicone Electrodes

A set of mixed uncracked NbO/silicone polymers electrodes were obtained by mixing the required volumes of 0.2 mol dm^{-3} $(NbCl_5)_2$ in EtOH , glymo and water, (to give 9:9:82 and 8:12:80 Nb/Si/H_2O percentage molarities) and spreading a 6μl drop of the resulting solutions on 2 cm^2 of an ITO glass electrode and heating in the oven at 335-353K and for between 18-24 hours.

9.4.9 Composite Electrodes

As with the thick niobium oxide films (section 9.4.2), a 0.05 ml drop of 0.5 mol dm^{-3} $(NbCl_5)_2$ solution in EtOH was spread over 2cm^2 of ITO glass and then spun at different speeds (1000-1500rpm) for different times (1-10secs). The electrode was then placed in 1 mol dm^{-3} sulphuric acid for 1minute to gel, excess acid gently blown off and the thick gel edges removed. These soft films were then dipped in either a glymo/MeOH/water mixture or a

5:13:82 Nb:Si:water mixture or a 9:9:82 Nb:Si:water mixture and spun again to remove excess second coating, this second spin being done at the same spin rate and time as the first film. The electrodes were then heated in an oven at 335K for 3 hours. Higher temperatures were tried but the films cracked. Like the single layer thick soft niobium oxide films it was found that the most reproducible uniform films were obtained by spinning at 1250 rpm for 3 seconds and by applying a second coat containing a 5:13:82 Nb:Si:water mixture.

9.5 Chapter 5, General

Cyclic voltammetry and chronoamperometry. Measurements were carried out using a combined pulse/scan generator and potentiostat (Pine Instruments RDE4 or homebuilt) and a Graphtec XY recorder. The three electrode cell configuration is shown in Fig. 9.3(a). Electrolytes used were: 1.0 mol dm^{-3} H_2SO_4 or 0.5 mol $dm^{-3}Bu^n_4NPF_6$ (Aldrich, 98% recrystallised) in HPLC grade acetonitrile (Aldrich). All potentials reported vs SCE (standard Calomel Electrode). The cell was N_2 purged before use. Chronoabsorptiometry and spectra were recorded using the cell depicted in Figure 9.3(b), which could be inserted directly into the cell-block of a Phillips PU8720 UV-Vis Spectrometer. Here a Pt quasi-reference was used instead of the SCE. Between three and six electrodes of each type were investigated. Diffusion coefficients and electrochromic efficiencies are quoted as mean values, the diffusion coefficients to a 99% confidence interval(see Appendix 2).

Electrochemical Impedance Measurements. The electrode (exposed area 1 cm^2) was mounted in a three-electrode cell with SCE reference electrode and ITO counter electrode, and 1.0 mol dm^{-3} H_2SO_4 electrolyte at 293 K. Data was collected by a Solartron 1255 Frequency Response Analyzer and 1286 SI Electrochemical Interface.

Electrode Fabrication

9.5.1 Thick Nb_2O_5/ITO Electrode

A 5 x 1 x 0.3 cm ITO (indium tin oxide, Phosphor Products, 20Ω/square) glass electrode was ultrasonically cleaned then coated with a 50 µl drop of 0.5 mol dm^{-3} $(NbCl_5)_2$ (Aldrich) in spectroscopic EtOH (Aldrich), and this was then spun at 1250 rpm for 3 seconds

Fig. 9.3

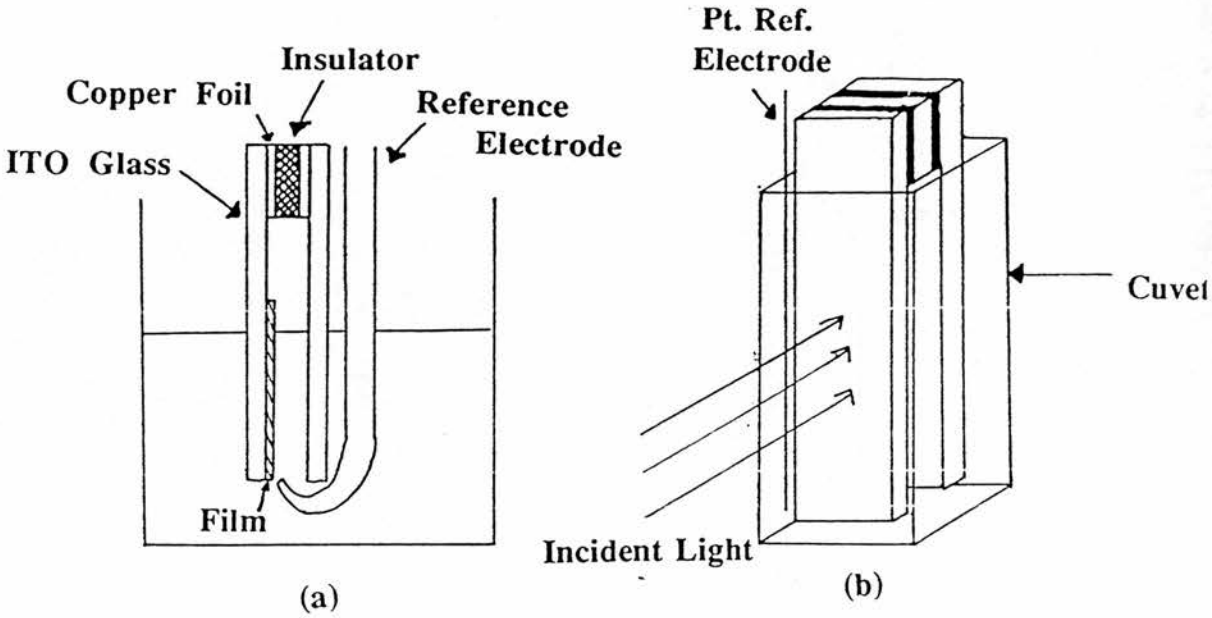

Fig. 9.3. The three electrode cell configuration used for (a) chronoamperometry, (b) chronoabsorptiometry experiments.

on an upturned Pine Electrodes Rotator, so that 2 cm^2 was covered. The electrode was then placed in 1.0 mol dm^{-3} H_2SO_4 for 1 minute for complete hydrolysis and gelation. This gave an even coating ca. 5 μm thick as measured by micrometer and SEM. The edges of the film were ca. 5 -10 μm thicker than the central part. Excess water was very gently blown off with a low velocity air stream at an angle of ~ 10° to the gel. The edges were stripped off and replaced by silicone grease in order to mask the exposed underlying ITO. The final Nb_2O_5/ITO electrode was 1.2 cm^2 in area.

9.5.2 Nb_2O_5/Silicone Composite Electrode

A Nb_2O_5/ITO electode was prepared as in section 9.5.1 but without the silicone grease applied to the exposed ITO, then dipped for 3 seconds in a composite silicone containing sol. The composite sol contained: 10.0 cm^3 0.2 mol dm^{-3} $(NbCl_5)_2$ (Aldrich) in spectroscopic EtOH (Aldrich), 2.3 cm^3 3-Glycidoxypropyltrimethoxysilane (Glymo) (96% Aldrich) and 1.17 cm^3 demineralised water. The resulting solution thus contained Nb:Si:H_2O in the molar ratios 5:13:82. The electrode was then spun at 1250 rpm for 3 seconds to remove excess sol and dried at 60°C for 3 hours.

9.5.3 Thin (0.1μm) Films of Nb_2O_5

Thin films of Nb_2O_5 were produced by applying 50μl drops of 0.05 mol dm^{-3} solution of $(NbCl_5)_2$ in EtOH to 5 x 1 x 0.3 cm ITO (Indium Tin Oxide, Phosphor Products, 20Ω/square) glass electrodes. The electrodes were then spun at 2000 rpm for 2 minutes and finally dried at 393K for 2 hours. SEM revealed the films to be of the order of 0.1μm thickness and all the films thus produced were crack-free, and hence could be used in the electrochemical experiments. Measurements of film weight gave film densities in the region of 3.9-4.1 g cm^{-3}.

9.5.4 Ethylene Glycol Gels

A 0.5 mol dm^{-3} solution of $(NbCl_5)_2$ in ethylene glycol was prepared and mixed with water in a 10:1 H_2O:Nb ratio and spread onto ITO glass (a) immediately, and (b) after 45

minutes of hydrolysis. After 4 days at 293K, the soft white gel electrodes (thickness ca. 50μm) were tested for electrochromic properties.

9.5.5 NbO/Silicone Gel Electrodes

A set of mixed uncracked NbO/silicone polymers electrodes (thickness ca. 15μm) were obtained by mixing the following volumes of 0.2 mol dm^{-3} $(NbCl_5)_2$ in EtOH, glymo and water: 10.0 ml, 1.78 ml, 1.30ml respectively for a 9:9:82 Nb:Si:H_2O solution and 10.0ml, 2.66ml and 1.42ml for the 8:12:80 solution. Then a 6μl drop of the resulting solution was spread on 2 cm^2 of ITO glass and heated in the oven at 335-353K for 18 or 24 hours.

4.5.6 Assumptions in the Calculation of D_H+ For The Thick Films

In calculating D_H+ from the slope of the i vs $t^{-1/2}$ graph (Figs. 5.8(a) and (b)), certain assumptions have been made, in order to extract a value for D_H+.

From eq(5.4) it is evident that D can be calculated if one knows either C, the concentration of reactant centres, or L and Q_{Tot}, the thickness and total charge passed, respectively. Cabanel et al[25] took C to be equal to the external electrolyte concentration, for which there seems to be no justification. Other workers [26-28] assumed C was proportional to the density of the films – this latter method is more justifiable, however we were unable to use this assumption as the concentration of the reactant sites decreased every cycle due to the cracking and peeling of the films.

In order to obtain D_H+ we calculated d and Q_{Tot}. d was taken to be the ex-situ thickness of the film, ie any increase in film thickness due to solvent swelling has not been taken into account. Q_{Tot} was calculated from the amount of charge passed on the colouration cycle during semi infinite diffusion. Fig. 9.4 shows i vs $t^{-1/2}$ graph of a typical polymer electrode.[29] The point t_d marks the end of the semi infinite diffusion and corresponds to the colour front reaching the internal interface of the film, as shown in Fig.9.5 (a).[29,30]

Fig. 9.4

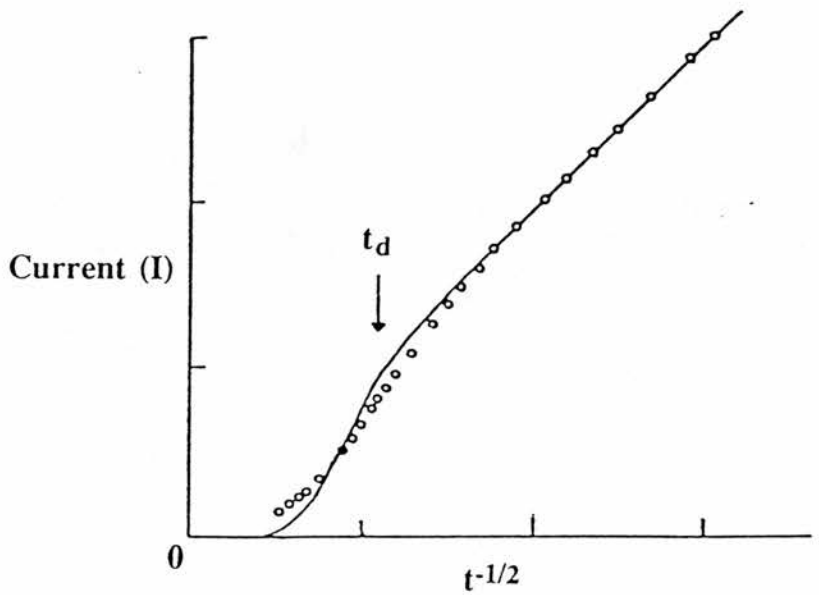

Fig. 9.4. I vs $t^{-1/2}$ graph of a typical polymer electrode showing t_d, where (o) are the experimental data and (—) the theoretical fit. Taken from reference 29.

Fig 9.5

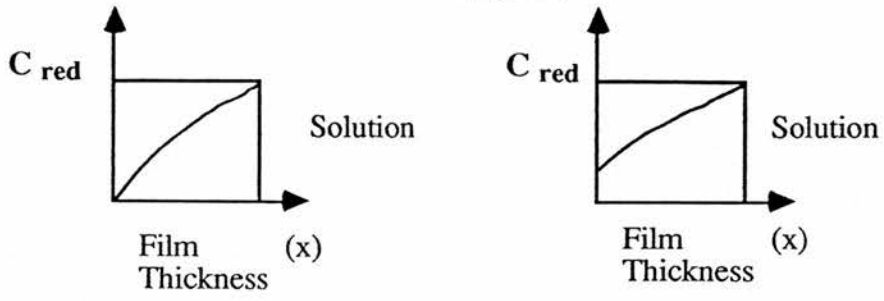

(a) (b)

Where C is the concentration of reactant centres and C_{red} is the conc. of reduced reactant centres. If $t>t_d$ then a concentration gradient like that shown in Fig. 9.5 (b) occurs, whilst still being diffusion controlled, the Cottrell equation is no longer obeyed and hence the graph deviates from the Cottrell slope. t_d for the composite electrode is 9 seconds and thus Q_{td} can be measured from the chronoamperometry experiments. As $2Q_{td} \sim Q_{Tot}$, this allows a value of Q_{Tot} to be calculated.[30]

9.6 Chapter 6, General

Cyclic voltammetry (CV) and chronoamperometry were carried out using a combined pulse/scan generator and potentiostat (Pine Instruments RDE4) and a Graphtec XY recorder in a standard three electrode cell. The working electrode was a home-built glassy carbon electrode (4 mm diameter), the microelectrode was a home-built platinum microelectrode (50 μm diameter) and the counter electrode was a platinum wire. All equipment and glassware were vacuum dried over P_2O_5 and all the electrochemistry was done with degassed solutions under N_2. Background CV's of the Nb-free solvents showed no electrochemistry in the regions being examined. Chronoamperometric experiments were analysed graphically or via a Macadios (G.W. Instruments) electrochemical interface to a Macintosh SE/30. Analysis programs for the calculation of D and n were written in Quickbasic (Microsoft).

9.6.1 Non-Aqueous Electrochemistry

The non-aqueous solvents used for the electrochemical measurements were acetonitrile (AN) and dimethylformamide (DMF), both were anhydrous grade (Aldrich) redistilled over 3Å

sieves. The supporting electrolyte was 0.1 mol dm^{-3} $Bu^n_4NPF_6$ (Aldrich recrystallized, vacuum dried over P_2O_5). Throughout the non-aqueous electrochemistry work ferrocene has been used as an internal standard after the proposal of Gagne et al.[6] Initially a quasi Pt reference electrode was used to observe the electrochemistry under investigation and then ferrocene was added as a reference redox couple. However, where ferrocene was found to react with the compounds under investigation (chapter eight) the reference electrode, $Ag/Ag^+NO_3^-$ (0.01 mol dm^{-3}), TBAHFP (0.1mol dm^{-3}) was used, which in turn was standardized to ferrocene in a separate AN solution. Ferrocene is a useful internal reference as it has a known $E_{1/2}$ of 0.400V vs N.H.E.[6] In all non aqueous solutions when diphenylanthracene was added to the solution, to check electrode conformation, ΔE_p for its redox couple was found to be 90mV.

9.6.2 Aqueous Electrochemistry

Concentrated HCl (Aldrich, lab grade) or 0.1 mol dm^{-3} KOH solution (Aldrich, A.C.S.) were used as the solvent and electrolyte systems. For the aqueous electrochemistry a saturated calomel electrode (SCE) (Russell pH Ltd) was used. A platinum disc electrode (diameter 6mm) working electrode was also used in conjunction with the carbon electrode described in section 9.6.

Niobium Precursor compounds

9.6.3 General

The $(NbCl_5)_2$ and ferrocene (vacuum dried over P_2O_5) were lab grade (Aldrich). $CsNbCl_6$ was made by the standard preparation (see section 9.2.1).[1] $(Nb(OR)_5)_2$ where R = Me, Et and Pr^i were prepared as before (see section 9.2.2). $NbOCl_3$ species were prepared in situ by the addition of 2 equivalents of demineralised water and identified by ^{93}Nb NMR, $NbOCl_3.(AN)_2$ has a peak at -498ppm (FWHM~850Hz) and $NbOCl_3$ in DMF has a peak at -500ppm (FWHM~1200Hz).[31]

9.6.4 $NbCl_5$.AN

^{93}Nb NMR of $(NbCl_5)_2$ added to warm (315K) anhydrous acetonitrile gives a peak at -55ppm (500Hz wide) and is indicative of the monomer adduct, $NbCl_5$.AN.[10]

9.6.5 $(NbCl_5)_2$ in DMF

Before carrying out the electrochemistry of $(NbCl_5)_2$ in DMF we investigated whether $(NbCl_5)_2$ reacts with this solvent. Dissolution of $(NbCl_5)_2$ in anhydrous DMF gave a ^{93}Nb N.M.R signal at 1.5ppm (FWHM 30Hz). Both the position and linewidth reflect the lower pseudo-octahedral symmetry about Nb in the dimer $(NbCl_5)_2$ compared to $[NbCl_6]^-$ which was used as the NMR reference. Furthermore 2.5 mol dm^{-3} solutions of $(NbCl_5)_2$ were prepared (under N_2) in warm anhydrous DMF (343K) and allowed to cool. The yellow precipitate formed was washed with cold benzene (under N_2) and vacuum dried over P_2O_5 for 4 days. The yellow solid showed no proton spectra in deuterated toluene thus we conclude that the only species present in the DMF solution is the dimer $(NbCl_5)_2$. In separate experiments we have found that $(NbCl_5)_2$ is hydrolysed as follows:

$$(NbCl_5)_2 + H_2O \rightleftharpoons NbOCl_3 + [NbCl_6]^- + 2H^+ + Cl^- \qquad (9.1)$$

However, in our electrochemical experiments there was no ^{93}Nb NMR evidence for either $NbOCl_3$ (-500ppm[10]) or $NbCl_6^-$ (0ppm), implying that the solution is anhydrous.

9.6.6 "Amorphous" $K_7HNb_6O_{19}.13H_2O$

$K_7HNb_6O_{19}.13H_2O$ was prepared by the method of Edlund et al.[32] 10g of Nb_2O_5 (Aldrich, 99.9%) was fused with 20g KOH (Aldrich, 99.99%) in a nickel crucible to form a clear melt. This was then dissolved in 200ml of distilled water and filtered. Equal amounts of ethanol (Aldrich, lab grade) were added, the solution stirred vigorously, the precipitate filtered and washed with cold ethanol. The precipitate was then recrystallised from water twice to give $K_7HNb_6O_{19}.13H_2O$. This was characterized by X-ray powder diffraction (see Fig. 9.6(a)) (and matched the theoretical powder diffraction for $K_7HNb_6O_{19}.13H_2O$ calculated from the X-ray crystal pattern of $Na_7HNb_6O_{19}.13H_2O$[33] using a Stoe modified version of the Lazy Pulverix program) and FTIR (see Fig. 9.7(b)).

Fig 9.6

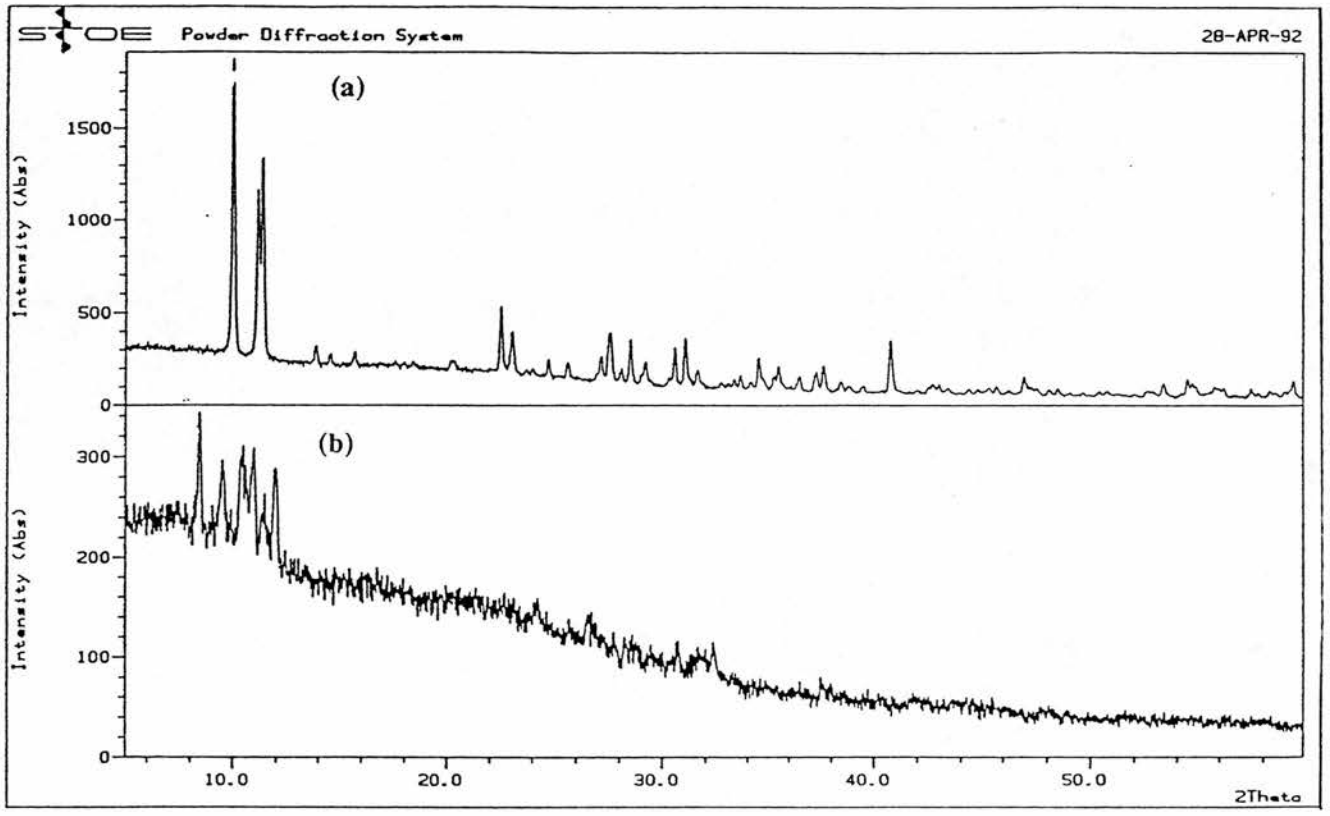

Fig. 9.6. The X-ray powder diffraction pattern of (a) $K_7HNb_6O_{19}.13H_2O$ crystals; (b) "amorphous" $K_7HNb_6O_{19}.13H_2O$ (first precipitate).

Fig. 9.7

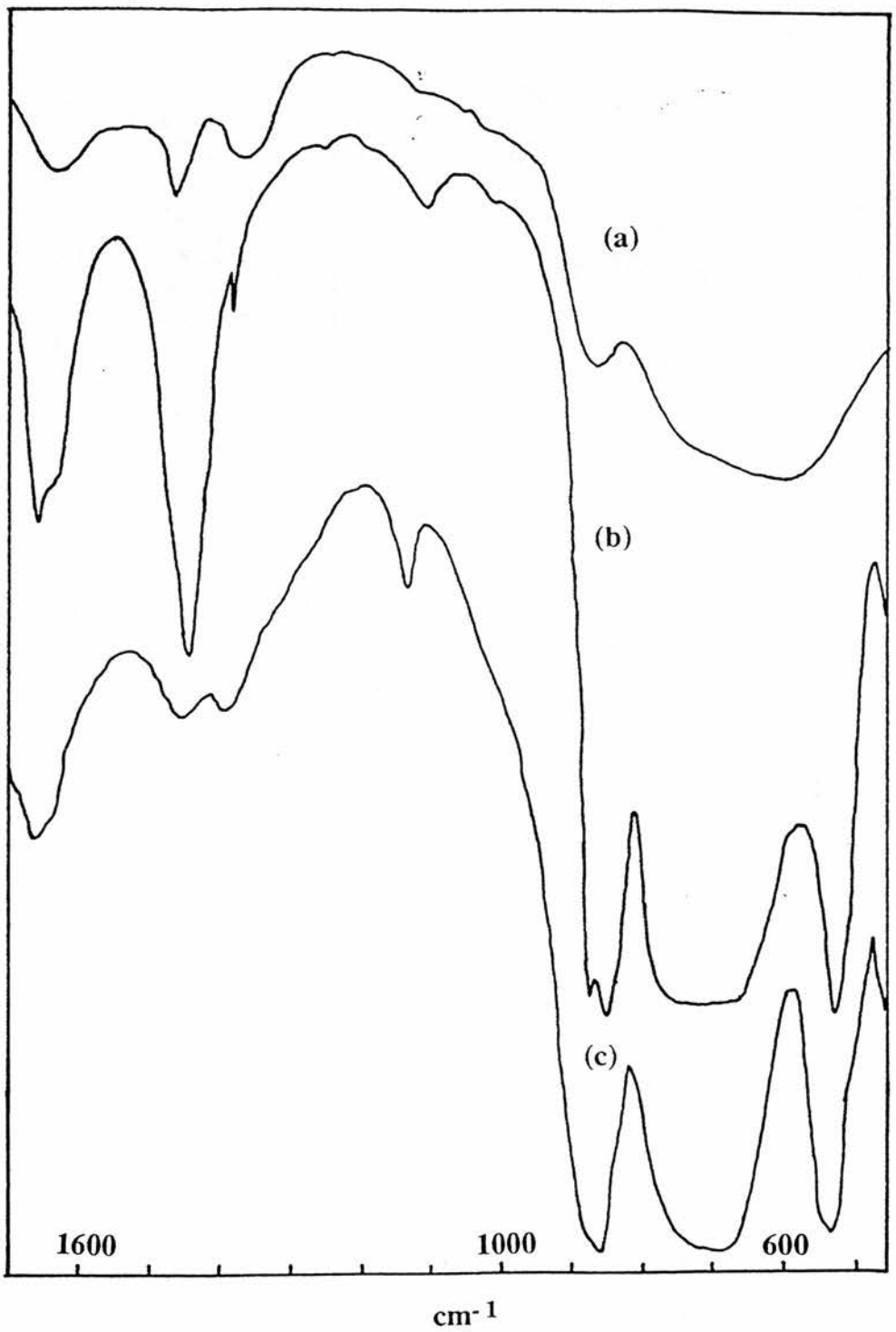

Fig. 9.7. FTIR spectra of $K_7HNb_6O_{19}.13H_2O$ and products where (a) is film formed by electrodeposition from $K_7HNb_6O_{19}.13H_2O$ solution, (b) is $K_7HNb_6O_{19}.13H_2O$ (crystals) and (c) is $K_7HNb_6O_{19}.13H_2O$ (first precipitate, ie "amorphous" $K_7HNb_6O_{19}.13H_2O$).

Unfortunately $K_7HNb_6O_{19}.13H_2O$ is only sparingly soluble in aqueous solution, even 1.0 mol dm^{-3} KOH. However the first precipiate is far more soluble (rather than the third) allowing electrochemical solutions to be prepared. Figs. 9.6(b) and 9.7(c) show the powder diffaction and FTIR of the first precipitate. Fig. 9.7(c) shows the three strong bands at 850, 700(br) and 520 cm^{-1} characteristic of $[Nb_6O_{19}]^{8-}$ but without the strong peak at 1450 cm^{-1} and the weak peak at 880 cm^{-1} characteristic of $K_7HNb_6O_{19}.13H_2O$ (see Fig. 9.7(b)). Similarly Fig. 9.5(b) shows a set of peaks in the 9.0-14.0 2θ region characteristic of $[Nb_6O_{19}]^{8-}$ species. That these peaks do not match a single compound is indicative of a mixture of cations being present.[34] This implies the formation of $[Nb_6O_{19}]^{8-}$ units but no long range crystallinity and this first precipitate has been dubbed "amorphous" $K_7HNb_6O_{19}.13H_2O$. 0.002 mol dm^{-3} solutions of "amorphous" $K_7HNb_6O_{19}.13H_2O$ were prepared in 0.1mol dm^{-3} KOH but no redox chemistry for this species was observed.

9.6.7 Calculation of The Rate Constant from Cyclic Voltammetry

For an ec system, the book "Instrumental Methods.In Electrochemistry"[35] contains a working curve for the estimation of the rate constant (k) of the chemical reaction. This is a plot of $\log(k\tau)$ vs $I_{p,a}/I_{p,c}$ where τ is $\Delta E/\nu$. ΔE is the difference between $E_{1/2}$ (the half wave potential) and E_2 the switching potential, ie the potential at which the sweep is reversed. ν is the scan rate. By comparison of experimentally derived values of $I_{p,a}/I_{p,c}$ with the working curve, values of $\log(k\tau)$ are obtained. As ΔE and ν are known for each of the values of $I_{p,a}/I_{p,c}$, the rate constant can be calculated.

9.6.8 Calculation of the Diffusion Coefficients from Chronamperometry

As we have seen in section 5.2.1, the current for a macroscopic electrode, under semi-infinite diffusion conditions, is given by:

$$i(t) = \frac{nFAD^{1/2}C}{\pi^{1/2}\, t^{1/2}} \qquad (9.2)$$

Where n is the number of electrons, t is the time taken (sec), D is the diffusion coefficient of the molecular species (cm^2s^{-1}), A is the macroscopic area of the film (cm^2), F is the Faraday

constant, C is the concentration of molecular species (mol cm^{-3}).

Similarly, for a single disc microelectrode with hemispherical diffusion dominating (see section 5.8.), the limiting plateau current (i_l) is given by:

$$i_l = 4nFDCr \qquad (9.3)$$

Where r = radius of electrode, n = number of electrons, F = Faraday constant, D = diffusion coefficient (cm^2s^{-1}), C = concentration of molecular species in solution. Thus by conducting chronoamperometry experiments (using a macroscopic area electrode) and obtaining CV's by cycling around the redox potential with a microelectrode we are able to find the slope of the i vs $t^{-1/2}$ plot and the limiting plateau current. These give two simultaneous equations in D and n (assuming C, r and A are known) which are solved for D and n.

9.7 Chapter 7, General

All niobium compounds investigated were prepared as in sections 9.6.4-7. The electrodeposition experiments were conducted using the same general experimental as described in sections 9.6-9.6.2, but with the following additions:- (i) platinum disc working electrodes (1mm and 6 mm diameter) were used in addition to the carbon electrode; (ii) all working electrodes were polished consecutively with 5, 1 and 0.25 μm diamond polish (Engis Ltd, Hyprez Five Star grade), washed in acetone, sonicated in an acetone bath for 30 minutes, washed again with demineralised water and acetone and finally dried at 80°C; (iii) an SCE reference electrode was used in all systems.

Film formation was checked visually, and then electrochemically by cycling the electrodes in 1.0 mol dm^{-3} H_2SO_4 between 0.2V and -1.0V in order to observe any characteristic Nb_2O_5 electrochromic CV's. Films thus found were analysed using FTIR, powder X-ray diffraction and SEM EDAX.

9.7.1 Superoxide Generation

0.0025 mol dm^{-3} solutions of $(NbCl_5)_2$ or $(Nb(OR)_5)_2$ (where R = Et or Pr^i) in acetonitrile, DMF or DMSO (Aldrich, HPLC grade, redistilled over CaH_2) with 0.1 mol dm^{-3} supporting electrolyte were prepared. The electrolyte was either tetra butyl ammonium hexafluorophosphate (TBAHFP) or tetrabutyl ammonium dihydrogen phosphate (TBADHP) (Aldrich, 97% recrystallised from acetonitrile, vacuum dried over P_2O_5). TBADHP is not soluble in DMF. O_2 was bubbled into the solutions at ~$1cm^3s^{-1}$ through a sintered glass frit.

The $O_2 + e^- \rightleftharpoons O_2^-$ redox was observed at -1.0V (E_{pc} = -1.05V, E_{pa} = -0.95V, vs SCE) and the second reduction of oxygen, $O_2^- + e^- \rightarrow O_2^{2-}$ at -1.8V.[36,37] O_2 was bubbled through the AN and DMF solutions whilst a constant potential of -1.8→-2.0V was applied. In DMSO a potential of -1.1V was applied (see section 7.1.1). Table 9.1 gives a summary of the types of electrode, metal precursor, solvent, electrolyte, and period of electrolysis. No metal oxide film was ever observed.

Table 9.1

Summary of Superoxide Generation Electrodeposition Experiments				
Electrode	Nb Precursor	Electrolyte	Solvent[a]	Electrolysis Time (hr)
C	$(Nb(OEt)_5)_2$	TBAHFP	DMF	4-16
Pt	$(Nb(OEt)_5)_2$	TBAHFP	DMF	1-16
Au[b]	$(Nb(OEt)_5)_2$	TBAHFP	DMF	1-16
C	$(Nb(OPr^i)_5)_2$	TBAHFP	DMF	$1^1/_2$
Au[b]	$(NbCl_5)_2$	TBAHFP	DMF	1-16
C	$(NbCl_5)_2$	TBADHP	AN	1
C	$(Nb(OEt)_5)_2$	TBADHP	AN	2
Au[b]	$(Nb(OEt)_5)_2$	TBADHP	AN	1-16
C	$(NbCl_5)_2$	TBAHFP	DMSO	1-10

(a). -1.8→-2.0V (vs SCE) was applied in AN or DMF solutions, -1.1V (vs SCE) in DMF solutions.

(b). 6mm diameter Au disc electrode.

9.7.2 Reduction of Teriary Alcohols

The two tertiary alcohols investigated were triphenyl methanol (TPM) (KochLight, puriss grade, $(C_6H_5)_3COH$) and 9-fluorenemethanol (9F) (Aldrich, 99%, $(C_6H_4)_2C(CH_3)OH$), recrystallised from DMF and vacuum dried over P_2O_5 for 3 days. The working electrode was a hanging mercury drop electrode prepared from a 1mm dia. Pt electrode and triply distilled mercury. 0.1 mol dm^{-3} solutions of TPM and 9F in anhydrous DMF, containing 0.1 mol dm^{-3} tetrabutyl ammonium hexafluorophosphate and 0.0025 mol dm^{-3} $(Nb(OEt)_5)_2$ were electrolysed at -2.90V and -2.50V (vs SCE)[38] respectively to give niobium oxide films. SEM EDAX analysis indicated the sole presence of niobium, and the abscence of mercury. FTIR for both sets of films showed a broad featureless band from 400-950 cm^{-1} characteristic of niobium/oxygen bonds (see section 9.3.3 and Fig. 9.2 (a-c)).

9.7.3 Reaction of Niobium with H_2O_2

1.5-3.0g of tungsten and molybdenmum metal have been dissolved in 10 ml of 30% H_2O_2 and subsequently electrodeposited as oxides.[39] Unfortunately, not even 0.1g of niobium metal (Aldrich, -60 mesh, 99.8%) appears to dissolve in 10ml of 30% H_2O_2. Addition of 1-5ml of conc HNO_3 to the solution also failed to dissolve the niobium.

9.7.4 "Amorphous" $K_7HNb_6O_{19}.13H_2O$

"Amorphous" $K_7HNb_6O_{19}.13H_2O$ was prepared as in section 9.6.7. and solutions of 0.002 mol dm^{-3} concentration in 0.1 mol dm^{-3} KOH were electrolysed at 1.6V and 1.95 V (vs SCE) for between 3-23 hours on a platinum electrode. This electrolysis produced protons which lowered the pH and white niobium oxide films were electrodeposited. These films gave no powder X-ray diffraction pattern implying that they are truly amorphous solids. The FTIR spectrum of a typical film is shown in Fig. 9.6(a) and seems to indicate a mixture of Nb_2O_5 and $[Nb_6O_{19}]^{8-}$ units. Cyclic voltammetry in 1.0 mol dm^{-3} H_2SO_4 revealed CV's characteristic of electrochromism (see Fig. 7.2). Repeating the experiments with C and ITO electrodes failed to form films.

9.7.5 $(NbCl_5)_2$ in Conc. HCl

Electrolysing 0.1 mol dm^{-3} solutions of $(NbCl_5)_2$ in conc HCl (Aldrich, lab grade) at -1.00V (C electrode) and -0.5V (Pt electrode) (vs SCE) to increase the pH of the solutions and hence electrodeposit Nb_2O_5 failed to form a film but gave a precipitate of Nb_2O_5. FTIR of these washed precipitates dried at room temperature and 150°C gave identical spectra to those shown in Fig. 9.1(a) and (c), confirming that hydrated Nb_2O_5 was being formed.

9.7.6 Mixed Organic/Aqueous Systems

1.08 ml of conc. HCl was added to 10 ml of 0.1 mol dm^{-3} $(NbCl_5)_2$ in AN or DMF ($Nb:H_2O$ = 1:20). Electrolysing at -1.20V (vs SCE) (C and Pt electrodes) gave H_2 gas and a Nb_2O_5 precipitate (similar to that found in 9.7.5), but no film.

9.8 Chapter 8, General

UV/Vis spectra were obtained on a Phillips PU8720 UV/Vis spectrometer using a 0.5mm path length cell. ESR spectra were obtained on a Bruker ER 200 D spectrometer with low temperature attatchment. ^{93}Nb NMR were run on a Bruker MSL 500 spectrometer, ^{1}H on a WP80 and ^{2}D, ^{14}N on an AM300 spectrometer. FTIR (Perkin Elmer 1720) and Raman (Spex 1403 interfaced to a DM1B computer with Coherent Radiation Innova 90-6 Ar^+ laser excitation at 514.5 nm, power < 100 mW at the sample) spectroscopic data are within $\pm$ 1 cm^{-1}.

9.8.1 Dicaesium hexachloroniobate(IV), $Cs_2[Nb(IV)Cl_6]$

On addition of ferrocene (Aldrich, 98%, 0.19g, 1 mmol) to a solution of $CsNbCl_6$ (section 9.2.1) (0.44g, 1 mmol) in 50 ml acetonitrile, followed by ultrasonication, a purple solid (Cs_2NbCl_6) is precipitated (under N_2, at 293K). The Cs_2NbCl_6 was filtered off under N_2 and vacuum dried over P_2O_5. Yields were essentially quantitative. The sample was identified by comparison with the spectroscopic data described in a previous high temperature preparation.[40] Elemental microanalysis confirmed there was no C or H present. UV/Vis (nujol mull): λ_{max}/nm (relative intensities), 400 (1.0), 543 (0.95). FTIR: ν(Nb-Cl) 310 (ν_3, t_{iu})

Fig. 9.8

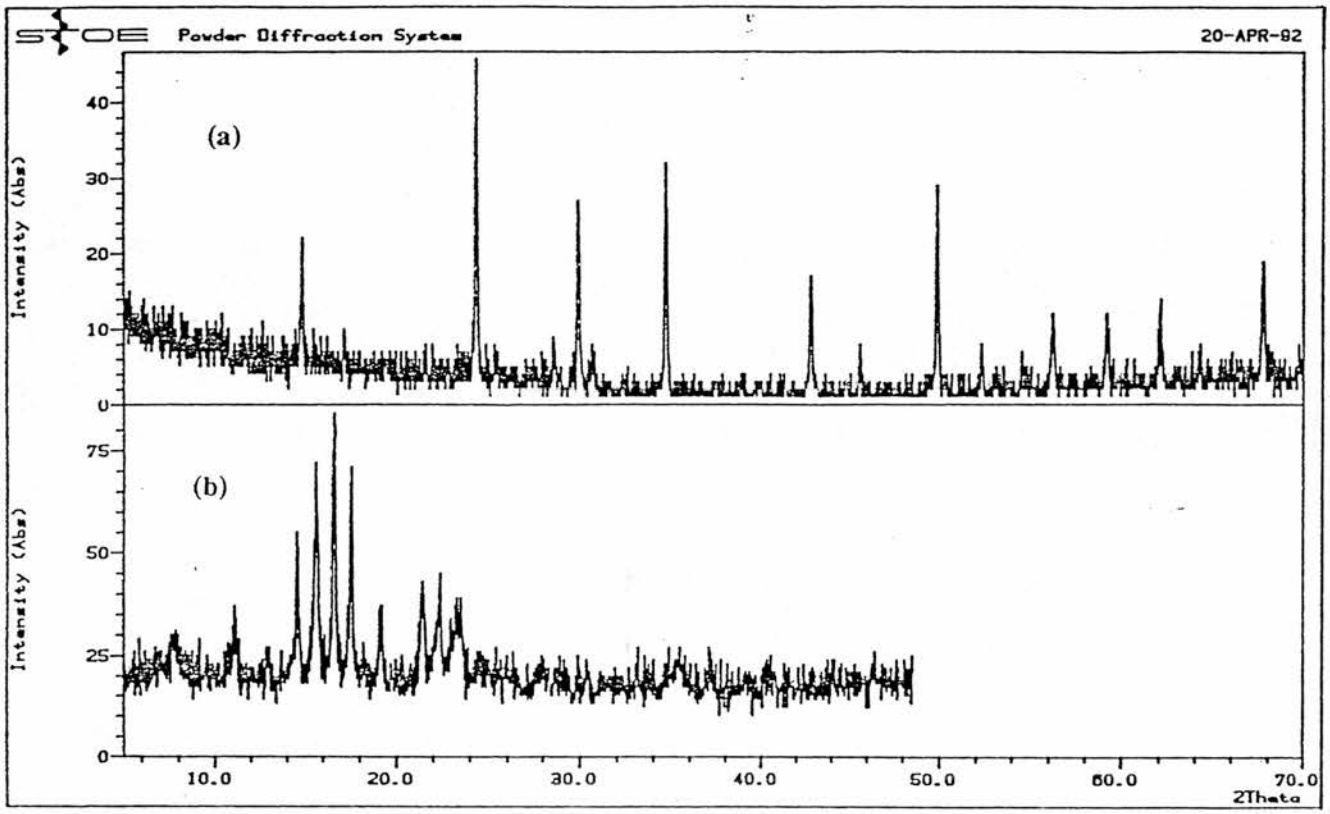

Fig. 9.8. X-ray powder diffraction patterns of (a) Cs_2NbCl_6 and (b) $Cp_2FeNbCl_6$.

cm^{-1}, Raman: 328 (ν_1, a_{1g}), 156 (ν_6, t_{2u}) cm^{-1} cm^{-1} (matches that given by Nakamoto[2]). The compound is insoluble in both organic solvents and 10.2 mol dm^{-3} HCl,[40] and we found no ^{93}Nb NMR solid state signal, implying that paramagnetic Nb^{IV} was present. See Fig. 9.8(a) for powder X-ray diffraction pattern.

9.8.2 Bis(cyclopentadienyl)iron hexachloroniobate(V), $Cp_2Fe[NbCl_6]$

Addition of ferrocene (Aldrich, 98%, 4.65g, 0.025 moles) to $(NbCl_5)_2$ (13.5g, 0.05 moles) in 100 ml dry AN yielded 11.24g (0.0227 moles) of washed and dried $Cp_2FeNbCl_6$ (under N_2, at 293K). (Addition of a further 4.65 g of ferrocene gave no more precipitate.) The blue-black precipitate $Cp_2FeNbCl_6$ was filtered under N_2, washed and recrystallised from acetonitrile and dried under vacuum over P_2O_5. Anal. Calc. for $C_{10}H_{10}FeNbCl_6$: C, 24.27; H, 2.04; N, 0.0. Found: C, 24.04; H, 1.91; N, 0.07. FTIR (cm^{-1}): 1420, 1110, 1000, 860 420 cm^{-1} (ferricenium[9]); 330cm^{-1}. (cf. $Cs[NbCl_6]$[9] ν(Nb-Cl) 333cm^{-1}). ^{93}Nb solid (magic angle) NMR, 5 kHz spinning rate, δ = 5ppm (indicating $[NbCl_6]^-$), referenced to $Cs[NbCl_6]$ external standard. No ^{13}C or ^{93}Nb NMR solution spectra found for this Nb(V) compound. See Fig. 9.7(b) for powder X-ray diffraction pattern (isomorphous with K_2PtCl_6).

9.8.3 Bis(1-methyl cyclopentadienyl)iron hexachloroniobate(V), Cp_2'$Fe[NbCl_6]$

Addition of 0.107g 1,1'-dimethylferrocene (Aldrich, 97%, 0.5 mmol) and 0.135g $(NbCl_5)_2$ in 10 ml dry AN gave a green solution. Removal of the solvent gave a green precipitate which was stored under N_2. FTIR (cm^{-1}):- 1364, 1234, 1054, 1027, 871, 797. This matched the FTIR spectrum of dimethylferricenium dodeca-tungstosilicic acid prepared by the standard method of Wilkinson et al (dimethylferrocene in ethanol/water is oxidised by H_2SO_4 and precipitated by the addition of dodeca-tungstosilicic acid to give blue-green dimethylferricenium dodeca-tungstosilicic acid).[41]

9.8.4 Bis(pentamethyl cyclopentadienyl)iron hexachloroniobate(V), Cp_2*$Fe[NbCl_6]$

Addition of 0.155g decamethylferrocene (0.5 mmol) and 0.135g $(NbCl_5)_2$ in 10 ml dry AN gave a green solution. Removal of the solvent gave a green precipitate which was stored

under N_2. FTIR (cm^{-1}):- 1072, 1012, 864, 580, 520, 442. This matched the FTIR spectrum of decamethylferricenium dodeca-tungstosilicic acid prepared by the standard method of Wilkinson et al (decamethylferrocene in ethanol/water is oxidised by H_2SO_4 and precipitated by the addition of dodeca-tungstosilicic acid to give green decamethylferricenium dodeca-tungstosilicic acid).[41]

9.8.5 Ammonium Chloride

The ammonium chloride crystals produced by the hydrolysis of acetonitrile were washed with cold acetonitrile, dried at 80°C. FTIR matched identically that of commercial ammonium chloride (Aldrich, ACS reagent). Anal. calc:- H, 7.53: N, 26.18. Found:- H, 7.53; N, 25.81; C, 0.90.

9.8.6 NMR Studies of Acetonitrile Hydrolysis Reactants and Products

In order to elucidate a mechanism for the hydrolysis, a series of NMR studies were undertaken at 293K. The studies had to be done in deuterated acetonitrile as the addition of water to solutions of $(NbCl_5)_2$ in non-coordinating solvents caused the immediate precipitation of Nb_2O_5. 0.1 mol dm^{-3} solutions of $NbCl_5$.AN (AN = acetonitrile) and 0.05 mol dm^{-3} solutions of $NbCl_5$.BN (BN = phenyl acetonitrile) were prepared. To these solutions were then added either 2 or 3 equivalents of H_2O ii) 3 equivalents of MeOH and 2 equivalents of H_2O. Multinuclei NMR spectra were then run on these solutions to follow the reactions occurring.

9.8.7 $NbCl_5$.BN

1.35g of $(NbCl_5)_2$ was dissolved in excess (20ml) phenyl acetonitrile, (Koch Light, puriss grade, redistilled over P_2O_5), and sonicated for 1 hour at 60°C (under N_2). Removal of solvent gave a brown solid, $NbCl_5$.BN. ^1H spectra, 7.53ppm, 5H (phenyl), 3.925ppm, 2H (CH_2).

9.8.8 $Nb(OH)Cl_4$.BN

Addition of 2 or 3 equivalents of water to a 0.05 mol dm^{-3} solution of $NbCl_5$.BN in CD_3CN gives $Nb(OH)Cl_4$.BN. ^1H spectra, 7.50ppm (5H), 3.90ppm (2H).

9.8.9 $NbCl_5$.AN

1.35g of $(NbCl_5)_2$ was dissolved in excess (20ml) acetonitrile, (Aldrich, anhydrous grade, redistilled over CaH_2), and sonicated for 1 hour at 60°C (under N_2). Removal of solvent gave a yellow solid, $NbCl_5$.AN. ^1H spectra (in CD_3CN), 2.425ppm (obtained by adding a further 10 eq. of CH_3CN), ^{93}Nb spectra, -55ppm.

9.8.10 $Nb(OH)Cl_4$.AN

Addition of 2 or 3 equivalents of water to a 0.1 mol dm^{-3} solution of $NbCl_5$.BN in CD_3CN gave $Nb(OH)Cl_4$.BN. ^1H spectra, 2.325ppm. ^{93}Nb spectra, -495ppm.

References

1. D.Brown, "Inorganic Synthesis", Vol 9, ed. S.Y.Tyree Jr., McGraw-Hill Book Grp., 1967, p88-91.
2. K.Nakamoto, " Infrared and Raman Spectra of Inorganic and Coordination Compounds", J. Wiley and Sons, Chichester, 1978, p155.
3. D.C. Bradley, W. Wardlaw and A. Whitley, *J. Chem. Soc.,* 1955, 726.
4. M. Schönherr and L. Kolditz, *Z. Chem.,* 1970, **10**, 72.

5a. R.D. Werder, R.A. Frey, Hs.H. Gunthard, *J. Chem. Phys.*, 1967, **47**, 4159.

5b. I.R. Beattie, T.R. Gilson, G.A. Ozin, *J. Chem. Soc (A)*, 1968, 2765.

6. H. Preiss, *Z. anorg. allg. Chem,* (1961), **311**, 121.
7. L.G. Hubert-Pfalzgraf, J.G. Reiss, *Inorg. Chem.*, (1975), **14**, 2854.
8. J.G. Riess, L.G. Pfalzgraf, *Bull. Soc. Chim. Fr.*, 1968, 2401.
9. J.G. Riess, L.G. Pfalzgraf, *Bull. Soc. Chim. Fr.*, 1968, 4348.
10. D.C. Bradley, C.E. Holloway, *J. Chem. Soc.(A)*, 1968, 219.
11. L.G. Hubert-Pfalzgraf, J.G. Riess, A.A.Pinkerton, *Inorg. Chem.*, (1978), **17**, 663.
12. R.G. Kidd and H.G. Spinney, *Inorg. Chem.,* 1973, **12**, 1967.
13. D.L. Kepert, R.S. Nyholm, *J. Chem. Soc.*, 1965, 2871.
14. L.G. Hubert-Pfalzgraf, J.G. Riess, *J. Chim. Phys.*, (1973), **70**, 646.
15. "Vogel's Textbook of Practical Organic Chemistry", 4th edt., J. Wiley and Sons, London, 1984, p485.

16a. "The Aldrich Library of IR Spectra", ed C.J. Pouchert, Aldrich Chem. Comp., 1978, p1330(A).

16b. "Sol-Gel Science", Eds C.J. Brinker, G.W. Scherer, Academic Press, 1990, p204.

17. A.I. Vogel "Textbook of Quantitative Inorganic Analysis", Longman, 1971.
18. A. A. McConnell, J.S. Anderson and C. N. R Rao *Spectrochim Acta, Part A* , 1976 , **32A**, 1067.
19. M. Dartiguenave and Y. Dartiguenave *Bull. Soc. Chim. Fr.*, 1968, 171.
20. M. Dubinin, *Chem. Rev.*, 1960, **60**, 235.
21. M. Dubinin, V.A. Astakhov, *Adv. Chem. Ser.*, 1971, **102**, 69.

22 G. Wilkinson, J.M. Birmingham, *J. Am. Chem. Soc.*, 1954, **76**, 4281.

23. P.N. Kapoor, R.C. Mehrotra, *J. of Less Common Metals*, 1965, **8**, 339.

24. N. Young, J.A. Crayston, manuscript in preparation.

25. R. Cabanel, J. Chaussy, J. Mazuer, G. De la Bouglise, J.C. Jubert, G. Barral and C. Montella, *J. Electrochem. Soc.*, 1990, **137**, 1444.

26. N. Machida, M. Tatsumisaga and T. Minami, *J. Electrochem. Soc.*, 1986, **133**, 1963.

27. R.S. Crandall and B.W. Faughnan, *Appl. Phys. Lett.*, 1976, **28**, 95.

28 S.K. Mohapatra, *J. Electrochem. Soc.*, 1978, **125**, 284.

29. A.R. Hillman, "*Polymer Modified Electrodes*" ,, 203.

30. R.W. Murray, "*Electroanalytical Chemistry*",1985, p191.

31. R.G.Kidd and H.G.Spinney, *Inorg. Chem.*, 1973, **12**, 1967.

32. D.J. Edlund, R.J. Saxton, D.K. Lyon, R.G. Finke, *Organometallics*, 1988, **7**, 1692.

33. A. Goiffon, E. Philippot, M. Maurin, *Revue de Chimie minerale*, 1980, **17**, 466.

34. Stoe Stadi-P powder diffraction database.

35. Southampton Electrochemistry Group, "Instrumental Methods in Electrochemistry", Ellis Horwood, London, 1990, p251-282.

36. D.T.Sawyer, E.J. Nanni, "Oxygen and Oxy Radicals in Chemistry and Biology", Academic Press, 1981, p15-44.

37. D.T. Sawyer, J.S. Valentine, *Acc. Chem. Res.*, 1981, **14**, 393.

38. H. Lund, H. Doupeux, M.A. Michel, G. Mousset, J. Simonet, *Electrochim Acta*, 1974, **19**, 629.

39. L.H. Dao, A. Guerfi, M.T. Nguyen, K.Arai, "Proceedings of the Symposium on Electrochromic Materials" Eds. M.K. Carpenter, D.A. Corrigan, The Electrochem. Soc. Vol 90-2, Philadelphia, 1990, p30.

40. D.P. Johnson, R.D. Bereman, *J. Inorg. Nucl. Chem.*, 1972, **34**, 679.

41. G. Wilkinson, M. Rosenblum, M.C. Whiting, *J. Am. Chem. Soc.*, 1952, **74**, 2125.

Appendix 1

The condensation reactions of niobium hydrolysis species can be represented by:

$$Nb(OH)_{za} + Nb(OH)_{zb} \rightarrow NbONb + H_2O \qquad (A.1)$$

where z_a and z_b are the coordination numbers of hydroxide ligands bound to the niobium and $z \geq 3$ for a branched polymer gel.[1]

Assuming hydrolysis is fast, that $[Nb(OH)_{za}] \sim [Nb(OH)_{zb}] = c$ (and initially after hydrolysis $c = C_o$) and no catalyst is present, then by application of Flory's classical kinetics for polymer formation:[2]

$$kc^2 = \frac{-d[Nb(OH)_{za}]}{dt} \qquad (A.2)$$

or $\quad kt = c^{-1}$ - constant (A.3)

then $\quad C_o kt = (1-p)^{-1}$ - constant (A.4)

(where p is extent of reaction, $c = (1-p)C_o$)

At the gel point:[1] $p = (z-1)^{-1}$ (A.5)

then $\quad C_o kt_g = 2$ - constant (A.6)

As C_o is a fraction of the original niobium concentration [Nb] then:

$$t_g = m[Nb]^{-1} \qquad \text{where m is a constant} \qquad (A.7)$$

Thus gel times are expected to be inversely proportional to the original niobium concentration.

1. C.J. Brinker, G.W. Scherer, "Sol-Gel Science", Academic Press, London, 1990, p315-6.
2. "Kinetics and Mechanisms of Polymerization", ed. D.H. Solomon, Marcel Dekker, New York, 1972, p7.

Appendix 2

The "normal" or "mean" value ($\bar{x}$) of a set of n data points is calculated as:[1]

$$\bar{x} = \frac{\Sigma x_i}{n} \qquad (A.8)$$

The standard deviation (s) of this distribution is expressed as:[1]

$$s = \left(\frac{\Sigma\{x_i\}^2}{n} \right)^{1/2} - (\bar{x})^2 \qquad (A.9)$$

The standard error of the mean, $\hat{\sigma}_{\bar{x}}$, is expressed as:[1]

$$\hat{\sigma}_{\bar{x}} = \frac{s}{\{n-1\}^{1/2}} \qquad (A.10)$$

This enables us to calculate the probability of finding the population mean within a given confidence limit. For a 99% confidence limit, the term is:[1]

$$\bar{x} \pm 2.576 \hat{\sigma}_{\bar{x}} \qquad (A.11)$$

Eq A.11 was used to find the quoted 99% confidence limits on the diffusion coefficients.

1. "Statistical Analysis in Geography", C.K. Ballantyne, Dept. Of Geography and Geology, St Andrews, 1989, p1-18.

Publications

(1) "Electrochromic Nb_2O_5 and Nb_2O_5/Silicone Composite Films Prepared by Sol-Gel Processing", G. Rob Lee and Joe A. Crayston, *J. Mater. Chem.*,**1**, 1991, 381.

(2) "Buckminsterfullerene, The 3rd Allotrope of Carbon", Rob Lee, *Chem. and Ind.*,**10**, 1991, 349.

(3) "^{93}Nb NMR Studies of $NbCl_5$ Solvolysis by Alcohols", G. Rob Lee and Joe A. Crayston, *Dalton Trans*, 1991, 3073.

(4) "Sol-Gel Processing of Transition Metals", G. Rob Lee and Joe A. Crayston, to be submitted to *Advaced Materials*.